The role of the c-Jun ubiquitin ligase Fbw7 in the nervous system

Anett Jandke

A thesis submitted for the degree of Doctor of Philosophy at the University of London

February 2008

Mammalian Genetics Laboratory

Cancer Research UK

London Research Institute

UMI Number: U591760

UMI

Dissertation Publishing

UMI U591760

ProQuest

I, Anett Jandke, confirm that the work presented in this thesis is my own. Where information has been derived from other sources, I confirm that this has been indicated in the thesis.

Abstract

Fbw7 belongs to the family of F-box proteins, which function as substrate recognition subunits of SCF complexes. Fbw7 controls the stability of several proteins including cyclin E, the Notch intracellular domain and c-Myc. In 2004 our lab additionally identified phospho-c-Jun as an Fbw7 substrate. c-Jun is part of the AP-1 transcription complex, whose activity is strongly induced in response to numerous signals such as growth factors, cytokines and extracellular stresses. Furthermore elevated phospho-c-Jun levels induce neuronal apoptosis. To investigate the significance of c-Jun regulation by Fbw7 in the nervous system, I generated mice harbouring a floxed fbw7 allele, *fbw7$^{f/f}$*. *fbw7$^{f/f}$* mice were bred to various Cre transgenic lines that express the Cre recombinase under nervous system specific promoters to obtain mice with a tissue specific deletion of Fbw7.

I confirmed published results that ubiquitous deletion of Fbw7 mediated by PGK-Cre is lethal. To delete Fbw7 at the stage of neuronal precursors, *fbw7$^{f/f}$* mice were crossed to the Nestin-cre line (*fbw7$^{\Delta N}$*). These mice die perinatally and show an increase in apoptosis at E16. As the lethality of the *fbw7$^{\Delta N}$* mice does not allow the investigation of Fbw7 in the adult nervous system, further crosses, using other cre-transgenic lines, were set up. Fbw7 deletion in postmitotic neurons (*fbw7$^{\Delta pN}$*) causes a Parkinson's disease like phenotype with a severe hindlimb tremor and a reduced cortical cellularity. Fbw7 deletion in the cerebellar vermis (*fbw7$^{\Delta Cb}$*) resulted in cerebella that are characterised by a reduced size, foliation defects accompanied by an astrocytic gliosis and a phospho-c-Jun dependent Purkinje cell loss. Concomitant deletion of c-Jun in in the cerebellum (*fbw7$^{\Delta Cb}$:c-jun$^{\Delta Cb}$*) partially rescues the cerebellar phenotype caused by Fbw7 deletion.

Thus the data in this thesis demonstrate a role for Fbw7 in cerebellar development and the central nervous system and identify c-Jun as an essential Fbw7 substrate in the nervous system.

Table of Contents

7

List of Figures

12

List of Tables

Abbreviations

aa	amino acid
AD	Alzheimer's Disease
AP-1	Activator Protein 1
ATP	Adenosine Triphosphate
BSA	Bovine Serum Albumin
BrdU	5-Bromodeoxyuridine
Cgc	Cerebellar Granule Cells
CIP	Calf Intestine Phosphatase
CNS	Central Nervous System
CP	Cortical Plate
CRUK	Cancer Research UK
C-terminus	Carboxy-terminus
DAPI	4',6-diamidino-2-phenylindole
DMEM	Dulbecco's Modified Eagle's Medium
DNA	Desoxyribonucleic acid
ERK	Extracellular signal Regulated Kinase
EGL	External Granule Layer
dNTP	deoxyribonucleotide triphosphate
DT-α	Diphteria Toxin alpha
ES cells	Embryonic Stem Cell
Fbw7	F-box-protein 7 (also knows as Sel-10, Ago, Fbxw6)
FCS	Foetal Calf Serum
GFAP	Glial Fibrillary Acidic Protein

15

GFP	Green Fluorescent Protein
GSK-3	Glycogen Synthase Kinase 3
Hepes	4-(2-hydroxyl)-1-piperazine ethane sulphonic acid
HD	Huntington's Disease
HRP	Horseradish Peroxidase
H&E	Haematoxilin & Eosin
IF	Immunofluorescence
IHC	Immunohistochemistry
IZ	Intermediate Zone
JNK	c-Jun-N-terminal-Kinase
kb	kilobase
kD	kilodalton
LB	Luria-Bertani Medium
LSM	Laser Scanning Microscope
MAPK	Mitogen Activated Protein Kinase
MAPKK	Mitogen Activated Protein Kinase Kinase
MAPKKK	Mitogen Activated Protein Kinase Kinase Kinase
MEFs	Mouse Embryonic Fibroblasts
ML	Molecular Layer
MLK	Mixed Lineage Kinase
Mr(kD)	Relative molecular weight in Kilodaltons
Neo	Neomycin
NES	Nuclear Export Signal
NF200	Neurofilament 200
NFAT	Nuclear Factor of Activated T cells

NLS	Nuclear Localisation Signal
Notch-ICD	Notch Intracellular Domain
nt	Nucleotide
N-terminus	Amino terminus
PAGE	Polyacrylamide Gel Electrophoresis
PD	Parkinson's Disease
PBS	Phosphate Buffered Saline
PCR	Polymerase Chain Reaction
PFA	Paraformaldehyde
RNA	Ribonucleic Acid
RPM	Revolutions per minute
RT	Room Temperature
SAPK	Stress Activated Protein Kinase
SCF	Skp1-Cul1-Fbox complex
SDS	Sodium dodecyl sulfate
SD	Standard Deviation
Shh	Sonic Hedgehog
siRNA	Small inhibitory RNA
SVZ	Subventricular Zone
TE	Tris EDTA
TEMED	N,N,N',N'-tetramethyl-ethylenediamine
TH	Tyrosine Hydroxylase
Tris	2-amino-2-(hydroxymethyl)-1,3-propanediol
Vglut1	Vesicular Glutamate Transporter 1
Vglut2	Vesicular Glutamate Transporter 2

VTA	Ventral Tegmental Area
v/v	Volume per volume
VZ	Ventricular Zone
w/v	Weight per volume
WB	Western Blotting
wt	Wildtype

1 INTRODUCTION

1.1 <u>JNK signalling and the transcription factor c-Jun</u>

The Mitogen Activated Protein Kinase (MAPK) pathway mediates the response to numerous extracellular signals by regulating the activation of transcription factors, which in turn control cell growth, differentiation or apoptosis depending on the cellular context. The MAPK cascade is initiated upon stimulation of various receptors such as hormone and growth factor receptors, cytokine receptors or in response to environmental stresses such as UV-irradiation or osmotic shock (reviewed in (K. J. Cowan and K. B. Storey, 2003)). Activation of these receptors leads to the recruitment of adaptor molecules to the relevant receptors, which then activate small GTP-binding proteins. These in turn activate a cascade consisting of multiple tiers of serine/threonine kinases such as the MAPKinase Kinase Kinase (MAPKKK), MAPKinase Kinase (MAPKK) and MAPKinases (MAPKs). There are three subclasses of MAPKs: the extracellular signal regulated kinases (ERK), the stress activated MAPKs including the 38 kD protein kinases (p38), and the c-Jun-N-terminal kinases (JNKs) (T. S. Lewis et al., 1998).

With regards to the JNK pathway MKK4 (SEK1) and MKK7 (SEK2) are the two MAPKKs that activate JNKs through the dual phosphorylation of a Thr-Xaa-Tyr motif (Figure 1.1 A) (B. Derijard et al., 1994). MKK4 is primarily activated by environmental stress and can additionally activate p38 (reviewed

in (R. J. Davis, 2000)). In contrast MKK7, is specific for JNKs and is activated by generic stimuli such as anisomycin and UV irradiation and additionally by specific stimuli like tumour necrosis factor (TNF) and interleukin-1 (IL-1) (C. W. Chow et al., 1997; C. Tournier et al., 2001). Studies using mice and mouse embryonic fibroblasts (MEFs) deficient for MKK4, MKK7 or both have demonstrated that the JNK signalling pathway regulates not only apoptosis but is also essential for survival and organogenesis. Whilst $mkk4^{-/-}$ and $mkk7^{-/-}$ MEFs are resistant to anisomycin or heat shock induced JNK activation, $mkk4^{-/-}$ embryos exhibit severe defects in liver formation and the liver cells undergo massive apoptosis (D. Yang et al., 1997; H. Nishina et al., 1999; C. Tournier et al., 2001). This apparent ambiguity of the resistance against UV induced apoptosis in MEFs and an increase in apoptosis during organogenesis shows that the effects of MAPK signalling are strongly dependent on the cellular context and that MKK4 and MKK7 are important mediators of MAPK signalling.

A
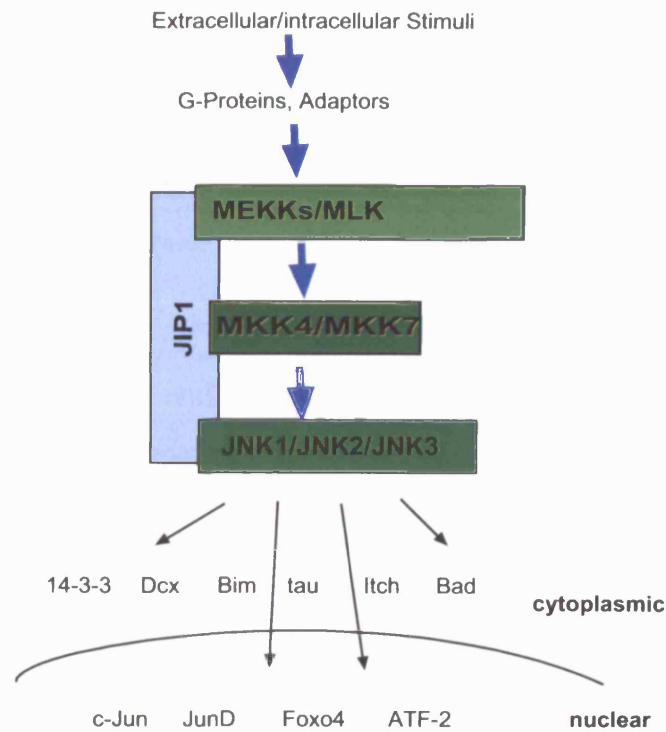
B

Figure 1.1 The JNK signalling cascade and the transcription factor c-Jun. A) JNK signalling is activated upon extracellular stimuli and is relayed via small G-Proteins and adaptor molecules to a kinase cascade. Upstream kinases such as MEKK and MLKs activate their downstream kinase which are in case of JNK signalling MKK4 and MKK7. This causes activation of c-Jun N-terminal kinases (JNKs) which then phosphorylate various cytoplasmic and nuclear substrates as indicated. The JNK-interacting protein JIP acts as a scaffold for the signalling cascade. B) Domain structure of c-Jun. JNK binds within the δ domain and activates c-Jun by phosphorylation at S63/73 and Thr91/93 in the transactivation domain. c-Jun dimerises with other AP-1 components via its c-terminal leucine zipper (L-Zip). Binding to target genes occurs via the DNA binding domain (DBD).

1.1.1 <u>The physiological role of JNKs</u>

The JNKs JNK1, JNK2 and JNK3 are encoded by 3 different genes and and are also known as the Stress Activated Protein Kinases (SAPKs): SAPK-γ, SAPK-α and SAPK-β respectively. They show a distinct expression pattern and while JNK1 and JNK2 are expressed ubiquitously, JNK3 is found predominantly in the brain and testis (S. Gupta et al., 1996; C. Y. Kuan et al., 1999). Additionally, the different JNKs appear to have an at least partially redundant function in the organism as mice bearing a single deletion for either JNK1 or JNK2 are viable whereas concomitant deletion of JNK1 and JNK2 results in embryonic lethality (C. Dong et al., 1998; C. D. Yang DD, Whitmarsh AJ, Barrett T, Davis RJ, Rincón M, Flavell RA., 1998; K. Sabapathy et al., 1999). Although JNKs were named after their major target c-Jun, it became apparent over the last years that JNKs can additionally phosphorylate and activate JunB, JunD, Elk-1 and ATF-2, (reviewed in (M. A. Bogoyevitch and B. Kobe, 2006)). Furthermore the Nuclear-Factor-of-Activated-T-cells (NFAT-4)(C. W. Chow et al., 1997), p53 (S. S. Shklyaev et al., 2001), c-Myc and a number of non-nuclear substrates including the microtubule associated protein Tau (H. Yoshida et al., 2004) and the ubiquitin E3 ligase Itch (M. Gao et al., 2004) have been identified as JNK substrates. Thus JNK signalling is not only a part of the cellular stress response and mediates apoptosis, it also regulates mechanisms such as cytoskeletal rearrangements, the immune response and protein degradation (see also 1.2.3).

With regards to the role of JNKs in the nervous system it was shown that the response to apoptotic stimuli also varies in different JNK knockout mice. While deletion of JNK1 or JNK2 does not alter the response to kainate induced neuronal apoptosis, mice lacking the brain specific JNK3 are resistant to kainate induced excitotoxicity (D. D. Yang et al., 1997). Kainate receptors are found throughout the brain and are activated by the primary excitatory amino acid glutamate and their specific agonist kainate, which mimics the effect of glutamate. Administration of kainate causes an increase in the intracellular Ca^{2+} levels and the calcium dependent release of the excitatory neurotransmitter glutamate. This excess of glutamate leads to neuronal apoptosis and this mechanism is also known as excitotoxicity (J. W. Ferkany and J. T. Coyle, 1983; S. F. Giardina et al., 1998). Kainate receptors are located presynaptically where the presence of nanomolar kainate concentrations increases the glutamate release into the synapse and postsynaptic kainate receptors participate in the mediation of synaptic currents (reviewed in (J. Lerma, 2003)). Brain regions that are sensitive to kainate express high levels of the GluR6 and K2 kainate receptor genes and Savinainen et al have shown that after GluR6 receptor activation the PSD-95 protein anchors the JNK upstream kinases MLK2 and MLK3 to the glutamate receptor complex, which subsequently results in JNK activation (W. Wisden and P. H. Seeburg, 1993; A. Savinainen et al., 2001). In 1999 Behrens et al demonstrated that the excitotoxic effect in hippocampal neurons is dependent on c-Jun phosphorylation at the N-terminal S63/73 residues as jun^{AA} mice that harbour mutations of these residues to alanines are resistant to kainate induced excitotoxicity (A. Behrens et al., 1999). The fact that JNK signalling is an essential mechanism in the regulation

of survival signals in neurons is further supported by the fact that $jnk3^{-/-}$ mice

but also $jnk2^{-/-}$ neurons are partially protected from apoptosis upon

administration of MPTP, a neurotoxic drug that induces loss of dopaminergic

neurons (S. Hunot et al., 2004). However $jnk1^{-/-}$ neurons are not protected in

this system indicating that there are distinct roles of the different JNK isoforms

in the brain (reviewed in (S. Brecht et al., 2005)).

1.1.2 <u>The transcription factor c-Jun</u>

One of the downstream targets of the JNK cascade is the transcription

factor c-Jun, which is the cellular counterpart to the transforming protein v-Jun

of the chicken retrovirus ASV17. To activate c-Jun, JNK first binds to the N-

terminal δ domain in c-Jun and phosphorylates residues Ser63/Ser73 and

Thr91/Thr93 located within the transactivation domain of c-Jun (Figure1.1 B)

c-Jun forms homo- or heterodimeric complexes with proteins such as JunB,

JunD, members of the Fos protein family or ATF-2 to generate the activator-

protein-1 (AP-1) transcription complex. The AP-1 complex binds to a

consensus sequence (AP-1 sites) found in promoters and enhancers of a great

variety of genes and is involved in the regulation of cell growth, transformation

and in the response to stress (E. Shaulian and M. Karin, 2002).

Regarding c-Jun in the nervous system, Herdegen et al. observed that

c-Jun is upregulated in response to injury, while the other components of the

AP-1 complex were not induced to the same extent (T. Herdegen et al., 1997)

(T. Herdegen et al., 1998). In 2004 the role of c-Jun in the nervous system was

further clarified in a study that used mice that lack c-Jun specifically in cells of

the neuronal lineage (c-$jun^{\Delta N}$ mice) (G. Raivich et al., 2004). c-$jun^{\Delta N}$ mice

develop normally but display defects in the axonal regeneration after injury while at the same time apoptosis in response to the injury was reduced.

The importance of c-Jun phosphorylation in neuronal apoptosis was underlined in a study that characterised jun^{AA} mice, where the N-terminal phosphorylation sites S63/S73 in the transactivation domain were mutated to alanines (A. Behrens et al., 1999). As the $jnk3^{-/-}$ mice the jun^{AA} mice are resistant to kainate-induced apoptosis, which demonstrates a requirement for c-Jun phosphorylation in the initiation of neuronal cell death. Also cultured sympathetic neurons from jun^{AA} mice display a significant delay in apoptosis induced by trophic factor deprivation (C. G. Besirli et al., 2005). Other *in vitro* experiments in rat cerebellar granule cell cultures (cgcs) and rat sympathetic neurons demonstrated that overexpression of a dominant negative c-Jun construct protects these neurons from apoptosis, thereby supporting the model that N-terminal phosphorylation of c-Jun is a crucial event in neuronal apoptosis (J. Ham et al., 1995; A. Watson et al., 1998). Apart from its role in neuronal apoptosis after insults, an active JNK pathway and phosphorylated c-Jun have been observed in neurodegenerative diseases. In brains from patients with Alzheimer's disease (AD) activated c-Jun was found in neurofibrillary tangles and was connected to amyloid depositions (A. G. Pearson et al., 2006; A. Thakur et al., 2007). Furthermore c-Jun phosphorylation has been linked to Huntington's disease (HD) (M. Garcia et al., 2004) and the death of dopaminergic neurons in a mouse model for Parkinson's disease (PD) (M. G. Willesen et al., 2002). In summary, while c-Jun is dispensable for brain development, c-Jun and c-Jun phosphorylation play an important role in axonal regeneration, neuronal apoptosis, and neurodegenerative diseases.

In 2004 it was found that the F-box protein Fbw7 targets specifically phosphorylated c-Jun for subsequent proteasomal degradation (A. S. Nateri et al., 2004). Fbw7 is one component of a so-called SCF-E3 ligase complex, which mediates the attachment of small ubiquitin molecules to a substrate and thereby marks it for subsequent degradation. Since I was investigating the role of Fbw7 in the nervous system, I will give a short overview about ubiquitination, E3 ligases and c-Jun degradation in the following section. I will then summarise the literature on Fbw7, its substrates and regulation and give a short introduction into the nervous system.

1.2 Protein ubiquitination, E3 ligases and c-Jun

1.2.1 Ubiquitination targets proteins for different intracellular events

Ubiquitin is a 76 amino acid molecule, which can be attached to other proteins either as a monomer or as a chain of ubiquitin residues and thereby alter the fate of the modified protein. An ubiquitin chain is generated by the linkage of ubiquitins via lysine residues present at various positions in the ubiquitin molecule whereby the lysine residues that are used for the ubiquitin linkage determine the fate of the ubiquitinated protein (Figure 1.2A). The presence of a chain of multiple ubiquitin residues that are linked via their lysine 48 (K48 linkage) marks a protein for subsequent proteasomal degradation. A polyubiqutin chain that is linked via lysine 63 (K63 linkage) is not targeted for degradation but is instead involved in other cellular processes such as intracellular signalling, transcription, transformation or DNA repair (reviewed

in (A. Isaksson et al., 1996; M. Muratani and W. P. Tansey, 2003; D. Mukhopadhyay and H. Riezman, 2007)). In addition there is also the possibility that a protein can be monoubiquitinated at either one or multiple sites, which was shown to regulate endocytosis of receptor tyrosine kinases (Figure 1.2B) (K. Haglund et al., 2003). In any ubiquitination reaction the ubiquitin attachment is mediated by a cascade of enzymes that finally leads to the formation of a thioester-bond between the C-terminus of ubiquitin and the e-amino group of a lysine in the substrate. The enzymes involved in this ubiquitination process are the ubiquitin-activating enzyme (E1), the ubiquitin conjugating enzyme (E2) and the ubiquitin ligases (E3s). E3 recognise and bind the substrate and finally mediate the attachment of ubiquitin moieties (see below) (Figure 1.2C). The initial steps of the ATP dependent ubiquitin activation and E2 conjugation are not described in detail in this introduction as my work focussed on the E3 ligase Fbw7 and for a review of the initial ubiquitination steps see (C. M. Pickart and M. J. Eddins, 2004).

Interestingly the number of E3 ligases is higher than the number of E2 ligases, which in turn is higher than the number of E1 enzymes identified so far (C. M. Pickart, 2001). The E3 ligases are the final and crucial adaptor molecules between the ubiquitination complex and the substrate, and are therefore responsible for the specificity. The high number of E3s may reflect the number of target proteins, however, this does not mean that any given E3 ligase has only one substrate. Indeed one E3 ligase can have many substrates that all share a specific recognition sequence, for instance a so-called phospho-degron, where a protein is recognised for ubiquitin attachment depending on its phosphorylation state. Additionally one substrate can also be targeted for

degradation by more than one E3 ligase, which has been shown to be the case for c-Jun (see below 1.2.3).

The result of the multi step ubiquitination cascade is always the attachment of an ubiquitin moiety to the substrate. Originally it was believed that all three enzymes are necessary for the ubiquitination of a protein and it was only elucidate recently that ubiquitination can also take place in the absence of an E3 ligase. Even more, in addition to the attachment of one ubiquitin molecule after the other to form a chain on the substrate also whole previously assembled ubiquitin chains can be attached (W. Li et al., 2007).

Ubiquitination is not a final modification and can be reversed by means of deubiquitinating enzymes (DUBs) and ubiquitin specific proteases (USPs) and an increasingly complex network of regulated ubiquitination and deubiquitination of proteins emerges. For instance, the Anaphase Promoting Complex (APC) E3-ligase activity in yeast is antagonised via USP44, which deubiquitinates the APC coactivator Cdc20 (F. Stegmeier et al., 2007). Importantly the first USP for the E3-ligase Fbw7, USP28, was recently identified and found to antagonise Fbw7 mediated ubiquitination (N. Popov et al., 2007).
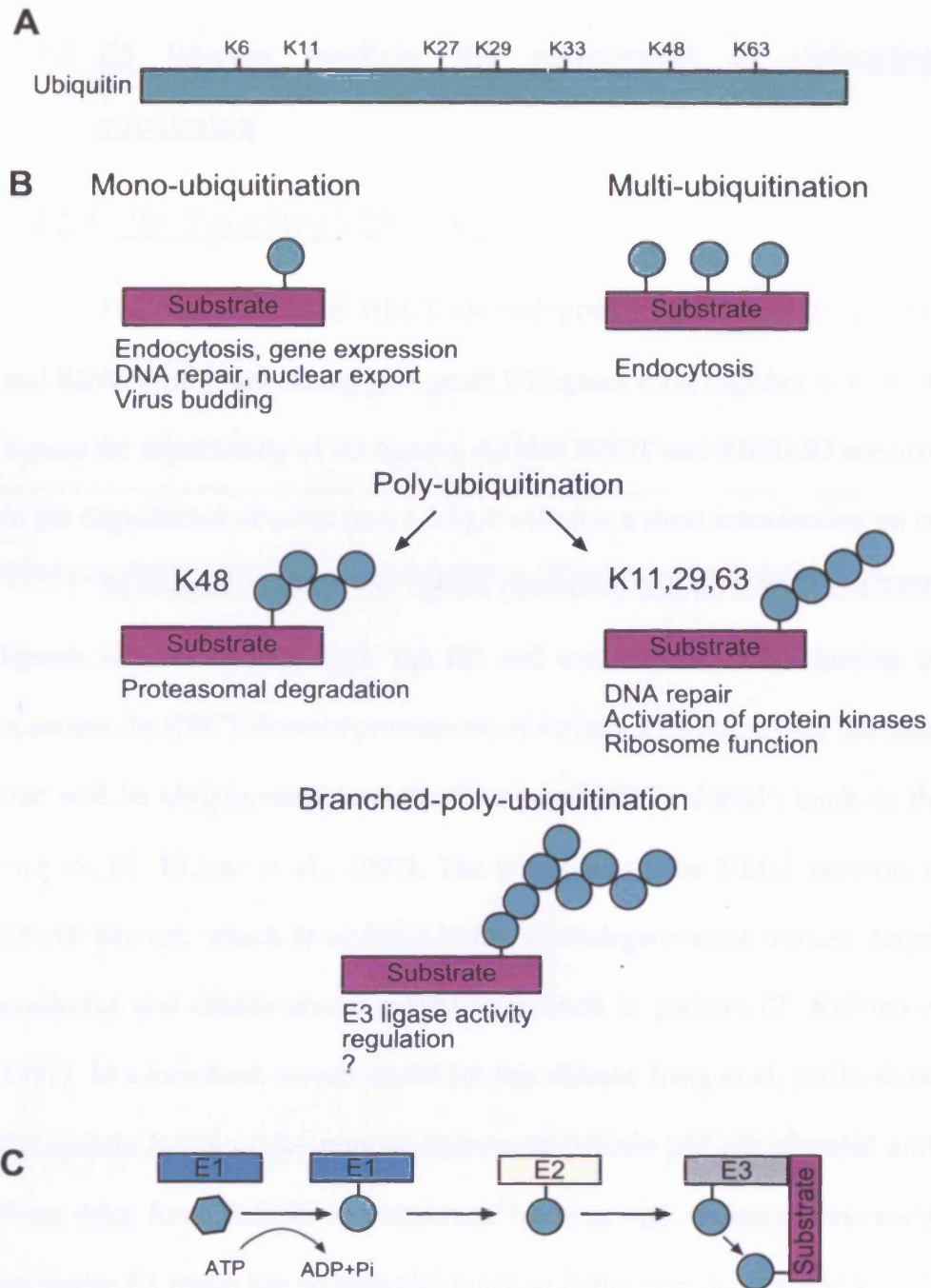
Figure 1.2 Ubiquitination targets proteins for a variety of processes
A) The 76 Amino acid ubiquitin molecules contains a variety of lysine
residues (K6 to K63) that are used to link the ubiquitins to the substrate
and during the polyubiqutin chain formation. Figure from Woelke et al.,
2007 B) Proteins can be ubiquitinated in different ways. Ubiquitination
was shown to be involved in a variety of cellular events listed below the
different ubiquitination modes C) Ubiquitination is mediated via a cascade
of three different enzymes. The E1 ubiquitin activating enzyme and E2
ubiquitin conjugating enzyme prepare the attachment of the ubiquitin
moiety via the E3 ligase to the substrate. Figure modified from Haglund&
Dikic,2005.

1.2.2 E3 ligases mediate the attachment of ubiquitins to substrates

1.2.2.1 HECT and RING E3 ligases

The two classes of HECT (homologous to E6-AP-carboxy terminus) and RING (really interesting new gene) E3 ligases form together with the F-box ligases the superfamily of E3 ligases. As also HECT and RING E3 are involved in the degradation of c-Jun (see 1.2.3), I will give a short introduction on them.

In contrast to the F-box ligases (discussed below) HECT and RING E3 ligases interact directly with the E2 and mediate the ubiquitination of the substrate. In HECT domain proteins the N-terminus interacts with the substrate that will be ubiquitinated, and the C-terminal HECT domain binds to the E2 enzyme (S. Kumar et al., 1997). The prototype of the HECT proteins is the E6-AP protein, which is mutated in the neurodegenerative disease Angelman syndrome and causes severe mental retardation in patients (T. Kishino et al., 1997). In a knockout mouse model for this disease Jiang et al. could show that the protein levels of the tumour suppressor protein p53 are elevated and that these mice have deficits in contextual learning and memory, indicating this particular E3 ligase has an essential function in the nervous system (Y. H. Jiang et al., 1998). Another example for a HECT-E3 is Itch, which regulates the degradation of Notch, c-Jun and JunB and which will be described in more detail later (see 1.2.3) (L. Qiu et al., 2000; D. Fang and T. K. Kerppola, 2004; M. Gao et al., 2004).

RING E3 ligases were named after their characteristic cross brace structure that coordinates two zinc ions in its core and have been divided into two subgroups, one group contains the RING proteins that exert their function as monomers, whereas the other group contains RING E3s that are part of multimeric complexes such as the Skp1-Cul1-F-box (SCF) complex or the Von Hippel Lindau (VHL) complex (T. Kamura et al., 1999). In the case of single subunit RING E3s the RING domain facilitates the ubiquitination of a substrate that is recognises by another domain of the protein. Examples for such a single subunit RING-E3 ligase are c-Cbl where the target protein is recognised via its SH2 domain (C. A. Joazeiro et al., 1999) and Mdm2, which has a crucial role in mediating the degradation of the tumour suppressor p53 (S. Fang et al., 2000). There is also emerging evidence that the interaction between these E3-ligases and their substrates is tightly regulated by posttranslational modifications. In case of Mdm2, for example, it was demonstrated that not only p53 is protected from Mdm2 mediated degradation when acetylated, but also that acetylation of Mdm2 itself impairs its function on p53 (X. Wang et al., 2004). Additionally specific adaptor molecules have been identified that can interact with E3 ligases that were originally thought to act as monomers. The adaptor molecule Numb, for instance, binds to the transcription factor gli1 thereby targeting it for Itch mediated degradation (L. Di Marcotullio et al., 2006).

1.2.2.2 F-box E3 ligases and the SCF complex

The SCF complex is a multi protein complex named after its components Skp-1:Cul1:F-box (Figure 1.3A) A further component of the SCF complex is the Rbx1 RING protein, which in this context acts as an adaptor for

the E2 ligase and not as a self-standing E3 ligase. An ubiquitin will be attached to a substrate via the E2 enzyme bound to Rbx1, which in turn is bound to the Cul1 C-terminus. The Cul1 N-terminus binds to Skp1, which also binds the conserved F-box domain of the F-box proteins (P. K. Jackson and A. G. Eldridge, 2002).

F-box proteins, such as Fbw7, act as a connector between the otherwise conserved complex and the specific substrate. There are three groups of F-box proteins and while the F-box domain is common to all of them, they differ in their C-termini, which can be composed of either a so-called WD-40 repeat region, a leucine rich repeat region or a variable region (J. T. Winston et al., 1999). In all cases the C-terminus is responsible for the binding of the substrate that is to be ubiquitinated. Ten WD-40 repeat F-box proteins have been identified so far and they have various functions, expression patterns and substrates. Fbw1 for example can be found in the nucleus as well as the cytoplasm and mediates the degradation of β-catenin (M. Kitagawa et al., 1999). Fbw2 is mainly expressed in the liver but not in the brain and localises to the cytoplasm (M. Miura et al., 1999). Another example is Fbw8, which forms a complex with Cul7 and Cul1 and Tsunematsu et al. showed that Fbw8 is required during the development of the placenta in mice (R. Tsunematsu et al., 2006). Thus, although these proteins share the same conserved domains such as the F-box and the WD-40 region, and bind to the same components of the SCF complex, their function is highly specific and diverse. Fbw8, for example, was found to interact with c-Myc but does not bind within the myc-box domain 1 as Fbw7 does (see also 1.3.3.2). Instead Fbw8 interacts with c-Myc via the myc-box domain 2 and the helix-loop-helix motif (H. B. Koch et

al., 2007). Considering that with Fbw7 and Skp2 there are already two E3 ligases involved in c-Myc degradation (see also 1.3.3.2) the interaction of Fbw8 with c-Myc adds further complexity to this mechanism and shows again that one substrate can be targeted by different E3 ligases for degradation. Nevertheless it remains largely elusive how these interactions are orchestrated. The studies published so far for c-Jun and c-Myc degradation usually focus on one particular E3 ligase in but do not consider effects of the other known specific E3 ligases on the given target protein.

1.2.3 c-Jun degradation

The first reports describing that c-Jun can be ubiquitinated and degraded via the proteasome pathway were published in 1994 and 1996 (M. Treier et al., 1994; A. M. Musti et al., 1996). Treier et al. demonstrated that the δ domain of c-Jun is important for its degradation and Musti et al. observed that differences in the δ domain of c-Jun, and JunD account for their different ubiquitination kinetics and thus different half live times of the proteins (A. M. Musti et al., 1997). However, in those two publications, however, no specific E3 ligases for the Jun family members were identified.

In 2003 it was shown that c-Jun binds to the RING protein Cop1 and that Cop1 binding to c-Jun downregulates AP-1-dependent transcription (E. Bianchi et al., 2003). A year later in 2004 Wertz et al. described a ternary complex consisting of Cop1, hDet1 and Cul4A, which mediates the degradation of c-Jun independent of JNK signalling or the presence of the δ-domain (I. E. Wertz et al., 2004). While it is not clear whether this complex acts in a phosphorylation independent manner or requires the phosphorylation at other

sites outside the δ-domain, an regulatory mechanism for the Cop1-hDet-c-Jun interaction has recently been elucidated. Savio et al. showed that a splice variant of Cop1, Cop1D, acts as a dominant negative regulator of Cop1. Savio et al observed an initial decrease in the Cop1/Cop1D ratio in response to UV, which is then followed by an increase in Cop1/Cop1D ratio. Savio et al conclude that these alterations in the Cop1 isoform ratios offer a mechanism for the finetuning of c-Jun levels in response to UV. Immediately after UV irradiation c-Jun activity increases the sensitivity of cells to p53 mediated apoptosis and c-Jun levels can be downregulated by the Cop1-hDet1-Cul1 complex. Once Cop1D is sufficiently upregulated it dimerises with Cop1 and sequesters it away from the E3 ligase complex. This leads to an increase in c-Jun levels, which mediate cell cycle re-entry (M. G. Savio et al., 2007).

Apart from Cop1 the F-box protein Fbw7 (A. S. Nateri et al., 2004; W. Wei et al., 2005) and the HECT-E3 ligase Itch (M. Gao et al., 2004) were found to mediate c-Jun ubiquitination and degradation (Figure 1.4A). Firstly, Gao et al. observed that the overexpression of an upstream kinase of the JNK signalling pathway such as MEKK1 or a dominant active JNKK2-JNK1 construct in 293 cells caused polyubiquitination of c-Jun in an Itch dependent manner. However, also c-Jun constructs harbouring either single or double mutations of the S63 and S73 residues to alanines were ubiquitinated to the same degree as wt c-Jun. Gao et al. next analysed the ubiquitination of a jun^{Ala} mutant where additionally to the S63/73 and T91/93 residues the threonine residues at positions 89, 90 and 95 were changed to alanines. In the presence of Itch this jun^{Ala} construct was ubiquitinated to the same extent as wt c-Jun. Based on these experiments Gao et al. concluded that Itch mediates the

ubiquitination of c-Jun independent of the phosphorylation status in the c-Jun transactivation domain (M. Gao et al., 2004). Interestingly, Gallagher et al. showed in 2006 that Itch itself is phosphorylated and thereby regulated by JNK signalling (E. Gallagher et al., 2006). The phosphorylation of Itch at various residues in its proline-rich region results in the disruption of an intramolecular interaction between its N- and C-terminal region, which on the one hand allows Itch to exert its function as an E3 ligase, but on the other hand decreases its stability by promoting its autoubiquitination. Additionally to Itch, the F-box E3 ligase Fbw7 can antagonise the levels of phosphorylated c-Jun and two different Fbw7 binding sites were identified, whereby one lies within the δ domain and the other one is located more c-terminal (see also chapter 1.3.3.1) (A. S. Nateri et al., 2004; W. Wei et al., 2005). By using c-Jun constructs, in which the phosphorylated residues were mutated to alanines both groups established that c-Jun has to be phosphorylated to be ubiquitinated by Fbw7 (A. S. Nateri et al., 2004; W. Wei et al., 2005).

In summary, three different E3 ligases for c-Jun have been identified so far: Itch, Cop-1 and Fbw7. The analysis of the binding sites for these E3 ligases reveals that all three ligases recognise different motifs in the c-Jun protein (Figure 1.4B). Furthermore the initial characterisation of these E3:c-Jun interactions demonstrated that the recognition of c-Jun as a substrate is regulated by a variety of different mechanisms: the phosphorylation of either the substrate (Fbw7:c-Jun interaction) or the E3 ligase itself (Itch-c-Jun interaction). Furthermore the recognition of c-Jun as a ubiquitination target can be regulated by other factors that sequester components of the ubiquitination

machinery as shown for the Cop-1:c-Jun interaction. The existence of different mechanisms that regulate c-Jun abundance suggests that dependent on the cellular context or extracellular stimulus different E3 ligases might be involved in regulating c-Jun levels. However, how the activity of the different E3s towards c-Jun is orchestrated still remains to be investigated.
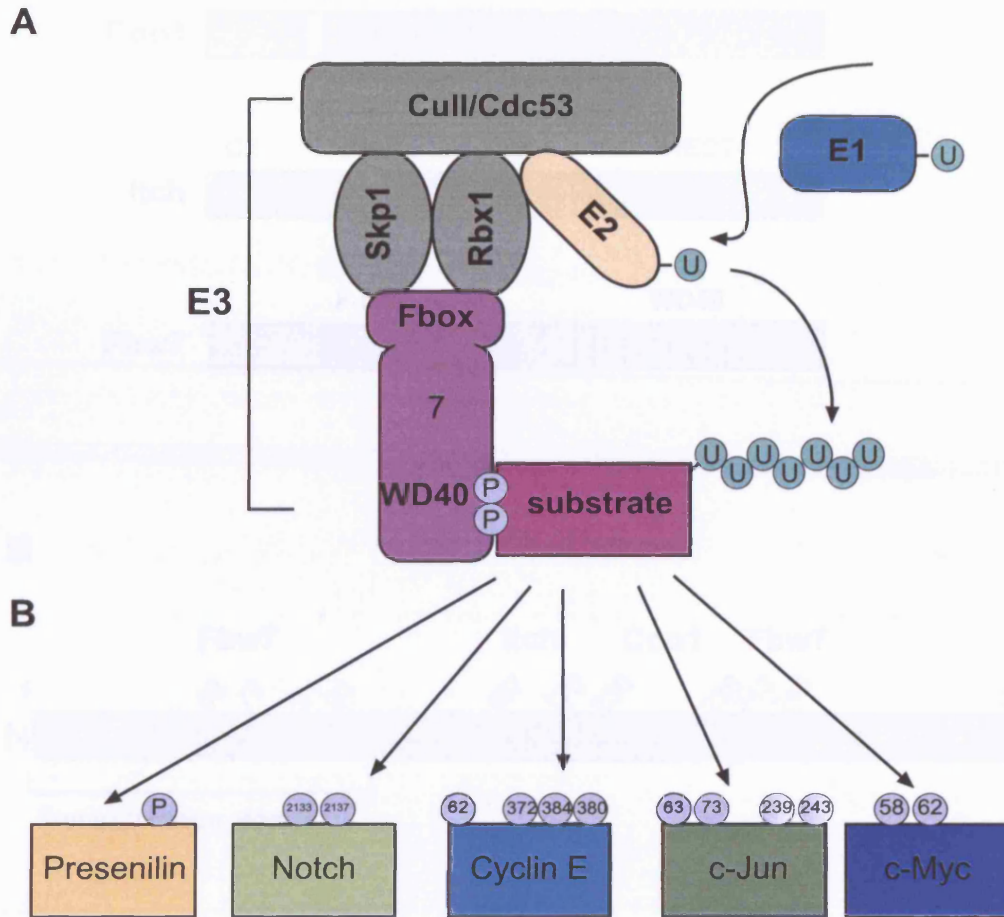
Figure 1.3 Fbw7 is part of the multimeric SCF-E3 ligase complex and confers the substrate specificity. A) The ubiquitin is activated by an E1 ubiquitin activating enzyme and is attached via an E2 ubiquitin conjugating enzyme and the multimeric SCF-E3 ligase to the substrate B) Substrates have to be phosphorylated to be recognised by the SCF^{Fbw7}complex. Phosphorylated residues required for recognition by Fbw7 are indicated in grey. For a detailed description of Fbw7 substrates see chapter 1.3.3.
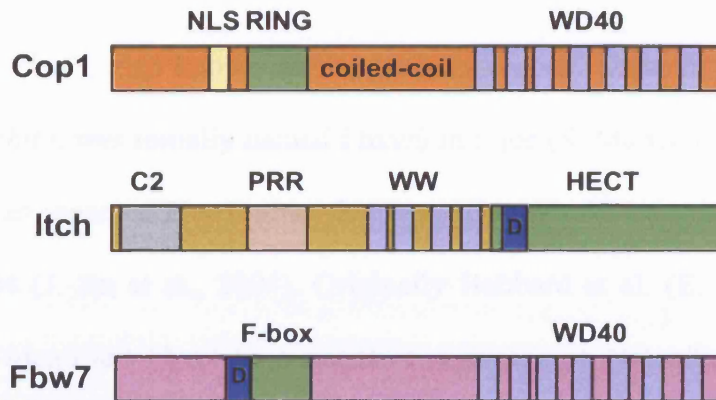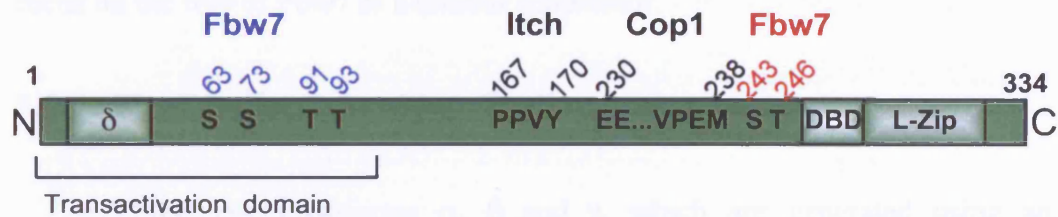
Figure 1.4 Three different E3 ligase recognise c-Jun A) Domain structure of the 3 identified c-Jun E3 ligases.The substrate binding domains (WW and WD40 respectively) are in light blue, the catalytic E3 domains are shown in green.Dark Blue square: D-domain. B) All E3 ligases for c-Jun bind at different sites. Fbw7, Cop1 and Itch binding sites on the mouse c-Jun amino acid sequence are indicated. For data on the two Fbw7 binding sites see also chapter 1.3.3.1. RING: Really Interesting New Gene domain, PRR: Proline rich region, NLS: Nuclear Localisation Signal, C2: C2-domain

1.3 <u>The Fbw7 protein</u>

Fbw7, also known as Sel-10 in *c.elegans*, Cdc4 in yeast and Ago in *drosophila*, was initially named Fbxw6 in mice (S. Maruyama et al., 2001) but was later renamed Fbw7 when the nomenclature of F-box proteins was unified in 2004 (J. Jin et al., 2004). Originally Hubbard et al. (E. J. Hubbard et al., 1997) identified Fbw7 as a negative regulator of Notch/lin-12 signalling in *c.elegans*. Since then various other substrates have been described including c-Jun, c-Myc, and cyclin E. I will now summarise how Fbw7 interacts with its substrates and as many of these substrates are known oncogenes, I will also focus on the role of Fbw7 as a tumour suppressor.

1.3.1 <u>Fbw7 isoforms and localisation</u>

Fbw7 has 3 isoforms α, β and γ, which are generated using an alternative first exon, followed by 10 common exons (Figure 1.5A) The unique exon 1 of the Fbw7 isoforms plays a crucial role in determining their localisation and function. While the α and γ isoforms are present in the nucleus and nucleoli, the β isoform is found in the cytoplasm (M. Welcker et al., 2004a). In addition the three isoforms show a tissue specific expression pattern with the β isoform being expressed mainly in brain, heart and testis, while the other isoforms are found in various tissues (C. H. Spruck et al., 2002).

A detailed study, conducted by Welcker et al. identified several localisation signals within the Fbw7 sequence that can explain the distinct

localisation patterns of the different isoforms (Figure 1.5B)(M. Welcker et al., 2004a). A nuclear localisation signal (NLS) in the α-exon of Fbw7 is responsible for its nuclear localisation and upon deletion of the respective residues this nuclear isoform localises to the cytoplasm. Additionally the N-terminus of the α-isoform is sufficient to translocate GFP to the nucleus, clearly indicating the presence of an isoform specific NLS (M. Welcker et al., 2004a). Furthermore, Welcker et al. could demonstrate that the N-terminus of the β-isoform contains a nuclear export signal (NES). In addition to the localisation signals identified by Welcker et al., I identified another NLS in the common region in between the F-box domain and the WD40 repeat region. Mutagenesis of this NLS (GFP-Fbw7-ΔN-4A) abolishes the nuclear localisation of a GFP fusion construct, containing only the common region of Fbw7 (GFP-Fbw7-ΔN), and distributes it back to the cytoplasm (A. Jandke, 2003).

The ability of Fbw7 to translocate between different cellular compartments, either upon deletion or mutagenesis of various domains, gives rise to the speculation that Fbw7 localisation might be regulated by yet to be defined mechanims. It is feasible to speculate that substrate recognition might be achieved or impaired via signals that bind and mask localisation signals, and thereby affect the localisation and subsequently access to substrates in different cellular compartments.

1.3.2 Fbw7 isoforms can act sequentially on a substrate and dimerise

Various studies have demonstrated that the different Fbw7 isoforms can interact and cooperate in their action towards substrates. A study by van Drogen

et al. demonstrated that multi-ubiquitination of cyclin E, one of the Fbw7 substrates, is achieved by the initial binding of Fbw7-α to cyclin E, which is followed by binding of the prolyl isomerase Pin1 to this complex (F. van Drogen et al., 2006). This in turn facilitates the binding of the second isoform, Fbw7-γ, to cyclin E. Their finding of a sequential interaction of both Fbw7 isoforms is supported by the existence of a cancer mutation in Fbw7-α, which cannot interact with Pin1 and thereby stabilises cyclin E (F. van Drogen et al., 2006). Data from $pin1^{-/-}$ mice strengthen this model, as in these animals cyclin E protein levels are deregulated (E. S. Yeh et al., 2006). Van Drogen and colleagues speculate that the sequential binding of different Fbw7 isoforms to a single substrate might be a general mechanism for the action of Fbw7 on its targets and a recent study using $pin1^{-/-}:p53^{-/-}$ mice supports this model(K. Takahashi et al., 2007). In this study the authors observed an increase in Notch-1-intracellular domain (Notch1-ICD) and Presenilin levels with both proteins being Fbw7 targets (see chapter 1.3.3.4). However, the authors did not relate the observed increase of these substrates to the role of Pin1 in Fbw7-mediated protein degradation and did not look at the effects on other substrates of Fbw7 such as c-Jun or c-Myc.

In line with the idea that Fbw7 isoforms can cooperate or interact, a so-called D-domain (dimerisation domain) directly upstream of the F-box domain was recently identified (W. Zhang and D. M. Koepp, 2006; M. Welcker and B. E. Clurman, 2007). Both groups investigated the interaction of different Fbw7 isoforms and used N- and C-terminal truncated constructs to map possible Fbw7 dimerisation sites. They observed that all isoforms have the ability to homo- and heterodimerise in various combinations *in vitro* (W. Zhang and D.

M. Koepp, 2006) and *in vivo* (W. Zhang and D. M. Koepp, 2006; M. Welcker and B. E. Clurman, 2007). Co-immunoprecipitation experiments showed that homodimerisation is more efficient than heterodimerisation. Additionally the heterodimerisation of the β-isoform with the others (α or γ) was very weak, which is perhaps not surprising considering the different cellular compartments where these isoforms are expressed (M. Welcker and B. E. Clurman, 2007). The same study also demonstrated that the dimerisation can alter the localisation of the complex. Performing co-overexpression studies in U2OS cells the authors observe that a cytoplasmic mutant of the γ-isoform, localises to the nucleus upon dimerisation with the α-isoform, whereas co-overexpression of the β and γ isoform did not result in an altered localisation (M. Welcker and B. E. Clurman, 2007). Welcker et al. further investigated whether the dimerisation affects the substrate ubiquitination. By using a dimerisation defective mutant where the four amino acids that are required for dimerisation are deleted, and by monitoring cyclin E levels, they observed that dimerisation is not strictly required for Fbw7 to exert its function. This is in contrast to the study of Zhang et al. who found that dimerisation is essential for cyclin E proteolysis. These authors used a cycloheximide protein synthesis block to determine the proteolysis of the cyclin E pool over time and observed a stabilisation when using the D-domain mutant, which contains a deletion of exon2, 3 and 4. Since the deletion domain mutant used by Welcker et al. spans only the 4 amino acids that are required for dimerisation this shows that dimerisation is indeed not completely required for Fbw7 function. Furthermore

both studies concluded that the functionality of the D-domain is not dependent on the presence of the F-box domain or the WD-40 repeats.

In summary it has been clearly demonstrated that more than one Fbw7 molecule can be involved in the ubiquitination of a substrate and that a ternary complex might be formed, either involving an Fbw7 dimer or another intermediate such as Pin1. Hao et al. have recently confirmed the dimerisation model for SCF-mediated ubiquitination by providing crystallographic data and additionally suggest that a model of "substrate cross-ubiquitination" is also feasible (B. Hao et al., 2007). This model proposes that a ubiquitin moiety can be attached more efficiently by a second SCF complex, present on the same substrate molecule, or even on a different E3 substrate molecule in close proximity (Figure 1.5C) Therefore, the interaction between the different Fbw7 isoforms and between Fbw7 and its substrates appears to be highly complex and most likely not all mechanisms or even substrates have yet been identified. As all substrates are potentially affected in Fbw7 knockout animals, I will now recapitulate the published data on the substrates known to date.

A

B

C
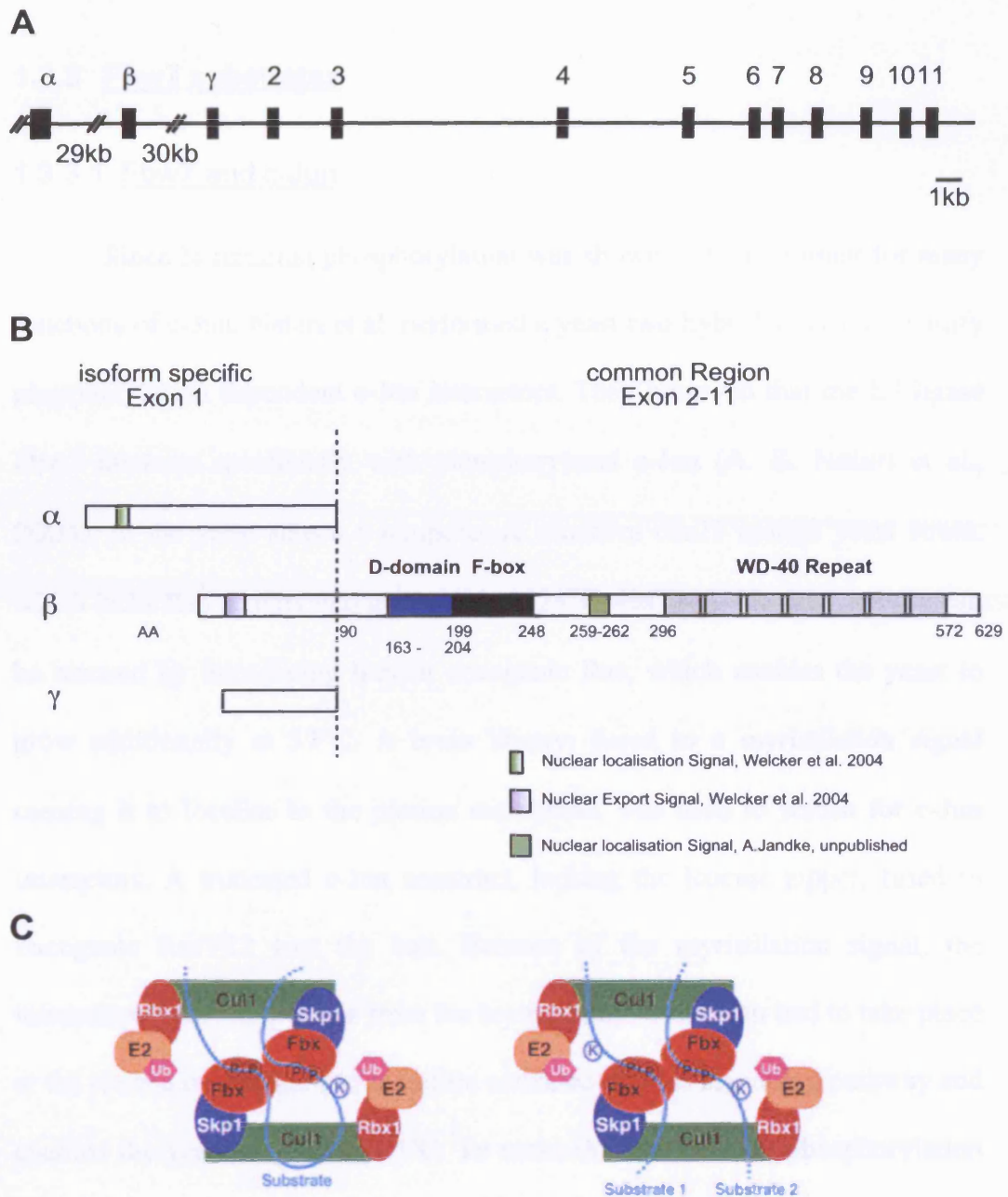
Figure 1.5 Genomic locus and domain structure and dimerisation of Fbw7. A) The *fbw7* gene is located on Chromosome 3 and has 3 isoforms that result from an alternative exon 1. Exon 2 to 11 are common to all 3 isoforms. Figure from Spruck et al., 2002 B) Domain structure of the Fbw7 protein. In addition to the F-box domain and the WD-40 propeller Nuclear Export Signals (NES) and Nuclear Localisation Signals (NLS) are located at the indicated locations. A dimerisation domain is located directly N-terminal to the F-box domain, Figure modified from Welcker & Clurman,2007 C) Models of substrate ubiquitinination by multiple SCF ligases. With either one substrate bound (left), or two substrates (right) it is feasible that the lysine residue for ubiquitination is better presented to the adjacent SCF complex than to the originally binding one (Figure from Hao et al., 2007)

1.3.3 **Fbw7 substrates**

1.3.3.1 Fbw7 and c-Jun

Since N-terminal phosphorylation was shown to be important for many functions of c-Jun, Nateri et al. performed a yeast two-hybrid screen to identify phosphorylation dependent c-Jun interactors. They observed that the E3-ligase Fbw7 interacts specifically with phosphorylated c-Jun (A. S. Nateri et al., 2004). In the yeast screen a temperature sensitive cdc25 mutant yeast strain, which lacks Ras activity and grows only at 25°C was used. The Ras activity can be rescued by introducing human oncogenic Ras, which enables the yeast to grow additionally at 37°C. A brain library, fused to a myristilation signal causing it to localise to the plasma membrane, was used to screen for c-Jun interactors. A truncated c-Jun construct, lacking the leucine zipper, fused to oncogenic RasV12 was the bait. Because of the myristilation signal, the interaction between proteins from the brain library with c-Jun had to take place at the plasma membrane and therefore activated the Ras signalling pathway and enabled the yeast to grow at 37°C. To make the screen c-Jun phosphorylation dependent, a constitutive active MKK7-JNK1 fusion construct under the control of the Met3 promoter, which caused reliable c-Jun phosphorylation in absence of Methionine, was employed. After identifying Fbw7 as an E3 ligase for phosphorylated c-Jun, the interaction was verified in an *in vitro* translation system where it was confirmed that Fbw7 and phosphorylated c-Jun co-immunoprecipitate. Using a peptide-binding assays Nateri et al. established that

the interaction requires the phosphorylation of c-Jun at its S63/S73 and T91/93

residues (A. S. Nateri et al., 2004). Therefore previous reports showing that

the N-terminal region of c-Jun is involved in its degradation were confirmed

(M. Treier et al., 1994).

More recently, another study also demonstrated the interaction between

Fbw7 and c-Jun (W. Wei et al., 2005). However, regarding the location of the

Fbw7 binding site on c-Jun both publications show conflicting data. Whereas in

the study by Nateri et al. Fbw7-β binds the same residues that are also

phosphorylated by JNK, namely Ser63 and Ser73, Wei et al. could not confirm

this interaction but showed that all Fbw7-isoforms recognise c-Jun

phosphorylated at Thr 239, which lies within a phospho-degron, a consensus

sequence for Fbw7 recognition (Figure 1.6C). They further elucidated that an

initial phosphorylation of Ser 243 is followed by GSK-3 mediated

phosphorylation of Thr239 and this generates the recognition site for Fbw7

(Figure 1.6A and C). Based on these data Wei et al. propose a model whereby

the Fbw7 binding site is generated by two sequential phosphorylation steps

whereby the second phosphorylation is mediated by GSK-3. This model is

similar to the one previously identified for the binding of Fbw7 to c-Myc (see

also 1.3.3.2). To support this model the authors present data for an inverse

correlation between the GSK-3 activity and c-Jun levels in various cell lines

and show that v-jun can escape Fbw7-mediated degradation because the

required priming phosphorylation site at S243 is mutated to phenylalanine.
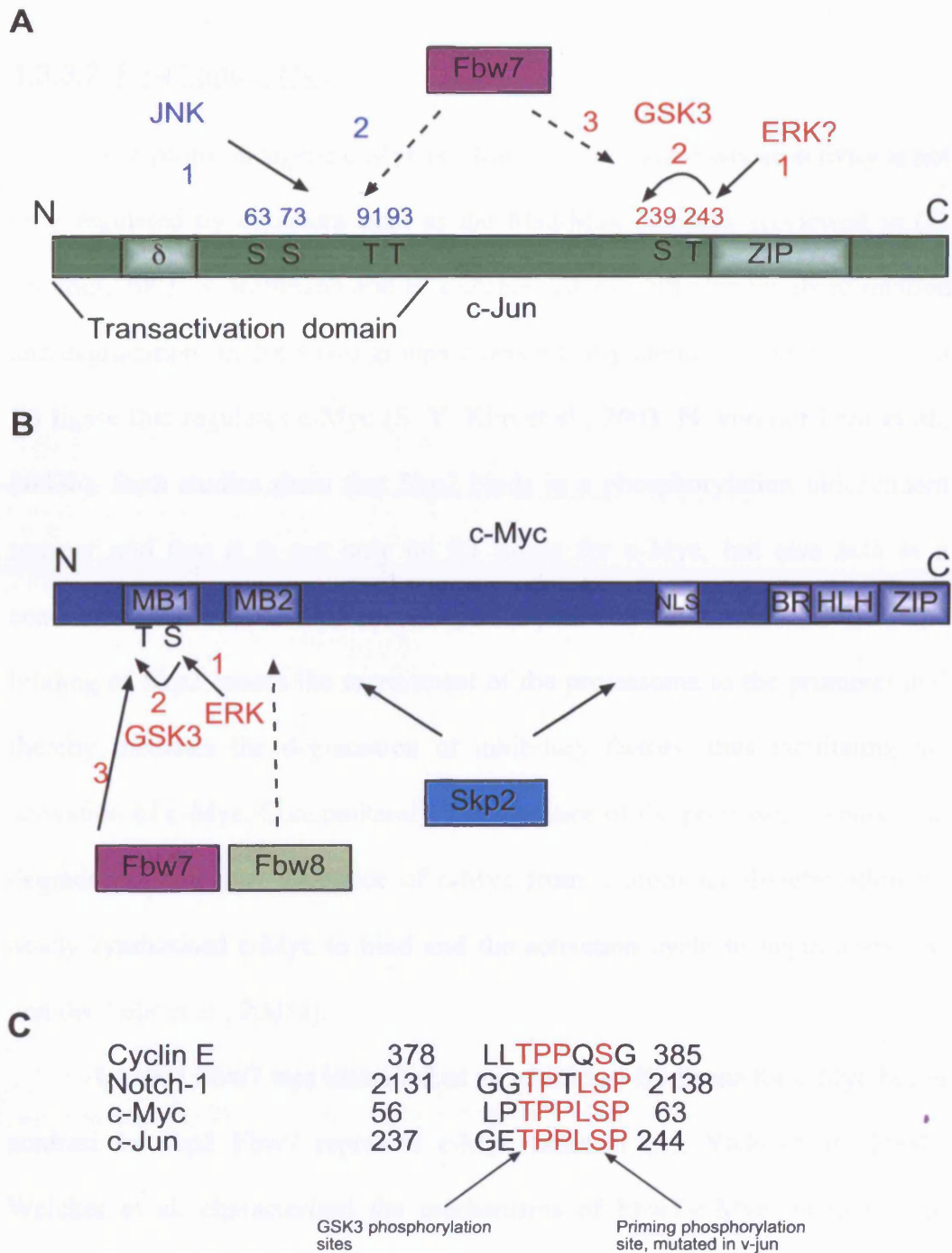
Figure 1.6 Fbw7 recognises a phospho-degron in c-Jun and c-Myc
A) Two different models (blue and red) are proposed for Fbw7:c-Jun interaction. Nateri et al. published that c-Jun is recognised at S63/S73 and T91/93 residues (blue). Wei et al (red) showed that Fbw7 binds in a C-terminal phosphodegron site, whereby S239 has to be phosphorylated by GSK3 after a priming phosphorylation of T243 by ERK. B) c-myc degradation is facilitated by three E3 ligases as indicated. Fbw7 requires a priming phosphorylation at S62 to allow GSK3 to phosphorylate T59 which is subsequently recognised by Fbw7. Skp2 acts in a phospho-independent manner. The role of Fbw8 is not clarified yet. C) Phospho-degron sites identified in Fbw7 substrates, Conserved residues are in red. Figure from Wei et al.,2005

1.3.3.2 Fbw7 and c-Myc

The proto-oncogene c-Myc is a transcription factor whose activity is not only regulated by cofactors such as the Mad/Max complex (reviewed in (B. Luscher, 2001; S. Rottmann and B. Luscher, 2006)), but also by ubiquitination and degradation. In 2003 two groups independently identified Skp2 as the first E3 ligase that regulates c-Myc (S. Y. Kim et al., 2003; N. von der Lehr et al., 2003b). Both studies show that Skp2 binds in a phosphorylation independent manner and that it is not only an E3 ligase for c-Myc, but also acts as a coactivator. This apparent discrepancy is explained with a model whereby the binding of Skp2 causes the recruitment of the proteasome to the promoter and thereby mediates the degradation of inhibitory factors, thus facilitating the activation of c-Myc. Concomitantly, the presence of the proteasome causes the degradation and thus clearance of c-Myc from a promoter thereby allowing newly synthesised c-Myc to bind and the activation cycle to begin anew (N. von der Lehr et al., 2003a).

In 2004 Fbw7 was identified as an additional E3 ligase for c-Myc but in contrast to Skp2 Fbw7 represses c-Myc function (M. Yada et al., 2004). Welcker et al. characterised the mechanisms of Fbw7-c-Myc interaction in more detail and identified a complex cascade of events leading to Fbw7 mediated c-Myc degradation (M. Welcker et al., 2004b). Using mutagenesis analysis of c-Myc and different truncated cDNAs for Fbw7, they demonstrated that GSK-3 mediated phosphorylation of c-Myc at residue T58 is required for Fbw7-mediated c-Myc turnover. However, a prerequisite for the

phosphorylation of T58 by GSK-3 is, that the S62 residue is already phosphorylated (Figure 1.6B). Interestingly the phosphorylation of S62 is mediated by the Ras/Mek/Erk pathway and was previously shown to stabilise c-Myc *in vivo* (R. Sears et al., 2000). Furthermore, S62 is also phosphorylated by JNK (K. Noguchi et al., 1999) and thus it appears that the initial phosphorylation is required for signalling pathways, whilst the second one is required to target c-Myc for degradation and thereby effectively switches the pathway off. Interestingly, Welcker et al. mention in their discussion of this study that the nervous system specific form of myc family members, N-myc, is also a substrate of Fbw7 although data for this are not shown (M. Welcker et al., 2004a).

1.3.3.3 Fbw7 and cyclin E

Cyclin E promotes G1/S transition in the cell cycle by binding to and activating the Cyclin dependent Kinase 2 (Cdk2) and cyclin E levels are tightly regulated on both the transcriptional level and the protein level during the cell cycle (H. Matsushime et al., 1994; T. Moroy and C. Geisen, 2004). Additionally different ubiquitination mechanisms ensure that cyclin E is expressed at appropriate time points in the cell cycle. Cul3, for instance, mediates the degradation of cyclin E when it is not bound to Cdk2, whilst cyclin E bound to Cdk2 is targeted for degradation by Fbw7 (J. D. Singer et al., 1999; H. Strohmaier et al., 2001; M. Welcker et al., 2003; J. D. McEvoy et al., 2007). Altogether four phosphorylation sites are essential for cyclin E degradation by Fbw7. They are T62, S372, T380 and T384 whereby the latter 2 are located within a phospho-degron sequence (Figure 1.6C). Also in case of cyclin E the second

phosphorylation step, at T380, is mediated by GSK-3 and is dependent on a priming phosphorylation of S384 a kinase, here Cdk-2. Activation of Cdk-2 therefore causes increased degradation and ubiquitination of cyclin-E as part of a regulatory feedback loop (M. Welcker et al., 2003).

Interestingly the Ras-MAPK pathway interferes with Fbw7 mediated degradation of cyclin E and overexpression of oncogenic Ras in rodent cells stabilised cyclin E levels (A. C. Minella et al., 2005). Surprisingly this report showed that there is no change in the phosphorylation status of the phospho-degron in cyclin E. However, this could be explained by the fact that the α and γ isoform can cooperate in the attachment of ubiquitins to cyclin E upon Pin1 mediated isomerisation of the initial Fbw7-α binding site (F. van Drogen et al., 2006). If Ras signalling would either directly or indirectly affect the function of Pin1, cyclin E could accumulate without alterations in its phosphorylation at the Fbw7 substrate recognition site. It was for example shown that Pin-1 cooperates with oncogenic Ras, binds to phosphorylated c-Jun and thereby increases its transcriptional activity towards the cyclinD1 promoter (G. M. Wulf et al., 2001). Thus the Pin-1 isomerase could act to stabilise Fbw7 substrates in the context of Ras signalling.

1.3.3.4 Fbw7, Notch and Presenilin

The Notch signalling pathway plays a crucial role during cell differentiation and development of the nervous and vascular system. Notch signalling and subsequent expression of Notch target genes is tightly regulated. Notch signalling is triggered by the binding of ligands such as Delta/Serrate/Lag to Notch. These ligands are present on the surface of a

neighbouring cell and bind to the extracellular domain of the full length Notch protein, which then leads to the sequential cleavage of Notch by several proteases. The result of this cascade is the release of the Notch intracellular domain (Notch-ICD). The Notch-ICD then translocates to the nucleus to activate Notch target genes. Presenilin is part of the γ-secretase complex that cleaves Notch to generate the Notch-ICD but is also involved in the cleavage of the amyloid precursor protein APP, a protein involved in AD (reviewed in (J. Shen and R. J. Kelleher, 3rd, 2007)). By mediating the degradation of Presenilin and the intracellular domains of Notch1 and Notch4, Fbw7 regulates the Notch pathway on two levels (G. Wu et al., 1998),(C. Oberg et al., 2001; J. Li et al., 2002). Firstly, it determines the abundance of an enzyme required for Notch cleavage. Secondly, Fbw7 mediates the degradation of the nuclear Notch-ICD and thereby antagonises the active signalling pathway.

Notch signalling is also a major determinant for cell fate decisions in the nervous system. It is involved in maintaining neuronal progenitor cells at the precursor stage and promotes an astrocytic cell fate in glial progenitor cells (reviewed in (A. Louvi and S. Artavanis-Tsakonas, 2006)). Thus deletion of Fbw7 could have severe effects on cell fate decisions and development. Since deletion of Fbw7 should lead to an accumulation of Presenilin, this would cause an increase in the Notch-ICD and increased target gene activation. Furthermore the ubiquitination of the Notch-ICD would be impaired. Therefore one would expect an upregulation of Notch signalling in Fbw7 knockout animals leading to a differentiation defect. Interestingly Notch4 was found to be upregulated in a tumour study using $fbw7^{+/-}$ mice in a $p53^{-/-}$ background, demonstrating that Fbw7 deletion causes an increase in the Notch-ICD (J. H. Mao et al., 2004).

Moreover the early embryonic lethality at E10.5 and vascularisation defects of $fbw7^{-/-}$ embryos were attributed to elevated Notch1 and Notch 4 levels (see also 1.3.6) as Notch signalling is also a major pathway in vascularisation processes (A. Karsan, 2005).

In addition to Fbw7, Notch can also be degraded by the RING E3 ligase Itch which recognises the N-terminal region of the Notch-ICD (L. Qiu et al., 2000). So far one model proposes that Itch mediates the degradation of the Notch-ICD in the cytoplasm whilst Fbw7 exerts its function in the nucleus (E. C. Lai, 2002). However, the detailed mechanisms of how these two E3s are orchestrated, have not been investigated.

1.3.3.5 Fbw7 and SREBP

The sterol regulatory element binding protein (SREBP) family of transcription factors is involved in regulating cholesterol and lipid metabolism. SREBPs have to be cleaved in a similar manner to Notch to become active and these active fragments can then exert their function on target genes before subsequently being degraded (M. T. Bengoechea-Alonso and J. Ericsson, 2007). In 2005 Sundqvist et al. demonstrated that SREBP1a, SREBP1c and SREBP2 are degraded by the Fbw7-α and Fbw7-γ isoforms (A. Sundqvist et al., 2005). As with the other Fbw7 substrates including c-Jun, c-Myc and cyclin E, the recognition of SREBP's by Fbw7 depends on GSK-3 mediate phosphorylation. Inhibition of SREBP phosphorylation prevents Fbw7 mediated degradation and siRNA mediated depletion of Fbw7 enhanced SREBP levels in U2OS cells. Thus these data add another substrate to the list of Fbw7-targets.

1.3.4 Fbw7 and Parkin

Parkin is a 52 kD RING E3, which is frequently mutated in autosomal-recessive juvenile Parkinsonism (AR-JP). Mutations in Parkin were found in all domains of the protein including the N-terminal Ubiquitin like domain (UBL), the C-terminal RING1 and RING2 domains and the In-Between-Ring domain (IBR) (reviewed in (I. F. Mata et al., 2004)). Parkin-substrates include α-synuclein, synphilin-1 (K. K. Chung et al., 2001) and PAEL-R (Y. Imai et al., 2001). α-synuclein is a protein found in Lewy-bodies, one hallmark of Parkinson's disease (PD) (M. G. Spillantini et al., 1997). Furthermore, mutations in α-synuclein are found in an autosomal-dominant form of PD (M. H. Polymeropoulos et al., 1997). In 2003 Staropoli and colleagues reported that Fbw7 interacts with Parkin and thereby enhances ubiquitination of cyclin E (J. F. Staropoli et al., 2003). They mapped the interaction between Parkin and Fbw7 to the Fbox domain of Fbw7 and the two RING domains of Parkin. An additional weaker interaction takes place between the UBL domain of Parkin and the WD-40 repeat region of Fbw7. Considering the binding domains identified, one would expect that Fbw7 and Parkin might degrade each other. However, even though Fbw7 mediates some ubiquitination of Parkin, the majority of the Fbw7-Parkin-complex regulates the degradation of cyclin E. The authors went on to investigate the function of Parkin in a neuronal model system and observed that Parkin protects postmitotic neurons (cerebellar granule cells as well as dopaminergic midbrain neurons) from kainate induced excitotoxicity. At the time of publication c-Jun and c-Myc had not been identified as a substrate for Fbw7, however, it would be interesting to test what

other substrates Fbw7-Parkin complex targets for ubiquitination. Given that c-Jun is upregulated in response to kainate administration it would be interesting to examine whether a Parkin-Fbw7 complex is able to antagonise the accumulation of phospho-c-Jun as well (A. Behrens et al., 1999).

1.3.5 Fbw7 in tumorigenesis

Since many substrates of Fbw7 are involved in cell cycle progression as well as tumorigenesis, it is not suprising that mutations of Fbw7 have been found in various cancers. In 2004 Reed et al. studied several cancer cell lines and tumours and found a correlation of loss of function mutations of Fbw7 and elevated cyclin E level (S. Ekholm-Reed et al., 2004). In this study 20% of the investigated endometrial tumours showed Fbw7 mutations and an accompanying loss of heterozygocity. Mutations in the α-isoform of Fbw7 correlated strongly with a misregulation of cyclin E whereas the Fbw7-β-isoform specific mutations did not. Misregulation in the context of this study meant not only elevated expression levels but also expression of cyclin E at non-appropriate timepoints during the cell cycle.

Another role of Fbw7 in tumorigenesis was elucidated in 2003 in a study by Kimura et al. (T. Kimura et al., 2003), who identified Fbw7-β as a transcriptional target gene of the tumour suppressor p53. In this study a microarray on a p53-mutated gliobastoma cell line was performed after wild-type (wt) p53 was transferred back into the cells. Here Fbw7 was found to be upregulated after p53 transfer. Furthermore electro-mobility shift assays identified a p53-binding site in exon 1 of the β-isoform. Accordingly, Fbw7-β expression is upregulated in a p53 dependent manner after UV and genotoxic

stress, whereas the induction of the Fbw7-α isoform is not dependent on p53 proficiency. Additional luciferase assays demonstrated that p53 could bind to the identified site and induce Fbw7-β expression. Based on these data a model was proposed, wherein the β-isoform is needed to maintain cells in a permanent cell cycle arrest and this would correlate with the observed high Fbw7-β expression levels in the brain.

In line with the above study a role for Fbw7 as a p53-dependent haplo-insufficient tumour suppressor was elucidated in 2004 (J. H. Mao et al., 2004). This study is based on the multiple-hit-theory for cancer. Using mice heterozygous for p53 ($p53^{+/-}$), which form tumours after a longer latency than $p53^{-/-}$ mice, the question arose whether there are any differences in the tumours of those two mouse strains. Using microsatellite markers to detect loss of heterozygocity (LOH) in these two groups of mice the authors found an extensive LOH on chromosome 3 in tumours from $p53^{+/-}$ mice. LOH on chromosome 3, which also harbours the fbw7 gene, was apparent in almost 100% of p53 heterozygous mice and this loss of one Fbw7 allele was sufficient to accelerate tumour development in the p53$^{+/-}$ background, but not in the p53$^{-/-}$ mice. Therefore these data suggest that loss of Fbw7 and/or other genes precedes the loss of wt p53 allele (J. Perez-Losada et al., 2005). In addition to the previously identified p53-binding site, this study identified further nine putative response elements in the Fbw7-α, four in the Fbw7-β and five in the Fbw7-γ promoter. However, the extent to which these putative response elements are indeed targets of p53-mediated regulation remains elusive.

The finding that Fbw7 expression can be used as a prognostic marker in tumour analysis and that expression of the β isoform is suppressed in gliomas further supported the role of Fbw7 as a tumour suppressor, (Z. Gu et al., 2007; M. Hagedorn et al., 2007).

1.3.6 The Fbw7 knockout mice

Based on the diverse nature of the Fbw7 substrates such as the oncogenes c-Jun and c-Myc, the cell cycle regulator cyclin E, and cell fate determining factor Notch, it was expected that a knockout of Fbw7 has detrimental effects on cell growth and differentiation and is incompatible with viability in a mouse model. In November 2004 Tetzlaff and colleagues demonstrated that deletion of Fbw7 causes embryonic lethality at E10.5 (M. T. Tetzlaff et al., 2004). A month later Tsunematsu et al. (R. Tsunematsu et al., 2004) came to the same conclusion. Both studies generated a germline knockout of Fbw7 but used different targeting strategies.

Tetzlaff et al. aimed to conditionally delete exon 5 and 6 by flanking them with two loxP sites and flank the neomycin cassette with Flp sites, altogether a very similar approach to the one presented in this thesis. However, the authors did not observe any Flp mediated deletion of the selection marker at ES cell level after electroporation of a Flp expression vector. As the Cre electroporation was more successful, they generated $fbw7^{+/-}$ mice, which developed normally and did not show any tumours for up to one year. Intercrosses of those animals were subsequently used to generate the $fbw7^{-/-}$ mice. However, the intercrosses did not produce any knockout offsprings and the time of embryonic lethality was determined to be E10.5. At E8.5 mutant

animals were indistinguishable from wt animals whereas at E9.5 mutants were smaller, developmentally delayed and neural tube closure was incomplete.

On the other hand, Tsunematsu et al. decided to generate Fbw7 knockout animals by replacing the first five exons with a neomycin cassette. Like Tetzlaff they found that knockout of Fbw7 is lethal at E10.5 and resulted in an incomplete closure of the neural tube. Interestingly the Fbw7 knockouts generated by both groups demonstrate similar, but not identical abnormalities in heart and vascular development.

Tetzlaff found that there were subtle delays in heart chamber maturation as well as defects in yolk sack vascularisation. Furthermore the embryos showed defects in vessel formation and had nucleated blood cells. Western blotting for the Notch intracellular domain and for Notch target genes showed that the Notch dependent transcripts of Hes1, Herp1 and Herp2 are more abundant in knockout animals. In addition the protein levels of the Notch1 and Notch4 ICDs were increased, which was also the case for cyclin E protein levels relative to the amount of mRNA. Therefore Tetzlaff et al. came to the conclusion that the defects in haematopoietic and vascular development cause the observed lethality.

Tsunematsu et al. performed a similar analysis of the $fbw7^{-/-}$ embryos, did not find any accumulation of the ICD of Notch1 or Notch3 but also observed accumulation of Notch4. The expression of the Notch target gene Hey1, was also enhanced. This led to the conclusion that elevated Notch4-ICD levels are responsible for the observed phenotype, which is supported by data on Notch4 transgenic mice, which show similar vascularisation defects (H. Uyttendaele et al., 2001). With regards to cyclin E as an Fbw7 substrate,

Tsunematsu et al. did not find changes in cyclin E protein levels or in its associated kinase Cdk2. However, in contrast to Tetzlaff et al., the relative protein levels in relation to mRNA amounts were not assessed.

Given that other targets of Fbw7, such as c-Jun and c-Myc, were identified in the same year as the Fbw7 knockout was published, neither of the groups investigated the effects of Fbw7 deletion in relation towards these substrates.

1.3.7 Summary

The studies on Fbw7, its substrates and interaction partners demonstrated that Fbw7 is involved in a great variety of cellular processes such as transcriptional regulation, cell cycle, neurodegeneration and tumourigenesis. Furthermore it became apparent that in many cases more than one E3 ligase is involved in targeting a substrate for degradation. However, it is still an open question how the interaction of the different E3s is orchestrated in the cell and to date no regulatory mechanism for Fbw7 or the orchestration of different E3s on c-Jun have been published.

Interestingly, Fbw7 only targets phosphorylated proteins for degradation and thus often mediates the termination of an active signalling cascade. A prerequisite for the recognition by Fbw7 is a GSK-3 phosphorylation of a serine residue often located in a so-called phospho-degron. This in turn requires an initial priming phosphorylation by another kinase such as JNK, ERK or Cdk2. Furthermore the involvement of Pin1-mediated isomerisation appears to be a common denominator in creating the recognition sites for Fbw7 binding and subsequent degradation.

It is also obvious from the literature that the α and γ isoform are similar in their nuclear localisation and have, at least a partially redundant function. Both are involved in the degradation of c-Myc, cyclin E and SREBP. Fbw7-β is not only localised differently and is less stable than the other isoforms, but is also the isoform that was found to act as a p53-dependent tumour suppressor (S. Ekholm-Reed et al., 2004) (J. H. Mao et al., 2004). Moreover the β-isoform is brain specific and its substrate, c-Jun, was shown to regulate neuronal apoptosis and axonal regeneration. Therefore to elucidate the role of Fbw7 and particularly Fbw7-β towards c-Jun, I generated various conditional Fbw7 knockout lines. As the conditional knockouts were directed to the nervous system, I will now give a brief introduction into neuronal development and the nervous system.

1.4 The mouse nervous system

1.4.1 Development of the nervous system

During the initial gastrulation the different germinal layers known as endoderm, mesoderm, and ectoderm are established. Neurulation is the next step in embryonic development and occurs around E8.5 in the mouse. Out of the three germinal layers, the ectoderm, and more precisely the neural plate, gives rise to the nervous system which is initiated by the formation of the neural tube (reviewed in (A. J. Copp et al., 2003)) Subsequently the three primary brain vesicles, the prosencephalon (forebrain), mesencephalon (midbrain) and rhombencephalon (hindbrain) are formed at the rostral end of the neural tube and subsequently give rise to all parts of the brain.

During the development of the brain, cells proliferate, differentiate and migrate, sometimes over long distances, to reach their final position. Over the last decades neuronal development and cell migration have been extensively studied. One of the most investigated brain regions with regards to neuronal development is the cerebral cortex. I will summarise some of the data concerning the cortical development in the following section, as this brain region is also affected in the Fbw7 conditional knockout lines presented in this thesis.

1.4.2 Neuronal differentiation in the cerebral cortex

After the primary brain vesicles have formed, the secondary vesicles of the forebrain, the telencephalon and the diencephalon, are generated (Figure 1.7A). The pallium gives rise to the cerebral cortex and the hippocampus and the formation of all brain regions relies on an orchestrated interaction of morphogenic clues, differentiation steps and migratory events. As a first step distinct anterior-posterior and dorsal-ventral domains are defined as the result of the coordinated expression of different morphogenic factors (reviewed in (S. W. Wilson and J. L. Rubenstein, 2000)). Finally, two different modes of cell migration lead to the cortical layering that is observed in the adult. One form of migration is the radial migration of cells from the inside towards the brain surface. The other mode of migration is the tangential migration, whereby cells migrate orthogonal to the radial direction (Figure 1.7B, green arrow). Both pathways are important during cortical development and were reviewed extensively (O. Marin and J. L. Rubenstein, 2001, 2003). Most of the cortical neurons that use γ-aminobutyric acid (GABA) as a neurotransmitter originate in

the telencephalon and reach the cortex via tangential migration where they then switch to a radial migration pattern. In contrast, cortical pyramidal neurons and some inhibitory neurons originate in the ventricular zone (VZ) and the subventricular zone (SVZ) of the cortex and move radially outwards (Figure 1.7B). Radial migration is largely, but not solely, dependent on glia cells (radial glia) that form a scaffold along which neurons are able to migrate during development. After the migration is finished radial glia cells become astrocytes. As corticogenesis takes place between E11 and E18 in the mouse embryo, the initial cortical structure, the so-called preplate, is split into the marginal zone, and subplate. The cortical layering then takes place in an inside out pattern (Figure 1.7C), whereby earlier born neurons lie deeper within the cortex and mainly originate from the VZ. The SVZ is involved in the generation of the outer cortical layers.

The importance of correct cortical layering is revealed in a number of mouse mutants but also in human diseases. In humans defects in the *lis1* and *doublecortin* genes result in a severely impaired cortical lamination and a disease called lissencephaly where patients are often mentally retarded (reviewed in (C. Lambert de Rouvroit and A. M. Goffinet, 2001)) Doublecortin interacts with the ubiquitin protease DFFRX which ubiquitinates it and is involved in regulating the localisation of doublecortin (G. Friocourt et al., 2005). One of the earliest models for cortical dysplasias in animals was the *reeler* mouse, which displays severe cortical and cerebellar lamination defects, resulting in an ataxic phenotype (G. D'Arcangelo et al., 1995). Polleux et al. later demonstrated that the rate of neurogenesis at early developmental stages is slower with a lower frequency of differentiating cell divisions in *reeler* mice.

However, at the end of corticogenesis neurons are generated at a higher rate and together these alterations ultimately lead to the observed aberrant cortical lamination (F. Polleux et al., 1998). Another molecule involved in neuronal migration is Cdk5 and in animals that lack Cdk5 the cortical inside out lamination is inverted and earlier born neurons are found superficial to later born neurons (E. C. Gilmore et al., 1998). One activator of Cdk5 is p35 and it was demonstrated that mice lacking p35 also display cortical lamination defects (T. Chae et al., 1997). Interestingly, p35 is regulated via the ubiquitin-proteasome-pathway and although the responsible E3 ligase has not been identified to date, it was shown that phosphorylated, activated p35 is ubiquitinated and degraded (G. N. Patrick et al., 1998). The cytoplasmic adaptor protein Dab1 which is involved in regulation of neuronal migration, is phosphorylated and degraded in response to reelin signalling and is then recognise by the E3 ligase component Cullin5 (L. Feng et al., 2007; G. Kerjan and J. G. Gleeson, 2007).

Together these studies demonstrate that defects in cortical lamination can arise at different stages of cortical development during the initiation or stop of migration but also during migration itself. A number of cytoskeletal associated proteins and signalling molecules are involved in neuronal migration and also the ubiquitin/proteasome system has recently emerged as a potential regulator of this process.
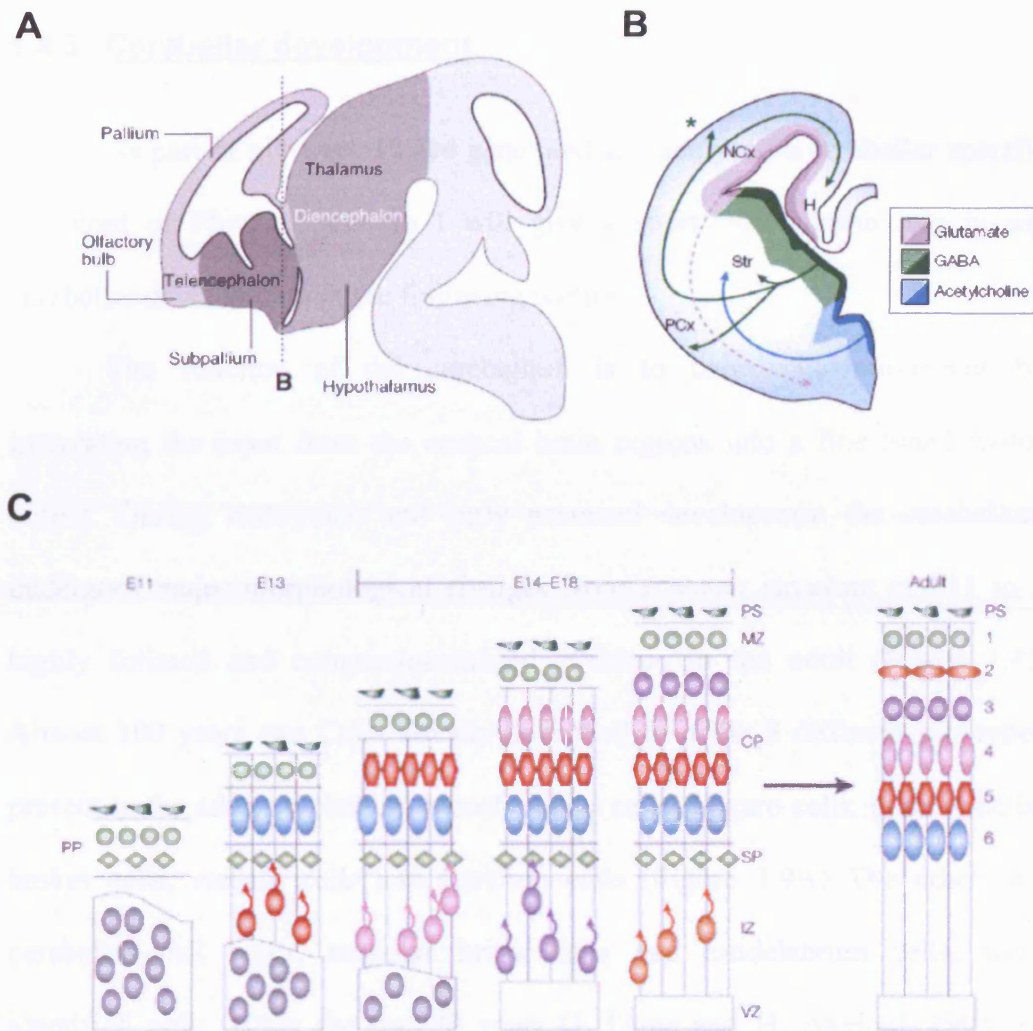
Figure 1.7 Anatomical organisation of the developing forebrain and cerebral cortex A) Anatomical organisation of the developing forebrain. Scheme of a sagittal section through the brain of an E12.5 mouse showing the main subdivisions of the forebrain, the diencephalon and the telencephalon. In the telencephalon, the pallium is depicted in lighter gray than the subpallium.Figure from Marin and Rubenstein, 2003. (B) Scheme of a transverse section through the telencephalon of an E12.5 mouse indicating the two migation modes, radial migration and tangential migration. Neurons that use different neurotransmitter originate in distinct brain regions and migrate over long distances.Depending on the neurotransmitter and other morphogenic clues they bypass brain regions (green arrow)or switch migration modes from tangential to radial (green askterisk) Figure from Marin and Rubenstein, 2001 C) Corticogenesis lasts from E11 to E18 in the mouse embryo. The early formed preplate (PP) is split by later generated neurons into the Marginal zone (MZ) and the subplate (SP). Neurons in the Cortical Plate (CP) are generated in an "inside-out" pattern whereby later generated neurons have to pass previously generated ones. In the adult cortex the different neurons are visible as layers 1 to 6. Figure from Gupta et al, 2002.

1.4.3 Cerebellar development

As part of my work I have generated and analysed a cerebellar specific knockout of Fbw7. Therefore I will give a short introduction into mouse cerebellar development in the following section.

The function of the cerebellum is to coordinate movement by integrating the input from the cortical brain regions into a fine tuned motor output. During embryonic and early postnatal development the cerebellum undergoes major morphological changes from a planar structure at E11 to a highly foliated and compartmentalised structure in the adult (Figure 1.8). Almost 100 years ago Cajal already described 6 of the 8 different cell types present in the adult cerebellum namely Golgi cells, Lugaro cells, granule cells, basket cells, stellate cells and Purkinje cells (Figure 1.9A) The other two cerebellar cell types, unipolar brush cells and candelabrum cells, were identified only within the last 20 years (J. Laine and H. Axelrad, 1994; E. Mugnaini and A. Floris, 1994). I will now focus on Purkinje cells and granule cells and the way information is relayed within the cerebellum.
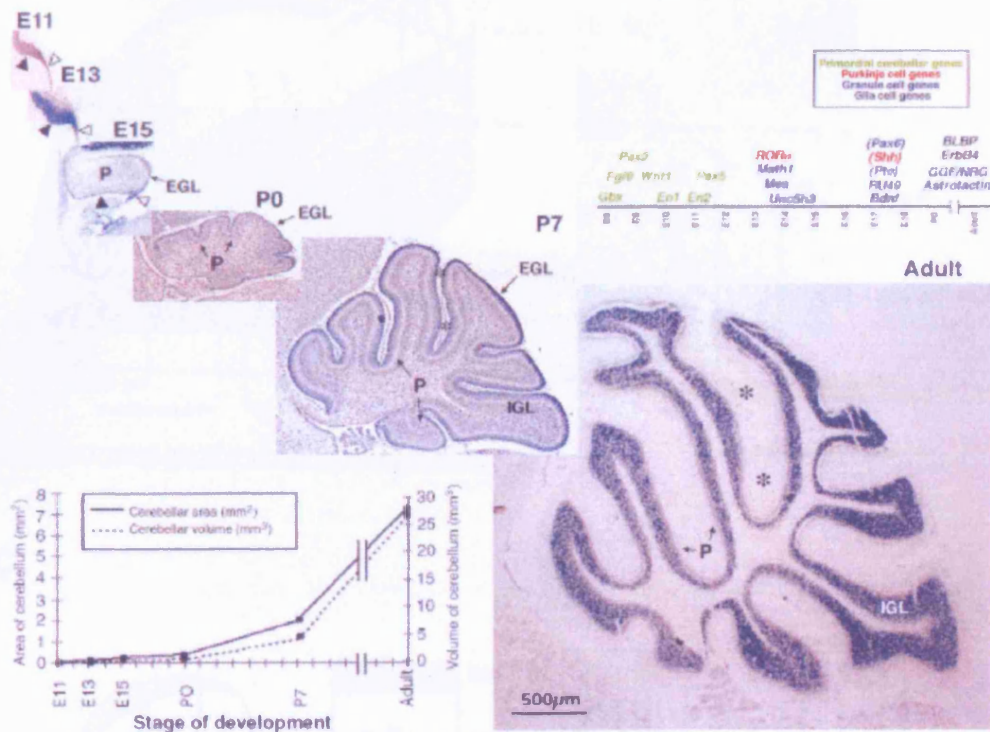
Figure 1.8 Structure and development of the cerebellum Sagittal sections of a mouse cerebellum from embryonic days E11, E13 and E15, P0 (day of birth),P7 and adulthood, are shown from left to right in the center of the figure to highlight the changes in size and complexity during development. In the photomicrographs, asterisks denote the primary fissure, P (with accompanying small arrows) points to the Purkinje cell layer, IGL: internal granule cell layer and EGL: external granular layer. In the three embryonic pictures, the filled arrowheads point to the ventricular neuroepithelium, and the unfilled arrowheads point to the germinal trigone. The scale bar for all photomicrographs is the same. The graph in the lower inset emphasizes the change in cerebellar size. The axis on the left shows the area of the sections that are pictured, the axis on the right provides estimates of the total cerebellar volume at these ages. The timeline in the upper right inset illustrates genes/loci, known to have relatively specific effects on cerebellar development when mutated. The position of genes along the timeline denotes the most likely point at which the effects of the mutant gene are manifested. Genes critical to the earliest stages of cerebellar development are shown in green. Those genes that are specific to granule cell, Purkinje cell, or radial glial cell development are shown in blue, red, or black, respectively, with genes in parentheses of presumed cellular localisation. Figure and legend from D. Goldowitz et al.,1998.
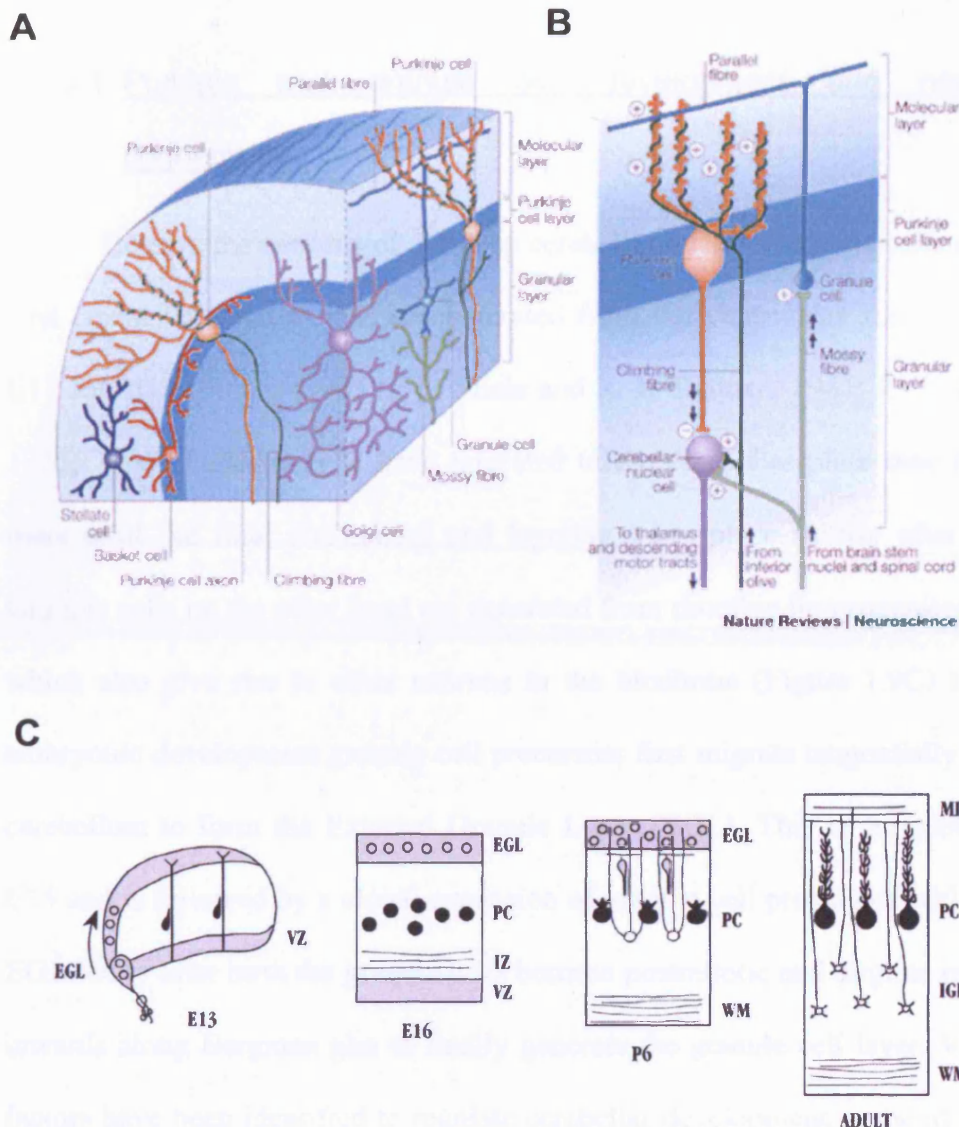
Figure 1.9 Cells, synaptic connections and migration in the cerebellum
A) Location and connection of the different cerebellar cells in the adult.
B) Synaptic circuits in the cerebellum. There are two main afferents to
the cerebellar cortex: climbing fibres and mossy fibres.The ascending
axons of the granule cells branch in the Molecular Layer (ML) to form
the parallel fibres, which make excitatory synaptic contacts with Purkinje
cells and ML interneurons i.e. stellate and basket cells. Figures A and
B from Apps and Garwicz, 2005 C) Migration in the cerebellum. At E13
(left), both of the principal neuron classes are specified. While Purkinje
cells (PCs) become postmitotic (filled circles) and migrate through the
wall of the cerebellar anlage, Granule cell precursors (unfilled circles)
migrate along the roof. In the perinatal period,P6, granule cells become
postmitotic and migrate inwards, along the Bergmann glia, to take their
position below the PCs. In the adult (right), the connections of the granule
neurons and thePCs are established. Granule cells extend parallel fibers,
which synapse on dendrites of the PCs. EGL, External germinal layer;
VZ,ventricular zone; WM, white matter; IZ, intermediate zone: IGL, internal
germinal layer. Figure from Hatten et al., 1999.

1.4.3.1 Purkinje and granule cell development and neuronal connectivity

Besides the neurons of the deep cerebellar nuclei, Purkinje cells are the first cerebellar neurons that are generated from the ventricular zone between E11 and E13 (Figure 1.9C) (I. L. Miale and R. L. Sidman, 1961; E. T. Pierce, 1975). Once Purkinje cells have migrated to the cerebellar plate they remain there until the final positioning and layering takes place shortly after birth. Granule cells on the other hand are generated from rhombic lip progenitor cells, which also give rise to other neurons in the hindbrain (Figure 1.9C) During embryonic development granule cell precursors first migrate tangentially in the cerebellum to form the External Granule Layer (EGL). This is completed by E15 and is followed by a clonal expansion of granule cell precursors within the EGL. Only after birth the granule cells become postmitotic and migrate radially inwards along Bergman glia to finally generate the granule cell layer. Various factors have been identified to regulate cerebellar development, some of which are depicted in the graph in Figure 1.8. Of these factors Sonic hedgehog (Shh) is secreted by Purkinje cells during cerebellar development and was shown to be required for granule cell precursor proliferation and Bergman glia differentiation (V. A. Wallace, 1999; P. M. Lewis et al., 2004). In line with these findings are the observations that loss of Purkinje cells results in a reduction of granule cells, which is for example the case in the *lurcher* mice (N. Dumesnil-Bousez and C. Sotelo, 1992). Also in the *staggerer* mice, Purkinje

cells degenerate, and this leads to an ataxic phenotype (R. L. Sidman et al., 1962; K. Herrup and R. J. Mullen, 1979).

One crucial step in relaying information in the cerebellum, as well as in other parts of the brain, is the formation of synaptic connections (Figure 1.9B) There are two major input pathways in the cerebellum known as the climbing fibres and the mossy fibres. Of those two only the climbing fibres make direct contact with the Purkinje cells with a 1:1 match, meaning one climbing fibre contacts only dendrites from one Purkinje cell. On the other hand the input of mossy fibres is relayed to Purkinje cells via granule cells by means of the so-called parallel fibres. As parallel fibres extend perpendicular to the plane of Purkinje cell dendrites and can extend over several millimetres of respective cerebellar folia, the input from one mossy fibre has an effect on multiple Purkinje cells (Figure 1.9B). Additionally other cells of the cerebellum such as stellate and basket cells synapse on parallel fibres to participate in the integration of input signals. Therefore all information is relayed onto Purkinje cells. Interestingly it was found that, with exception of the granule cells, all other cerebellar cortical neurons form inhibitory synapses with their targets, which in many cases are Purkinje cells. Furthermore, Purkinje cells are the sole cerebellar output neurons of this signalling cascade and project to the deep cerebellar nuclei. Therefore they are key players in cerebellar information processing and it is perhaps not surprising that mutant mice with Purkinje cell defects display the above-described severe phenotypes.

1.4.3.2 c-Jun in the cerebellum

S. Estus and J.Ham were the first to suggest that c-Jun is important in neuronal apoptosis based on *in vitro* experiments in which they used cultured sympathetic neurons (S. Estus et al., 1994) (J. Ham et al., 1995). They found that withdrawal of the trophic factor NGF from cultured rat superior cervical ganglia triggers the initiation of a cell death program, which includes the induction and phosphorylation of c-Jun. To assess whether c-Jun and other Jun family members are essential in mediating neuronal apoptosis Estus et al. microinjected purified antibodies against c-Jun, allowed the cells to recover and then either cultured them in the presence or absence of NGF for 40 hours. Subsequent fluorescent staining against rabbit IgG identified injected neurons and a Hoechst staining was used to score for chromatin integrity as either uniform, condensed or undetectable. Neurons deprived of NGF that were injected with antibodies against c-Jun but not JunB or JunD were largely protected from apoptosis and displayed normal chromatin whilst neurons in the presence of Control non-immune IgG underwent apoptosis and displayed a condensed or non-existent chromatin (S. Estus et al., 1994). At the same time Ham et al. demonstrated that the NGF withdrawal induced cell death in sympathetic neurons can be blocked by the microinjection of a dominant negative c-Jun expression vector, which lacks the N-terminal transactivation domain but is still able to dimerise and bind to DNA. Furthermore overexpression of c-Jun in this system is sufficient to induce cell death even in the presence of NGF (J. Ham et al., 1995).

In 1998 the role of c-Jun phosphorylation was confirmed in an *in vitro* culture model of rat cerebellar granule cells (cgc). Cultured cgcs are maintained under depolarising conditions (i.e. high K^+ levels) and lowering the potassium levels in the culture medium or serum withdrawal induces apoptosis (S. R. D'Mello et al., 1993). By using a phospho specific antibody for the c-Jun S63 residue Watson et al. observed in cgcs that phospho-c-Jun levels are elevated shortly after the reduction of K^+ levels in the culture medium and occur before c-Jun protein levels are increased and apoptotic alterations in the chromatin appear (A. Watson et al., 1998). Experiments using either a phosphorylation mimicking construct (*jun^{Asp}*) or phopshorylation deficient construct (*jun^{Ala}*) where the transactivation domain phosphorylation sites are mutated, confirmed that the death of cgcs upon either serum deprivation or low K^+ level is phospho-c-Jun dependent and that overexpression of the jun^{Asp} construct is sufficient to induce apoptosis under normal growth conditions (A. Watson et al., 1998).

At the same time the role of c-Jun in the cerebellum was elucidated *in vivo* in a detailed analysis of naturally occurring mouse mutants that display cerebellar defects such as the *weaver* and *Purkinje cell death (pcd)* mice (F. Gillardon et al., 1995; A. Migheli et al., 1997). In both mouse lines either granule cell precursors or Purkinje cells die during early postnatal development. Migheli and Gillardon observed that in both cases the dying cells express high levels of c-Jun, thus indicating that c-Jun also plays a role *in vivo* in the regulation of neuronal apoptosis in the cerebellum.

In addition to the role for c-Jun in neuronal apoptosis, it has also been reported that c-Jun is upregulated in regenerating neurons after injury (J. D. Leah et al., 1991). It was shown that deletion of c-Jun in the nervous system

leads to defects in axonal regeneration (G. Raivich et al., 2004). As Purkinje cells in the cerebellum were known not to possess regenerative capacities, Carulli et al. wanted to address the question whether overexpression of c-Jun *in vivo* under the Purkinje cell specific L7 promoter can induce Purkinje cell regeneration (D. Carulli et al., 2002). Overexpression of c-Jun does not affect the normal Purkinje cell development and is also not able to provide Purkinje cells with the ability to regenerate after injury, demonstrating that overexpression of c-Jun in Purkinje cells is not sufficient to trigger a regenerative program. However the Purkinje cell survival was reduced in the *in vitro* culture system of cerebellar slices derived from these *c-jun* transgenic animals, indicating that the effect of c-Jun is strongly dependent on the cellular and experimental context and that one has to be careful to draw conclusions from *in vitro* experiments about the *in vivo* effects and vice versa.

1.4.4 The nigrostriatal system

Since one of the mouse lines investigated in this thesis displayed behavioural defects that have been observed in neurodegenerative diseases such as Parkinson's disease (PD) and Huntington's disease (HD), I will give a short introduction into the nigrostriatal pathway and mouse models for both pathologies.

The nigrostriatal system is one of the different dopaminergic circuits in the brain (Figure 1.10A) and is involved in the regulation of voluntary movements. The loss of neurons in this particular pathway is the cause of PD and HD. The striatum is the crucial mediator of incoming cortical information and relays this information to neurons in the substantia nigra. Two different

pathways are used to achieve this relay and to subsequently generate a controlled motor movement (Figure 1.10B). The first pathway is the direct pathway from the cortex via the striatum to the medial globus pallidus and substantia nigra (blue arrow Figure 1.10B). The second pathway is the indirect pathway (Figure 1.10B red arrows) that links the striatum with the globus pallidus from which neurons extend to the subthalamic nucleus and finally subthalamic neurons connect to the substantia nigra and the medial globus pallidus (the same target areas as in the direct pathway) (reviewed in (C. J. Zeiss, 2005)).

Neurons from the ventral tegmental area (VTA), which lies medial to the substantia nigra (Figure 1.10A, right), also project to the striatum and pallidum. The VTA is part of the so-called ventral mesostriatal system, which is involved in the regulation of motivated reward related behaviour (reviewed in (S. J. Cragg, 2006)).

All neurons of the striatal system use a variety of neurotransmitters such as GABA, glutamate but some of them additionally use dopamine. Dopamine is synthesised from the amino acid tyrosine (Figure 1.10C) and in histological sections the presence of the enzyme tyrosine hydroxylase (TH) is used to identify dopaminergic neurons. Additionally, stainings for the glutamate decarboxylase 67kD isoform (GAD-67), an enzyme needed for the generation of the inhibitory neurotransmitter GABA, can be used to characterise neurons and projections in the striatum. Administration of the neurotoxic drug MPTP, for instance, causes an increase in GAD-67 levels in the striatum whilst L-Dopa treated PD patients display normal GAD-67 levels (M. T. Herrero et al., 1996).

Thus the analysis of TH and GAD-67 can give indications of whether the nigrostriatal pathway is lesioned or if neurons are degenerated or lost.

Degeneration and the subsequent loss of TH positive neurons in the substantia nigra pars compacta, which is part of the direct pathway, is the cause of PD. This loss leads to a decrease in dopamine levels and can be treated by the administration of the dopamine precursor L-Dopa. L-Dopa, in contrast to dopamine, is able to cross the blood-brain barrier and is converted into dopamine in the CNS (Figure 1.10C)(P. Huot and A. Parent, 2007). Concerning the genetic origin of PD, mutations in the Parkin RING E3 ligases itself as well as mutations in UCH-L1, an ubiquitin hydrolase associated with Parkin, and other genes have been identified (H. C. Ardley et al., 2004; I. F. Mata et al., 2004). To date there are four studies in which the authors have deleted Parkin with the aim to elucidate the role of Parkin in the pathogenesis of PD (for an extensive review see (S. M. Fleming et al., 2005)). Interestingly, no degeneration of dopaminergic neurons could be observed in the substantia nigra or striatum in all four of these mouse models (M. S. Goldberg et al., 2003; J. M. Itier et al., 2003; R. Von Coelln et al., 2004; F. A. Perez and R. D. Palmiter, 2005). Only one study reported a loss of TH positive neurons in the locus coeruleus (R. Von Coelln et al., 2004). Although some of the Parkin deficient mice display behavioural defects in form of a reduced startle response, alterations in their exploratory behaviour or in learning (J. M. Itier et al., 2003) (R. Von Coelln et al., 2004), no striking phenotype such as a tremor or ubiquitin positive inclusions, which are hallmarks of PD, were found in any of these studies. Although the loss of the Parkin E3 ligase alone was not sufficient to cause PD symptoms, it lead to alterations in dopamine and norepinephrine

levels. In all of these Parkin-knockout mouse studies the neurotransmitter levels, as determined by high performance liquid chromatography (HPLC), were changed. Itier et al. and Goldberg et al. observed that the levels of dopamine are increased in brains of Parkin deficient mice and von Coelln reported a reduction in norepinephrine levels due to the loss of TH positive neurons in the locus coeruleus. Norepinephrine as well as epinephrine are produced in chatecholaminergic neurons via the sequential action of different enzymes and can thus be also used as readout for the functionality of these neurons (Figure 1.10B).

Whilst dopaminergic neurons die in PD, the first neurons affected in HD are the medium spiny neurons in the striatum. In the striatum 95% of neurons are GABA-ergic medium spiny neurons and it appears that they are particularly sensitive to the presence of a polyglutamine segment. This polyglutamine segment is the result of a mutation of the *huntington* gene. In normal conditions 6-37 CAG repeats, which are translated into glutamines, are present near the 5' end of the gene. In case of HD this glutamine repeats are expanded to around 50 repeats and in severe cases to more that this (reviewed in (J. F. Gusella and M. E. MacDonald, 2000)). The overexpression of CAG repeats in mice results in a hindlimb clasping phenotype; a resting tremor and handling associated seizures and can therefore be used as a mouse model for HD (L. Mangiarini et al., 1996). Also in HD inclusions are formed. They are immunopositive for polyglutamine but also for ubiquitin, suggesting that the ubiquitin-proteasome system is important in this neurodegenerative disease as well (M. L. Maat-Schieman et al., 1999).
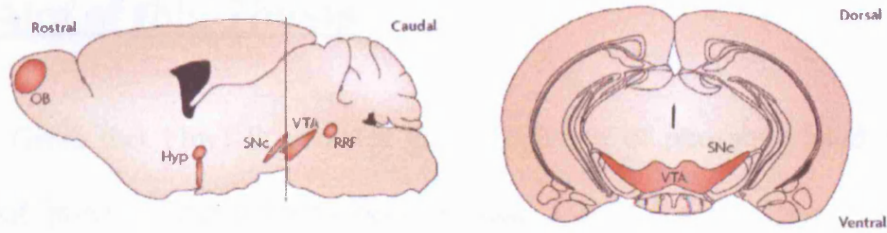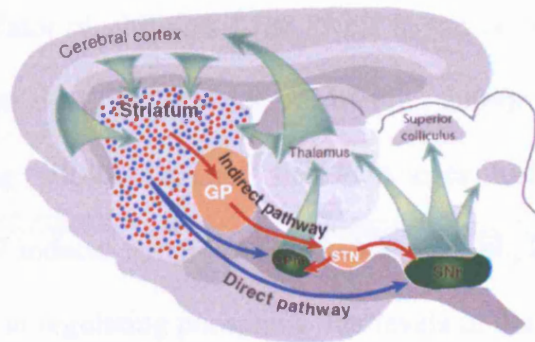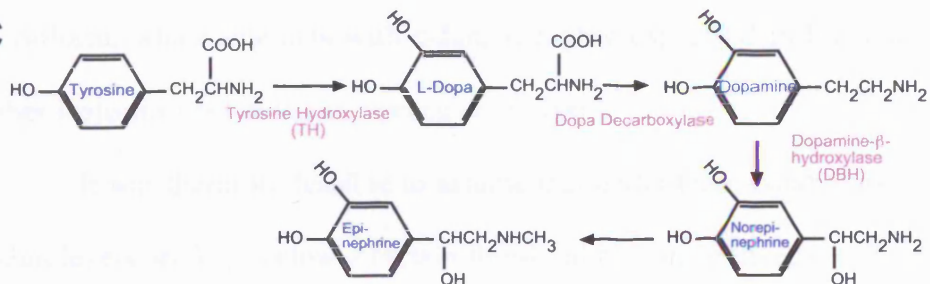
Figure 1.10 The nigrostriatal pathway A)Dopaminergic neurons in the mouse brain. left sagittal right: coronal section cut at the level indicated left. OB: olfactory bulb RRF: retrorubral field VTA:ventral tegmental area SN:substantia nigra Hy:hypothalamus Figure from Smidt and Burbach, 2007 B)There cerebral cortex and thalamus provide excitatory input (green arrows)to the striatum, the main nucleus of the basal ganglia. The output originates from the medial globus pallidus(GPm) and the substantia nigra pars reticulata(Snr) and is directed to the thalamic nuclei which project to the frontal areas of the cerebral cortex. The direct pathway (blue) originates from striatal projection neurons whose axon extend directly to the GPm and SNr output nuclei. The indirect pathway originates from striatopallidal neurons (red) whose axons terminate within the Globus pallidus(GP). Neuron in the GO project to the subthalamic nucleus (STN) which projects to the GPm and SNr. Thus striatopallidal neurons are connected indirectly through the GP and STN with the output neurons. Figure from Gerfen, 2006,C) Dopamine, Norepinephrine and Epinephrine are synthesises sequentially from the amino acid tyrosine by means of the indicated enzymes.

1.5 <u>Aim of this Thesis</u>

Given that Fbw7-β mediates the degradation of phosphorylated c-Jun and that previous publications demonstrated a role for phospho-c-Jun in neuronal apoptosis and axonal regeneration, we hypothesised that Fbw7 might act as a key regulator of phospho-c-Jun levels in the brain (A. Behrens et al., 1999; A. S. Nateri et al., 2004; G. Raivich et al., 2004). Additionally *in vitro* experiments using siRNAs against Fbw7 in cgcs had demonstrated that depletion of Fbw7 induces apoptosis (A. S. Nateri et al., 2004). The idea that Fbw7 is involved in regulating phospho-c-Jun levels in the nervous system was further supported by the fact that among the three different Fbw7 isoforms, the β isoform, which interacts with c-Jun, is highly expressed in brain whilst the other isoforms are not (C. H. Spruck et al., 2002).

It was therefore feasible to assume that under basal conditions phospho-c-Jun levels are kept below a certain threshold by constitutive, Fbw7 mediated, phospho-c-Jun degradation. We further hypothesised that upon an insult, such as stress or injury, phospho-c-Jun levels rise above this threshold and thereby trigger apoptosis in neurons. According to this model, Fbw7 would be a crucial regulator of JNK signalling during neuronal development and differentiation.

To test the threshold model that Fbw7 targets phospho-c-Jun for degradation in the nervous system, we decided to conditionally delete Fbw7 in the nervous system. If Fbw7 would indeed be a key regulator of phospho-c-Jun levels in the brain, a lack of Fbw7 should result in elevated levels of

phospho-c-Jun and possibly other Fbw7 substrates, as well as an increase in neuronal apoptosis.

To allow a temporal and spatial analysis of the role of Fbw7 in the nervous system we decided to generate various conditional knockout lines where Fbw7 is deleted in either different neuronal populations or at different timepoints during development. The obtained results should be further validated with regards to whether elevated c-Jun or phospho-c-Jun levels could be the cause of the phenotype. Therefore fbw7 conditional knockout mice should be crossed to floxed -c-jun mice (c-$jun^{f/f}$) that are available in the lab to obtain conditional double knockout animals. If the phenotype were c-Jun dependend, further crosses to mice homozygous for jun^{AA} allele, where N-terminal phosphorylation of c-Jun is no longer possible, would allow asking the question whether this effect is mediated via the phosphorylated form of c-Jun.

Taken together the overall aim of my thesis was to investigate the role of Fbw7 in the nervous system by generating condition Fbw7-knockout mice, with the focus on the role of Fbw7 in regulating phospho-c-Jun.

2 MATERIALS AND METHODS

2.1 Reagents

2.1.1 Chemicals and enzymes

Reagents were obtained from Amersham, BDH, BioRad, Calbiochem, Cell Signalling Technologies, Clontech, Fisher Scientific, Gibco, Invitrogen, Merck, Molecular Probes, New England Biolabs, Qiagen, Sigma Aldrich, Stratagene and GE-Healthcare. Distilled H_2O, PBS, 5M NaOH, 0.5M EDTA, LB medium, sterile glycerol were provided by Cancer Research UK Central Services.

2.1.2 Antibodies

All HRP-conjugated secondary antibodies used for western blotting were from Jackson laboratories. The secondary antibodies for immunohistochemistry were all from Vector laboratories: biotinylated goat and rabbit, biotinylated rabbit and rat, biotinylated horse and mouse. For immunofluorescence vector goat anti rabbit alexa 555 or 488 antibodies were used. The following primary antibodies were used. Dilutions are given for either use in Western blotting (WB) or immunohistochemistry (IHC). If antibodies were used for immunohistochemistry the antigen retrieval method is also indicated:

MW: microwaving, C: Citrate Buffer pH 6

T: trypsin

Table 2.1: Primary antibodies

Antigen	Antibody name	Source	Dilution & application
Actin	α–actin	Sigma Aldrich	1:2000 WB
Calbindin	α–Calbindin	Chemicon	1:400 IHC MW/C
c-Jun	c-Jun H79	Santa Cruz	1:500 WB 1:120 IHC MW/C
Fbw7	F7-3B7	Cancer Research UK	1:500 WB
GAD67	α–GAD 67	Sigma Aldrich	1:1000 IHC MW/C, 12'
GFAP	α–GFAP	Dako Cytomation	1:400 IHC MW/C
NeuN	α–NeuN	Chemicon	1:1000 IHC MW/C
Parvalbumin	α–Parvalbumin	Swant	1:1000 IHC MW/C
Tyrosin Hydroxylase	α–TH	Chemicon	1:500 IHC T
Vesicular glutamate transporter 1	α–Vglut1	Chemicon	1:1000 IHC MW/C

Antigen	Antibody name	Source	Dilution & application
Vesicular glutamate transporter 2	α–Vglut2	Chemicon	1:1000 IHC MW/C

2.1.3 Oligonucleotides

Oligonucleotides were obtained from Sigma Aldrich. The following primers were used.

Table 2.2 Primers for generation of conditional Fbw7 targeting construct.

Primer	Sequence
Fbx7F1(nt437)	5'-ctg cga ttg agg cat ttg agg gtg-3'
Fbx7F2(nt536)	5'-tac agc act tgg tcc agc ctc ctc-3'
Fbx7F3(nt 5935)	5'-cac tgc ttc atc cta gtc tcc ctg -3'
Fbx7R1(nt 4639)	5'-gca tat tct aga gga ggg tat cgg -3'
Fbx7R2 (nt 4751)	5'-tca ctg gac agc tgc cac tct agc-3'
Fbx7R3 (nt 8908)	5'-tgg tca tca tgc cct ttc agc acc -3'
Fbx7F4Bcl1(nt4428)	5'-actg tgatca ctt ttt aaa aat gac att gtc cca gaa g-3'
Fbx7R4Bcl1(nt6032)	5'-agtc tgatca tac ctg ttt aca aaa cag aag att ctc c-3'
Fbx7F5 (nt 4212)	5'-cat cat tca tac aat gat cct gaa ccc tc-3'
Fbx7R5 (nt 6169)	5'-cct cac tcg tca gtg ctc tct acc-3'
ScrFlrt1	5'- cg gtt gtt agt gaa gta ggt ctc -3'

Primer	Sequence
ScrFlrt2	5'- tg cta ctt cca ttt gtc acg tcc -3'
ScrFbx7-1 (nt 7635)	5'- at aca ggg act aca agc atg tgg -3'
ScrFbx7-2 (nt 7778)	5'- at cac aca ctg tct caa ctc acc-3'

Table 2.3 Primers for sequencing of knockout targeting construct

Primer	Sequence
SeqFe4(nt3247)	5'- ctg tcc atg gtt cca ctg ctc -3'
SeqRe4-1(nt 3530)	5'- gtt atg cac cca taa cca c -3'
SeqRe4-2(nt 3571)	5'- gtg tca acc ata atg agc agg -3'
SeqFe4 (nt 3247)	5'- ctg tcc atg gtt cca ctg ctc -3'
SeqFe5 (nt 5426)	5'- gtc cta gca aga tgc tca gcc -3'
SeqRe5 (nt 5735)	5'- cat cta ctc tca ctc aca gcc -3'
SeqFe6 (nt 7138)	5'- gtt cag tgc tgc aca gcc c -3'
SeqRe6 (nt 7475)	5'- gag tta cac tgc agc caa cac -3'

Table 2.4 Primers for genotyping of used mouse strains

Target site	Primer	Sequence
Cre	Cre 1	5'-cgg tcg atg caa cga gtg atg agg-3'
	Cre 2	5'-cca gag acg gaa atc cat cgc tcg-3'
Flp	Flp1	5'-cac tga tat tgt aag tag ttt gc-3'
	Flp2	5'-ctagtgcgaagtagtgatcagg-3'

Target site	Primer	Sequence
fbw7-loxP1	F7-PCR1	5'-cag tgg agt gaa gta caa ctc tgg-3'
	F7-R1	5'-gca tat tct aga gga ggg tat cgg -3'
	F7-Delta 2	5'-g gcc agc ctg gtc tgt ata gag -3'
	NeoS	5'-cctcgtgctttacggtatcgc-3'
fbw7-loxP2	Fbx7F3 (nt 5935)	5'-cac tgc ttc atc cta gtc tcc ctg -3'
	Fbx7R5 (nt 6169)	5'-cct cac tcg tca gtg ctc tct acc-3'
Floxed *c-jun*	LoxPCR5	5'-ctcataccagttcgcacaggcggc-3'
	LoxPCR6	5'-ccgctagcactcacgttggtaggc-3'

Table 2.5 Primers for RT-PCR

Target site	Primer name	Sequence
Fbw7-E2	F7-Fw 367	5'-cca tgt tca gca aca cca ac-3'
Fbw7-E7	Rev 925	5'-cggttgccaacaaaactgtag-3'
c-Jun	Jun Ol 14	5'-gccagcaactttcctgacc-3'
	Jun Ol 15	5'-ggttagcctgggctgtgcg-3'
GAPDH	GAPDH	5'-gcc cat cac cat ctt cc-3'
	GAPDH	5'-ggg atga tgt tct ggg cag c-3'

Table 2.6 Primers used for generation of in situ hybridisation probe

Probe	Primer	Sequence
Exon 2/5	F7-E2-BamH1-fw	5'-gga tcc gga cca tgg ttc tga agt tcg-3'
	F7-E5-EcoR1 rev	5'-gaa ttc tac att tct ctc tcc aga gaa ggt t-3'

Probe	Primer	Sequence
Exon4/5	F7-E5-BamH1 fw	5'-gga tcc cac tct atg tgc ttt cat tcc tg-3'
	F7-E5/2-EcoR1 rev	5'-gaa ttc cct ctt ctt tac att tct ctc tcc ag-3'

2.1.4 Bacterial strains

E. coli strain: *Application:*

DH5α   cloning

XL1-blue   cloning

Bacterial cultures were stored as 30 % glycerol stocks at -80 °C.

2.1.5 Plasmids

Plasmid	Source	Use
pcDNA 3.1+	Invitrogen	knockout construct
pDTA (Asp)	in house	knockout construct
pFlrt1	in house	knockout construct
pgem3Z	Invitrogen	In situ probe

2.1.6 Mouse Strains

Mouse line	Reference
Nestin-Cre	(F. Tronche et al., 1999)
Engrailed2-cre	(D. L. Zinyk et al., 1998)
Synapsin-cre	(C. Hoesche et al., 1993; Y. Zhu et al., 2001)
TH-cre	(D. M. Gelman et al.,

Mouse line	Reference
	2003)

2.2 Methods

2.2.1 DNA techniques

2.2.1.1 Long template PCR for amplification of the *fbw7* locus fragments

The PCR for the amplification of the genomic sequences for the Fbw7 knockout construct from isolated genomic DNA were performed using the Long-template-Expand-PCR kit (Amersham). The Polymerase therein is a mixture of the fast Taq polymerase and a slow proofreading Tgo-polymerase. Taq, which has no proofreading ability, tends to fall off the PCR template when it incorporates an incorrect base. In this case the proofreading Tgo polymerase can reinitiate at this position and correct the error (W. M. Barnes, 1994; S. Cheng et al., 1994). Therefore, by combining these two enzymes one gets quick amplification of long templates with the benefit of proofreading (B. Frey, Suppmann, B., 1995). For all PCRs Buffer 3, provided with the kit, was used. Final concentrations of reagents are listed in (Table 2.7). The two programs used for amplification of the long and short homology arm are listed below (Table 2.8,Table 2.9).

Table 2.7 PCR composition for long template amplification of genomic DNA

Reagent	Concentration of Stock	Final concentration
Buffer 3	10x	1x
dNTP	2.5mM	0.35mM
Primer 1	25mM	0.5mM
Primer 2	25mM	0.5mM
Polymerase	5 U/μl	1.5 U/μl
Template	50ng/μl	2.5ng/μl
H_2O		ad 20μl

Table 2.8 PCR program for amplification of genomic DNA between 0.5 and 3 kb

Temperature	Time	Additional number of cycles
94°C	2:00	
94°C	0:10	
57°C	0:30	30 cycles
68°C	2:00	
68°C	7:00	
4°C	for ever	

**Table 2.9 PCR program for amplification of genomic templates between 3
and 6 kb**

Temperature	Time	Additional number of cycles
94°C	2:00	
94°C	0:10	
63°C	0:30	30 cycles
68°C	4:00	
68°C	7:00	
4°C	for ever	

2.2.1.2 PCR for screening of ES cell clones for targeting

To screen the DNA from ES-cell clones for insertions of the knockout
construct a nested PCR was performed using the Qiagen Taq polymerase. The
primer pair ScrFbx7.2/ScrFlrt7.2 was used for the initial PCR from the isolated
ES-cell clones with 2μl of DNA. For the nested PCR the primer pair
ScrFbx7.1/ScrFlrt7.1. and 2μl of the initial PCR reaction were used (Table
2.11).

Table 2.10 PCR reaction for screening ES cell clones for gene target insertion

Reagent	Concentration of Stock	Final concentration
10x Buffer	10x	1x
dNTP	25mM	1mM
Primer 1	100µM	0.12µM
Primer 2	100µM	0.12µM
Polymerase	5 U/µl	0.5 U/µl
Template	50ng/µl	2.5ng/µl
H_2O		ad 20µl

Table 2.11 PCR program for screening ES cell clones and genotyping

Temperature	Time	Additional number of cycles
94°C	1:00	
94°C	1:00	
52°C	1:00	40 cycles
72°C	3:00	
72°C	10:00	
4°C	for ever	

2.2.1.3 Isolation of genomic DNA

Solutions: Proteinase K, Melford

        1x Tail Buffer :   50mM Tris HCl, pH 8.0

                              100mM EDTA, pH 8.0

                              100mM NaCl

                              1% SDS (w/v)

                              0.5 mg/ml ProK (added fresh)

        5M NaOH

        Isopropanol

Genomic DNA for genotyping of stock mice was either obtained from Ear- or tail biopsy samples. To detect Fbw7 deletion, samples of the respective organ were taken and processed in the same way. Samples were incubated overnight in 500µl tail buffer containing proteinase K at 56°C. The next day 200µl 5M NaOH was added and mixed thoroughly. The sample was spun down at 16000g for 10 min and the supernatant transferred to a new tube. To this 500µl isopropanol was added and mixed again. After 5 minutes of centrifugation at 16000g at room temperature the supernatant was discarded and the precipitated DNA left to dry. Finally the DNA was taken up in 300µl H_2O and left to dissolve for at least 1 hour on a shaker. 2µl were subsequently taken for the PCR reaction.

2.2.1.4 Genotyping

Genotyping was performed using primers flanking the loxP sites and at intermediate steps screening for insertion and deletion of the Neomycin cassette

(Figure 3.4). The PCR was carried out using the Qiagen Taq polymerase and PCR composition as described in Table 2.11. and primers as in Table 2.4.

2.2.1.5 Preparation of plasmid DNA

Plasmid purification on a small or large scale was performed with the Qiagen Mini or Maxi Prep kits, respectively. Bacteria were grown in 5 ml (Mini prep) or 250 ml (Maxi prep) cultures containing the appropriate selection antibiotic. Plasmid concentrations were determined as described in Chapter 2.2.1.6. In the case of cloning experiments, the plasmid insert was sequenced using insert or plasmid specific primers (2.2.1.8).

2.2.1.6 Quantification of DNA

DNA concentrations were quantified in a spectrophotometer at a wavelength of 260 nm after dilution in H_2O. An OD_{260} of 1 corresponds to 50 µg DNA/ml double stranded DNA. To assess the purity the absorbance ratio $OD_{260/280}$ was recorded additionally. It was usually between 1.6 and 1.8.

2.2.1.7 Restriction digest

Restriction digests were carried out in 20 µl reaction volumes containing 1 µg DNA, 5 units restriction enzyme (New England Biolabs), 2 µl 10x restriction buffer supplied with the enzyme and 1x BSA if required. Samples were incubated according to the manufacturers instructions for 1 hour to overnight, before the reaction was stopped by adding 5x sample buffer (Bromphenol blue in 50% glycerol, 1mM EDTA pH 8.0).

2.2.1.8 DNA sequencing

Fluorescent cycle sequencing was performed with the ABI dye terminator kit (Perkin Elmer). 3.2 pmol gene or vector specific primer were mixed with 500ng double stranded DNA, 8 μl ABI reaction mix and H_2O to a final volume of 20μl. Cycle sequencing conditions were as below (Table 2.12).

Table 2.12 PCR program for DNA sequencing

Temperature	Time	Additional number of cycles
96°C	2:00	
96°C	0:10	
50°C	0:05	25 cycles
60°C	4:00	
4°C	for ever	

To remove primers and dye terminators, samples were purified using ethanol precipitation of DNA. Capillary sequencing was performed on an Applied Biosystems 3730 DNA Analyser. Sequences were aligned with Sequence Navigator (ABI) using DNA strider software.

2.2.1.9 DNA agarose gel electrophoresis

Depending on the size of the DNA, 0.8 – 2% (w/v) agarose was dissolved in TAE buffer (Tris-HCl pH 8.0, 20 mM acetic acid, 1 mM EDTA). Ethidium bromide was added to a final concentration of 0.5 μg/ml. Samples were mixed with 5x sample buffer (Bromphenol blue in 50% glycerol, 1mM

EDTA pH 8.0) and separated in TAE depending on the gel size between 50 and

140 Volts constant.

2.2.1.10 Gel purification of DNA fragments

The desired DNA fragment was cut out from an agarose gel and the

DNA was isolated and purified from the gel slice with the GFX PCR DNA and

Gel Band Purification Kit (GE-Healthcare).

2.2.1.11 Ligation

Gel purified DNA fragments and vectors were mixed at a molar ratio of

approximately 5:1 and ligated with 400 Units of T4 DNA-ligase (New England

Biolabs) in a 20 µl reaction volume for either 1 hour at room temperature or

overnight at 16 °C. 5 µl of the ligation was then transformed using competent

bacteria (see also Chapter 2.2.1.12).

2.2.1.12 Bacterial transformation

A 50 µl aliquot of competent XL1-Blue cells was mixed with 5 µl

ligated DNA or 100 ng plasmid and incubated on ice for 30 minutes before

being heat shocked at 42°C for 45 seconds and left on ice for further 5 minutes.

450 µl LB medium was added and the reaction was incubated at 37°C for

1hour. 150- 200µl were spread on a LB plate containing the appropriate

antibiotic and incubated overnight at 37°C.

2.2.1.13   Southern blotting

For southern blotting the digested DNA was run on an agarose gel as described in 2.2.1.9. The DNA was depurinated by soaking the gel in 0.25N HCl for 15 minutes and the depurination was completed by rinsing the gel in dH$_2$O. The DNA was subsequently denatured by immersion of the gel in a solution of 1.5M NaCl and 0.5M NaOH for 25 minutes. For further neutralisation the gel was soaked in a solution containing 1.5M NaCl and 0.5M Tris-HCl (pH8.0) for 30 minutes. The DNA was transferred onto a Nitrocellulose membrane by capillary blotting over night using SSC (3M NaCl, 0.3M sodium citrate) as the transfer buffer and UV crosslinked using a Stratlink-crosslinker (Stratagene) onto the membrane at 700 for 30 seconds. To confirm the transfer from the agarose gel onto the membrane, the gel was stained with Ethidiumbromide after the transfer. The southern probe was radioactively labelled using the Stratagene Push column beta shield device and NucTrap probe purification column (Stratagene) according to the manufacturers instructions. For the probe hybridisation the Qick Hyb Hybridisation solution (Stratagene) was used to prehybridise the membrane for 15 minutes at 68°C. Boiling for 5 minutes denatured the labelled probe and it was left on ice for 3 minutes before it was added to the prehybridised blot. The hybridisation reactions was left for 1 hour at 68°C. After the hybridisation the membrane was washed twice for 15 minutes at room temperature with 2x SSC buffer containing 0.1% (w/v) SDS. A further wash was performed at 60°C with a 0.1x SSC buffer containing 0.1% (w/v) SDS. The signal was detected by exposing the membrane over the weekend at -80°C.

2.2.2 RNA techniques

2.2.2.1 RNA extraction using TRIzol

Solutions: TRI-Reagent (Sigma)

Chloroform

Ethanol

Tissue samples were extracted and immediately snap frozen in liquid nitrogen. For RNA extraction the sample was homogenized in an appropriate amount of TRI reagent usinge a 25G needle. The mixture was incubated at RT for 15-30 minutes to allow complete homogenization. 0.2ml Chloroform was added per ml of TRI reagent used. The mix was shaken vigorously and incubated for further 2-3 minutes at RT to allow separation of phases. Samples were then centrifuged for 15minutes at 4°C and the aqueous phase transferred to a new tube. To this 0.5ml isopropanol was added per ml of TRI reagent used and the mix was shaken vigorously incubated at 15 to 30 minutes at RT followed by a further centrifugation step at 4°C for 15minutes. Finally the RNA was washed twice with 70% (v/v)Ethanol, dissolved in H_2O and stored at -80°C for further use.

2.2.2.2 First Strand synthesis from RNA using SuperscriptIII

Reagents: SuperscriptIII Kit (Invitrogen)

RNA was isolated as described above (2.2.2.1) and used as a template for first strand synthesis. The composition of the RT mix is given in Table 2.11 and Table 2.14.

Table 2.13 Composition of Superscript III first strand synthesis RT-PCR reaction initial mix

Reagent	Final Concentration
RNA	5µg
Oligo dT primer	5µM
dNTP Mix	1mM
DEPC treated H$_2$O	to 10µl

The initial mix (Table 2.13) was incubated at 65°C for 5 minutes and placed on ice for one minute. Subsequently the final reagents were added as listed in Table (Table 2.14) and the PCR done according to table 2.15. After the final incubation on ice samples were spun down, 1µl Rnase H added and the samples incubated for further 20 minutes at 37°C to allow degradation of the initial mRNA template. The newly generated cDNA was stored at -20°C.

Table 2.14 Superscript RT PCR reaction mix

Reagent	Amount
10x RT buffer	2µl
25mM MgCl$_2$	4µl
0.1M DTT	2µl
RNAse OUT (40U/µl)	1µl
SuperScript III RT (200U/ml)	1µl

Table 2.15: PCR program for first strand synthesis using SuperscriptIII

Temperature	Time/minutes
50°C	50:00
85°C	5:00
4°C	for ever

2.2.2.3 In situ hybridisation

Probes for in situ hybridisation were generated using common DNA techniques described (2.2.1). The DNA for the probe was amplified from mouse-Fbw7-β cDNA using primers as in Table 2.6. The DNA was linearised and given to the Cancer Research UK in situ hybridisation service for labelling and incubation. Images were acquired using a darkfield microscope, Adobe Photoshop and the Q Capture imaging software plugin for photoshop.

2.2.3 Tissue culture techniques

2.2.3.1 Maintenance of mammalian cells

HEK293T cells (Invitrogen) were maintained in growth medium (DMEM supplemented with 10 % foetal calf serum, 4.8 mM glutamine and antibiotics (penicillin/streptomycin, Gibco). For the passaging the cells were washed once with PBS (137 mM NaCl, 3.35 mM KCl, 10 mM Na_2HPO_4, 1.84 mM KH_2PO_4, pH 7.2) and then incubated in 1x trypsin (Gibco) until the cells detached from the plate. Cells were then either seeded into a new flask (1:5 for maintenance) or seeded into dishes or plates at the desired cell density for the experimental procedure.

2.2.3.2 Transient transfection

Transient transfections in HEK293T cells were carried out with Lipofectamine 2000 (Invitrogen) according to the manufacturers instructions. Cells were then incubated in optimem in the presence of the reaction mix, containing plasmid DNA and Lipofectamine 2000. The reaction mix was prepared in polypropylene tubes. After 4 hours cells were washed with PBS and normal growth medium (DMEM with 10% fetal calf serum) was added back. The transfection efficiency was between 70 to 95% as judged by visual examination of GFP transfected cells under a tissue culture microscope equipped with a fluorescent unit (GFP filter set and a mercury lamp).

2.2.3.3 Storage and recovery of mammalian cells

For storage in liquid nitrogen HEK293A cells were trypsinised and spun at 200g for 5 minutes in swing bucket centrifuge (Heraeus). The cell pellet of one confluent T75 flask was resuspended in 3 ml growth medium, containing 20 % foetal calf serum and 10 % sterile DMSO. Cells were frozen at -80 °C in 1 ml aliquots in a Cryo-1°C-Freezing Container (Nalgene) filled with isopropanol to allow slow freezing (1°C/min). After a week, cells were transferred to liquid nitrogen for long-term storage. To recover cells, aliquots were rapidly thawed at 37 °C in a water bath and added to one T75 flask, containing 25 ml of growth medium. The medium was replaced the following day, after the cells had attached to the plastic.

2.2.4 Protein techniques

2.2.4.1 Protein quantification

Protein concentrations of samples were measured using the BioRad protein assay reagent. BSA standards and samples were diluted in 800 μl H_2O and incubated with 200μl protein assay reagent. The absorbance at $OD_{595}nm$ was measured and compared to the standard curve to calculate protein concentrations.

2.2.4.2 Preparation of cell lysates and SDS-PAGE

HEK293T cells were washed once with ice cold PBS, and then detached using a cell scraper. Cells were spun down for 3 min at 200g, and lysed on ice for 15 min in Cell Lysis Buffer (Cell Signalling) plus protease inhibitors (250 μM PMSF, 50 μg/ml chymostatin, 0.5 μg/ml leupeptin, 50 μg/ml antipain, 0.5 μg/ml pepstatin A, 0.1 mg/ml pefabloc). Nuclei and insoluble debris was removed from lysates by centrifugation in a microcentrifuge (10 min, 16000g, 4°C). Protein concentrations were determined (Chapter 2.2.4.1) and samples were mixed with 4x sample buffer and loaded onto an SDS gel.

2.2.4.3 Preparation of tissue lysates and SDS-PAGE

Organs were removed and stored in ice-cold PBS containing protease inhibitors. They were passed through a 70μm cell strainer using a plunger of a syringe and taken up in 1x Lysis buffer (Cell Signalling) and sonicated for 5 intervals of 10 seconds at 10 microns amplitude. After further 10 minutes on ice, cells were spun for 10 min at 4°C to remove the insoluble fraction. The

supernatant was transferred to a new tube, and the protein concentration determined (2.2.4.1)

2.2.4.4 SDS-polyacrylamide gel electrophoresis

Solutions:

APS (Ammoniumpersulphate) 10% (w/v) in water

TEMED (Sigma)

Acrylamide-Bisacrylamide Solution (Protran) 37.5: 1

Running Buffer: 50x, for 10 litre

     Glycine   1400g

              Tris   300g

              SDS   50g

Laemmli sample- buffer: 4x :

              4ml 10% SDS (w/v)

              1.6ml 1M Tris (pH 6.8)

              20% Glycerol (v/v)

              5% β-Mercaptoethanol (v/v)

              ad 10ml H_2O

              Bromphenol Blue

The stock solution is stored at -20°C without β-mercaptoethanol

Before loading, samples were boiled for 3 minutes. Equal amounts of protein were loaded per lane, and separated on either 8 % SDS-PAGE gels or 10 % SDS-PAGE gels using a 45mA current until the dye front reached the bottom of the gel. See below for composition of gels. Gel systems used were

either 1.5mm Cambridge electrophoresis mini gels or if stated NuPage-4%-12%

Bis-Tris pre-cast gels.

Table 2.16 Composition of SDS-PAGE running gel

Component	8% Gel	10% Gel
H_2O	18.5 ml	15.9 ml
30% acrylamide mix	10.7 ml	13.3 ml
1.5M Tris (pH 8.8)	10 ml	10 ml
10% SDS	0.4 ml	0.4 ml
10% APS	0.4 ml	0.4 ml
TEMED	0.024 ml	0.016 ml

Table 2.17 Composition of SDS PAGE stacking gel

Component	Volume
H_2O	6.8 ml
30% acrylamide mix	1.7 ml
1.5M Tris (pH 8.8)	1.25 ml
10% SDS	0.1 ml
10% APS	0.1 ml
TEMED	0.01 ml

2.2.4.5 Western blotting

Solutions:

Transfer buffer:	10x Stock
	390mM Tris
	480nM Glycine
	0.37% SDS
	ad 1 litre
Dilution to 1x in:	200ml Methanol
	100ml 10x Stock
	700ml H_2O
Blocking Buffer:	5% (w/v) Milk in TBST
TBST:	137mM NaCl
	10mM Tris,pH 7.4
	0.1% (v/v) Tween

For transfer of the separated proteins from the SDS-Page a semi-dry blotting chamber was used. Whatmann 3mm filter paper and the nitrocellulose membrane were cut to the size of the running gel. Both were equilibrated in transfer buffer prior to use. The transfer-sandwich is built from the anode to the cathode as follows: 3 slices of filter paper, nitrocellulose membrane, gel and three slices of filter paper. Possible air bubbles in the blotting sandwich were removed by rolling a pipette over the sandwich. The proteins were transferred at 0.8 mA/cm^2 for 1hr. Transfer and equal protein loading was tested with Ponceau S (Sigma-Aldrich) staining. Blots were blocked by incubating the

membrane in blocking buffer for 1 hour at room temperature or overnight at

4°C. Membranes were then incubated with the primary antibody in blocking

buffer for at least 1 hour at room temperature, after which they were washed 3x

in TBST and incubated with the secondary HRP-conjugated antibody (Jackson)

diluted 1:10000 in blocking buffer. Membranes were washed 3 x 10 minutes in

TBST incubated in enhanced chemiluminescence substrate (ECL, GE

Healthcare) and developed.

2.2.4.6 Immunohistochemistry on paraffin embedded tissues

Solution: 10% NBF:

10% Formalin

4g NaH_2PO_4

6.5g Na_2HPO_4

ad 1 litre

Tissues were dissected and fixed overnight at room temperature in 10%

NBF. On the following day the NBF was replaced with 70% (v/v) Ethanol. The

processing, embedding and antibody stainings were performed by the Cancer

Research UK Experimental Histopathology laboratory. Briefly, formalin fixed

paraffin embedded sections were de-waxed in xylene and dehydrated by

passage through a graded series of IMS washes ultimately into water. Sections

were microwaved in citrate buffer for 15 minutes and then transferred to PBS.

Slides were incubated in 1.6% hydrogen peroxide for 10 minutes. Normal goat

serum diluted to 10% in 1% BSA was used as a blocking step for 30 minutes.

Primary antibodies diluted in 1% BSA was added for 1-2 hours. Sections were

washed in PBS prior to applying secondary antibody for 45 minutes at room

temperature. Sections were washed in PBS and then incubated in ABC for 30 minutes prior to washing. DAB solution was applied for 2-5 minutes and development of the colour reaction was monitored microscopically. Slides were washed in PBS, stained with a light haematoxylin, dehydrated, cleared and then mounted. The antibody dilutions and antigen retrieval method is given in Table 2.1. Pictures were taken using an Axiovert upright microscope (Zeiss) with 2.5x, 20x, 40x and 100x objective. For the image acquisition and quantification of events and area measurements the axiovision software (Zeiss) was used.

The Experimental Histopathology Laboratory, CRUK, performed fluorescent staining of brain sections. For the imaging I used a Zeiss LSM 510 confocal microscope equipped with a Zeiss 40x, 1.4NA Differential Interference Contrast (DIC) Plan-Apochromat or Phase Contrast oil-immersion objective, controlled by Zeiss LSM 510 software. Images were collected using the 493nm line of an argon laser and the 543nm and 633nm lines of a helium-neon laser with 4x or 8x averaging.

2.3 Animal Techniques

2.3.1 Animal housing and husbandry

Animals were housed according to the UK guidlines for the animal health and welfare in the animal facilities of Cancer Research UK either in 44 Lincoln's Inn fields or Clare Hall facilities.

2.3.2 Animal culling

Unless stated otherwise animals were culled according to Schedule 1 of the Animal Scientific Procedures Act 1986 either by lethal injection with Euthanal, placement in a CO_2 chamber, or cervical dislocation. For preparation of cerebellar granule cells pups of 6-7 days of age were decapitated if needed.

2.3.3 BrdU injection

Solutions: 200mg/ml BrdU (Sigma Aldrich) in PBS

To investigate proliferation in the cerebellum, either the pups or the time mated pregnant females were injected intraperitoneal with BrdU at 100μg/g bodyweight and housed for 2 hours after injection. At the end of the 2 hour period animals were culled according to the home office guidelines (2.3.2) and brains were extracted. For birthdating experiments time mated pregnant females were BrdU injected at the indicated day of pregnancy with 100μg/g bodyweight. At indicated timepoints, pups were extracted culled and subject to immunohistochemistry studies.

2.3.4 Behavioural Tests

2.3.4.1 Pole Test

The pole test was performed according to Matsuura et al with slight modifications (K. Matsuura et al., 1997). Animals of two month of age were acclimatised to the pole one day before the test and tested on day two. The pole consists of a retort stand wrapped in duct tape to generate a rough surface. The half and bottom of the pole are marked for time measurements. The pole was

wiped with 70% (v/v) ethanol between animals. On acclimatisation day the animals were placed on top of the pole and allowed to walk down the pole 3 times without taking the time. At the bottom of the pole a thick layer of nesting material ensured that no mice were hurt in case they fall. On the test day animals were placed on top and the walk down the pole was monitored with a Digital camcorder (Sony). This was carried out in 3 consecutive runs. The time needed to walk down was subsequently stopped on the video recording. Behavioural abnormalities such as stopping and letting go of the pole were noted as well. The two best times (judges as continuous runs, no falls) were taken and averaged per animal.

2.3.4.2 Hanging wire test

2 month old animals were used for the hanging wire test. The experiment was performed over a two-day period leaving one day for acclimatising the animals to the experimental set-up and using day two for testing. Animals were placed on top of a wired cage lid and the lid was raised up and down 3 times to promote the animal to grip. Afterwards the cage lid was turned resulting in the animal hanging below the cage lid. The time until the animal either falls or climbs on top was measured. A cut off time of 30 seconds was chosen after which the cage was turned back to starting position if the animal did not let go or climb on top. A thick layer of nesting material was placed at the bottom to ensure no animal was hurt if it fell. After 3 times the animal was either valued "Hang" if the animal kept hanging over the 30 seconds or climbed on top 2 out of 3 times. Animals were counted as "Fall" if they let go 2 out of 3 times.

2.3.4.3 Gait analysis

To assess whether animals are ataxic a gait analysis was performed. Briefly, the animals' front paws were marked with orange non toxic ink and the back paws with purple non toxic ink. Animals were placed in a U-chanel layered with filter paper. As the mouse walks along, one can trace the footprints and measure stride length, distance of front paws and back paws thereby seeing whether the mouse is ataxic.

2.3.5 Statistical Analysis

The statistical analysis of data was performed using the Graphpad Prism software. If two groups of mice were compared, an unpaired two-tailed T-test was performed. When more than one group were compared, analysis of variance (Anova) was used with a Kruskal Wallis Post test. Unless otherwise stated the Data are presented as Mean+/-SD and p values are indicated as follows: $p < 0.05$: * , $p < 0.01$: **.

2.3.6 Quantification of neurons:

All neurons quantified were counted manually and comparable brain regions for each experiment were chosen. Do to the chosen brain regions and different stainings (HE, NeuN in different experiments different counting methods were used for the analysis. At least 3 animals were quantified per genotype, the numbers of animals are indicated as n in the respective chapters.

2.3.6.1 Purkinje cell quantification

The number of Purkinje cells was counted in mid-sagittal sections. The length of the Purkinje cell layer in the whole cerebellar section was measured using the Axiovision software (Carl Zeiss). The Purkinje cell density was obtained by dividing the number of Purkinje cells counted devided by the Purkinje cell layer length.

2.3.6.2 Quantification of neurons in E 18.5 brains

Comparable regions of interest (ROIs) with a fixed size in the cortical plate, intermediate zone and midbrain were chosen in sagittal sections as indicated in Fig 4.3. The neurons were counted manually in H&E stained sections taken at 20x and 10x magnification using the event count tool in the metamorph software (Molecular devices). To obtain comparable datasets, the neuron number counted was normalised to the fixed sized area as cells/mm^2.

2.3.6.3 Quantification of neurons in adult cortices of $fbw7^{\Delta pN}$ animals

Comparable Regions of interest (ROIs) of the different cortical layers were chosen in coronal sections of comparable regions as indicated in Fig 6.8. The neurons were quantified manually in NeuN stained sections taken at 20x magnification using the event count tool in the metamorph software (company). To obtain comparable datasets, the neuron number was normalised as cells/mm^2.

2.4 Supplementary material on DVD

2.4.1 Description of movies M1 and M2

$fbw7^{ApN}$ animals display a strong hindlimb tremor when allowed to grip a cage lid with their front paws. M1: control M2: $fbw7^{ApN}$

2.4.2 Description of movies M3 and M4

$fbw7^{ApN}$ animals display a caterpillar like walking pattern in the pole test and need longer to climb down the pole. M3: control M4: $fbw7^{ApN}$

3 GENERATION OF THE FBW7 CONDITIONAL KNOCKOUT MICE

3.1 Generation of the targeting construct for Fbw7 deletion

The Cre-loxP system is a widely used system to generate conditional knockout mice and it is based on the activity of the Cre recombinase towards so called loxP sites, which are partially palindromic 34bp sequences (reviewed in (U. Muller, 1999)). The recombinase will excise the region in between two loxP sites if they have the same orientation, or will invert the region between them if they are orientated opposite to each other. If the Cre expression is driven by a tissue specific promoter, a selective deletion can be achieve in the respective tissue and the severe defects of a germline knockout can be avoided (reviewed (C. Gaveriaux-Ruff and B. L. Kieffer, 2007)). To obtain mice that harbour an allele where a specific sequence, such as an exon, is flanked by two loxP sites ("floxed"), a targeting vector has to be cloned first. In general, this vector contains the genomic target sequence and two loxP sites, one 5' and one 3' of the targeting sequence. Additionally, two homology regions to the genomic sequence that surround the targeting sequence have to be present so that the construct can insert into the genome by homologous recombination. The floxed targeting construct will be transfected into ES cells where it should integrate into the genome. Therefore to select for the stable insertion and against random

integrants, a positive and negative selection marker have to be present in the targeting vector (reviewed (C. Gaveriaux-Ruff and B. L. Kieffer, 2007)).

For the *fbw7* targeting construct I flanked exon 5 by two loxP sites in the same orientation and inserted the homology arms on either side of it. Exon 5 was chosen because it encodes the major part of the F-box domain and is common to all isoforms (Figure 3.1A). As exon 5 spans 125 bases, the deletion causes a frameshift mutation and thus the resulting message should be be subjected to nonsense mediated decay and subsequently lead to the loss of the Fbw7 protein (reviewed in (M. W. Hentze and A. E. Kulozik, 1999)). A neomycin cassette was used as a positive selection marker and Frt sites that flanked the neomycine cassette allowed that it could be excised after the successful targeting. The negative selection marker was a Diphteria-toxin-α (DT-α) cassette, located outside of the homology arm. Therefore cells that have randomly integrated the whole targeting vector die due to the toxin expression, whereas cells that integrated the vector by homologous recombination will have lost the DT-α cassette and are viable (Figure 3.1B). The presence of loxP sites around the targeting region and Frt sites around selection marker allows the sequential crossing of mice to firstly obtain the floxed *fbw7$^{f/f}$* animals and subsequently to generate the tissue specific knockout of Fbw7 (Figure3.1 C).

The targeting construct for the floxed *fbw7* allele was generated using a four step cloning strategy (Figure 3.2). The single cloning steps are described below. For all cloning techniques such as digest, PCR and sequencing the methods described in Chapter 2.2.1 were used.
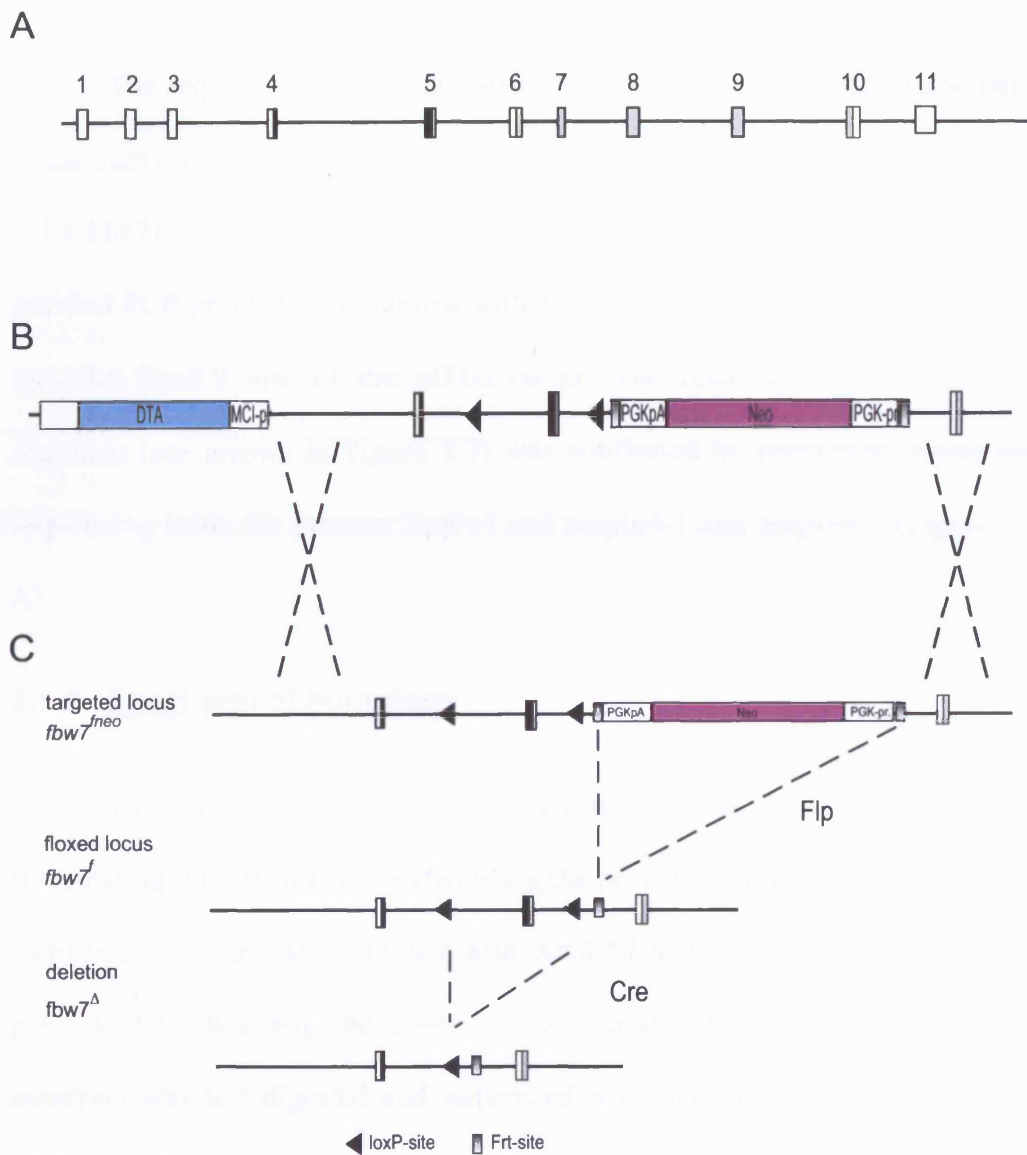
Figure 3.1 Targeting construct and strategy to obtain Fbw7 conditional knockout mice. A) genomic organisation of the *fbw7* locus. *fbw7* contains 11 exons (rectangles) whereby exon 5 encodes for the major part of the F-box domain (dark filled rectangles). B) targeting construct used to insert loxP sites around exon 5. Blue: DT-α-negative selection marker, pink: neomycin cassette as a positive selection marker. The DT-α cassette is lost upon homologous recombination indicated by the dashed crosses C) final crossing strategy after obtaining animals harbouring the targeted floxed allele of *fbw7* to generate conditional knockout mice.

3.1.1 Long arm of homology

The sequence for the long arm of homology, covering exon 4 and parts of the surrounding introns, was cloned from mouse genomic DNA using primer pairs Fbx7F1/Fbx7R1 in a long template PCR reaction (chapter 2.2.1.1). The purified PCR product was digested with ScaI and the resulting fragment cloned into the EcoRV site of the pDTα-vector. The relative orientation of the fragment (see arrows in Figure 3.2) was confirmed by restriction digest and sequencing using the primers SeqFe4 and SeqRe4-1 and SeqRe4-2 (Figure 3.2 A).

3.1.2 Short arm of homology

The short arm of homology, spanning exon 6 and parts of the surrounding introns, was generated using the primers Fbx7F3 and Fbx7R3. The amplified fragment was digested with XbaI/NheI and inserted into XbaI cut pcDNA 3.1+ whereby the NheI site was destroyed. The resulting fusion construct was test digested and sequenced with SeqFe6 and SeqRe6 primers (Figure 3.2B).

3.1.3 Insertion of two lox P sites around exon 5 of Fbw7

To flank exon 5 of *fbw7* with two lox P sites, two BclI sites were introduced by PCR on genomic wt DNA. For this purpose the primers Fbx7F4BclI and Fbx7R4BclI contained a BclI site each. The amplified fragment was cut with BclI and cloned into the pFlrt vector, which contains a

BamHI site in between two loxP sites that can be ligated to BclI cut ends. This ligation additionally destroys the BamHI site. The sequence was confirmed using primers SeqFe5 and SeqRe5 (Figure 3.2C).

3.1.4 Construction of the final targeting vector

The short arm of homology was excised from the initial pcDNA3.1 vector using a XhoI/KpnI digest and inserted into the pFlrt vector which already contained the region spanning exon 5 flanked by two loxP sites (3.1.3). The long arm of homology including the negative selection marker DTA was cloned via NotI/SalI into the pFlrt vector. The final outcome is a targeting vector that contains the positive and negative selection marker in one orientation and the region of interest, here exon5 flanked by loxP sites, in the other orientation (Figure 3.2D).

3.1.4.1 Linearisation of the final targeting vector

The targeting construct was linearised using NotI and purified using common DNA methods (chapter 2.2.1) and given to the Cancer Research UK transgenic services for the ES cell transfection.

Figure 3.2: Cloning strategy for the conditional Fbw7 knockout construct. Arrows below constructs indicate the relative orientation For a detailed description plese refer to: A) Chapter 3.1.1 B) Chapter 3.1.2 C) Chapter 3.1.3 D) Chapter 3.1.4
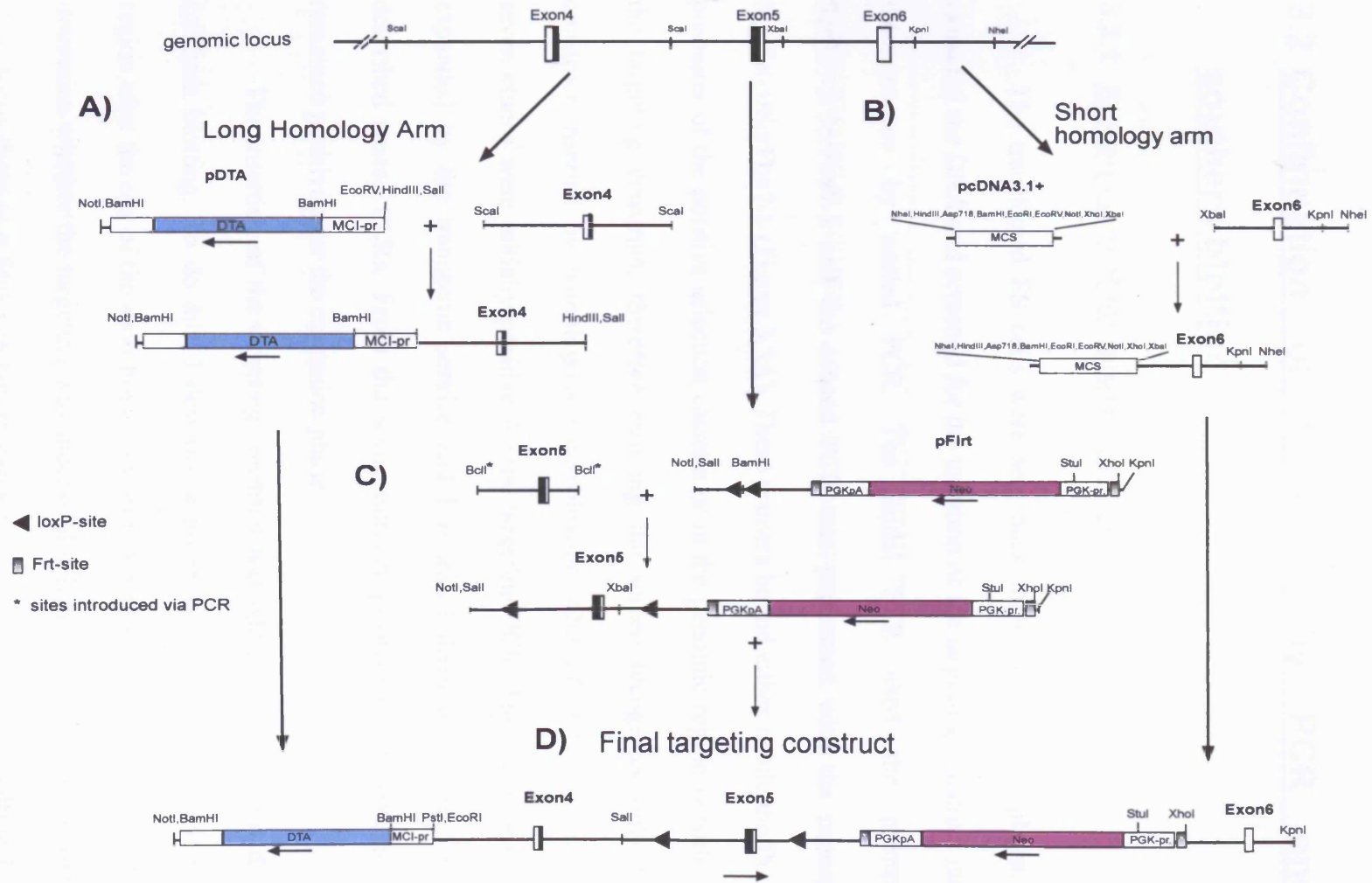
3.2 Confirmation of targeting by PCR and southern blotting

3.2.1 Screening PCR for target insertion in ES cells

The transfected ES cells were sent back to me in 96 well plates. I extracted the DNA and screened for the insertion of the targeting construct into the genome by nested PCR. The initial PCR used the primers ScrFlrt-2/ScrFbx7-2 and the second PCR was performed with the primers ScrFlrt-1/ScrFbx7-1 (Figure 3.3A). These primers bound either inside the PGK promoter of the positive selection cassette or in the genomic region outside of the targeting construct, therefore ensuring the screen recognises only the construct inserted by homologous recombination. Out of 864 transfections seven clones were initially positive for the targeting PCR. These clones were expanded by the transgenic service and I re-tested them using the above described nested PCRs. From the seven initially positive clones one clone remained positive after the expansion phase.

The insertion of the targeting construct was additionally confirmed by southern blotting. To do this, I designed a probe that binds in the genomic region after the end of the short homology arm. A StuI digest was performed to determine whether the targeting was successful (Figure 3.3A). In the genomic *fbw7* locus there is a StuI site before exon 4 and after exon 6, resulting in a 5735 bp fragment that is recognised by the probe upon digestion with StuI. Due to a StuI site present in the neomycin cassette, the probe detects a 2560 bp

fragment in the targeted *fbw7* locus. The southern blotting confirmed that the insertion of the targeting construct was successful (Figure 3.3B). The targeted ES cell clone was also used to establish the genotyping PCR. Using the primers F7-PCR1/F7R1 the amplification of the wt allele generates as expected a 287bp fragment whilst amplification of the floxed allele produces a 394 bp fragment (Figure 3.3C).This targeted ES cell clone was expanded and used for the injection into C57Bl/6 blastocyst (performed by the CRUK Transgenic services). A high level of coat colour contribution together with a bias to male chimeras (as the ES cell line is male) was indicative of an ES cell clone that contributes to the germline. After the expansion of the targeted mice by crossing them to Bl6, and removing the selection marker by breeding them with Flp-transgenic animals, *fbw7$^{f/f}$* mice were obtained.

3.2.2 Genotyping

The genotyping of the *fbw7* targeted and conditional knockout animals was performed using various primer combinations. For the genotyping of the targeted allele together with a deleted allele where the neomycine cassette was still present, a three primer PCR with primers F7-PCR1, F7-R1 and NeoS was (Figure 3.4A and C lane 1 and 3). The genotyping for mice derived from *fbw7$^{f/f}$* animals where the selection marker was excised, was performed using the primer combinations F7-PCR1, F7-R1 and Δ2 (red askterisks, Figure 3.4C). These three primers are able to detect the wildtype, floxed and deleted *fbw7* allele. An alternative genotyping PCR for the second loxP site was also established (Figure 3.4B). The size of the PCR fragments for the various possible alleles is given in Figure 3.4C.
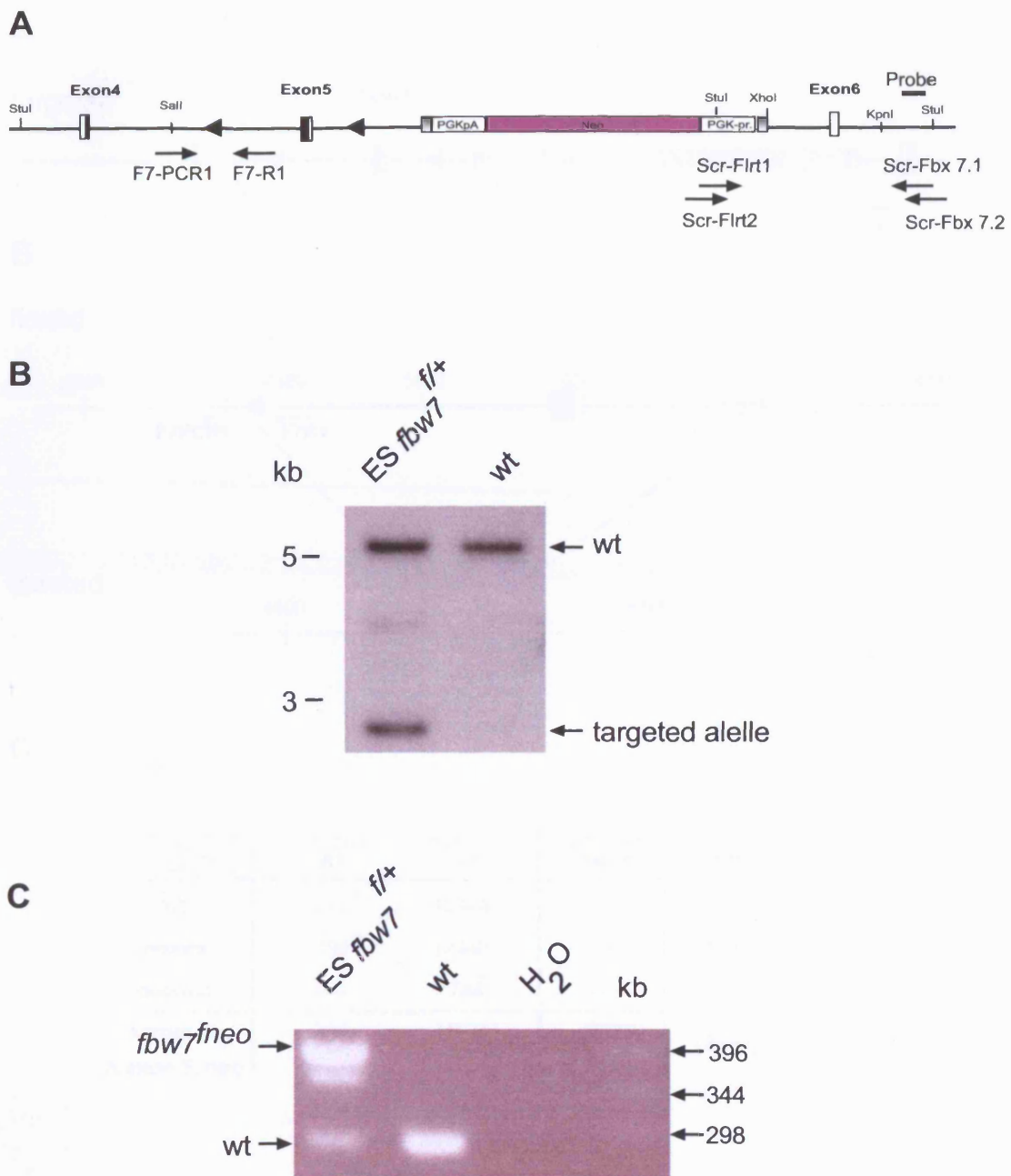
Figure 3.3. Southern blot, screening and genotyping PCR on the targeted _fbw7_^fneo^ allele A) Probe and primer design for southern blotting, screening and genotyping PCR. The genomic _fbw7_ locus contains a StuI site before exon 4 and after exon 6. These sites and an additional site within the neomycin selection cassette were used to confirm the targeting by performing a StuI digest. The probe detects a 2.6 kb band upon targeting and a 5 kB band in the wt _fbw7_ locus. Positions of primers used for the initial screening of ES cells are indicated. B) Southern blotting confirmed the targeting of the construct in the selected ES cell clone C) A PCR around the inserted 5' loxP site results in a 80 bp difference of the floxed versus wt PCR product. F7-PCR1 and F7-R1 primers are chosen within the intronic region around Exon 5 as indicated by the arrows in (A).
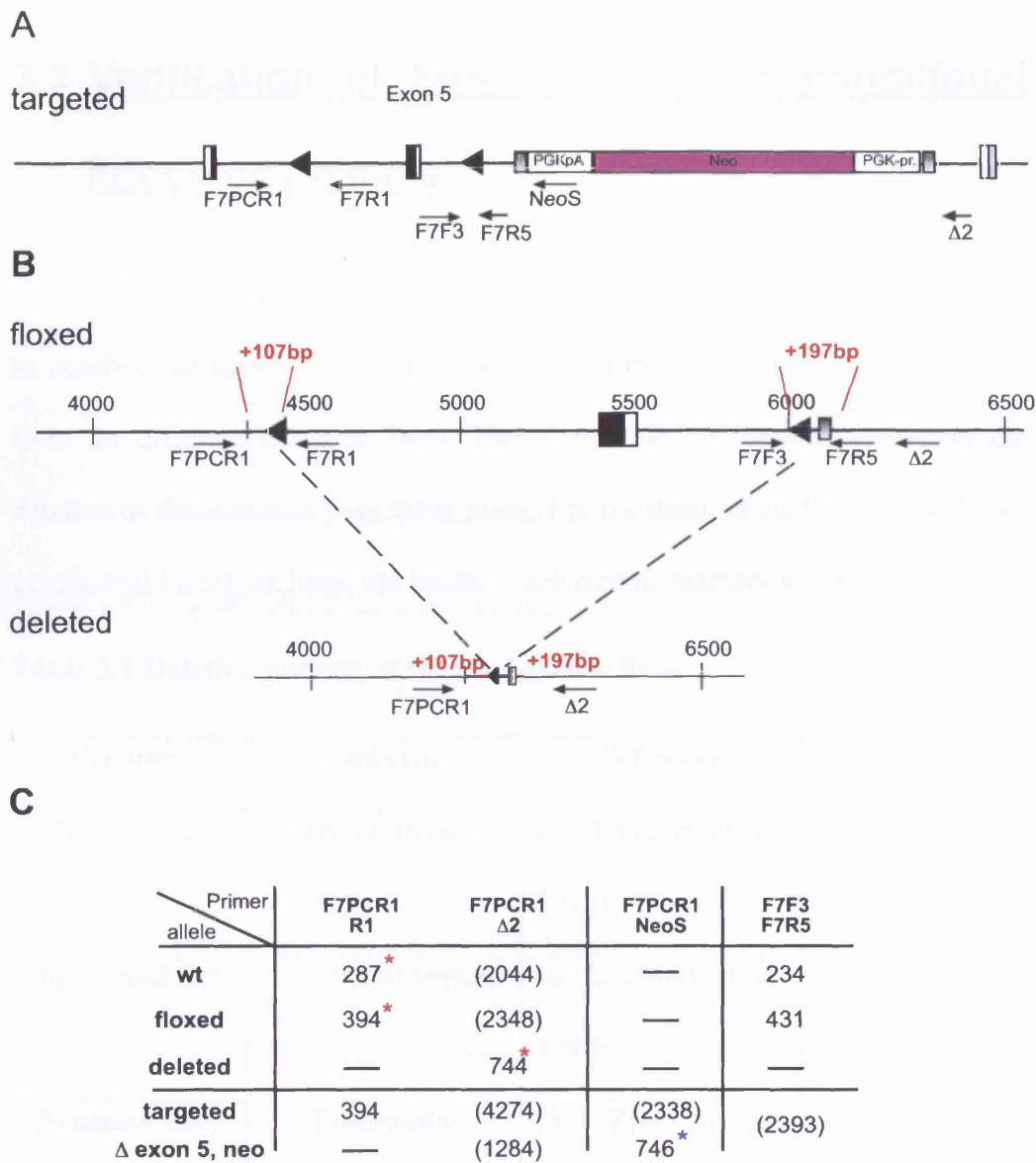
Figure 3.4 Genotyping primers for the targeted and deleted *fbw7* allele
A) Targeted *fbw7* locus containing the positive selection marker. Primer sites for genotyping are indicated B) Magnification of final floxed *fbw7* locus containing only exon 5 flanked by two loxP sites and the one remaining Flp site after excision of the positive selection marker. Annotations in red indicate additional bases that were inserted due to the cloning strategy.Numbers above the line indicated 500 bp distances on the genome and were used to locate the primer binding sites. C) Expected size of genotyping PCR bands using different primer combinations. Red askterisks indicate primers used for routine genotyping. The blue askterisk indicates primers used for genotyping *fbw7*$^\Delta$ allele that still contained the neomycine cassette.PCR products in brackets indicate that PCRs were not performed because the product would be very long for a conventional PCR.

3.3 <u>Verification of Fbw7 deletion in conditional knockout animals</u>

The first step in the analysis of the conditional *fbw7* knockout mice, was to confirm the knockout. To do this, I used various approaches and samples from the different knockout lines. Therefore table 3.1 summarises where the deletion in these mouse lines takes place. For the detailed analysis of the Fbw7 conditional knockout lines, the reader is referred to chapters 4 to 6.

Table 3.1 Deletion pattern of the used mouse lines

Cre line	Deletion	Reference	Chapter
Nestin Cre	Neural lineage	(F. Tronche et al., 1999)	4
Engrailed-2 Cre	Cerebellar vermis	(D. L. Zinyk et al., 1998)	5
Synapsin Cre	Postmitotic neurons	(Y. Zhu et al., 2001)	6

3.3.1 <u>Confirmation of Fbw7 deletion by RT-PCR</u>

To investigate to what degree deletion can be obtained on the message level, I used $fbw7^{\Delta Cb}$:c-$jun^{\Delta Cb}$ animals where *fbw7* and *c-jun* should be deleted in the cerebellar vermis but not the lateral sides (for a detailed description of this mouse line see chapter 5.). I extracted RNA from both parts of the

cerebellum and performed a reverse transcriptase PCR reaction using primers

binding in exon 2 and 7 of *fbw7*, primers for *c-jun*, which is only transcribed

from a single exon, *gapd* was used as a control (Primers are listed in Table 2.5).

The RT-PCR on wt fbw7 message should yield a 558 bp fragment. As I

anticipated that the exon 5-deleted message is subjected to nonsense-mediated

decay, I did not expect to detect an exon 5 deleted PCR product of 433bp. For

the lateral side I obtained the wt 558bp PCR fragment, however, I could also

detect a 433bp fragment in the vermis of the $fbw7^{\Delta Cb}$:c-$jun^{\Delta Cb}$ knockout

animals, suggesting that the deleted fbw7 message at least partially escapes

nonsense mediated decay. To verify that this smaller band is indeed *fbw7*

message, I purified the PCR band from the gel and sequenced it with the same

primers that I used to amplify it. The alignment to the wt sequence shows that

upon Cre expression exon 5 is deleted as expected (Figure 3.5B). Therefore the

message continues into exon 6, where two stop codons are present in a row

(green circle in Figure 3.5C). Thus the remaining message cannot be translated

into a functional protein since the F-box domain is missing and the WD-40

repeat region not present. If this truncated message would be stable and

translated, one could expect that three truncated proteins are generated, all

consisting of the first exon for each isoform and the common sequence up to

the stop codon. The predicted size for those proteins would be 20 kD (γ), 25 kD

(β) and 33 kD (α). However, this could not be verified as none of the available

antibodies are able to detect the endogenous protein (see 3.3.4 and discussion).

In case of the *c-jun* RT-PCR, I could detect a strong band in the lateral

part of the cerebellum and only a very weak band in the medial part, indicating

that c-jun was efficiently deleted (Figure 3.5A). The residual signal can

potentially be caused by contamination of the tissue preparation with non-deleted cells or by contamination of the RNA preparation with DNA. Since the *c-jun* genomic organisation does not contain introns, even small DNA contaminations are likely to be amplified.
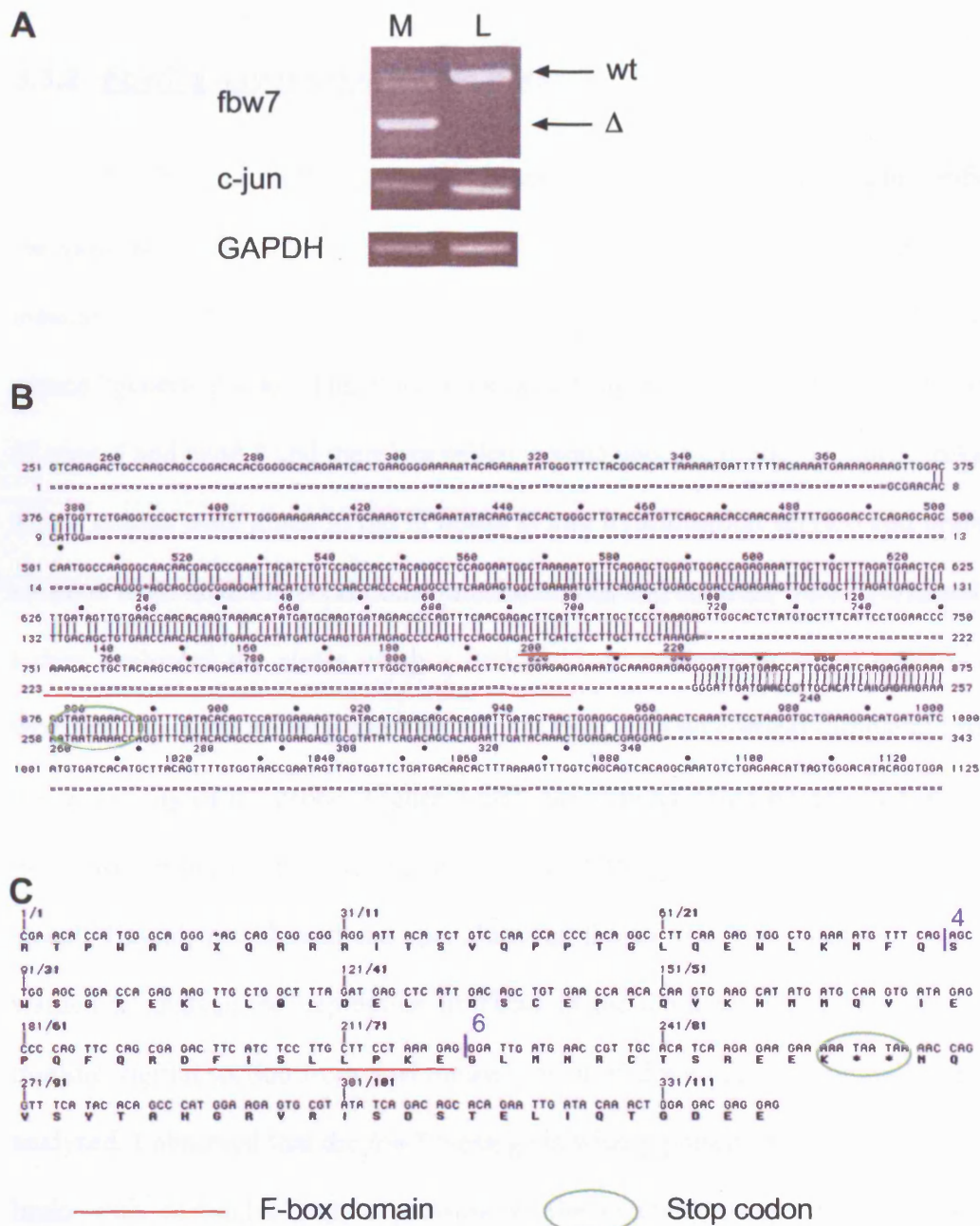
Fig 3.5 RT-PCR to confirm deletion of exon 5 of Fbw7 in the vermis of *fbw7*$^{\Delta Cb}$*cjun*$^{\Delta Cb}$ mice. A) Medial (M) and Lateral (L) samples of the cerebellar cortex were taken. RNA was extracted and RT-PCRs were performed for *fbw7*, *c-jun*, *gapdh* was used as control. The lower *fbw7* band in the medial sample and the band from the lateral part were excised and sequenced with the same PCR primers as used for amplification. B) Sequence alignment of the deletion PCR product to wt cDNA. Exon 5, which encodes for the major part of the F-box domain (red underlined) is deleted. C) Translation of obtained sequencing of the Δ band. The deletion of exon 5 causes a frameshift upon transition to exon 6 and a stop codon (green circle).

3.3.2 Fbw7 expression in the wt brain

To characterise the expression pattern of Fbw7 in wt brain and to verify the various knockout lines, I cloned *in situ* hybridisation probes for the *fbw7* message. One probe was designed to cover the sequence from exon 2 to 5, and named "generic probe". The other probe was designed to span only a small part of exon 4 and exon 5 and therefore called "exon5 specific probe" (Figure 3.6A). These probes were given to the in house *in situ* hybridisation service and brain sections from different conditional knockout lines and controls were hybridised. I then evaluated the slides using a dark-field microscope. A sense construct spanning the bases as the generic probe was used on a wt cortical sample to test the specificity of the probe (Figure 3.6B). No staining could be detected using the sense probe, confirming the specificity of the signal obtained antisense-signal. Having established the specificity of the *in situ* hybridisation, I first wanted to analyse the expression of Fbw7 in the adult wt brain. Therefore a midline sagittal section from a wt mouse was probed with the generic probe and analysed. I observed that the *fbw7* message is widely present in the adult mouse brain with particular high expression in the cerebral cortex, hippocampus, dentate gyrus and in some nuclei such as the pons and the inferior olive whilst in other regions such as the thalamus hardly any signal can be detected (Figure 3.7, Figure 3.10). Fbw7 is also expressed in the cerebellar granule cell layer, which is discussed below in more detail. The exon 5 specific probe gave a slightly weaker but otherwise identical signal as the generic probe on wt brains (data not shown).

A

B

sense   anti-sense
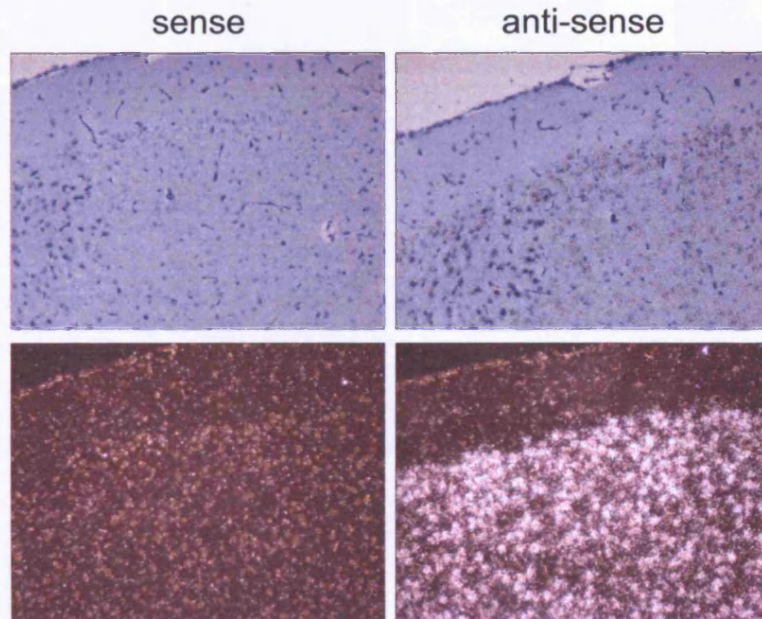
Figure 3.6 Design and validation of Fbw7 in situ hybridisation probes.
A) Partial cDNA sequence of the mouse Fbw7-β isoform with annotated
exon boundaries. The sequence of the generic *fbw7* in situ hybridisation
probe covers exons 2 to 5 and the exon 5 specific probe extends from
exon 4 to 5. All exons from exon 2 onwards are common to all three Fbw7
isoforms (see also Fig 1.5) B) A wt mouse cerebral cortex probed either
with the sense negative control or the antisense probe. No signal was
detected in the sense sample (which covers the same sequence as the
generic probe) whereas the antisense sample gave a signal in the cortex
indicating that probe binds specifically.
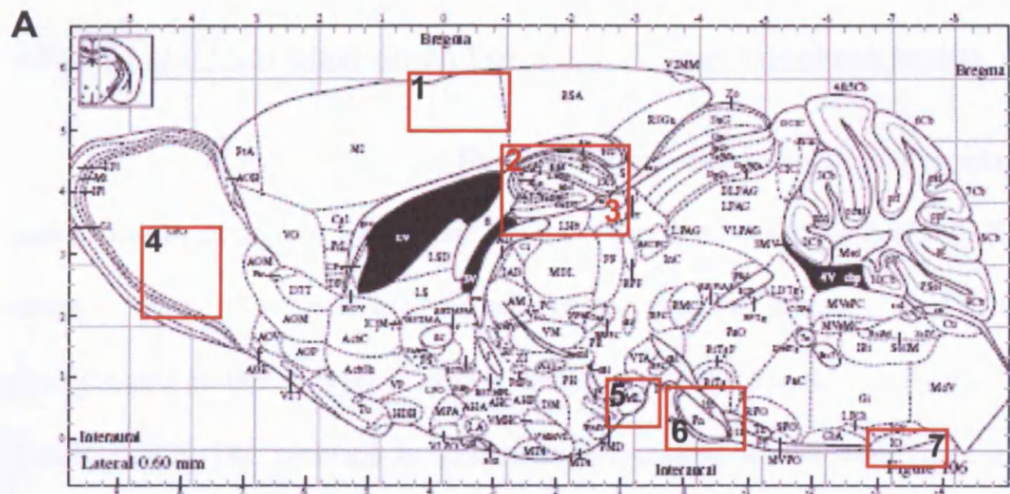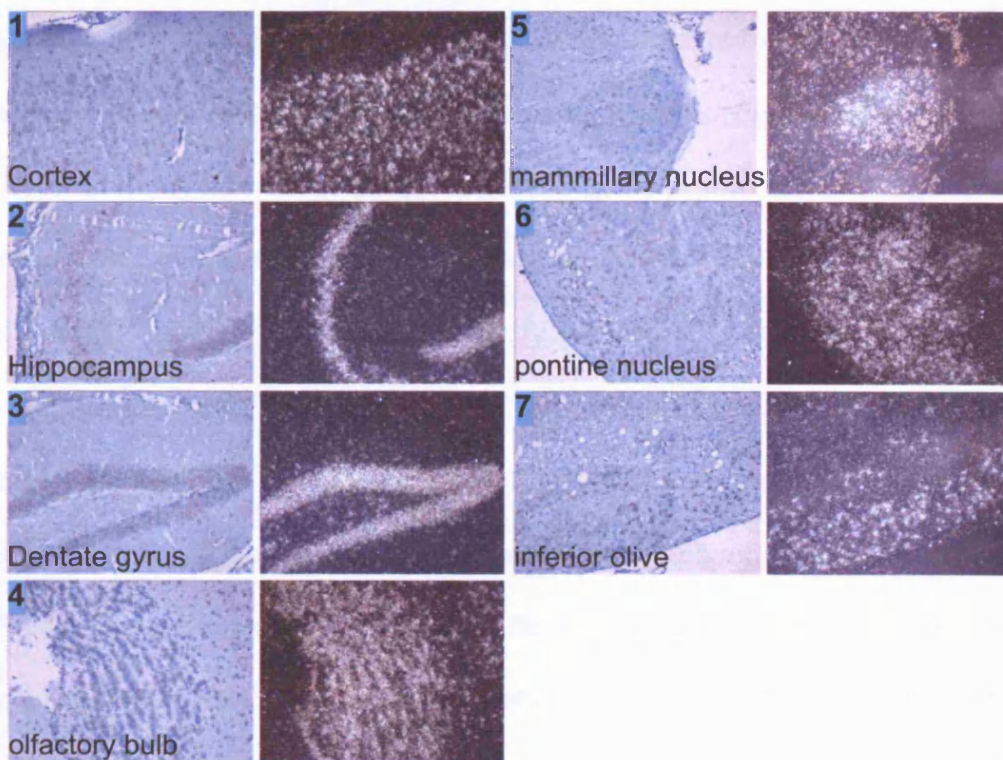
Figure 3.7 Detection of Fbw7 message in the wt brain A) scheme of a midline sagittal cut mouse brain.(from, Paxinos, 2002) Red numbered rectangles indicated areas of Fbw7 expression that are magnified in B. B) Areas of Fbw7 expression detected with the generic Fbw7 probe. Shown are brightfield and darkfield images of the resprective regions.

3.3.3 *In situ* hybridisation on Fbw7 conditional knockout brains

To verify the knockout of Fbw7 in the generated conditional knockout lines, sections of control and mutant animals were hybridised. In brains of E18 embryos where *fbw7* is deleted in cells of the neuronal lineage, $fbw7^{\Delta N}$, the strong signal in the embryonic cortex disappears in the knockout (Figure 3.8, panels 2, 2'). The message is also strongly reduced in the embryonic eye (Figure 3.8, panels 4, 4'), confirming previously published data that Nestin-cre mediated deletion also affects the eye (Y. Cang et al., 2006). A loss of the cortical *fbw7* hybridisation signal could also be observed in the adult $fbw7^{\Delta pN}$ animals where Fbw7 is deleted in postmitotic neurons (Figure 3.9 and Figure 3.10). In a montage image using the generic probe distinct areas of high Fbw7 expression such as the cortex, hippocampus, olfactory bulb are visible and in the $fbw7^{\Delta pN}$ animal this signal is strongly reduced (Figure 3.9). The residual signal in the $fbw7^{\Delta pN}$ cortex compared to the $fbw7^{\Delta N}$ brain that is present in brains probed with the generic (Figure 3.10 top panel) and the the exon 5 specific probe (Figure 3.10, bottom), can be attributed to cells still expressing Fbw7 since Synapsin-cre mediated deletion selective affects postmitotic neurons while Nestin-cre mediated deletion also causes deletion in glial cells. Additionally the signal in the dentate gyrus is strongly reduced in $fbw7^{\Delta pN}$ animals (Figure 3.10), confirming previously published results for the efficient cre-recombinase expression of the Synapsin-cre line in neurons and particularly the dentage gyrus (C. Hoesche et al., 1993). The *fbw7* message is also detected

in the cerebellar granule cell layer and this signal is reduced upon Engrailed-2

mediated deletion in the $fbw7^{\Delta Cb}$ brain (Figure 3.11).

Taken together these data demonstrate that the deletion of Fbw7 results

in a reduction of $fbw7$ message *in vivo* and suggest that the message is removed

by nonsense-mediated decay.
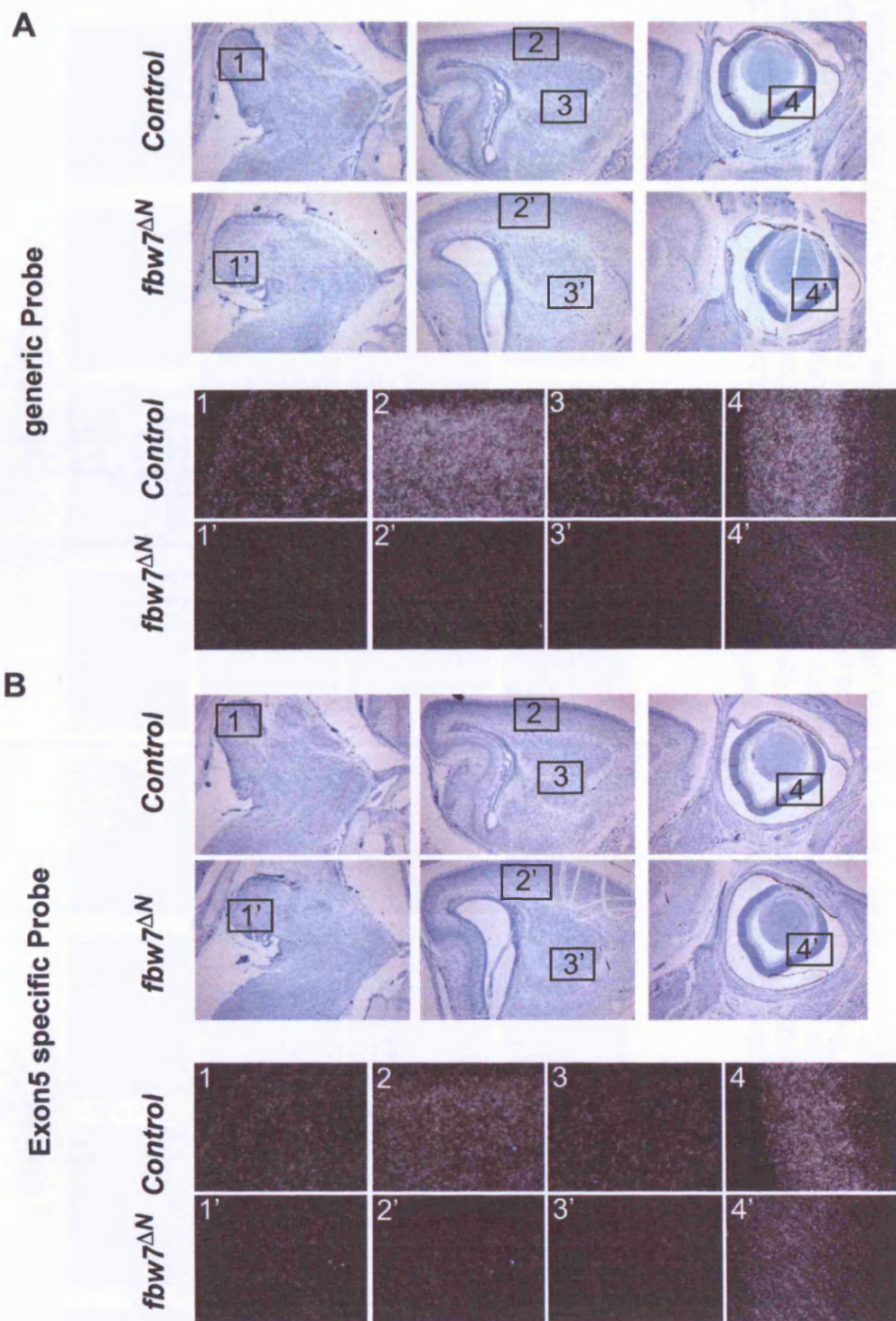
Figure 3.8 Fbw7 in situ hybridisation on E18 *Control* and *fbw7*$^{\Delta N}$ brains. A control and *fbw7*$^{\Delta N}$ brain were hybridised with either the generic probe (A) or the exon 5 specific probe (B). Overview images (blue panels) covering the cerebellum (left), cortex (middle) and eye (right) were taken at 5x magnification. Numbered areas were chosen for 50x magnification darkfield images. The reduction in signal particularly in the cortex (2,2') and eye (4,4') is visible in both probes.
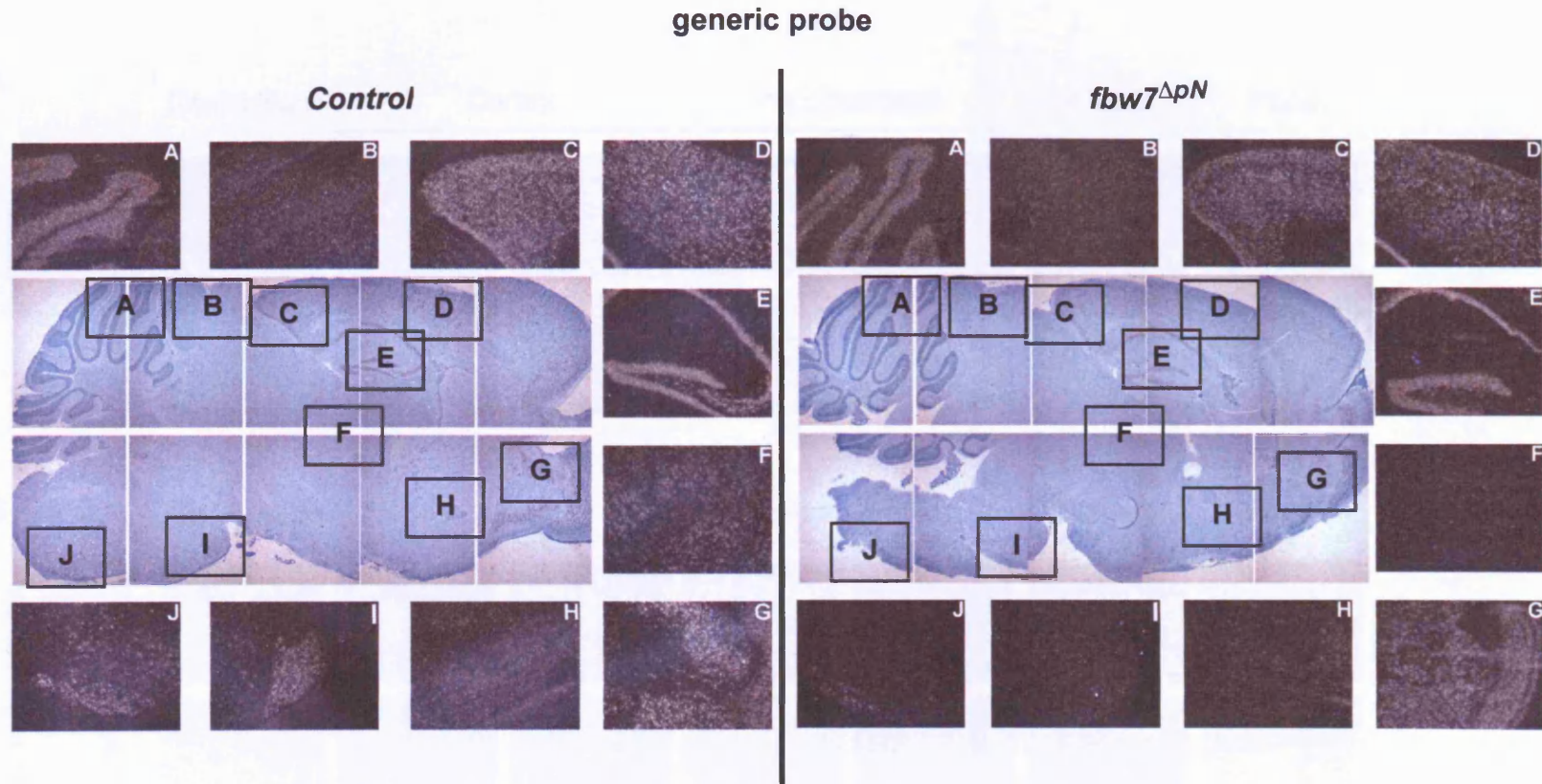
Figure 3.9 Reduction of in situ hybridisation signal in _fbw7_^{ΔpN} brain, I. The generic probe was used to highlight fbw7 message levels in the brain. The montage of transmissive images (blue) shows that the signal, visible as a grey/black staining, is strong in areas such as the cortex, hippocampus and olfactory bulb. Images of the areas indicated were taken at 10x magnification as darkfield images. The hybridisation signal is weaker in in the knockout brain. Regions that give a strong signal such as the cerebral cortex (C, D). hippocampus (E) and olfactory bulb (G) can be distinguished from regions with low _fbw7_ message such as the superior colliculus (B), thalamus (F) or nucleus accumbens (H). Message levels in the cerebellum (A), pons (I) and inferior olive (J) are also high.For more detailed images on the loss of hybridisation signal in the knockout brain see Figure 3.10.
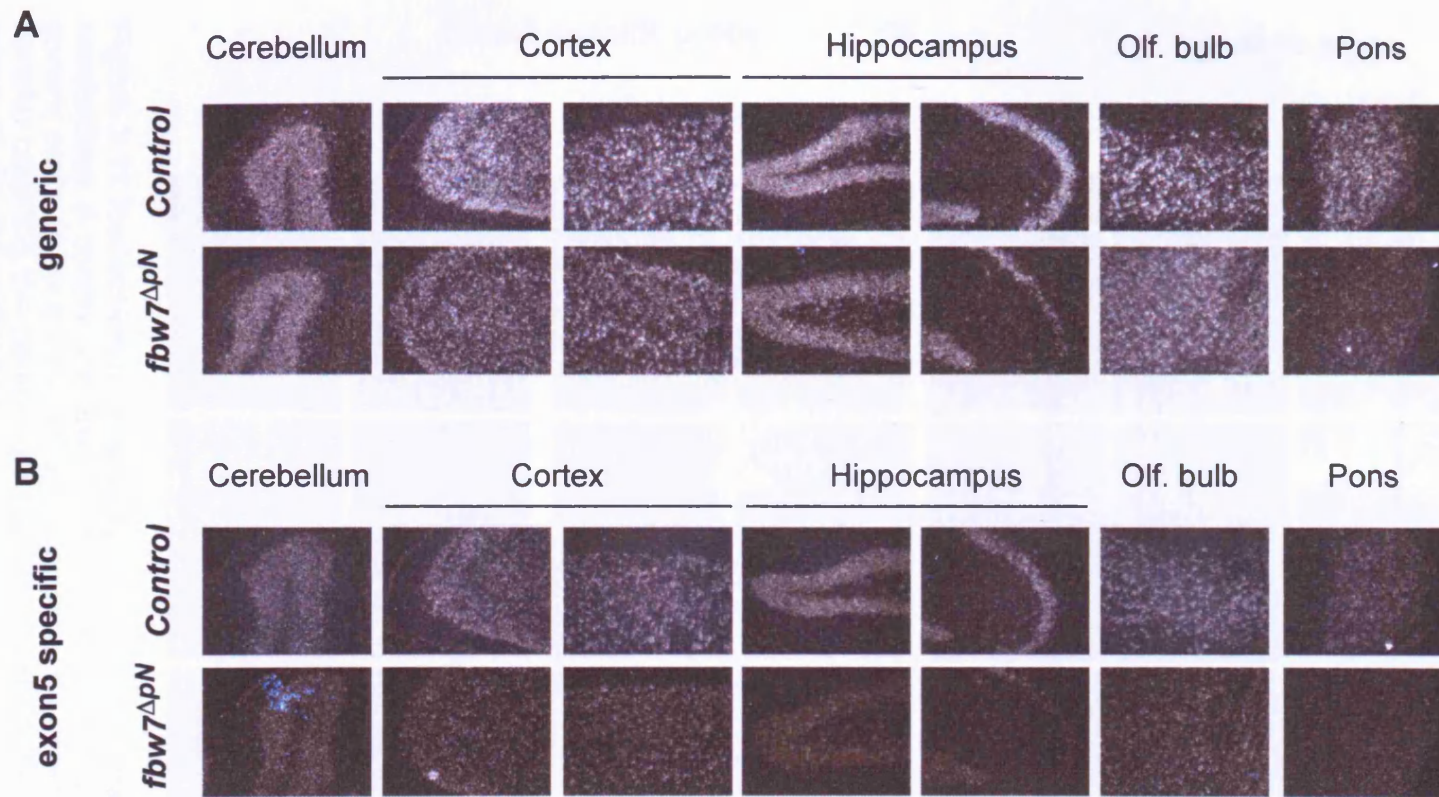
Figure 3.10 Reduction of in situ hybridisation signal in the *fbw7*$^{\Delta pN}$ brain, 2. Pictures of high expressing areas were taken at 20x magnification of sagittal cut brains hybridised with either the generic probe (A) or the exon 5 specific probe (B). The reduced hybridisation signal in the *fbw7*$^{\Delta pN}$ brain is visible with both probes, although a stronger reduction is detected with the exon 5 specific probe.
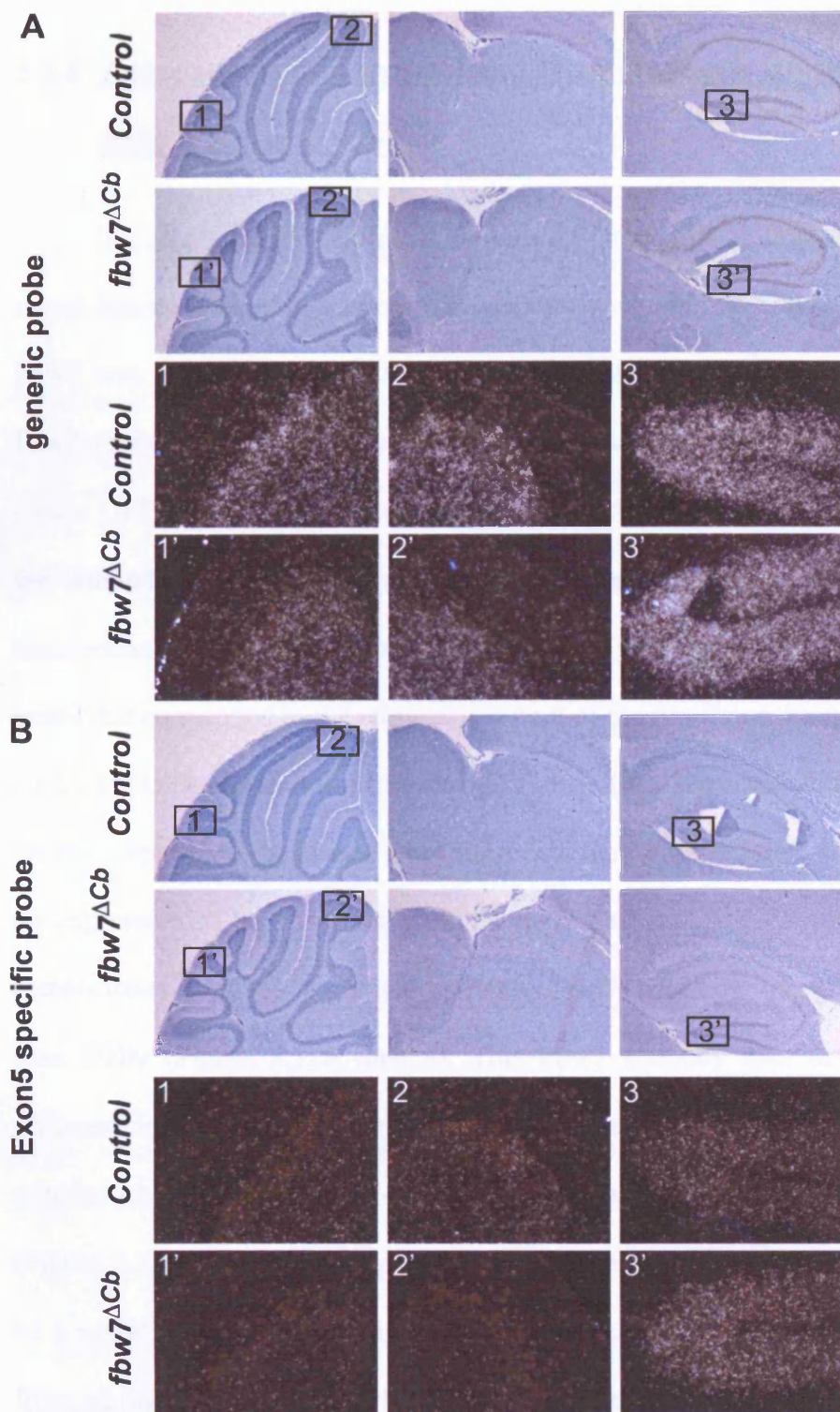
Figure 3.11 Reduction of in situ hybridisation signal in the fbw7$^{\Delta Cb}$ cerebellum. A control and fbw7$^{\Delta Cb}$ brain were hybridised with either the generic probe (A) or the exon 5 specific probe (B). Overview images (blue panels) covering the cerebellum (left) to the Hippocampus (right) were taken at 5x magnification. Numbered areas were chosen for 50x magnification darkfield images. The reduction in signal is present in both probes and in both cerebellar lobes (panels 1,2) whilst the dentate gyrus (panel 3) is not affected.

3.3.4 Assessment of a monoclonal Fbw7 antibody on transfected cells and tissue extracts

To detect the Fbw7 protein, an in-house monoclonal antibody that was raised against a peptide sequence within the first common exon (exon 2) of Fbw7 was generated by the CRUK monoclonal antibody service (in-house Fbw7 antibody). To test this antibody 293T cells were transfected with different mouse GFP-Fbw7-β fusion constructs that either contained or did not contain the antibody epitope (Figure 3.12A). Cells were harvested 24 hours post transfection and western blotting for Fbw7 or GFP was performed. Specific bands that correspond to the molecular weight of the Fbw7 construct fused with the 29 kD GFP protein were detected (Figure 3.10B). Upon the deletion of the antibody-epitope no band was recognised with the in-house Fbw7 antibody. As the expression of the construct could be confirmed using a GFP antibody, this demonstrates that the generated in-house Fbw7 antibody recognises Fbw7 specifically (Figure 3.12B lane 3). This Fbw7 antibody also detects the 3 different isoforms of the human Fbw7 protein as shown by transient transfection of human Fbw7-α, -β and -γ Flag-myc-expression constructs (Figure 3.12C). These overexpression data suggested that this antibody could be a useful tool in studying the conditional knockout mice. In tissue extracts from wt mice run on a 10% SDS-PAGE the in-house Fbw7 antibody detects a band of 80 kD kidney, liver, spleen and thymus (Figure 3.13A and data not shown). However, this band is hardly detectable in brain extracts (Figure 3.13A). The only strong band that is present in brain extracts of all animals

including Bl6 controls is a small non-specific 35kD band. I decided to test the

Fbw7 antibody on *fbw7$^{\Delta Cb}$:c-jun$^{\Delta Cb}$* protein extracts from the cerebellar vermis

and lateral sides. In these extracts western blotting for c-Jun can act as a

positive control as to whether the deletion is taking place as expected. With

regards to Fbw7 I observed that in this 8% SDS-PAGE a weak duplet of 85 and

75kD is detected. However, this duplet is still present in extracts from the

fbw7$^{\Delta Cb}$:c-jun$^{\Delta Cb}$ vermis, indicating that this band is not specific as western

blotting for c-Jun showed an efficient deletion (Figure 3.13B). Also in protein

extracts from *fbw7$^{\Delta N}$* E18 cortices or *fbw7$^{\Delta pN}$* brains no specific band for Fbw7

could be detected when using the in-house antibody that was previously

established to recognise Fbw7 in transfected cells. Ponceau staining, actin blots

and one lane loaded with a cell lysate of GFP-Fbw7-β transfected cells were

used as controls in these experiments to ensure that a) the proteins from the cell

lysates were transferred onto the nitrocellulose membrane and b) that the

antibody staining protocol worked. I tested different membranes (nitrocellulose,

PVDF), blocking agents (Milk, BSA) and buffers (TBS, PBS, TBST, PBST) to

ensure that the absence of a signal is not cause by the experimental setup. I

furthermore tested different Fbw7 antibody concentrations as well as different

tissue lysis protocols (data not shown).

Additionally to the in-house Fbw7 antibody there are commercial

antibodies available. These antibodies differ in their epitopes in comparison to

the in house antibody. A polyclonal Fbw7 antibody recognises a C-terminal

epitope (AB 12292, abcam) and should therefore recognise all Fbw7 isoforms

as the C-terminus is conserved. However, the provided datasheet does not

provide convincing information regarding the specificity for Fbw7. Another tested polyclonal Fbw7 antibody (PAB-10565) is directed against the N-terminus of the Fbw7-β-isoform. To assess these antibodies GFP-mFbw7-β was transfected into 293T cells and western blotting was performed with the same constructs as described in Fig.3.12. Whilst the in house antibody was used as a positive control and recognised the GFP-Fbw7-β fusion construct as described, the actin staining confirmed equal loading and the functionality of the used rabbit secondary antibody, blotting with the commercial antibodies did not result in any bands in any of the tested experimental conditions (as described for the in-house antibody on on tissue extracts), (data not shown). As these commercial antibodies have been unable to detect the overexpressed Fbw7 protein, they were not further analysed with respect to the endogenous protein. To overcome the lack of an antibody that can detect the endogenous Fbw7 protein, I have initiated the generation of further monoclonal and polyclonal Fbw7 antibodies that recognise the F-box domain of Fbw7 and these are currently being tested.
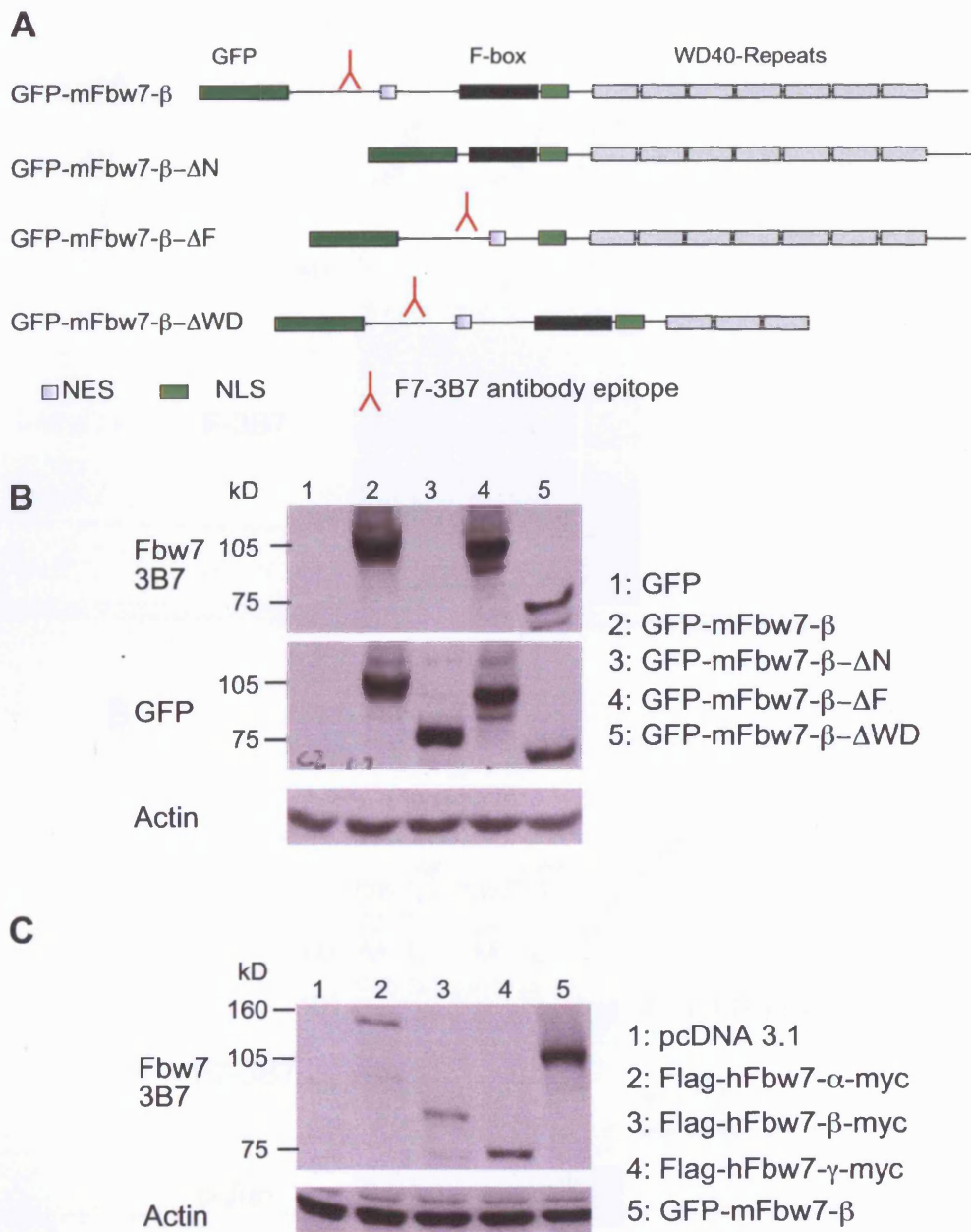
Figure 3.12 The F7-3B7 antibody is specific and detects all isoforms in transfected cells. (A) Scheme of GFP-Fbw7 fusion constructs used to test the Fbw7-3B7 antibody. The epitope is not present in the GFP-mFbw7-ΔN construct. B) 293T cells were transfected with the indicated Fbw7 constructs, whole cell lysates were prepared and western blotting performed. The Fbw7 Antibody recognises GFP-mFbw7-β fusion constructs that have the antibody epitope. The GFP-mFbw7-ΔN construct, which lacks the epitope, is not recognised, but it can be detected by reprobing the blot with a GFP antibody. The GFP band is not depicted in lane 1 as it runs at 30kD C) 293 cells were transfected with the three different human, flag-myc tagged Fbw7 isoforms. The antibody recognises all isoforms. The GFP-mFbw7-β fusion construct (Lane 5) is also recognised and runs 30kD higher than the Flag-myc-tagged human β-isoform (lane3) due to its fusion to GFP. The expression level of the Flag-myc tagged constructs is much lower than that the GFP fusion construct.
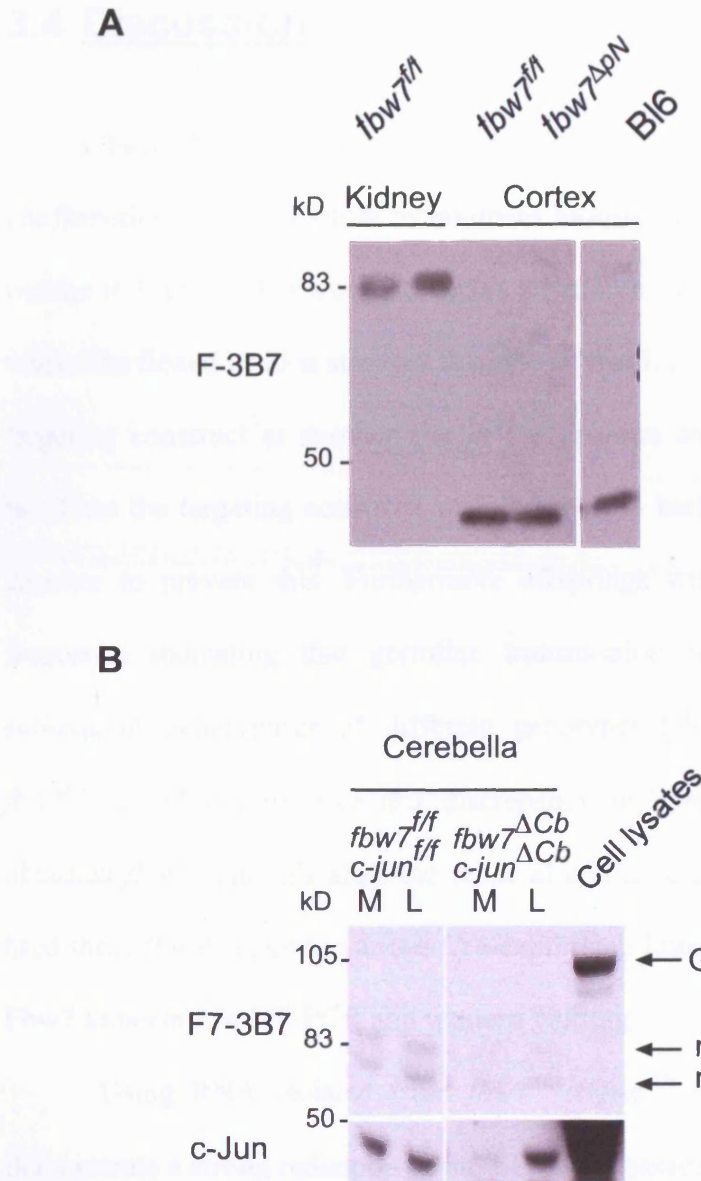
Figure 3.13 The F7-3B7 antibody does not work on brain tissue. A) Kidney and cortical sample of a control, $fbw7^{\Delta pN}$ and Bl6 animal were homogenises as described. The F7-3B7 antibody recognises different bands in kidney and cortical sample, but none is specific. C57-Bl6 and $fbw7^{f/f}$ cortical samples display the same pattern as the $fbw7^{\Delta pN}$ sample. B) The Fbw7 antibody does not work in $fbw7^{\Delta Cb}{:}c\text{-}jun^{\Delta Cb}$ brains where protein extracts were prepared from either the medial (M) or lateral (L) sides. c-Jun protein levels are strongly reduced in the cerebellar vermis in conditional double knockout animals, but no specific band for Fbw7 can be detected. ns: non specific

3.4 <u>Discussion</u>

I have described the generation of the targeted $fbw7^{fneo}$ mice and the confirmation of the targeting by southern blotting. Using the crossing strategy outline in Figure 3.1. Figure 3.3 shows a genotyping PCR on targeted ES cells where the floxed band is stronger than the wt band. A random integration of the targeting construct at another site in the genome could explain the stronger band but the targeting construct was designed to harbour a negative selection cassette to prevent this. Furthermore offsprings were born with mendelian frequence indicating that germline transmission had taken place and in subsequent genotypings of different genotypes ($fbw7^{f/f}$, $fbw7^{f/\Delta}$, $fbw7^{\Delta/+}$ or $fbw7^{f/+}$) I did not observe this discrepancy in band intensities anymore. I obtained $fbw7^{f/f}$ animals after the removal of the selection marker and having bred these $fbw7^{f/f}$ mice to various Cre-expressing lines, I wanted to confirm the Fbw7 knockout by RT-PCR and western blotting.

Using RNA isolated from $fbw7^{\Delta Cb}$:c-$jun^{\Delta Cb}$ cerebella I could clearly demonstrate a strong reduction of the wt $fbw7$ message in the medial part of the cerebellum compared to the lateral non-deleted part. Unexpectedly however, I detected a lower molecular weight band in the RT-PCR on the medial part of the $fbw7^{\Delta Cb}$:c-$jun^{\Delta Cb}$ cerebellum (Figure 3.5). The sequencing confirmed that this band corresponds to the exon-5 deleted $fbw7$ message and contained a premature stop codon and thereby confirmed that the Cre-mediated deletion takes place as anticipated. However, as exon 5 is in the middle of the $fbw7$

locus, I expected that the truncated message is subjected to nonsense-mediated decay upon successful recombination and is therefore not detectable by RT-PCR. The presence of the deleted band could indicate that the message is stable and has escaped nonsense-mediated decay. However, an alternative explanation may be that the observed band and especially its amount in comparison to the wt band in the lateral sample is the result of a saturated PCR amplification. Since I used 40 cycles in the PCR it is likely that amplification has reached saturation and therefore masks the real difference in the amounts between the wt *fbw7* RNA in the lateral sample and the truncated message in the medial sample. While this result clearly shows that exon 5 has been efficiently deleted from the medial part of the cerebellum it is more difficult to assess how much truncated message is present in relative terms, something which could be better addressed by quantitative PCR.

An additional approach that I used to verify the Fbw7 knockout was the analysis of the *fbw7* message levels by *in situ* hybridisation. For this purpose I analysed brain sections of the various conditional knockout lines that I generated during my PhD. I observed a strong reduction in the Fbw7 signal in all knockout brains (Figures 3.8 to 3.10). Especially in E18 *fbw7*$^{\Delta N}$ brains there was an almost complete loss of message indicating that the Fbw7 knockout was successful. This confirms the result from the RT-PCR that Fbw7 can be efficiently deleted upon cre-mediated recombination. Furthermore the *in situ* data strongly suggests that the strong band for the exon 5-deleted RT-PCR is indeed the result of a saturated PCR reaction and that the truncated Fbw7 message is indeed subjected to nonsense-mediated decay *in vivo*.

The confirmation of the Fbw7 knockout on protein levels by western blotting did not work so far. I used an in-house monoclonal Fbw7 antibody and I could clearly demonstrate that it recognises overexpressed Fbw7 constructs of all isoforms (Figure 3.10). Depending on the organ taken for western blotting, the in-house Fbw7 antibody recognises a band of an apparent molecular weight 80 kD in other organs than the brain. In brain samples there is a duplet present of 85kD and 75D (Figure 3.11B), however, when western blotting protein extracts from $fbw7^{\Delta Cb}$:c-$jun^{\Delta Cb}$ mice, no loss of bands could be detected. In contrast, the deletion of c-Jun was confirmed, demonstrating that these samples allow the comparison of deleted (medial) and non-deleted (lateral) parts of the cerebellum. In combination with the results obtained from the RT-PCR, in the *in situ* hybridisation this suggests that the observed bands are unspecific. The lack of a band, which can be clearly identified as Fbw7, could be explained by the instability of the protein. It is possible that Fbw7 is rapidly degraded and thus the detection is very difficult. Alternatively the two non-specific bands in organ extracts could mask an even weaker specific band.

When using the commercial antibodies on GFP-Fbw7 transfected cells, I could not observe any band in western blots (Data not shown), which was the reason why I did not continue to use them on tissues. Interestingly however, none of the companies provides convincing western blots in the datasheets that demonstrates that their antibodies work. I have therefore initiated the generation of further monoclonal and polyclonal antibodies that are directed against the F-box domain of Fbw7, however, these antibodies are still to be tested.

In conclusion I have generated $fbw7^{f/f}$ mice that allow a tissue-specific deletion of Fbw7 upon crossing them to Cre-transgenic lines. I furthermore

confirmed by RT-PCR and *in situ* hybridisation and RT-PCR experiments that

Fbw7 deletion takes place as expected in the mouse lines that I characterised

during my PhD.

4 UBIQUITOUS AND NESTIN-CRE MEDIATED FBW7 DELETION ARE LETHAL

4.1 PGK-cre mediated deletion of Fbw7 is lethal

When I started cloning the targeting construct for the conditional Fbw7 knockout, the function of Fbw7 *in vivo* had not been investigated. However, during the generation of the conditional knockout mice two papers were published, that demonstrated that the germ line deletion of Fbw7 is lethal (M. T. Tetzlaff et al., 2004; R. Tsunematsu et al., 2004) (see also chapter 1.3.6). In both studies the authors obtained $fbw7^{+/-}$ mice but intercrosses never resulted in any $fbw7^{-/-}$ offsprings. To confirm their results I decided to use the PGK-cre line and breed them to mice harbouring the targeted allele. The presence of the Cre-recombinase under the PGK promoter leads to ubiquitous deletion at early embryonic stages (Y. Lallemand et al., 1998). This cross leads to mice that harbour the deleted Fbw7 allele with the positive selection marker still present ($fbw7^{\Delta neo/+}$) (Figure 4.1A). Intercrosses of these mice did not give any homozygous $fbw7^{\Delta neo/\Delta neo}$ offsprings at weaning age (data not shown), thereby reproducing the data by Tetzlaff and Tsunematsu.

To further confirm their results that at E 9.5 $fbw7^{-/-}$ animals are still present, I set up a time mating of an $fbw7^{\Delta neo/+}$ intercross and genotyped the embryos at E9.5. In a litter of seven three animals were $fbw7^{\Delta neo/\Delta neo}$ as seen by

the presence of only the Δ band in the genotyping PCR. The genotyping PCR of

the other animals amplified an additional wt band, demonstrating that they are

heterozygous, $fbw7^{\Delta neo/+}$ (Figure 4.1B). Thus PGK-cre mediated deletion results

in a null allele and reproduces the published data for the germline knockout.

Since the other two groups had already characterised the effect of the

ubiquitous Fbw7 deletion (summarised in 1.3.6), I did not pursue this analysis

further and focussed instead on the generation and analysis of the conditional

knockout of $fbw7$ in the nervous system.

A
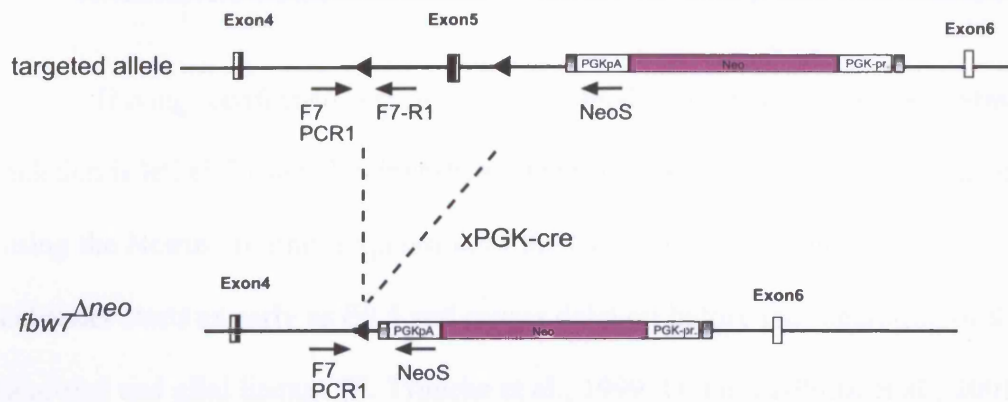
B
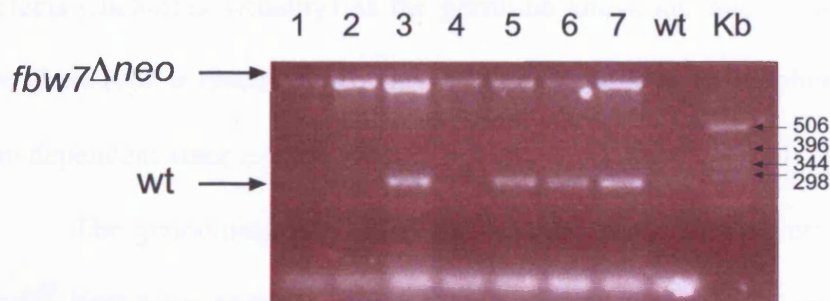
Figure 4.1 *fbw7^Δneo/Δneo* animals are still present at E 9.5 A) Mice harbouring the targeted *fbw7* allele were crossed with PGK-cre transgenic mice to obtain ubiquitious deletion of Fbw7. The neomycin cassette is still present in these crosses. Primers used for genotyping are indicated. B) Genotyping PCR on E 9.5 embryos from time mated *fbw7^Δneo/+* x *fbw7^Δneo/+* crosses. *fbw7^Δneo* homozygous mutant animals (numbers 1,2,4), detected by a PCR band amplified with primers F7-NeoS are still present at this developmental stage.

4.2 <u>Nestin-Cre Mediated deletion of Fbw7 is lethal</u>

Having confirmed previously published data that ubiquitous Fbw7 deletion is lethal, I wanted to investigate the role of Fbw7 in the nervous system using the Nestin-cre line. Expression of the Cre recombinase under the Nestin-enhancer starts as early as E9.5 and causes deletion before the separation of the neuronal and glial lineage (F. Tronche et al., 1999; D. Graus-Porta et al., 2001) (reviewed in (C. Gaveriaux-Ruff and B. L. Kieffer, 2007)). Using this line, I generated Fbw7 conditional knockout mice ($fbw7^{\Delta N}$) as well as double knockout animals for Fbw7 and c-Jun ($fbw7^{\Delta N}$:c-$jun^{\Delta N}$) in the nervous system. This was based on the hypothesis that, even if $fbw7^{\Delta N}$ mice displayed the same severe defects (including lethality) as the germline knockout, one would expect that the phenotype is rescued in the $fbw7^{\Delta N}$:$cjun^{\Delta N}$ animals, if the phenotype was c-Jun dependent since c-$jun^{\Delta N}$ animals are viable (G. Raivich et al., 2004).

The genotyping of 94 mice at weaning age, did not result in a single $fbw7^{f/f}$:$Nestin$-cre positive ($fbw7^{\Delta N}$) animals whilst the other genotypes were observed with the expected mendelian frequency (Figure 4.2A). The same was true for the $fbw7^{\Delta N}$:c-$jun^{\Delta N}$ animals where out of 38 mice no double mutants could be found at weaning age (Figure 4.2B). The fact that concomitant deletion of c-Jun was not able to rescue the lethality, was a first indication that the observed phenotype is not solely c-Jun dependent. To check at what time of gestation $fbw7$ deletion is lethal, I set up time-matings and the embryos were analysed at different time points. $fbw7^{\Delta N}$ animals are present throughout

embryonic development and are slightly smaller than the wt littermates (Figure 4.2C). As there are $fbw7^{\Delta N}$ animals present at E18, this led to the conclusion that $fbw7^{\Delta N}$ animals most likely die during or shortly after birth, at least eight days later than the germline knockouts, which display an incomplete closure of the neural tube and die around E10.5. These results clearly demonstrate that Fbw7 plays a role not only during very early development and neurulation but is essential also at later stages in the nervous system development.

A

fbw7		f/+ or Δ/+		f/f or f/Δ		+/+	
	Age	cre+	cre-	cre+	cre-	cre+	cre-
fbw7^{Δ/+},Nes-cre x fbw7^{f/+}	weaned	15	11	-	5	3	5
fbw7^{f/+}:c-jun^{+/+}:Nes-cre fbw7^{f/f}c-jun^{f/f} **	weaned	7	11	-	12		
fbw7^{f/+},Nes-cre x fbw7^{f/f}	weaned	9	9	-	7		
	E18	20	27	17	22		

B

	fbw7^{f/+}:c-jun^{f/+}		fbw7^{f/f}:c-jun^{f/+}		fbw7^{f/+}:c-jun^{f/f}		fbw7^{f/f}:c-jun^{f/f}	
	cre+	cre-	cre+	cre-	cre+	cre-	cre+	cre-
fbw7^{f/+}:c-jun^{f/+}:Nes-cre fbw7^{f/f}c-jun^{f/f}	3	2	-	1	2	9	-	6
fbw7^{f/+}:c-jun^{f/f}:Nes-cre fbw7^{f/f}c-jun^{f/f}					3	8	-	4

C

E 13.5   E 18.5

Control   *fbw7^{ΔN}*   *Control*   *fbw7^{ΔN}*
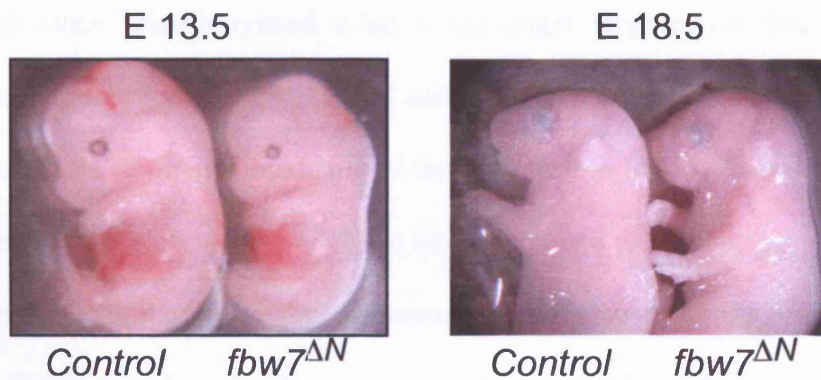
Figure 4.2 Nestin-cre mediated deletion of Fbw7 is lethal. A) Frequency of indicated genotypes at either weaning age and E 18.5. No *fbw7^{ΔN}* mutant are found at weaning age, whereas they were present at E18.5. (**: all animals are *c-jun^{f/+}* as this breeding was used to generate double knockout animals). B) No *fbw7^{ΔN}:c-jun^{ΔN}* are among animals genotyped at weaning age from crosses indicated right. No *fbw7^{ΔN}:c-jun^{ΔN}* or *fbw7^{ΔN}* animals were found, whereas *c-jun^{ΔN}* animals are viable, confirming published results. C) Photographs of control and *fbw7^{ΔN}* animals at indicated timepoints. *fbw7^{ΔN}* animals are smaller than wt littermates and are present at E13.5 and E18.5.

4.2.1 Reduced cellularity in *fbw7$^{\Delta N}$* animals at E18

H&E staining in *fbw7$^{\Delta N}$* E18.5 embryos showed that the brain does not display gross morphological defects however the cellularity appeared reduced (Figure 4.3B). To quantify this comparable regions were chosen in the cortical plate, intermediate zone and the midbrain and the cell density was quantified as described in 2.3.6. All three quantified regions display a significant 20-30% reduction in cellularity (Figure 4.3C). The reduced cellularity in the cerebellar primordium was not quantified due to the disruption of it in some samples and therefore too small sample numbers. The reduced cellularity is preceded by an increase in pyknotic nuclei at E16.5, a stage at which *fbw7$^{\Delta N}$* mutant animals also showed elevated phospho-c-Jun levels (Figure 4.4). This observation is consistent with the hypothesis that lack of Fbw7 leads to increased phospho-c-Jun levels since phosphorylated c-Jun is no longer targeted for degradation. However, as concomitant loss of Fbw7 and c-Jun did not rescue the phenotype, c-Jun cannot be the major mediator of the observed lethality. Therefore other substrates such as Notch and c-Myc are likely to play a role observed apoptosis and decreased cellularity, however immunohistochemistry stainings for c-Myc, N-myc, Notch-1 and cyclin E were inconclusive to date (data not shown). Additionally I performed western blotting experiments on brain lysates of control and knockout animals but was unable to detect any specific bands for these substrates (Data not shown).

Jörg Hoeck, another student in the lab, continued the analysis of the *fbw7$^{\Delta N}$* animals. He cultured neurospheres derived from E13.5 of *fbw7$^{\Delta N}$*,

fbw7$^{\Delta N}$:c-jun$^{\Delta N}$ and control brains to investigate the role of Fbw7 in neuronal

development further. By culturing the neurospheres in differentiation medium,

Jörg could show that cell fate decisions such as differentiation into O4 positive

oligodendrocytes, tujIII positive neurons is impaired and that these normally

exclusively expressed markers can in some cases be found in the same cells

(J.Hoeck personal communication). Additionally he observed that the number

of Nestin positive precursor cells is reduced in undifferentiated *fbw7$^{\Delta N}$*

neurospheres Therefore Jörgs work demonstrated that the lineage decision is

impaired in *fbw7$^{\Delta N}$* animals and he continues to investigate this (see also

discussion chapter 4.3).
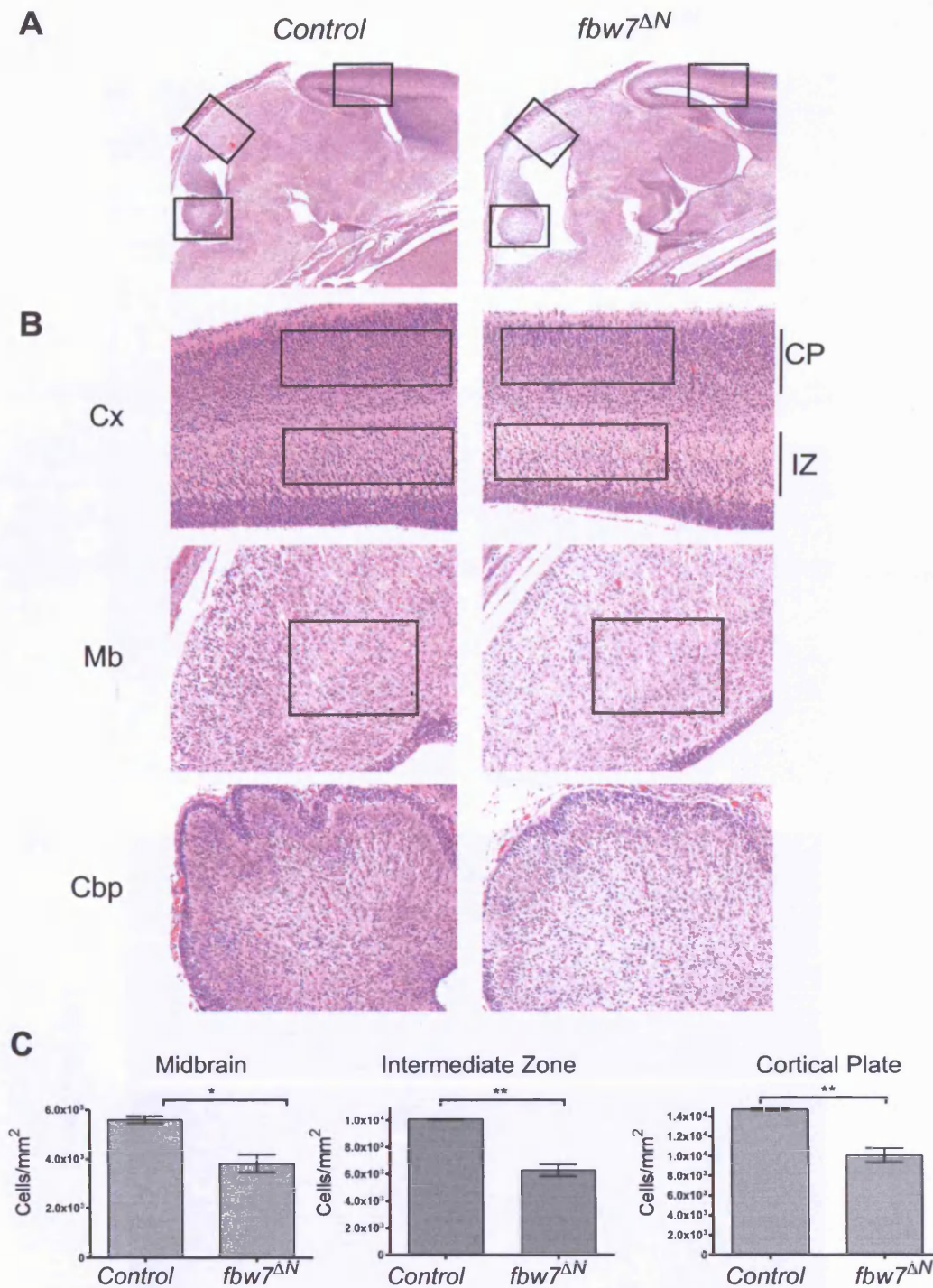
Figure 4.3 Reduced cellularity at E18 in *fbw7$^{\Delta N}$* brains A) H&E stain on sagittal sections from E18 embryos. Areas outlined in A are shown in B. B) The reduced cellularity is apparent throughout the brain Cx: Cortex with ventricular zone (VZ), intermediate Zone (IZ) and cortical plate (CP) , Mb: midbrain, Cbp: cerebellar primordium. Regions of the same size were used from the Cortical plate, Intermediate Zone and the midbrain as indicated and the number of cells quantified . The Mean +/- SEM of the number of cells in comparable regions for 3 *control* and 3 *fbw7$^{\Delta N}$* animals is shown in C),$p_{(MB)}$=0.0101, $p_{(IZ)}$ =0.0011,$p_{(CP)}$=0.0032
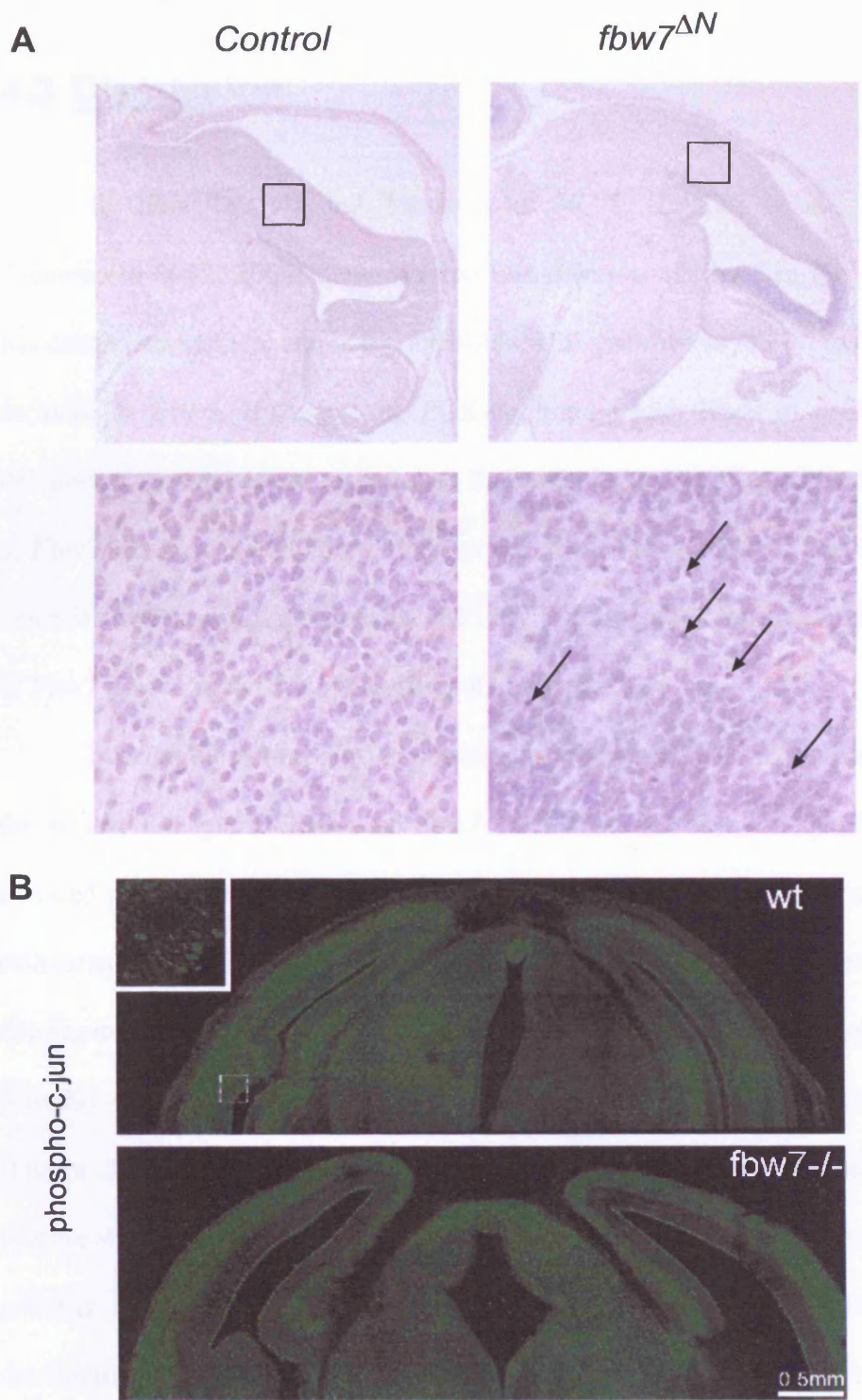
Figure 4.4 Increased apoptosis and elevated phospho-c-Jun levels at E16 in fbw7$^{\Delta N}$ animals A) H&E stainings on sagittal cut E16.5 brains indicates that the cellularity is still preserved at this stage but that the number of pyknotic nuclei (arrows) is elevated. B) Phosphorylated c-Jun levels in the developing mouse brain. E16 cereberal cortices of indicated mice were stained for phospho-c-Jun S 73 and a composite image taken.High phospho-c-Jun levels are present in the ventricular zone (Arrow) Picture in B courtesy of Gennadij Raivich, Department of Perinatal Brain repair, UCL, London

4.3 <u>Discussion</u>

In 2004 Tetzlaff and Tsunematsu (M. T. Tetzlaff et al., 2004; R. Tsunematsu et al., 2004) demonstrated that deletion of Fbw7 in the organism has detrimental effects and is incompatible with viability as *fbw7*$^{-/-}$ embryos die *in utero* at E10.5. By using the PGK-cre line, which leads to a ubiquitous deletion of Fbw7, I could recapitulate these results and confirmed that deletion of Fbw7 results in a null allele. Furthermore these data underline that due to its essential function in the organism, the only feasible approach to study the role of Fbw7 *in vivo* is the use of conditional knockout mice.

I used a Nestin-cre line to obtain mice where Fbw7 is deleted in cells of the neural lineage. Deletion of Fbw7 causes an increase in apoptosis and elevated phospho-cJun levels at E16.5, which subsequently leads to a reduced cellularity at E18.5. This demonstrates that Fbw7 is crucial during embryonic development for the survival of cells in the neural lineage. Interestingly, Fbw7 is highly expressed in the developing cortex as detected by *in situ* hybridisation (Figure 3.8), while phospho-c-Jun levels are high in the ventricular zone (Figure 4.4). The inverse correlation of Fbw7 and phospho-c-Jun expression patterns suggests that Fbw7 could regulate c-Jun levels during brain development. One could envisage that in differentiated cortical neurons high levels of Fbw7 antagonise phospho-c-Jun levels. As neurons differentiate during development they migrate radially from the ventricular zone toward the pial surface of the cortex. If phospho-c-Jun levels were downregulated by Fbw7

when cells exit the proliferative VZ and migrate towards the surface, Fbw7

deletion could impair migration and/or differentiation and this could ultimately

lead to the increase in apoptosis at E16 in $fbw7^{\Delta N}$ mice.

The fact that the Fbw7:c-Jun double knockout did not rescue the

phenotype strongly suggests that elevated phospho-c-Jun levels alone are not

the reason for the observed lethality. It is feasible to assume that Fbw7 might be

required to down regulate other substrates such as Notch or N-myc during this

period of embryonic development. Notch signalling is involved in maintaining

cells in a progenitor state during neuronal development and the regulation of

Notch levels by Fbw7 during nervous system development could explain the

differentiation defects that Jörg has observed in $fbw7^{\Delta N}$ neurospheres (reviewed

in (A. Louvi and S. Artavanis-Tsakonas, 2006)). After 11 days of culture in

differentiation medium the morphology of $fbw7^{\Delta N}$ Tuj-1 positive neurons and

O4 positive oligodendrocytes was severely impaired while the morphology of

GFAP positive cells (astrocytes and progenitors) was normal (Jörg Hoeck,

personal communication). This is in line with the fact that Notch signalling

promotes the astrocyte lineage decision and that therefore Fbw7 deficiency

might not affect cells of this lineage (W. Ge et al., 2002). Furthermore Notch

signalling needs to be antagonised to allow differentiation of progenitors into

neurons and oligodendrocytes (reviewed in (A. Louvi and S. Artavanis-

Tsakonas, 2006)). It is therefore conceivable that Fbw7 deletion impairs Notch

downregulation, leading to the observed phenotype. To test the hypothesis that

Notch signalling is indeed the major mediator of the observed phenotype, one

could differentiate $fbw7^{\Delta N}$ neurospheres in the presence of Notch signalling

inhibitors to see whether the differentiation defect can be rescued. Additionally, a similar role as for Notch in maintaining cells in a progenitor state was described for N-myc, another substrate of Fbw7 (P. S. Knoepfler et al., 2002) (M. Welcker et al., 2004a). It is therefore important to establish whether N-myc or Notch cause the observed phenotype. The reduced cellularity at E18 and the increase in pyknotic nuclei show that cells die in the $fbw7^{\Delta N}$ brain. It will be essential to establish whether the remaining cells are cells that have not been deleted or whether these cells are deleted and follow a different lineage fate that is not affected by Fbw7 deletion. The use of lineage markers such as tuj-1, NeuN, O4 on brain sections of different embryonic developmental stages will help to investigate this phenotype further. The set up of an Fbw7-antibody staining for immunohistochemistry to identify deleted cells is also essential as this would allow the discrimination of Fbw7 expressing and non expressing neurons.

Taken together the data obtained from the $fbw7^{\Delta N}$ embryos and neurospheres demonstrate that Fbw7 plays a role not only in very early neuronal development as shown by Tetzlaff and Tsunematsu, but also at later stages in brain development. The non-redundant role of Fbw7 in the brain is emphasised by the fact that the selective Fbw7 deletion in the neuronal lineage is sufficient to causes perinatal lethality. *In vitro* cultures of neurospheres showed that Fbw7 is required for proper lineage decisions as Fbw7 deletion impairs neuronal and oligodendrocyte differentiation. Although the lethality cannot be rescued by concomitant c-Jun deletion, the nature of the differentiation defects indicates that a major substrate of Fbw7 during neuronal differentiation might be Notch.

Having observed a severe phenotype upon deletion of Fbw7 in the neuronal lineage, I wanted to investigate whether Fbw7 plays a role in the adult nervous system as well. I therefore generated two further conditional Fbw7 knockout lines with Fbw7 being deleted either in the cerebellar vermis ($fbw7^{\Delta Cb}$) or in postmitotic neurons ($fbw7^{\Delta pN}$).

5 FBW7 DELETION IN THE CEREBELLUM LEADS TO A SMALLER VERMIS AND LOSS OF PURKINJE CELLS

To further investigate the role of Fbw7 in the nervous system I used the Engrailed-2-cre line and generated mice with a tissue specific deletion of Fbw7 in the cerebellar vermis ($fbw7^{\Delta Cb}$). The Engrailed2-cre mouse line was generated by Zinyk et al. with the aim to map the fate of cells in the mouse midbrain-hindbrain constriction (D. L. Zinyk et al., 1998). Zinyk et al. generated transgenic mice that express cre from the En2 enhancer and determined the time window of Cre-recombinase expression from E9 to E12. They crossed these animals with c-β-STOP-lacZ reporter line and obtained mice where Engrailed2-cre activity causes the excision of a floxed STOP and thus permits lacZ expression. Since the Cre mediated excision is heritable, all cells derived from cells where Cre was expressed between E9 and E12 remain lacZ positive even after the Cre expression is switched off (D. L. Zinyk et al., 1998). The analysis of lacZ positive cells showed that Purkinje cells and granule cells are affected by this deletion particularly in the medial part of the cerebellum, the vermis. Thus cells located in the dorsal midbrain-hindbrain constriction during Cre expression populate the medial cerebellum and although Purkinje cells and granule cells are not clonally related, there is a pool of precursors that specificially generate the medial domain of the cerebellum. This conclusion by Zinyk et. al supported a previous finding by Mathis et al. who

also identified a pool of precursors specific for the generation of the cerebellar vermis (L. Mathis et al., 1997). The engrailed2-cre line was subsequently used for the conditional knockout of the Rb protein in the cerebellum (S. Marino et al., 2003). Marino et al confirmed the specific deletion in the cerebellar vermis by a deletion PCR on En2cre:Rb$^{lox/lox}$ cerebella. For the deletion PCR cells were fractionated on a percoll gradient into one fraction containing larger cells such as astrocytes and Purkinje cells whilst the other fraction contained smaller cells such as granule cells and granule cell precursors and both fractions showed recombination (S. Marino et al., 2003) Additionally Marino et al performed a wholemount β-galactosidase staining in *En2cre:ROSA26^{loxP}* cerebella and presented a low resolution figure showning that β-galactosidase expression extends throughout the cerebellar vermis. However a high-resolution image for the cerebellar vermis was not presented. Marino et al also used the engrailed-2 cre line to analyse the conditional knockout of PTEN in the cerebellum and observed an enlargement of the cerebellar vermis (S. Marino et al., 2002). To re-analyse the affected cell population in the cerebellar vermis I obtained an *En2-cre$^+$:pten$^{flox/+}$p53$^{flox/+}$: Rosa26$^{flox/+}$* cerebellum and performed a β-galactosidase stain on a coronal cryosection (see appendix). In agreement with the previously described data the β-galactosidase stain was restricted to the cerebellar vermis. Higher magnification images confirmed that not only the granule cells are affected but also cells residing in the molecular layer and Purkinje cells are lacZ positive ie. derived from the Cre deleted precursor pool (see appendix bottom panel).

5.1 $fbw7^{\Delta Cb}$ mice have a smaller cerebellar vermis

$fbw7^{\Delta Cb}$ mice were born with mendelian frequency and mutant animals were indistinguishable from their wt littermates (data not shown). The macroscopic examination of the cerebellum showed that the cerebellar vermis is smaller in knockout animals, whereas the lateral sides of the cerebellum did not display a visible phenotype (Figure 5.1A). Heterozygous animals did not display any phenotype. H&E stainings on midline sagittal sections confirmed the size defect in the vermis and revealed that with regards to the cerebellar foliation, $fbw7^{\Delta Cb}$ animals do display additional fissures (arrows in Figure 5.1B). Otherwise the cerebellum was formed normally and no gross morphological defects in the molecular layer or granule cell layer could be identified in either the H&E or NeuN stain (Figure 5.1C). To analyse the $fbw7^{\Delta Cb}$ animals further, I used a number of histological markers for the different subpopulations of cells within the cerebellum (listed in Table 5.1). The GFAP stain demonstrated that although the morphology of the cerebellum is preserved in $fbw7^{\Delta Cb}$ animals, they display a strong gliosis (Figure 5.2A). Such a gliosis can occur as a reaction to neuronal dysfunction and degeneration (J. L. Ridet et al., 1997). It is conceivable to assume that based on the phenotype which I will describe in the following sections, this is the case.

Table 5.1 Histological Marker for cerebellar analysis

Marker	Population stained
NeuN	Granule cells
Calbindin	Purkinje cells
Parvalbumin	Stellate, Basket, Purkinje cells
GFAP	Bergmann glia
Neurofilament 200 (NF200)	Basket cell axons
BrdU	Proliferating cells after BrdU injection
Vglut2	Climbing fibre terminals
Vglut1	Parallel fibre terminals
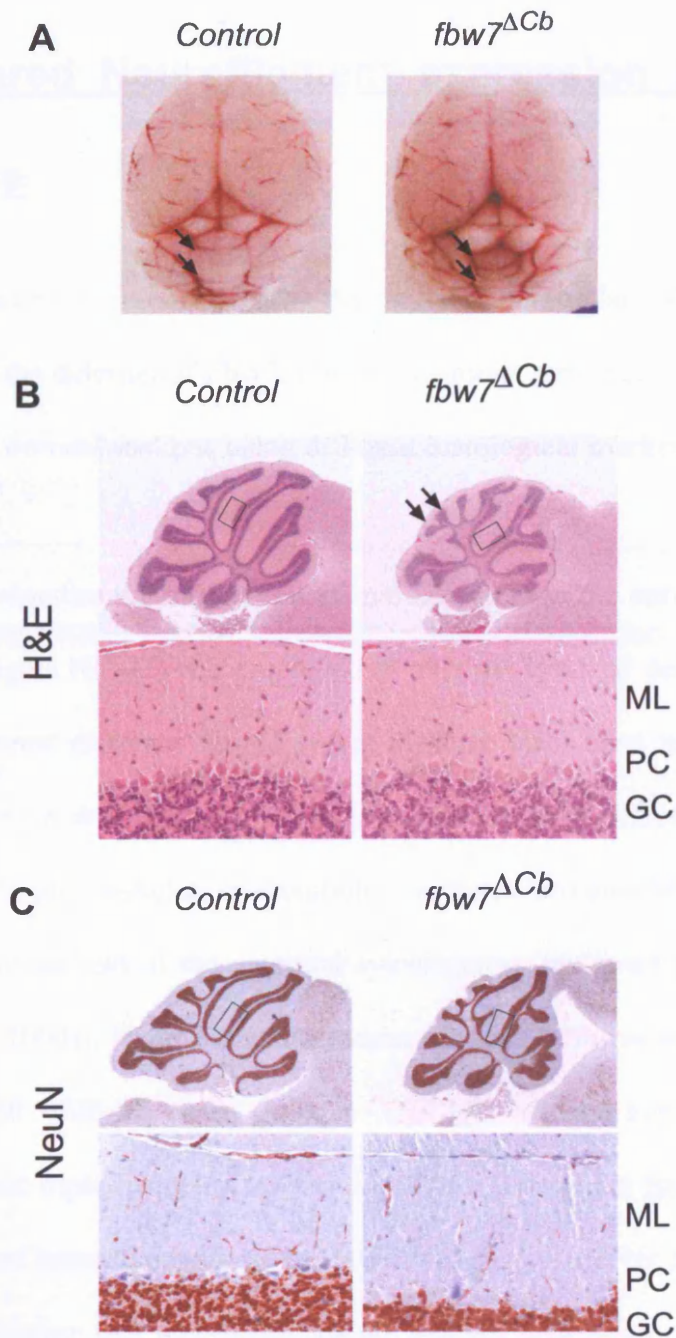
Figure 5.1 fbw7$^{\Delta Cb}$ animals have a smaller cerebellar vermis and foliation defects A) photographs of control and fbw7$^{\Delta Cb}$ brains. Arrows indicate the smaller cerebellar vermis and the foliation defects. B) H&E of midline sagittal brain sections of control and fbw7$^{\Delta Cb}$ animals confirming the smaller vermis and foliation defects. Arrows indicate the additional fissure observed in the mutants. High magnification pictures were taken from the region marked by a rectangle C) Normal morphology of the Molecular Layer and granule cell layer in fbw7$^{\Delta Cb}$ animals. ML: Molecular layer, PC: Purkinje cells, GC: granule cells

5.2 <u>Altered Neurofilament expression in *fbw7$^{\Delta Cb}$*</u>

<u>mice</u>

In order to investigate how the different cerebellar subpopulations are affected by the deletion of Fbw7, immunostainings were performed on midline sagittal and coronal sections using different histological markers (listed in table 5.1).

To visualise the basket cell axonal arborisation the anti NF-H antibody (NF-200, Sigma N4142) was employed as over the last four decades antibodies directed against different neurofilament proteins have been used as a tool to study cerebellar development. Neurofilaments are intermediate filaments and together with microtubules, microtubule associated proteins (MAPs) and other proteins they are part of the neuronal cytoskeleton (reviewed in (P. Grant and H. C. Pant, 2000)). Neurofilaments consist of three different subunits of ca 70 (NF-L), 160 (NF-M) and 200kDa (NF-H), which together form the neurofilament-triplet protein (A. Petzold, 2005). One of the first studies on the expression of neurofilaments in the brain was performed by Matus et al. and used an antiserum that was raised against isolated neurofilaments (A. I. Matus et al., 1979). Matus and colleagues observed an abundant staining in basket cell axons and small bundles of mossy fibre terminals without any staining in the cell bodies of the cerebellum. Electron microscopy showed enhanced neurofilament immunoreactivity in close proximity to Purkinje cells in the so-called basket or "pinceaus" of basket cells but no staining of Purkinje cells,

glial or granule cells (A. I. Matus et al., 1979). Julien and Mushinsky demonstrated in 1982 that neurofilaments can be phosphorylated (J. P. Julien and W. E. Mushynski, 1982) and Sternberg and Sternberg investigated whether phosphorylation also affects the recognition of neurofilaments in tissue sections and preparations (L. A. Sternberger and N. H. Sternberger, 1983). After testing different antibodies by western blotting on cytoskeletal preparations and immunohistochemistry on cerebellar sections that were either untreated or phosphatase treated, the authors concluded that some cell bodies and dendrites as well as some proximal axons contain non-phosphorylated neurofilaments whereas long fibres and terminal axons contain phosphorylated neurofilaments (L. A. Sternberger and N. H. Sternberger, 1983). Thus by 1983 it was established that neurofilaments are composed of distinct polypeptide subunits and that their phosphorylation influences the recognition of the antibody epitopes. This then led to a number of studies where new antibodies against neurofilaments were generated, characterised and compared to earlier publications. One of these studies which used an antibody against the NF-H polypeptide and studied the neurofilament expression in the rat cerebellum confirmed the observation of Matus et al. of a strong stain in basket cell axons and the absence of any immunoreactivity in cell bodies or perisomatic processes (N. Leclerc et al., 1985). Leclerc furthermore observed that the NF-H immunoreactivity becomes apparent at P12 in basket cell axons i.e. only after basket cells are terminally differentiated, which occurs between P6 and P10 in the rat (N. Leclerc et al., 1985). Another study compared antibodies against the different sized neurofilament subunits and also analysed them with regards to their phosphorylation specificity(M. Vitadello and S. Denis-Donini, 1990). This

study showed that the basket cell axonal staining observed by Matus and Leclerc is present upon the use of antibodies against the phosphorylated heavy neurofilament polypeptide whilst antibodies against NF-M and NF-L polypeptides additionally label parallel fibres (M. Vitadello and S. Denis-Donini, 1990). NF-L and NF-M are also expressed earlier, at P6 in the mouse cerebellum, than NF-H where immunoreactivity was absent again confirming the data obtained by Leclerc et al. in the rat cerebellum. A comparative study on the cat cerebellum by Riederer et al. summarised the data for different antibodies by presenting a series of sections stained at different developmental timepoints with various phospho-specific antibodies against either NF-H or NF-M (B. M. Riederer et al., 1996). This work confirmed that a phospho-specific NF-H antibody stains basket cell axons and pinceaus but not Purkinje cells. The antibody used in this thesis (Sigma, N4142) has been previously compared to the phospho-specific NF-H antibody NE-14 (characterised in (B. M. Riederer et al., 1996)) and gave a comparable staining pattern (J. Paysan et al., 2000). It has also has been used to visualise basket cell axons by immunohistochemistry (J. M. Huard et al., 1999). Furthermore this antibody has been employed in cerebellar cultures to distinguish axons from dendrites by using a co-stain with the SMI32 antibody that does recognise the non-phosphorylated form of the NF-H fragment thereby also stains dendrites (H. Marzban and R. Hawkes, 2007).

Using the anti NF-200 (Sigma, N4142) antibody on midline sagittal and coronal sections I observed that in wt animals the neurofilament staining is present in a regular, organised pattern in the lower half of the molecular layer where the basket cells reside (Figure 5.2B). In agreement with published data

161

the basket-like structures around the Purkinje cells, pinceaus, also display a strong immunoreactivity. In $fbw7^{\Delta Cb}$ animals the regular staining pattern is lost and the Neurofilament stain extends all through the molecular layer (Figure 5.2B). The baskets around Purkinje cells are still formed but display a stronger Neurofilament immunoreactivity that in wt controls and additionally a punctate pattern can be observed in coronal sections of $fbw7^{\Delta Cb}$ animals (Figure 5.2C arrows). To investigate whether c-Jun plays a role in the observed altered Neurofilament expression, $fbw7^{\Delta Cb}:c\text{-}jun^{\Delta Cb}$ double knockout animals were generated and analysed. Like the $fbw7^{\Delta Cb}$ animals, $fbw7^{\Delta Cb}:c\text{-}jun^{\Delta Cb}$ mice were born with mendelian frequency and did not show a behavioural phenotype (data not shown). Interestingly, the Normal Neurofilament expression was restored upon concomitant deletion of c-Jun (Figure 5.2C compare right with left panel), demonstrating that the alterations in the Neurofilament expression occur in a c-Jun dependent manner. To investigate whether the increased Neurofilament expression is caused by an increase in the number of cells residing in the molecular layer such as stellate and basket cells, I quantified those cells using parvalbumin as a marker (Figure 5.3). I counted the parvalbumin positive cells within two adjacent molecular layers in equivalent sections from wt and $fbw7^{\Delta Cb}$ animals. Parvalbumin positive Purkinje cells, which are bigger and lie at the interface between the molecular layer and granule cell layer, were not counted. Additionally I measured the thickness of the molecular layers to address the question whether the reduced cerebellar size is due to a reduced molecular layer thickness. No significant difference in the number of parvalbumin positive cells or in the molecular layer thickness could be

observed (Figure 5.3B and C). This strongly suggests that the aberrant

Neurofilament stain is not caused by alterations in cell number in the molecular

layer, but is rather a defect in the arborisation of basket cells.
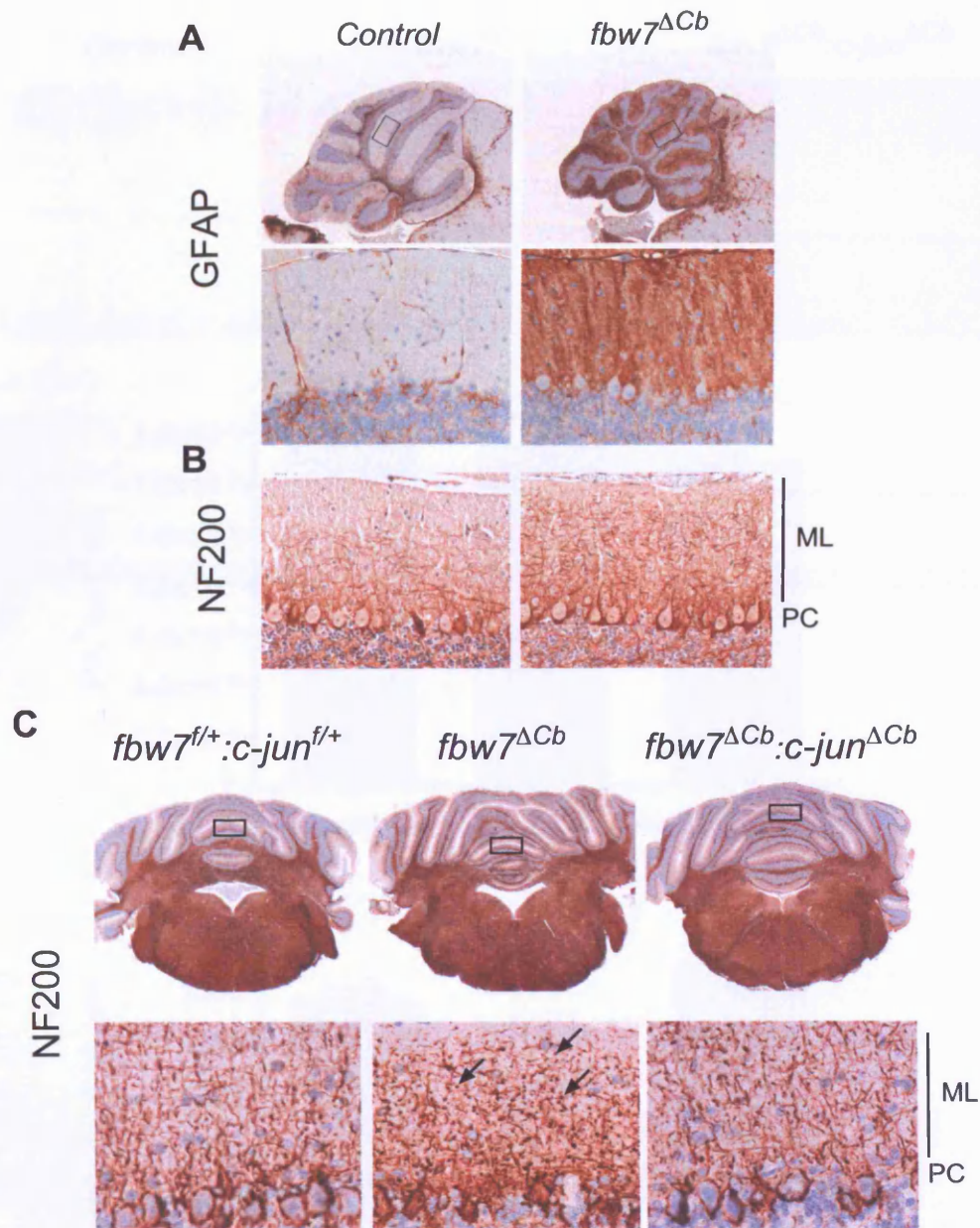
Figure 5.2 Aberrant Neurofilament expression and gliosis in the molecular layer of *fbw7^ΔCb* animals . A) Sagittal sections from control and *fbw7^ΔCb* cerebella. Knockout animals have a strong gliosis shown by the intensive GFAP stain in the Molecular Layer (ML). B) Neurofilament200 (NF200) expression in basket cell axons extends through the Molecular Layer and around Purkinje cells (PC) and is less organised and more intense in *fbw7^ΔCb* animals. C) Coronal sections of Fbw7 single mutant and Fbw7:c-Jun double Mutant cerebella stained with NF200. Top panelThe misorganisation of the cerebellar vermis is partially rescued upon concomitant c-Jun deletion. Bottom panel: The NF200 stain shows a punctate pattern (arrows) and is stronger in *fbw7^ΔCb* animals. NF200 expression is rescued upon concomitant c-Jun deletion (right image).

A

Control $fbw7^{\Delta Cb}$ $fbw7^{\Delta Cb}$:c-jun$^{\Delta Cb}$

PC

ML

PC

B

C
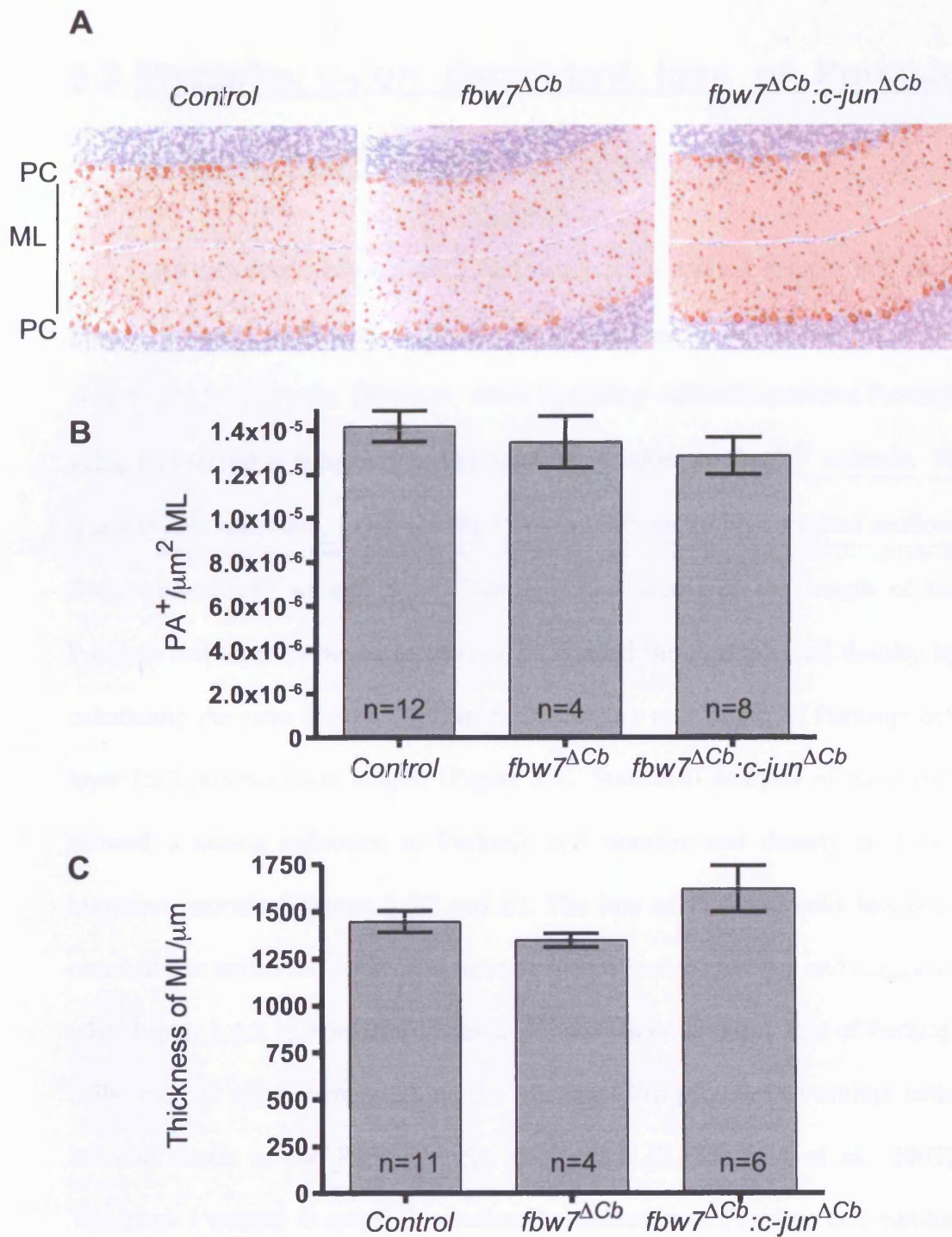
Figure 5.3 Thickness and cell number in the molecular layer are not altered in $fbw7^{\Delta Cb}$ and $fbw7^{\Delta Cb}$:c-jun$^{\Delta Cb}$ animals. A) Parvalbumin (PA) stained Molecular Layer in control, $fbw7^{\Delta Cb}$ and $fbw7^{\Delta Cb}$:c-jun$^{\Delta Cb}$ animals. PA positive (PA$^+$) cells were counted and the area of the Molecular Layer (ML) measured in this section. B) Quantification of Parvalbumin positive cells per square micrometer of ML shows no difference in the number of PA$^+$ cells C)The thickness of the Molecular layer in control and mutant animals is similar. Mean +/- SEM shown

5.3 Phospho c-Jun dependent loss of Purkinje cells in *fbw7$^{\Delta Cb}$* mice

As described above, *fbw7$^{\Delta Cb}$* animals have a normal granule cell layer (Figure 5.1) and there is no difference in the number of parvalbumin positive stellate and basket cells. However, when analysing calbindin positive Purkinje cells, I observed a reduction in Purkinje cell number in *fbw7$^{\Delta Cb}$* animals. To quantify this reduction, I counted the Purkinje cells in midline sagittal sections from 7-month-old wt and *fbw7$^{\Delta Cb}$* animals and measured the length of the Purkinje cell layer in the same section. I obtained the Purkinje cell density by calculating the ratio between Purkinje cell number and length of Purkinje cell layer (cell number/layer length) (Figure 5.4). Statistical analysis of these data showed a strong reduction in Purkinje cell number and density in Fbw7 knockout animals (Figures 5.4D and E). The loss of Purkinje cells has been correlated to ataxia for instance in mouse mutants such as *lurcher* and *staggerer* (see chapter 1.4.3.1). Furthermore mice that show a progressive loss of Purkinje cells, such as mice overexpressing the truncated Prp protein in Purkinje cells, become ataxic as the Purkinje cells degenerate (E. Flechsig et al., 2003). Therefore I wanted to establish whether the reduction in Purkinje cell number and density is the result of a progressive loss of Purkinje cells. I performed the same quantification in younger animals and additionally *fbw7$^{\Delta Cb}$:c-jun$^{\Delta Cb}$* double conditional knockout animals were analysed to establish whether the Purkinje cell reduction is c-Jun dependent. The loss of Purkinje cells in *fbw7$^{\Delta Cb}$*

animals is not progressive as in 2-month-old animals the Purkinje number and density were reduced to the same extent as in 7-month-old animals (compare $fbw7^{\Delta Cb}$ values in Figure 5.4 and Figure 5.5) suggesting that either the Purkinje cells are lost before this time point, or that there are less Purkinje cells present to begin with.

When comparing the double conditional knockouts I observed that the concomitant deletion of Fbw7 and c-Jun was not able to rescue the foliation defects observed in the $fbw7^{\Delta Cb}$ cerebella (Figure 5.5A, arrows) although the size defect observed in $fbw7^{\Delta Cb}$ cerebella was partially rescued (Figure 5.5B). Interestingly the Purkinje cell density was fully restored in $fbw7^{\Delta Cb}:c\text{-}jun^{\Delta Cb}$ cerebella, indicating that the loss of Purkinje cells is c-Jun dependent (Figure 5.5E). According to the working hypothesis deletion of Fbw7 causes elevated phospho-c-Jun levels, which could then lead to apoptosis and finally a reduction in Purkinje cells.

To address whether the loss of Purkinje cells is phospho-c-Jun dependent, I crossed $fbw7^{\Delta Cb}:c\text{-}jun^{\Delta Cb}$ mice with $fbw7^{f/f}:jun^{AA/AA}$ animals to obtain $fbw7^{\Delta Cb}:c\text{-}jun^{\Delta Cb/AA}$ mice. In addition to Fbw7, c-Jun is deleted on one allele and its N-terminal S63/S73 phosphorylation sites are mutated on the other, therefore the absence of Fbw7 can no longer lead to the accumulation of N-terminally phosphorylated c-Jun (A. Behrens et al., 1999). The quantification of Purkinje cell parameters demonstrated that the Purkinje cell density is rescued to the same degree as in $fbw7^{\Delta Cb}:c\text{-}jun^{\Delta Cb}$ cerebella and thus proves the hypothesis that the reduction in the Purkinje cell density is phospho-c-Jun dependent (Figure 5.6). However, the cerebellar area and foliation were still

altered, confirming the data from the $fbw7^{\Delta Cb}$:c-$jun^{\Delta Cb}$ cerebella which indicated that the cerebellar size and foliation defects are not solely c-jun dependent.

Purkinje cells are the cerebellar output neurons and receive their excitatory input from climbing fibres and parallel fibres and it has been demonstrated that Purkinje cell require synaptic input for the later stages of dentritogenesis ie the formation of their fine dendritic network (C. A. Baptista et al., 1994). Furthermore it has been shown that in the pcd mutants Purkinje cells degenerate during the early postnatal development presumably because they display disruptions in the synaptogenesis between the parallel fibres and the dendritic spines (S. C. Landis and R. J. Mullen, 1978). Therefore to investigate the Purkinje cell reduction further, the analysis was extended to the use of immunofluorescence of Purkinje cells and synaptic markers such as Vglut1 and Vglut2, which can be used to visualised parallel and climbing fibre synapses in the Molecular layer. Additionally, cerebella from 7-day-old animals were analysed as this is the time when the granule cells differentiate, and the Purkinje cells align in their respective plane between the Molecular layer and the granule cell layers and the expansion and formation of the cerebellar fissures takes place.
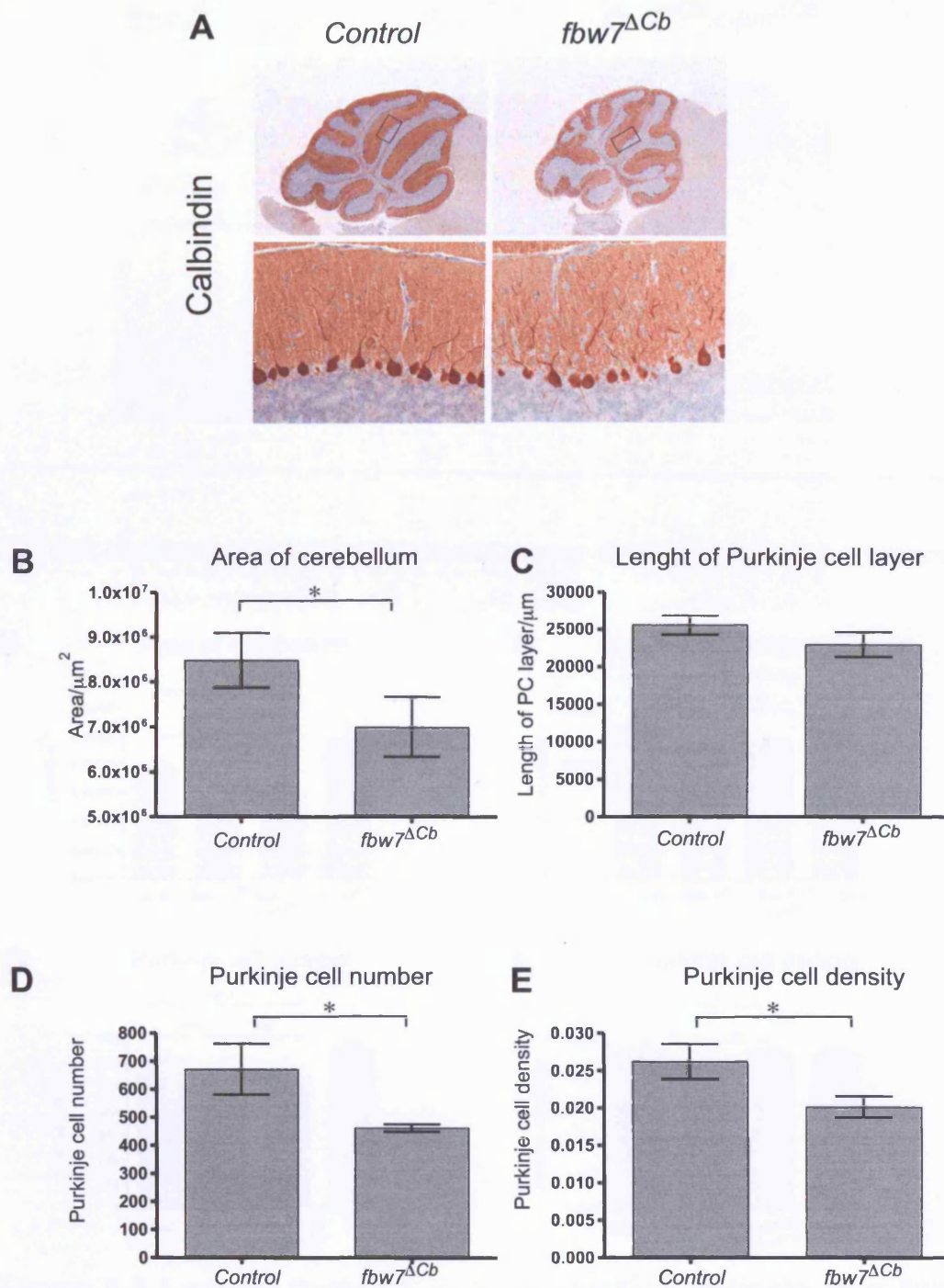
Figure 5.4 Loss of Purkinje cells in 7 month old fbw7$^{\Delta Cb}$ animals.
A) Calbindin stain on adult cerebella for Purkinje cells The loss of Purkinje cells is apparent. B-D: Quantification of cerbellar parameters. B) The cerebellar area is reduced in fbw7$^{\Delta Cb}$ animals (p=0.0463) C)Length of Purkinje cell layer in μm. (p=0.1015) D) The number of Purkinje cells per cerebellum is reduced in fbw7$^{\Delta Cb}$ animals (p=0.0171) E) To obtain the Purkinje cell density the ratio of D) over C) was calculated.The Purkinje cell density is reduced in fbw7$^{\Delta Cb}$ animals (p=0.0196) Controls: n=3, Mutants: n=3, Age 7 month, Mean+/-SD are shown
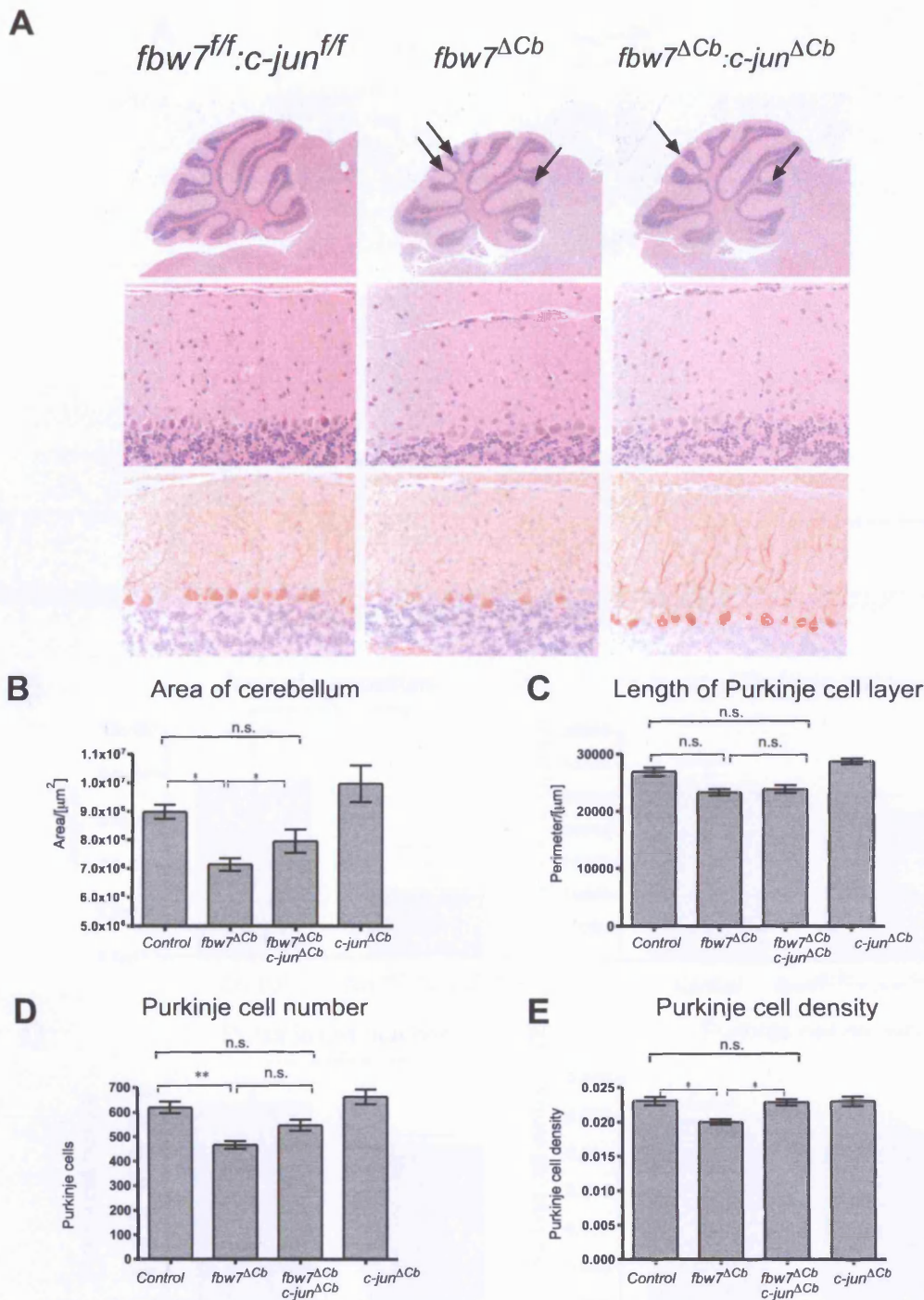
Figure 5.5 Loss of Purkinje cells in $fbw7^{\Delta Cb}$ animals is c-Jun dependent. A) H&E and Calbindin stain of Control, $fbw7^{\Delta Cb}$ and $fbw7^{\Delta Cb}$:c-$jun^{\Delta Cb}$ animals shows that the foliation defect is not rescued (arrows) B)-E) Quantification of cerebellar parameters B) The rescue in cerebellar sizeupon concomitant c-Jun deletion in only partial C) The lenght of the Purkinje cell layer is similar in $fbw7^{\Delta Cb}$ and $fbw7^{\Delta Cb}$:c-$jun^{\Delta Cb}$ animals. D) The Purkinje number is partially rescued upon concomitant c-Jun deletion. E) Rescue of Purkinje cell density in $fbw7^{\Delta Cb}$:c-$jun^{\Delta Cb}$ animals. Deletion of c-Jun in the cerebellum did not result in any significantly altered cerebellar parameters and is ftherefore not indicated in the graphs Control: n=11, $fbw7^{\Delta Cb}$: n=5, $fbw7^{\Delta Cb}$:c-$jun^{\Delta Cb}$ n=8, c-$jun^{\Delta Cb}$ n=3, Age: 2 month, Mean +/- SEM shown
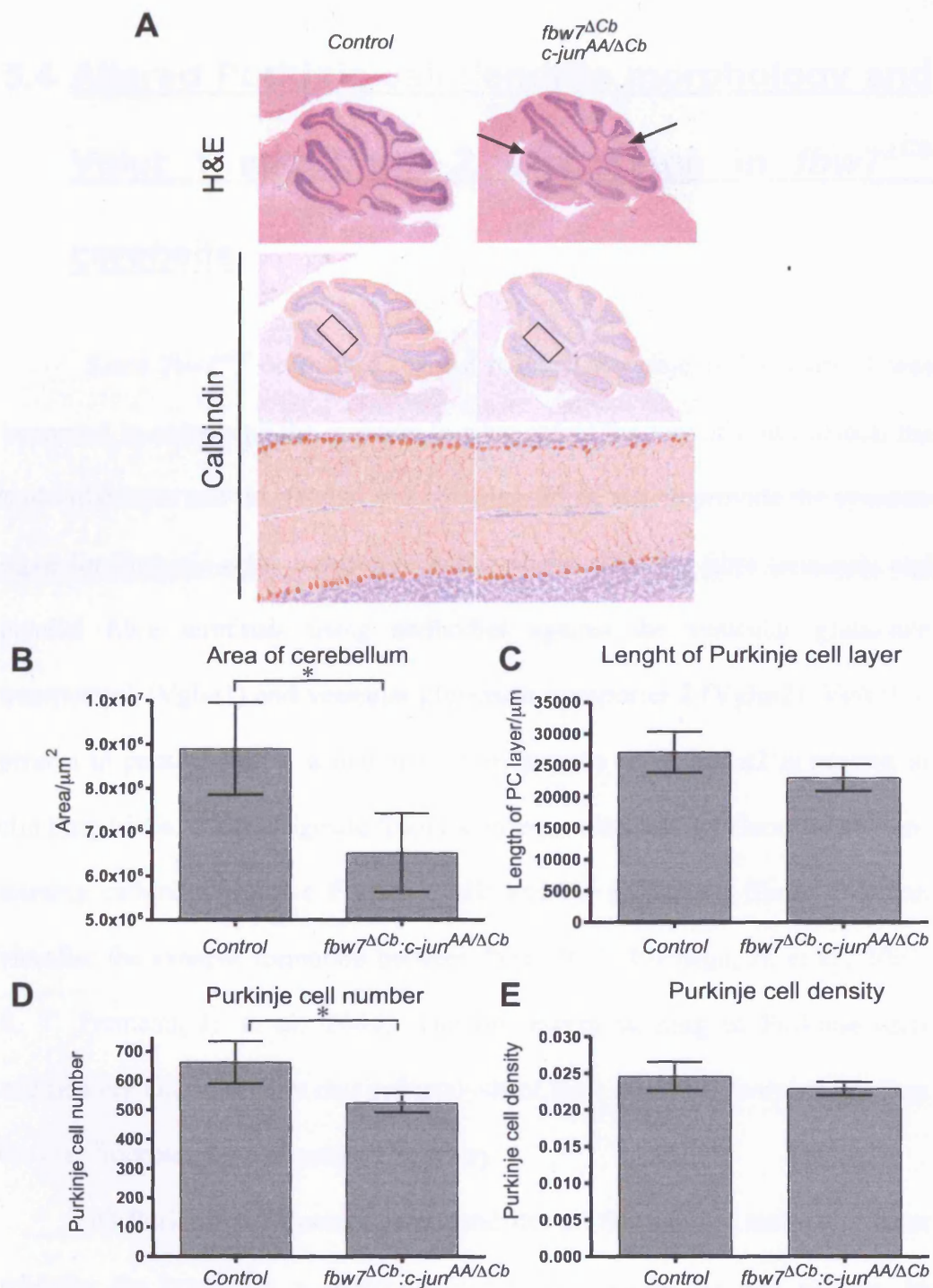
Figure 5.6 The loss of Purkinje cells is phospho-c-Jun dependent
Purkinje cell analysis in $fbw7^{\Delta Cb}{:}c\text{-}jun^{AA/\Delta Cb}$ animals. A) H&E and
Calbindin stain on adult cerebella of control and $fbw7^{\Delta Cb}{:}c\text{-}jun^{AA/\Delta Cb}$
animals. B-D: Quantification of cerbellar parameters. B) The cerebellum
is smaller than in controls, p=0.0138 C) The length of the Purkinje cell
layer is not significantly altered, p=0.0813 D) The Number of Purkinje
cells per cerebellum is reduced,p=0.0141 E) Purkinje cell density obtained
by dividing Purkinje cell number by Purkinje cell layer length, p=0.03429.
$Controls{:}$n=4, $fbw7^{\Delta Cb}{:}c\text{-}jun^{AA/\Delta Cb}{:}$n=4, Age: 4 Month, Mean+/-SD shown

5.4 Altered Purkinje cell dendrite morphology and Vglut 1 and Vglut 2 expression in $fbw7^{\Delta Cb}$ cerebella

Since $fbw7^{\Delta Cb}$ animals display a reduced Purkinje cell density, I was interested in addressing the question to what extent the loss of Fbw7 affects the molecular layer and the parallel and climbing fibres, which provide the synaptic input for Purkinje cells. I therefore analysed the climbing fibre terminals and parallel fibre terminals using antibodies against the vesicular glutamate transporter1 (Vglut1) and vesicular glutamate transporter 2 (Vglut2). Vglut1 is present in parallel fibres, which arise from granule cells. Vglut2 is present in climbing fibres, which originate from the inferior olive and by fluorescently co-staining calbindin positive Purkinje cells and the respective fibres, one can visualise the synapse formation between them (R. T. Fremeau, Jr. et al., 2001; R. T. Fremeau, Jr. et al., 2004). The fluorescent staining of Purkinje cells additionally allows a more detailed analysis of their dendritic morphology than the non-fluorescent immunohistochemistry.

Wt Purkinje cells extend their dendrites all through the molecular layer whereby the branching is increasingly refined towards the pial surface. In contrast $fbw7^{\Delta Cb}$ cerebella display a reduced punctate pattern of climbing fibre terminals and the arborisation of Purkinje cells is strongly reduced (Figure 5.7B arrows). In $fbw7^{\Delta Cb}$ cerebella the dendrites do not branch to the same degree as in wt Purkinje cells and no organised increase in higher degree branches

towards the surface can be observed. In $fbw7^{\Delta Cb}$:c-$jun^{\Delta Cb}$ cerebella the Purkinje cell morphology is only partially rescued with Purkinje cells displaying more dendrites that in $fbw7^{\Delta Cb}$ animals but there is still an obvious lack of the organised refined arborisation that is observed in wt cerebella.

Vglut2 positive climbing fibre terminals are visible as green spots along the red calbindin stained Purkinje cell dendrites in wt cerebellar sagittal sections (Figure 5.7A white arrows). Parallel to the lack of fine dendrites there appear also less Vglut2 positive dots in the molecular layer, however a definite conclusion about this cannot be made as neither the arborisation or the number of Vglut2 positive dots/dendrite was quantified. Also in $fbw7^{\Delta Cb}$:c-$jun^{\Delta Cb}$ cerebella (Figure 5.7B, right) the Vglut2 staining in respect to the present dendrites has to be quantified with regards to any possible rescue.

Within the cerebellum the parallel fibres form the only excitatory synapse on Purkinje cells dendrites. Originating from the granule cells, the parallel fibres extend along the cerebellar lobe and thus are able to make contact with a number of Purkinje cells. When comparing the staining pattern for parallel fibre terminals, using a co-stain for Vglut1 and Calbindin, cerebella from wt animals display a punctate Vglut1 staining pattern, which is apparent throughout the molecular layer (Figure 5.8A). The widely spread punctae indicate that synapses are formed on fine Purkinje cells dendrites. In $fbw7^{\Delta Cb}$ animals this staining has almost disappeared and only the stronger foci at the bigger Purkinje cell dendrites remained (Figure 5.8B). In $fbw7^{\Delta Cb}$:c-$jun^{\Delta Cb}$ cerebella, again a partial rescue of the $fbw7^{\Delta Cb}$ phenotype can be observed, with the punctate pattern being restored, but not to the full extent of the wt animal

(Figure 5.8 compare B right panel with A). However, also for this staining quantification is needed to allow for a definite conclusion regarding the phenotype and the partial rescue of the phenotype (see also discussion).

Taken together the immunofluorescence has demonstrated that there are not only fewer Purkinje cells in $fbw7^{\Delta Cb}$ animals, but that their arborisation is also reduced and the dendrites appear to be less directional towards the surface. Furthermore the number of synapses of parallel and climbing fibres in the molecular layer could be reduced, although quantification is still missing. The above experiments do not clarify whether the observed Purkinje cell phenotype is due to the loss of Fbw7 in Purkinje cell or a secondary effect from Fbw7 depletion in other cells such as granule cells (see also discussion chapter 5.7). However, the morphological defects of Purkinje cells as well as the Vglut1 and Vglut2 staining appear to be partially rescued by concomitant c-Jun deletion, which would be consistent with the hypothesis that c-Jun is a substrate for Fbw7 in the nervous system.

A *Control*

B

fbw7$^{\Delta Cb}$ *fbw7*$^{\Delta Cb}$*:c-jun*$^{\Delta Cb}$

Calbindin/Vglut2/Dapi

Figure 5.7 Impaired climbing fibre synapses in *fbw7*$^{\Delta Cb}$ animals. In wt cerebella the climbing fibres, shown in green, synapse on shafts of Purkinje Cell dendrites (white arrows). Purkinje cell dendrites extend through the molecular layer and the fine arborisation increases towards the pial surface. B) As Purkinje cells are missing in *fbw7*$^{\Delta Cb}$ animals, the number of climbing fibre-Purkinje dendrite synapses is reduced. Purkinje cell dendrite arborisation is impaired in *fbw7*$^{\Delta Cb}$cerebella and no fine branching as in the wt is observed. In *fbw7*$^{\Delta Cb}$*c-jun*$^{\Delta Cb}$ animals synapse formation is partially rescued. The Purkinje cell arborisation does not reach the same degree as in wt cerebella *fbw7*$^{\Delta Cb}$*c-jun*$^{\Delta Cb}$ cerebella.

A *Control*

B

fbw7^{ΔCb}   *fbw7*^{ΔCb}:*c-jun*^{ΔCb}
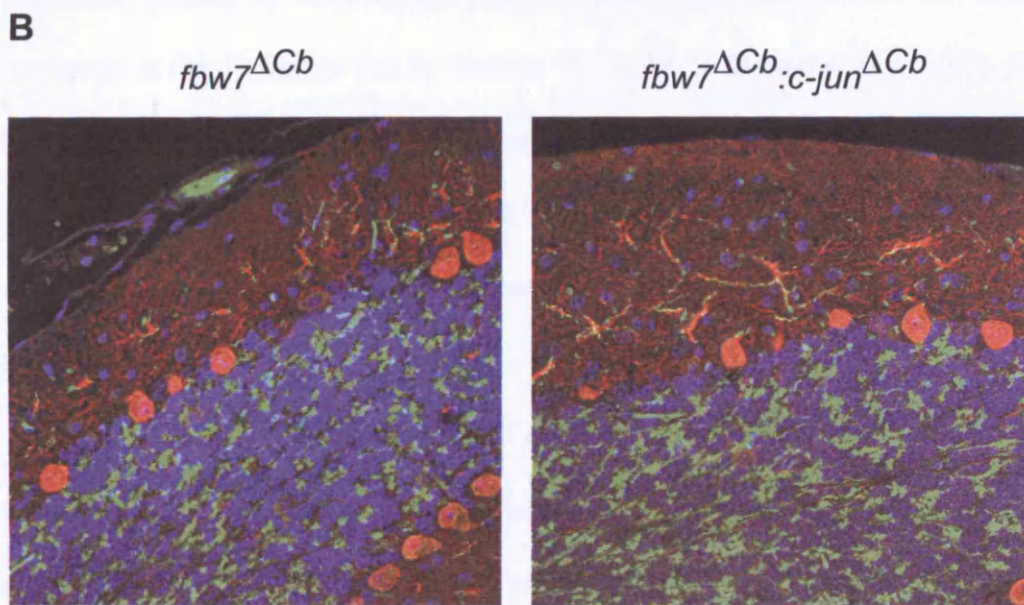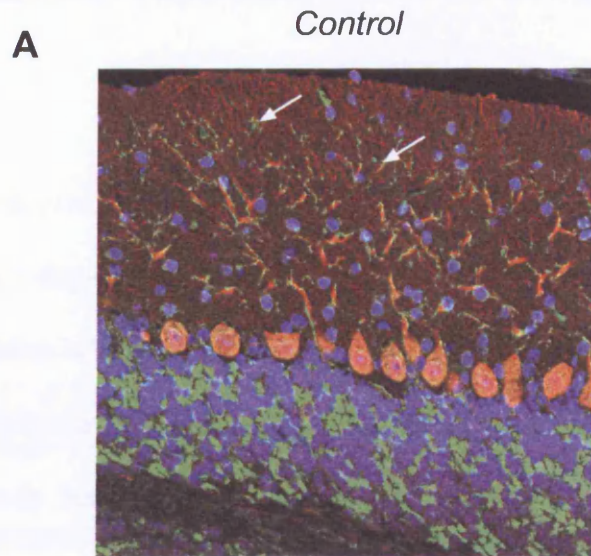
Calbindin/Vglut1/Dapi

Figure 5.8 Impaired parallel fibre synapses in *fbw7*$^{\Delta Cb}$ animals. A) In wt cerebelli parallele fibres run along the folia and synapse on Purkinje cell dendrites which is visible as green dots which extend through the molecular layer (white arrows). B) The number of parallele fibres in the Molecular Layer as indicated by a green staining in the Molecular Layer is reduced in *fbw7*$^{\Delta Cb}$ animals. Again the impaired Purkinje cell morphology can be observed. In *fbw7*$^{\Delta Cb}$:*c-jun*$^{\Delta Cb}$ animals the parallele fibre presence and synapse formation is partially rescued as also the Purkinje cell arborisation is partially rescued.

5.5 The *fbw7^{ΔCb}* phenotype is already apparent at

P07

To investigate the foliation and Purkinje cells defects further, I analysed cerebella from 7-day-old *fbw7^{ΔCb}* animals (P07) as this is the time where the cerebellar foliation is formed and cells migrate to their final position whilst at around P0 the granule cell precursors are still present in the EGL some of these cells have already become postmitotic at P07 and some started their inwards migration, passing by the Purkinje cells, to finally form the granule cell layer (reviewed in (M. E. Hatten and N. Heintz, 1995) (M. E. Hatten et al., 1997)). At the end of this differentiation process, around P14-P21, the EGL has disappeared and the cerebellar foliation is established with the molecular layer and granule cell layer separated by a monolayer of Purkinje cells reviewed in (D. Goldowitz and K. Hamre, 1998) (R. V. Sillitoe and A. L. Joyner, 2007).

Analysis of midline sagittal cut *fbw7^{ΔCb}* brains showed that at P07 the foliation defect and the gliosis that were observed in the adult animal are already present (Figure 5.9). The expression of NeuN starts when the precursor cells differentiate as they migrate inwards from the inner part of the EGL to form the granule cell layer (A. Sudarov and A. L. Joyner, 2007). In P07 *fbw7^{ΔCb}* animals as in wt animals the NeuN expression pattern begins at the inner part of the EGL (Figure 5.9 and Figure 5.10A). The additional fissure in *fbw7^{ΔCb}* animals could be the result of a hyper-proliferation during the postnatal expansion of the cerebellum. Therefore to analyse the proliferation in the

cerebellum, I injected P07 pups with BrdU and sacrificed the animals 2 hours post injection. I could find no difference in the BrdU positive cells outside the EGL at P07 suggesting that the migration is not altered at P07 in $fbw7^{\Delta Cb}$ animals (Figure 5.10B). As expected, the EGL is strongly labelled with BrdU (Figure 5.9 bottom panel), and it appears that there are slightly more BrdU positive cells in the EGL of $fbw7^{\Delta Cb}$ animals. Since $fbw7^{\Delta Cb}$ animals display an additional fissure, which can be due to a hyperproliferation in the EGL, the number of BrdU positive cells in the EGL during the first weeks of postnatal development needs to be quantified (Figure 5.10). However, as at P07 the cerebellar foliation defect is already apparent, potential differences in the EGL proliferation might be more efficiently addressed at earlier time-points such as P03 to P05 when the secondary fissures are formed, (reviewed in (A. Sudarov and A. L. Joyner, 2007)).

In P07 $fbw7^{\Delta Cb}$ animals a reduction in Purkinje cell density is already apparent (Figure 5.11). The Purkinje cell morphology is also altered. Purkinje cells of $fbw7^{\Delta Cb}$ animals have less dendrites and display a reduced arborisation pattern at P07 (Figure 5.12). In $fbw7^{\Delta Cb}:c\text{-}jun^{\Delta Cb}$ P07 sections it was apparent that although the Purkinje cell number is rescued, the morphology of Purkinje cells is only partially restored. Compared to $fbw7^{\Delta Cb}$ P07 Purkinje cells, Purkinje cells of $fbw7^{\Delta Cb}:c\text{-}jun^{\Delta Cb}$ mice have more dendrites, but full arborisation as seen in the wt cerebella is not recovered. The dendrites in $fbw7^{\Delta Cb}:c\text{-}jun^{\Delta Cb}$ Purkinje cells are widened and show an intensive calbindin stain (Figure 5.12). Thus Fbw7 deletion impairs the maturation and arborisation

of Purkinje cell in addition to playing a role during earlier Purkinje cell

development, as the loss of Purkinje cells is already present at P07.
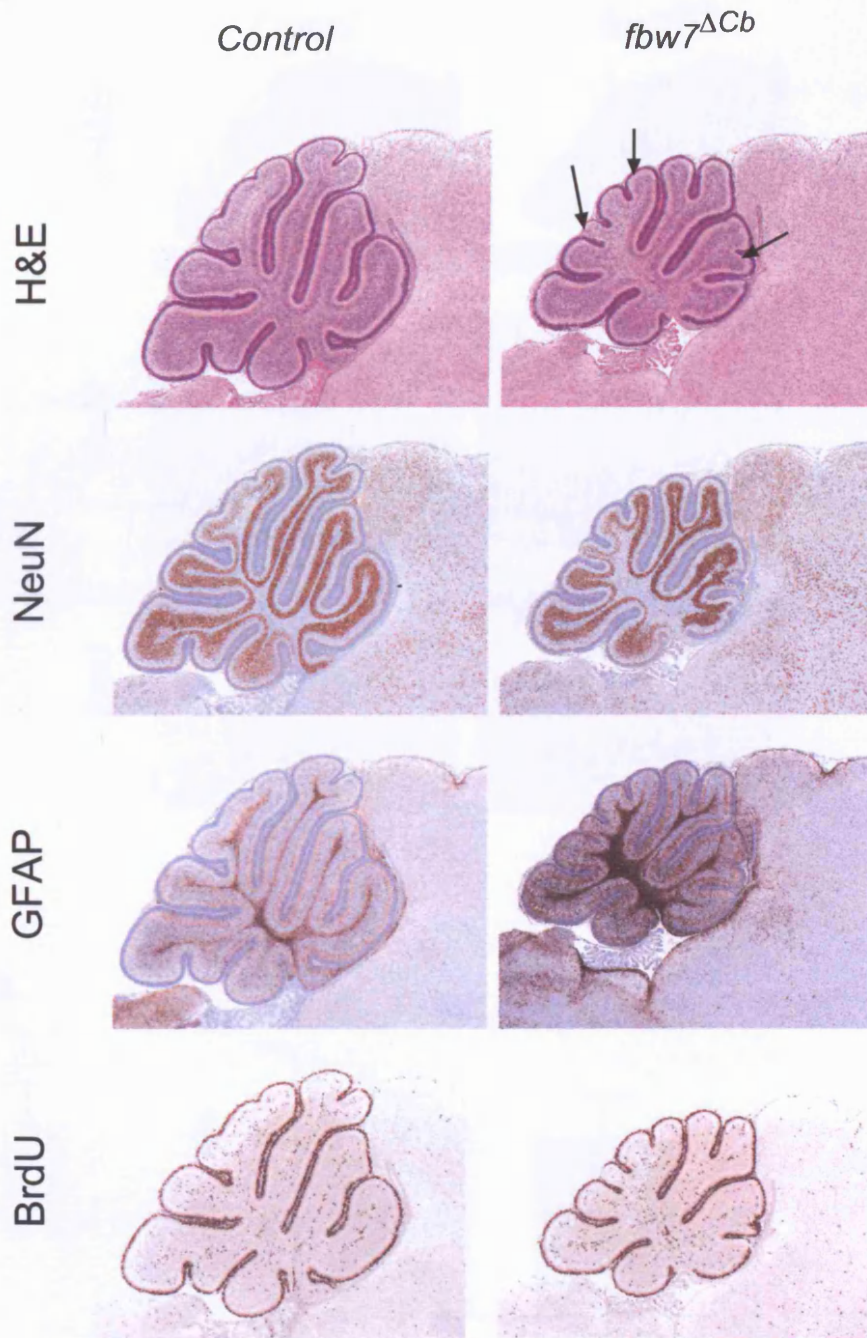
Figure 5.9 Foliation defects and gliosis are present in P07 in _fbw7_$^{\Delta Cb}$ animals A) Histological analysis of control and _fbw7_$^{\Delta Cb}$ animals at P07. The additional fissure (arrows) and the gliosis indicated by the stron GFAP stain are already present. The NeuN stained granule cell layer is normal and has already formed. BrdU labelling for two hours shows a comparable labelling of the still proliferative EGL and comparable number of BrdU positive cells inside the cerebellum (For quantification see Figure

A

Control $fbw7^{\Delta Cb}$

H&E

NeuN

BrdU

B

$BrdU^+$ cells outside the EGL

Control $fbw7^{\Delta Cb}$

n=5   n=5
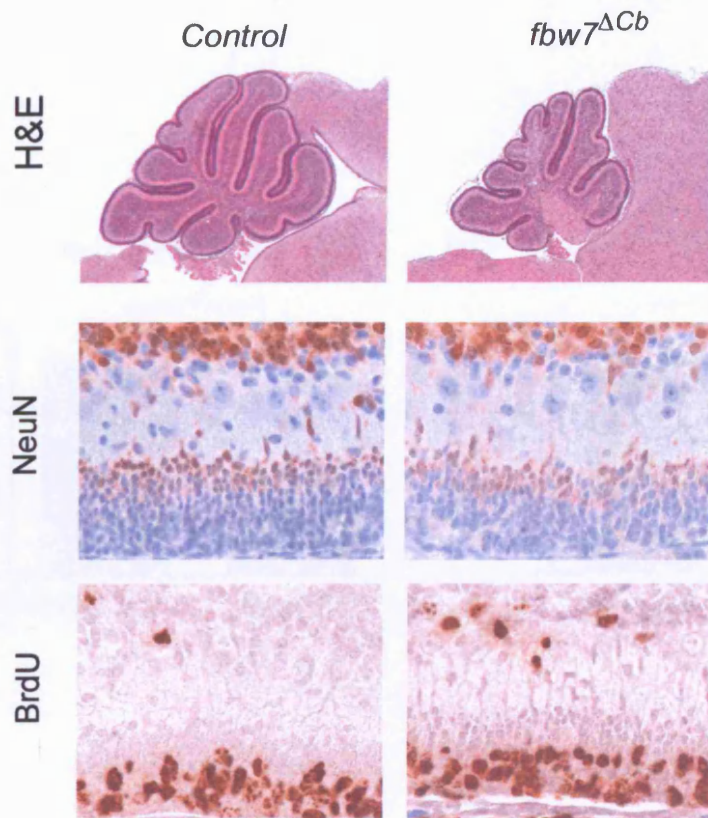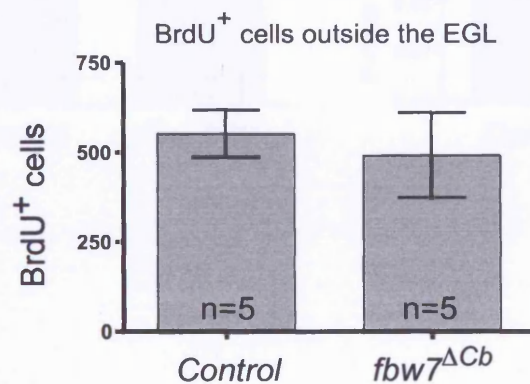
Figure 5.10 Normal granule cells and no difference in BrdU$^+$ cell inside the $fbw7^{\Delta Cb}$ P07 cerebella A)Midline sagittal sections of wt and $fbw7^{\Delta Cb}$ P07 brains. Middle: The NeuN staining confirms that granule cell differentiation and migration is normal in $fbw7^{\Delta Cb}$ animals. As cells leave the EGL and become postmitotic in the inner layer of the EGL, they start to express NeuN. Bottom: Proliferating cells were stained with BrdU for 2hours. No difference in the EGL thickness can be observed. B) Proliferation analysis of P07 brains following 2hrs after BrdU injection. BrdU positive cells outside the EGL were counted. No significant difference was observed. Mean +/- SEM shown, p=0.497: n.s.
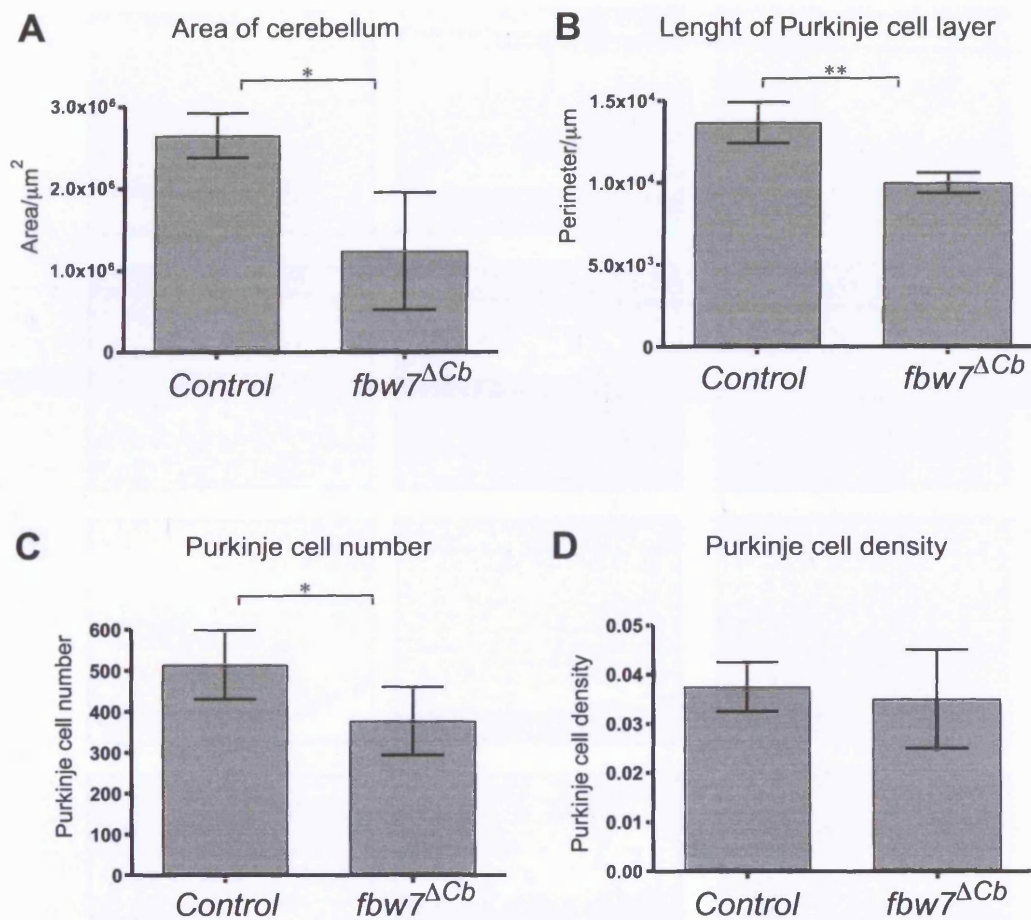
Figure 5.11 The Loss of Purkinje cells in *fbw7$^{\Delta Cb}$* animals is present at P07. Purkinje cell parameters were determined as described previously in sagittal sections of 1 week old control and *fbw7$^{\Delta Cb}$* animals A) There cerebellum is significantly smaller at P07, p=0.0103 B)Length of Purkinje cell layer, p=0.0019 C)The number of Purkinje cells per cerebellum is reduced, p=0.1143 D) The Purkinje cell density in knockout animals is reduced but not to the same extend as in adult animals, p=0.6704. Control:n=4,*fbw7$^{\Delta Cb}$*:n=4 Mean+/-SD shown
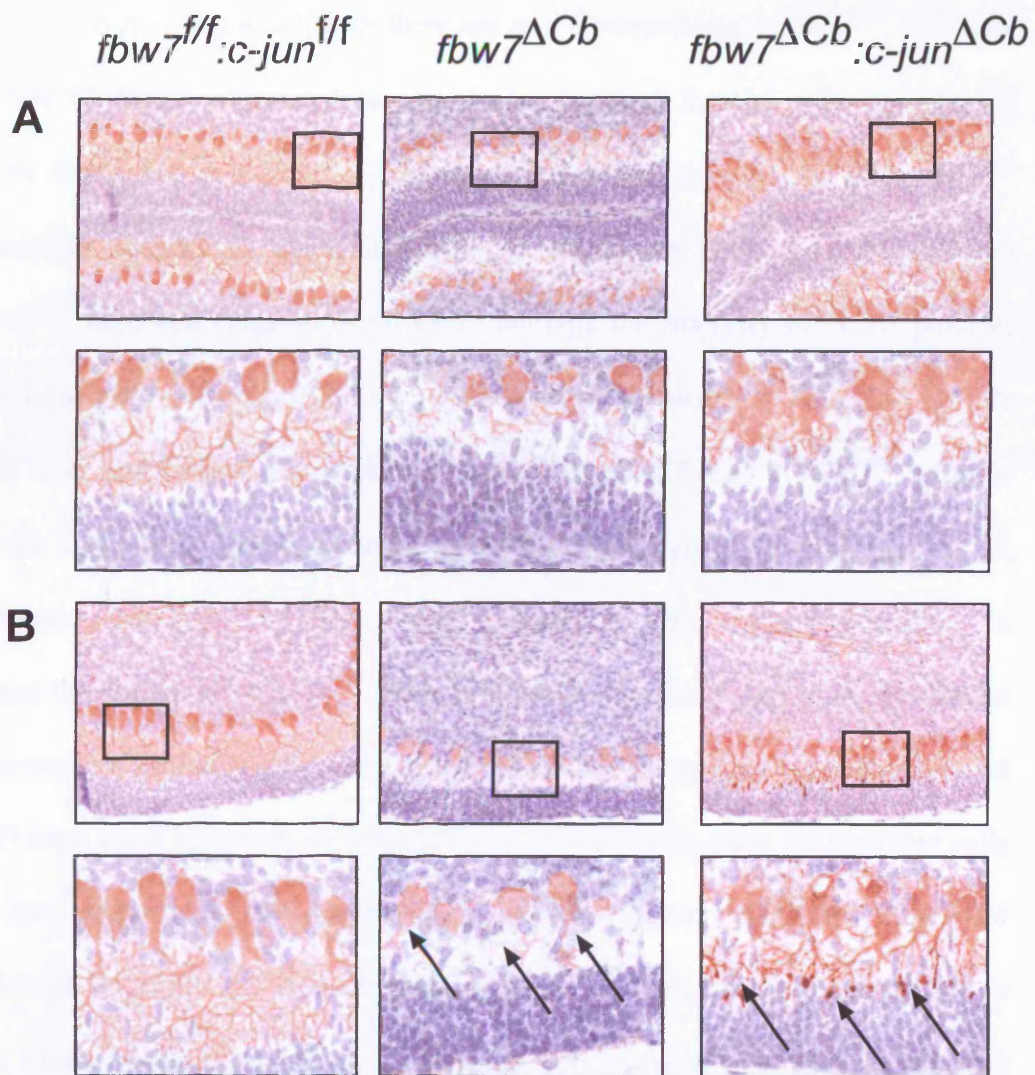
Figure 5.12 Concomitant c-Jun deletion partially rescues Purkinje cell arborisation defects in P07 fbw7$^{\Delta Cb}$ cerebella. The panel shows Calbindin stains on the indicated P07 cerebella.2 different area of the cerebellum were taken in A) and B) Purkinje cell arborisation in fbw7$^{\Delta Cb}$animals is severely impaired and partially restored in fbw7$^{\Delta Cb}$:c-jun$^{\Delta Cb}$ animals (arrows). Purkinje cells from fbw7$^{\Delta Cb}$:c-jun$^{\Delta Cb}$ do have more dendrites than fbw7$^{\Delta Cb}$ Purkinje cells, but they are less branched than in wt controls.The termini are wide and display a strong calbindin immunoreactivity.

5.6 Proliferation defects in E18 *fbw7$^{\Delta Cb}$* cerebella

To investigate whether there are any abnormalities in *fbw7$^{\Delta Cb}$* cerebella before the foliation takes place, time mated pregnant females were i.p. injected with BrdU for two hours. Analysis of proliferating cells in E18 *fbw7$^{\Delta Cb}$* cerebella showed an aberrant migration pattern of BrdU positive cells in *fbw7$^{\Delta Cb}$* cerebella (Figure 5.13). In wt animals the majority of BrdU positive cells are still residing in the EGL, start to migrate inwards to form the granule cell layer and a regular patterning is visible. The BrdU stain in *fbw7$^{\Delta Cb}$* animals in the inner part of the cerebellar primordium is more irregular (Figure 5.13, arrows). However, to assess the extent of the hyperproliferation, a quantification of BrdU positive cells in the EGL and inner part of the cerebellar primordium has still to be performed and further timepoints between E18 and P07 have to be analysed. In E18 cerebella the calbindin stain for Purkinje cells is less pronounced and appears more widely spread within the cerebellar primordium of *fbw7$^{\Delta Cb}$* animals than in the wt control, where it is restricted to the future Purkinje cell layer (Figure 5.13 bottom panel). As described in the 1.4.3.1 the fate of Purkinje cells is determined between E10 and E13 which is also the time where the Cre recombinase is active (E8.5 -12.5) (D. L. Zinyk et al., 1998). Although expression of the Cre recombinase is switched off, cells derived from deleted progenitor cells, will be Fbw7 deleted at all subsequent developmental stages. To investigate whether the Cre activity has immediate effects at E13, I analysed cerebella of E13 *fbw7$^{\Delta Cb}$* animals. The preliminary

data suggest that the E13 cerebellar primordium is formed normally and no difference in Ki67 positive proliferating cells or c-Jun protein levels could be found (Figure 5.14A). The staining with a calbindin antibody for developing Purkinje cells is very weak in both cases, most likely due to the fact that Purkinje cells are just developing and does not allow conclusions about the number of Purkinje cells. Analysis of E16 BrdU labelled cerebella gave not indication of proliferation defects at this stage and in contrast to the altered proliferation at E18, the number of BrdU labelled cells in E16 cerebella appeared comparable (Figure 5.14B).

Taken together the data from the analysis of E13 to P07 $fbw7^{\Delta Cb}$ animals allow the conclusion that the effects of the Fbw7 knockout in the cerebellum appears between E18 and P07 which is the time of extensive cell migration, expansion in cerebellar size and fissure formation.
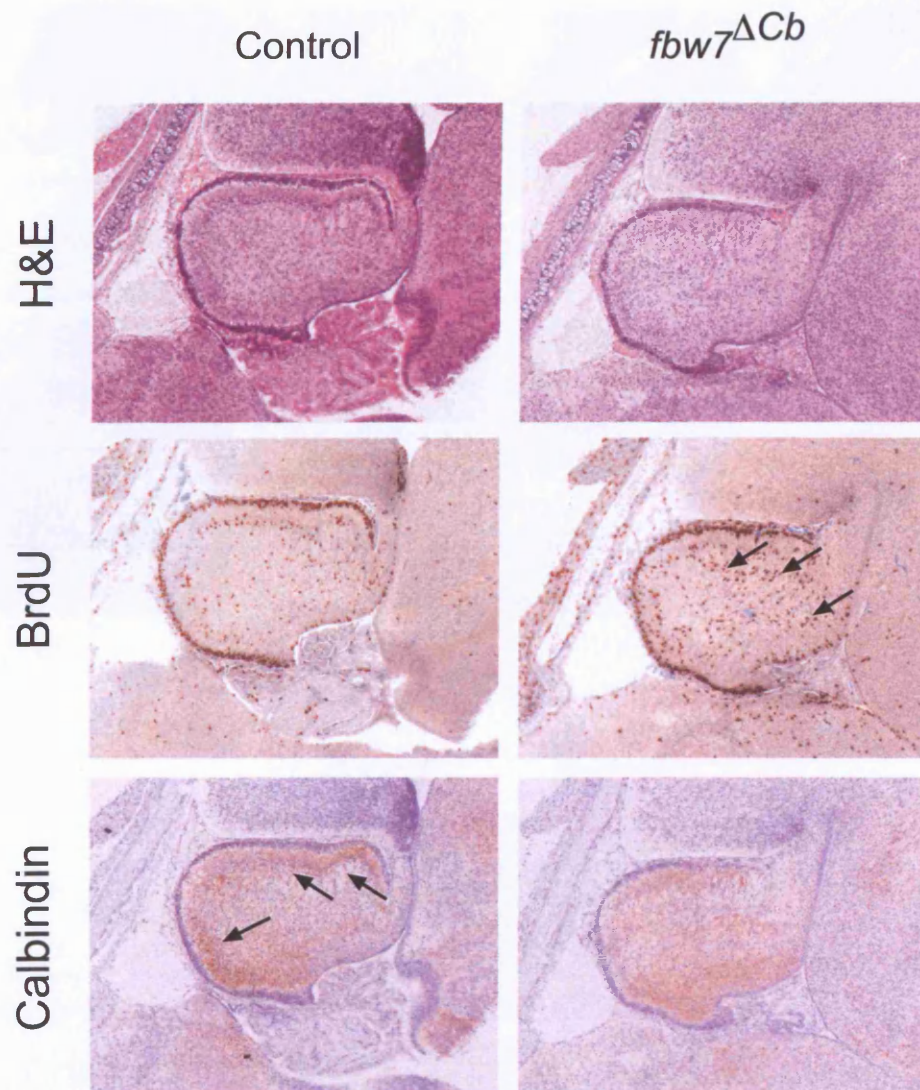
Figure 5.13 Aberrant proliferation in E18 *fbw7*$^{\Delta Cb}$ cerebella. Top: H&E (top), BrdU (middle) and Calbindin (bottom) stainings.The cerebellar foliation is not formed yet and there are no major differences in the gross appearence in the H&E stain of the cerebellar primordium. Middle: BrdU labelling (100ug/g bw. ip. 2hrs) shows a different proliferation pattern in *fbw7*$^{\Delta Cb}$ animals. More BrdU positive cells have migrated inwards (arrows) Bottom: The Calbindin stain is stronger and more evenly spread within the inner part below the EGL in control animals (arrows) than in mutants where it is weaker and more diffuse.

A

B
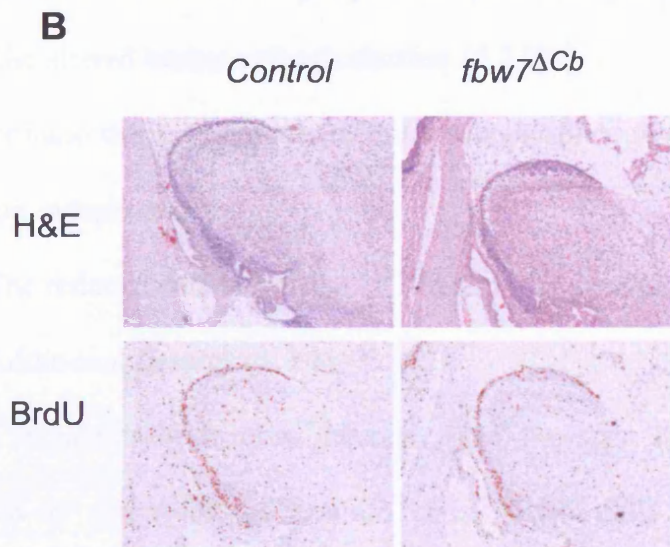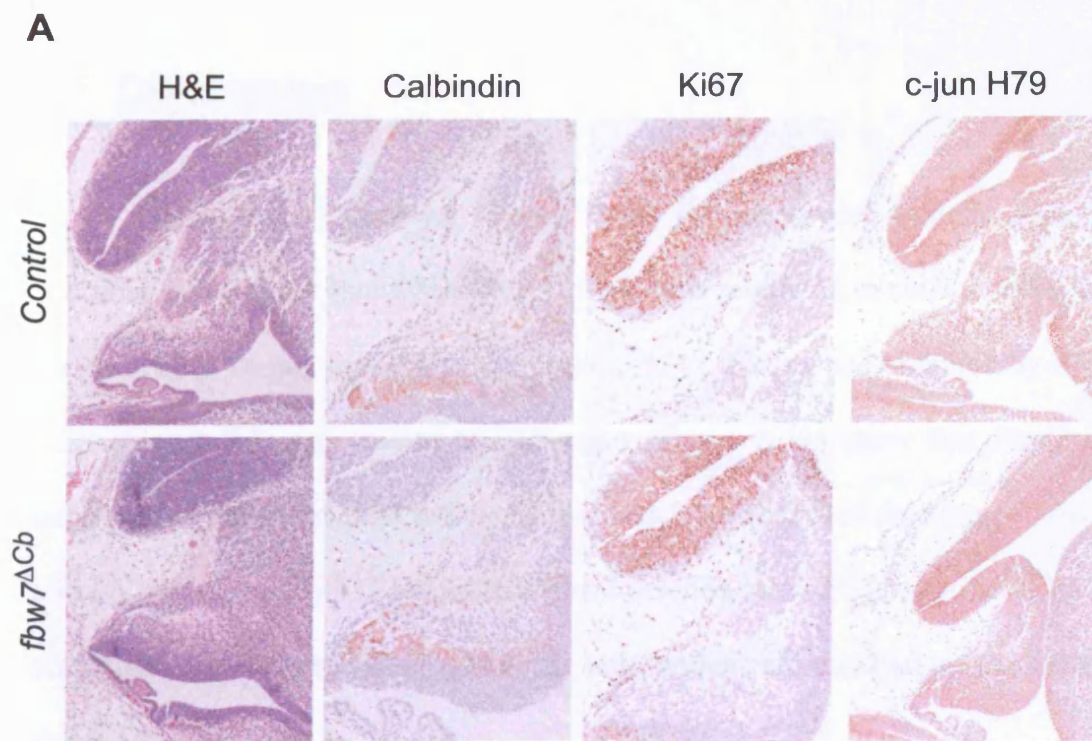
Figure 5.14 No defects in the cerebellar primordium at E13 and E16 in fbw7^ΔCb animals A) Cerebellar primordia of E13.5 embryos are comparable. Sagittal sections were stained with the antibodies indicated. Purkinje cell bodies cannot be detected with the Calbindin antibody at E13. Normal proliferation in the rhombic lip as indicated by Ki67 immunoreactivity. c-Jun (H79) expression is ubiquitious and higher c-Jun levels are detected in the proliferating area of the rhombic lip B) E16.5 time mated females were injected with BrdU for two hours and pups were analysed. The cerebellar primordia are comparable in size and structure and no difference in BrdU labelling can be observed.

5.7 **Discussion**

I have investigated the role of Fbw7 in the nervous system using a conditional knockout line where Fbw7 deletion is restricted to cells residing in the cerebellar vermis (see Appendix 1 and p.151). The results obtained by RT-PCR (Figure 3.5) and in situ hybridisation (Figure 3.11) show that Fbw7 is expressed in the cerebellum and that Engrailed-2 cre mediated deletion of Fbw7 takes place. Generally I observed that Fbw7 deletion caused a phenotype, which consisted of c-Jun dependent and c-Jun independent effects. Part of the c-Jun dependent phenotype is

1) The alteration in Purkinje cell density and morphology (5.7.1) and

2) The altered basket cell arborisation (5.7.2).

On the other hand there are aspects of the cerebellar phenotype in $fbw7^{\Delta Cb}$ mice that are c-Jun independent.:

3) The reduced cerebellar size (5.7.3) and

4) Additional fissures (5.7.4).

The in situ hybridisation detected $fbw7$ message in the granule cell layer, which is composed of granule cells, Golgi cells and mossy fibre terminals. Previous data from Nateri et al. demonstrated that in cultured cgcs Fbw7 message is present and that Fbw7 depletion by siRNA caused an increase in apoptosis suggesting that Fbw7 is indeed expressed in granule cells (A. S. Nateri et al., 2004). A detailed analysis regarding the Fbw7 protein levels and expression in different cerebellar populations has not been performed yet.

However, this will be necessary to elucidate which cells express Fbw7 and thus contribute to the observed phenotype as for all points mentioned above the reason for the phenotype can either be direct due to the loss of Fbw7 expression in the respective cell type, or indirect due to secondary effects caused by Fbw7 deletion elsewhere in the cerebellum. This is discussed in the following section.

5.7.1 Alterations in Purkinje cell density and morphology

Fbw7 deletion in the cerebellum results in a persistent 20% reduction in the Purkinje cell density in adult animals, which is rescued upon either concomitant deletion of c-Jun (Figure 5.5) or expression of a *c-jun* allele that cannot be phosphorylated (Figure 5.6). Therefore these data suggest that Fbw7 mediated regulation of phospho-c-Jun is important for Purkinje cell development before P07. The Purkinje cell arborisation defect, on the other hand, is only partially rescued in the $fbw7^{\Delta Cb}$:c-$jun^{\Delta Cb}$ and $fbw7^{\Delta Cb}$:jun^{AA} animals which suggests that additionally other substrates of Fbw7 play a role in the $fbw7^{\Delta Cb}$ phenotype. Furthermore, from the experiments conducted in this thesis, it is not possible to conclude whether the observed reduction in Purkinje cells and their reduced arborisation are due to the loss of Fbw7 in them or due to a secondary effect from, for instance, the deletion of Fbw7 in granule cells, which have been shown to be important for Purkinje cell development. Both possibilities of a direct or indirect effect and the possible involvement of other substrates are discussed below (chapters 5.7.1.1 and 5.7.1.2 , chapter 5.7.4).

5.7.1.1 Hypothesis I: The Purkinje cell defect is a secondary effect caused by Fbw7 deletion in other cerebellar cells

fbw7 message was detected by in situ hybridisation in the granule cell layer, but no convincing hybridisation signal in the Purkinje cell monolayer at the outer part of the granule cells was observed (Figure 3.11). This suggests that Fbw7 levels might be absent or low in the adult Purkinje cells and argues in favour of the hypothesis that the loss of Purkinje cells is a secondary effect. Although Purkinje cells are generated early during cerebellar development they develop their dendritic tree during the first 2-3 postnatal weeks (reviewed in (J. P. Kapfhammer, 2004)). Briefly, Purkinje cells start to polarise shortly before birth and develop an axon and non-branched dendrite. During the first postnatal days Purkinje cells extend more processes from their cell body and assume an intermediate "stellate" morphology. At this time the first input that reaches these Purkinje cells are climbing fibres whilst parallel fibres are just starting to develop (reviewed in (J. P. Kapfhammer, 2004)). Following the first postnatal week the dendrites start to elongate and an extensive synaptogenesis between Purkinje cell dendrites and the parallel fibres takes place (J. Altman, 1972c, b). Another study by the same authors made use of X-irradiation to kill granule, stellate and basket cells in neonatal rats and this subsequently caused mislocalisation of Purkinje cells whose dendrites lost their pial orientation and extend in a random fashion (J. Altman and W. J. Anderson, 1972). Additionally Baptista et al. demonstrated that isolated Purkinje cells do develop dendritic arbours when co-cultured with granule cells but that in the absence of them or co-culture with cells that provide only inappropriate input, the arborisation is

impaired and not as refined as under co-cultured conditions with granule cells (C. A. Baptista et al., 1994). Thus it has been shown that during early postnatal development Purkinje cells are dependent on appropriate afferent input from parallel fibres to form their characteristic dendritic tree. One could therefore envisage a model where Fbw7 deleted granule cells are not able to provide the required input and this subsequently leads to the observed defects in arborisation.

Another point supporting the hypothesis that the Purkinje cell defect is secondary to a granule cell phenotype is the reduced Vglut1 staining in the $fbw7^{\Delta Cb}$ knockouts. Altman et al. have demonstrated in 1972 that the axons of granule cells, the parallel fibres, are formed before their cell bodies move inwards to form the IGL (J. Altman, 1972a). Furthermore Altmans studies describe that as Purkinje cells mature, parallel fibre-Purkinje cell synapses are not present on the smooth primary dendrite, but only on secondary and ternary dendrites and form first on dendritic spines in the lower part of the molecular layer and subsequently in the upper part (J. Altman, 1972c). As the number of secondary and ternary fine dendrites was strongly reduced in $fbw7^{\Delta Cb}$ Purkinje cells, the reduced number of Vglut1 positive dots that indicate parallel fibre-Purkinje cell synapses in the molecular layer could just reflect the above described possible defect of granule cells in providing an appropriate input for Purkinje cell dendrite maturation.

The observation that the Vglut1 and Vglut2 stainings are only partially rescued upon concomitant deletion of Fbw7 and c-Jun (Figures 5.7 and 5.8) could be due to the fact that a potential granule cell defect is still present in $fbw7^{\Delta Cb}:c\text{-}jun^{\Delta Cb}$ animals and especially the Purkinje cell dendrites are not as

finely branched compared to wt animals at P07 (Figure 5.11). Nonetheless a partial rescue appears to take place with the Purkinje cell density being restored in the adult upon either deletion of c-Jun or expression of the jun^{AA} allele. The partial rescue of the phenotype where the foliation defect is not rescued in $fbw7^{\Delta Cb}$:c-$jun^{\Delta Cb}$ animals but Purkinje cell density is rescued, furthermore indicates that other substrates mediate the phenotype. One particular substrate could be N-myc whose possible involvement is discussed in chapter 5.7.3.

The further analysis of the obtained $fbw7^{\Delta Cb}$:c-$jun^{\Delta Cb/AA}$ cerebella by immunofluorescence with calbindin, Vglut1 and Vglut2 antibodies will be valuable in investigating the effect of Fbw7 during the cerebellar development. In *Drosophila*, the AP-1 complex has been shown to regulate synaptic plasticity of neuromuscular junctions through activation of CREB (S. Sanyal et al., 2002). Also in rats c-Jun and AP-1 have been implicated in memory formation, which is associated with formation of synapses (W. C. Abraham et al., 1993). Thus the generated cerebellar knockout lines could be a useful tool for the investigation of the role of c-Jun and phospho-c-Jun during synapse formation between parallel fibres and Purkinje cell dendrites. Purkinje cells and climbing and terminal fibre synapses can be labelled with the mentioned antibodies and one could therefore investigate the initial stages of the synapse formation in sections of cerebella from animals between P0 and P14 or culture cerebellar slices.

To test the hypothesis that granule cells are affected by the Fbw7 deletion in the cerebellum and loose their ability to promote Purkinje cell maturation it is essential to analyse the expression of Fbw7 during the cerebellar development and to determine whether Fbw7 is expressed in the

granule cell precursors and is required for their parallel fibre formation. The in situ hybridisation data obtained from the E18 $fbw7^{\Delta N}$ cerebellar primordium (Figure 3.8) do not allow a conclusion regarding the Fbw7 expression in distinct cerebellar populations in the cerebellar anlage. This could be either achieved by antibody stainings if in the future there are antibodies that can detect the endogenous protein, or by non-radioactive in situ hybridisation where cells of the cerebellar primordium can be additionally macroscopically characterised. A fractionation of cerebellar cells as performed by Marino et al could also be useful in distinguishing which cellular population is recombined successfully in the cerebellum and also expresses the Fbw7 protein. However, the latter would be dependent on a functional Fbw7 antibody (S. Marino et al., 2003).

To address whether the observed Purkinje cell defect is secondary to a granule cell defect one could also employ a granule cell specific conditional knockout line. Two groups have generated Cre transgenic lines in which the transcription of an activatable form of the Cre recombinase (CreER™ activated by tamoxifen and CrePR activated by antiprogestins) is either placed under the granule cell specific Math1 enhancer (L. M. Chow et al., 2006) or is expressed under the granule cell specific GluRε3 promotor (M. Tsujita et al., 1999). These lines could be useful to investigate to what extent granule cells cause the Purkinje cell defect. If the Purkinje cell defects were a consequence of Fbw7 deletion in granule cells, one would predict that deletion of Fbw7 in granule cells alone causes the same Purkinje cell phenotype as observed in the $fbw7^{\Delta Cb}$ mice.

5.7.1.2 Hypothesis II: Purkinje cells require Fbw7 during development and the observed defect is the result of Fbw7 deletion in precursors

If the observed defect were caused directly by the loss of Fbw7 in the cerebellar Purkinje cell precursors one could speculate that Purkinje cells are particularly sensitive to elevated phospho-c-Jun levels during embryonic development and therefore require Fbw7 activity (see Model in Figure 5.15). As there is no progressive loss of Purkinje cells after birth in $fbw7^{\Delta Cb}$ cerebella, one can further hypothesise that mature Purkinje cells do not express c-Jun and thus no regulation is required, possibly because they do not utilise an active JNK pathway. Alternatively Purkinje cells could be able to adapt and to tolerate increased phospho-c-Jun levels or that the JNK c-Jun pathway is controlled in an Fbw7 independent way.

Concerning the absence of the JNK-c-Jun pathway and c-Jun levels in the adult brain, a number of studies have demonstrated that in mature Purkinje cells c-Jun protein and message levels are below a detectable level, indicating that c-Jun is not employed during mature Purkinje cell function (T. Herdegen et al., 1995; M. Zagrebelsky et al., 1998; D. Carulli et al., 2002). Furthermore the JNK pathway does not appear to be active in mature Purkinje cells, as in mice overexpressing c-Jun under the Purkinje cell specific L7 promoter did not alter Purkinje cell arborisation, density or morphology. More importantly this did not result in elevated levels of phosphorylated c-Jun or an increase in Purkinje cell apoptosis (D. Carulli et al., 2002). As c-Jun phosphorylation is not induced in mature Purkinje cells, deletion of Fbw7 will most likely have no effect. The

inactivity of the JNK pathway is therefore a possible explanation why there is no progressive loss of Purkinje cell in the adult.

The fact that proteins of the JNK signalling cascade such as MKK4, JIP-1 and JIP-3 are expressed in mature Purkinje cells, nevertheless indicates that this signalling cascade has been used at some point in their life, possibly during development (J. K. Lee et al., 1999; J. B. Pellet et al., 2000; E. Miura et al., 2006). It is therefore feasible to assume that the loss of Purkinje cells during development can be caused by elevated phospho-c-Jun levels. Regarding the analysis of c-Jun during Purkinje cell development stainings with phospho-c-Jun specific antibodies have to be performed. Interestingly, in cerebellar slices derived from P09 c-Jun transgenic cerebella, Purkinje cell survival was reduced, implying that the JNK cascade and subsequently phospho-c-Jun levels can be activated under stress conditions, such as the *in vitro* culture, and mediate Purkinje cell death (D. Carulli et al., 2002). Therefore one could culture cerebellar slices obtained from $fbw7^{\Delta Cb}$ animals and predict that Purkinje cells would die in a similar manner as in slices from c-Jun transgenic animals, since the stress implied by the culture conditions appears to be sufficient to activate the JNK-Jun pathway.

Purkinje cells from $fbw7^{\Delta Cb}$ animals display an altered morphology by P07 and the number of dendrites is greatly reduced (Figure 5.7). The altered Purkinje cell morphology could also affect the formation of synapses within the cerebellum such that fewer Purkinje cell-parallel fibre and Purkinje cells-climbing fibre synapses are present in $fbw7^{\Delta Cb}$ animals (Figure 5.7 and 5.8). To test whether this hypothesis is valid one could cross floxed fbw7 mice to animals that express the Cre-recombinase under the Purkinje cell specific L7

promoter (J. Oberdick et al., 1990). If the defect were caused by loss of Fbw7 in Purkinje cells, these animals should recapitulate the observed Purkinje cell phenotype.

5.7.2 Altered basket cell arborisation

In addition to the loss of Purkinje cells, the basket cell arborisation is altered in $fbw7^{\Delta Cb}$ animals and could be rescued upon concomitant deletion of c-Jun (Figure 5.2). Although I did not quantify apoptosis by TUNEL staining in the ML, I did not find any difference in the number of parvalbumin stained basket and stellate cells (Figure 5.3) and therefore conclude that loss of Fbw7 does not lead to apoptosis in these cells but rather to an aberrant morphology of their axons. Interestingly the Neurofilament200 expressing basket cells and the stellate cells are derived from the same germinal layer, the ventricular zone, as the Purkinje cells. All three cell types belong to the class of GABA-ergic so it could also be possible, that loss of Fbw7 specifically affects neurons that use GABA as a neurotransmitter and are derived from the ventricular zone. To address this hypothesis, one could for instance perform *in situ* hybridisation on E13 and earlier cerebella. If Fbw7 were crucial in the ventricular zone, this would then lead to the prediction that also stellate cells should also display an altered morphology in the Fbw7 knockout. Whilst basket cells were investigated using a Neurofilament200 antibody, no detailed analysis of stellate cells was performed so far.

Basket cells inhibit Purkinje cells by means of their basket like synapses on the Purkinje cell somata but are at the same time connected to the parallel fibres which in the rat start to synapse on basket cells around postnatal day 8,

(J. Altman and A. T. Winfree, 1977) (reviewed in (R. V. Sillitoe and A. L. Joyner, 2007)). Therefore the possibility that the altered basket cell axonal arborisation is due to defects in the parallel fibres or their development is also given. Experiments as outlined under 5.7.1.1 will help to clarify this question as well. Similar to the Purkinje cells one would expect a recapitulation of the phenotype upon a granule cell specific deletion of Fbw7 if the basket cell arborisation were impaired as a secondary effect.

5.7.3 **Reduced cerebellar size**

All Fbw7 cerebellar knockout mice investigated in this study have a smaller cerebellar vermis, indicating that this is a c-Jun independent effect of the Fbw7 deletion. This phenotype can be caused by either less cells being present, or by an increase in apoptosis. Nateri et al. demonstrated that in wt cgcs siRNA mediated Fbw7 depletion causes an increase in apoptosis and if this occurred *in vivo* in granule cells, this could explain the smaller cerebellum (A. S. Nateri et al., 2004). Alternatively apoptosis could also occur at the early progenitor was described for the Engrailed-2 mediated conditional knockout of Notch-1 where mice also display a smaller cerebellum and a reduction in Purkinje cell density due to the loss of early precursor cells (S. Lutolf et al., 2002). The same study elucidated that in case of the Notch-1 cerebellar knockout the level of apoptosis in different progenitor populations peaks at E12, a day earlier than the time points I have investigated in the Fbw7 conditional knockout so far. Therefore the careful analysis of apoptosis in the granule cell layer by TUNEL assays at different timepoints during embryonic and postnatal development is mandatory to clarify whether apoptosis of granule

cell precursors or mature granule cells causes the smaller cerebellar vermis in

$fbw7^{\Delta Cb}$ animals. Math1, the earliest known marker for granule cells together

with TUNEL staining on time mated embryos could provide essential insights

of whether the defect in $fbw7^{\Delta Cb}$ animals is similar to the one observed in the

Notch-1 cerebellar knockout and deletion of Fbw7 causes a depletion at the

cerebellar precursor cell stage (F. Guillemot and A. L. Joyner, 1993; N. Ben-

Arie et al., 1997).

5.7.4 Additional fissures

The $fbw7^{\Delta Cb}$ animals display additional fissures in the cerebellum (Fig

5.1) that is already present at P07 (Fig. 5.9), however, the overall structure of

the cerebellar layers and shape is preserved. The formation of the cerebellar

lobes occurs in distinct phases whereby first the so-called four cardinal lobes

are formed at around E17.5 in mice and the other finer fissures develop

postnatally (reviewed in (R. V. Sillitoe and A. L. Joyner, 2007)). Work by

Corrales et al has shown that the fissure formation depends directly on the

levels of Shh signalling and that increased Shh signalling produces a more

complex foliation (J. D. Corrales et al., 2006) whilst the loss of Shh activity

causes a reduced foliation (P. M. Lewis et al., 2004). Shh is secreted by

Purkinje cells during normal cerebellar development and induces proliferation

in granule cell (V. A. Wallace, 1999; P. S. Knoepfler et al., 2002; A. M.

Kenney et al., 2003). N-myc is a crucial mediator of Shh-signalling and is

expressed in granule cell precursors where it is essential for proliferation (B. A.

Hatton et al., 2006) (T. G. Oliver et al., 2003). Welcker and colleagues found

that N-myc is also a substrate of Fbw7 and as the phospho-degron of c-Myc is

198

conserved in N-myc, it is possible that Fbw7 also regulates N-myc (Figure 5.16A)(M. Welcker et al., 2004a). Since the cerebellar foliation defects cannot be rescued by concomitant c-Jun deletion, this indicates that in addition to c-Jun other substrates that promote granule cell proliferation participate in the phenotype of the $fbw7^{\Delta Cb}$ animals. The hypothesis that granule cell precursors hyperproliferate is supported not only by the additional fissure but also the enhanced BrdU immunoreactivity at E18 in the cerebellar primordium, which however still has to be quantified (Figure 5.14). If N-myc were a substrate of Fbw7 in the EGL, this could explain such a hyperproliferation of granule cells. If Fbw7 could not degrade N-myc, one would expect an increase in proliferation, as observed at E18 in $fbw7^{\Delta Cb}$ animals, which could ultimately lead to the generation of an additional cerebellar fissure (see model in Figure 5.16B). The notion that there are more BrdU labelled cells in the EGL of P07 BrdU injected $fbw7^{\Delta Cb}$ animals does indicate that more proliferation takes place, and it is essential to quantify this in order to identify the precise timing of the hyperproliferation (Figure 5.10). The data from the Purkinje cell analysis also imply that cells of the granule cell layer proliferate more in the $fbw7^{\Delta Cb}$ animals than in wt animals. Whilst the Purkinje number is reduced to the same extent in P07 mice as in adult animals, the density is not. This indicates that the Purkinje cell layer length increases after P07 so that in the adult the Purkinje cell density is reduced in $fbw7^{\Delta Cb}$ vs. control cerebella. Since the Purkinje cell layer length is measured as the perimeter of the whole Purkinje cell layer, this furthermore predicts, that there must be more granule cells present.

The hypothesis that N-myc is a substrate of Fbw7 in the cerebellum is based on the assumption that Fbw7 is not only expressed in mature granule cells (Figure 5.9) but also in granule cell precursors. Experiments that can be done to investigate this include *in situ* hybridisation for Fbw7 on E18 cerebella when the EGL is still present as well as immunohistochemistry and western blotting experiments for N-myc to assess whether N-myc accumulates in the *fbw7*$^{\Delta Cb}$ and Fbw7:c-Jun double mutants. The finding that Fbw7 is suppressed in gliomas, and that downregulation of Fbw7 inversely correlated with an increase in N-myc levels, further supports the hypothesis that N-myc could be one major substrate of Fbw7 during cerebellar development (M. Hagedorn et al., 2007) (M. Bredel et al., 2005) In addition to the aforementioned stainings, another approach to investigate the Fbw7 deleted neurons in knockout mice would be to use GFP-reporter mice where Fbw7 deleted cells can be identified by their GFP expression. This cross would allow the tracing of Fbw7 depleted neurons in the cerebellum. This could also give insights whether Fbw7 expression can be correlated with certain classes of neurons such as GABA-ergic or neurons or to what extent Fbw7 deleted neurons die during development.

Genotypes

Protein levels	wt	$fbw7^{\Delta Cb}$	$fbw7^{\Delta Cb}$ $c\text{-}jun^{\Delta Cb}$	$fbw7^{\Delta Cb}$ $c\text{-}jun^{\Delta Cb/AA}$	
Progenitor cell	●	●	●	●	E13
Fbw7	++	--	--	--	
c-Jun	++	++	--	++	Development
phospho-c-Jun (predicted)	--	+++	--	--	

PC
BC
GC

P07
ML
GL
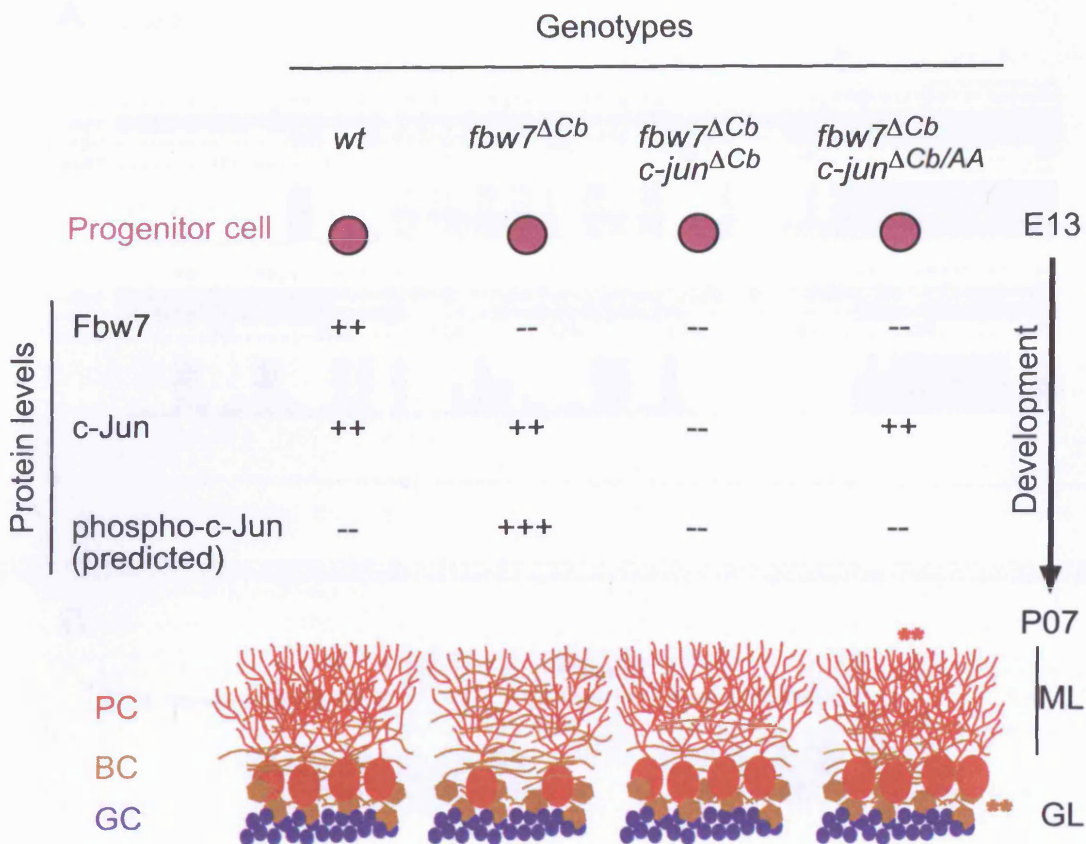
Figure 5.15 Model for Fbw7 mediated phospho-c-Jun regulation during cerebellar development Protein levels are indicated as ++ if present and -- if they are absent due to the knockout or successfully downregulated. Data obtained are summarised in this table. Left panel: As development from progenitor cells (purple) to mature Purkinje cells (red) and Basket cells (brown) proceeds, phospho-c-Jun levels need to be downregulated by Fbw7 to allow Purkinje cell maturation and dendritic arborisation.Basket cell axons (brown) surround Purkinje cells (red) and extend through the lower half of the Molecular layer (ML) and Purkinje cells receive input from basket cell axons. The Purkinje cell layer separates the ML from the granule cell layer (GL). In wt animals Purkinje cell dendrites form an elaborate network extending through the ML 2nd from left: If phospho-c-Jun accumulates due to the lack of Fbw7 less Purkinje cells are present, possibly because early precursors die, and the arborisation of the remaining Purkinje cells is reduces. The basket cell arborisation is impaired and extends through the whole Molecular layer. Concomitant deletion of c-Jun and Fbw7 (3rd from left) rescues the Purkinje cell number and basket cell arborisation. However, the number of dendrites is still reduced. The Purkinje cell number is also in $fbw7^{\Delta Cb}$:c-$Jun^{\Delta Cb/AA}$ mice(right panel), indicating that phosphorylated c-Jun is the cause of the observed phenotype. However, a detailed analysis of Purkinje cell dendrites and Basket cell axon morphology has still to be carried out and the normal morphology are predictions (askterisks).

A


```
              **    :   :* **::**:** *  **:: **.   :*   ..*.********* ************
c-Myc   MDFLEALETPQTATTMPLNVNFTNRNYDLDYDSVQPFFICDEEENFYHQQQQSELQPPAPSEDIWKKFELLPTPPLSPSR   80
n-Myc   ---------------MPG---MICKNPDLEFDSLQPCFYPDEDD-FYFGGPDS----TPPGEDIWKKFELLPTPPLSPSR   57
ruler   1.......10........20........30........40........50........60........70........80

              **.    **.:  *  *   *    ..*::   :    ***    *          :*:********* **
c-Myc   RSGLCSPSFVAVATSFSPREDDDGGGGNFSTADQLEMMTELLGGDMVNQSFICDFDDETFIKNIIIQDCMWSGFSAAAKL   160
n-Myc   AFPEHSPEPSNWATEMLLPEADLFG----NPAEEDAFGLGGLGGLTPNP-----------VILQDCMWSGFSAREKL     119
ruler   .......90.......100......110......120......130......140......150......160
```

B

Figure 5.16 Model for a putative role of N-myc as a Fbw7 target in granule cell development A) Alignment of the mouse c-myc and N-myc amino acid sequence. The phospho-degron is conserved (red rectangle), indicating that N-myc is likely to be a substrate of Fbw7. B) Granule cell development in the fbw7^ΔCb cerebellum. In the normal cerebellum Sonic hedgehog (Shh) induces N-myc expression. N-myc is degraded by Fbw7, and granule cell precursors (dark blue) differentiate (light blue) and migrate inwards. In fbw7^ΔCb animals N-myc induction by Shh is reduced due to the lack of Purkinje cells. However, as N-myc is not degraded by Fbw7, N-myc accumulates induces proliferation in the EGL which subsequently lead to more granule cells and the formation of an additional fissure in fbw7^ΔCb brains.

6 FBW7 DELETION IN POSTMITOTIC NEURONS CAUSES A TREMOR, HINDLIMB DEFECT AND REDUCED CORTICAL CELLULARITY

So far I have described two different approaches to investigate the role of Fbw7 in the nervous system. In the first approach Fbw7 was deleted in neuronal progenitor cells ($fbw7^{\Delta N}$) while in the $fbw7^{\Delta Cb}$ mice the deletion was restricted to a specific area in the brain, the cerebellar vermis. The data obtained from these two lines demonstrated that Fbw7 is essential during neurogenesis and synapse formation. Furthermore it became apparent that the Fbw7 knockout phenotypes contain c-Jun dependent and c-Jun independent components. The deletion of Fbw7 occurred during developmental stages where precursor cells are affected and in both cases a reduced cellularity or smaller cerebellum was observed. These results lead to the hypothesis that Fbw7 deficient cells might die at early stages of neuronal differentiation in these mouse lines.

To investigate the role of Fbw7 in postmitotic neurons, I used a mouse line where the Cre-recombinase is expressed under the control of the Synapsin-1 promoter to generate animals that are $fbw7^{f/f}$:$Synapsin$-cre^{+} ($fbw7^{\Delta pN}$). In this mouse line the Cre mediated deletion is limited to postmitotic neurons in the brain and in the spinal cord (C. Hoesche et al., 1993; Y. Zhu et al., 2001). The histological analysis of Zhu et al. with NeuN as a neuronal marker in lacZ reporter mice demonstrated that Cre activity is mainly

distributed in differentiated neurons outside the ventricular regions of the brain and spinal cord. Whilst neurons in the spinal cord, hippocampus and cerebral cortex where deleted efficiently, the lacZ immunoreactivity was low in the cerebellum and could only be observed in a few Purkinje cells but not in granule cells. Additionally the deletion does not affect glia (Y. Zhu et al., 2001). Hoesche et al have demonstrated by placing a chloramphenicol acetyl transferase reporter under this promoter that the activity starts at E12 and peaks at P20 (C. Hoesche et al., 1993).

6.1 *fbw7$^{\Delta pN}$* mice are infertile and smaller than their wt littermates

In general *fbw7$^{\Delta pN}$* animals were smaller than their wt littermates and this size difference was more pronounced in animals from larger litters (Figure 6.1A). However, *fbw7$^{\Delta pN}$* animals that have reached the weaning age did not loose weight, lived as long as their wt littermates, and did not develop tumours within 1 year of age (data not shown). To characterise the growth defect of *fbw7$^{\Delta pN}$* animals, the weight of the mice was taken once a week for the first 3 month after birth. It became apparent that male and female *fbw7$^{\Delta pN}$* animals are smaller (Figure 6.1B). I also observed that pups disappeared during the weight-taking period, probably because they were eaten. Although their genotypes could not be confirmed, it is likely that these animals were mutants because additionally about 10% of *fbw7$^{\Delta pN}$* animals had to be culled within two month after birth due to severe growth retardation and a severe hindlimb tremor whilst heterozygous mice did not display any phenotype. As the analysis of embryos

at different gestation levels between E15 and P0 demonstrated that $fbw7^{\Delta pN}$ embryos are present with mendelian frequency, I conclude that the observed submendelian frequency of $fbw7^{\Delta pN}$ mutants at weaning age is caused by early postnatal deaths and animals that had to be culled (Figure 6.1C). Additionally neither male nor female $fbw7^{\Delta pN}$ animals breed and therefore all further breedings were set up using a $fbw7^{f/f}$ males or females with the respective $fbw7^{f/+}$:Synapsin-cre$^+$ animal, which did not display any phenotype.

Figure 6.1 fbw7$^{\Delta pN}$ mice are present with submendelian frequency and are smaller than their wt littermates. A)Size comparison between a 1 year old fbw7$^{\Delta pN}$ animal and wt littermate showing that in some cases the weight difference persists through adulthood B) Weights from control and fbw7$^{\Delta pN}$ animals were recorded in 1 week intervals from birth onwards. fbw7$^{\Delta pN}$ animals are significantly smaller than their littermates over the period measured. p-values females: p=0.0042, males p<0.001 C) Obtained genotypes at weaning age and embryonic stages between E15 and P0

6.2 *fbw7$^{\Delta pN}$* animals have a hindlimb defect and tremor

During the handling of the mice I noticed that *fbw7$^{\Delta pN}$* animals have a hindlimb defect as they are unable to spread their hindpaws when suspended by their tail and instead keep them together or in some cases clasp them (Figure 6.2). Such defects are known to occur after treatment with neurotoxic drugs such as MPTP (W. Dauer and S. Przedborski, 2003) or in neurodegenerative diseases. For example, in a mouse model for HD, animals display a hindlimb defect (L. Mangiarini et al., 1996). Also, animals in which autophagy is impaired clasp their hindpaws (M. Komatsu et al., 2006). Additionally *fbw7$^{\Delta pN}$* animals have a tremor in their hindlimbs (see supplementary movie M1 and M2) and this tremor was in general more pronounced in mutant animals that had to be culled. Since the tremor and hindlimb defect are indicative of neurodegeneration, I further analysed the *fbw7$^{\Delta pN}$* animals using different behavioural tests before proceeding with the immunohistochemical analysis of the brains.

To assess whether the *fbw7$^{\Delta pN}$* mice are ataxic, I performed a gait analysis using a U-shaped channel where the feet of mice were marked with ink and the footprints were recorded on filter paper. Whereas the front- and hindpaw- prints of control animals almost overlap, this was not the case in the mutant animals. However, *fbw7$^{\Delta pN}$* animals are still able to walk straight (Figure 6.3A), indicating that the *fbw7$^{\Delta pN}$* animals are only mildly ataxic and their

hindlimb defect does not impair their gait severely. The reduced stride length of $fbw7^{\Delta pN}$ animals is explained by the size difference between $fbw7^{\Delta pN}$ mutants and controls (Figure 6.3B). While there was no difference in the width between the front paws of $fbw7^{\Delta pN}$ and control animals (Figure 6.3C), I noticed that the hindpaw width is slightly bigger in $fbw7^{\Delta pN}$ animals (Figure 6.3D). The wider hindlimb distance together with the hindlimb defect indicate that $fbw7^{\Delta pN}$ mice are either not strong enough to support their bodyweight and spread their hindlimbs or that they have alterations in the neuro-muscular connection.
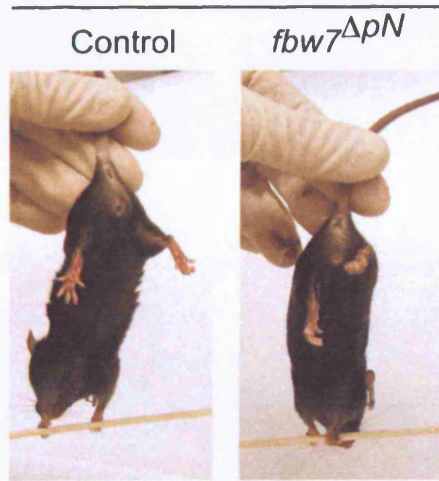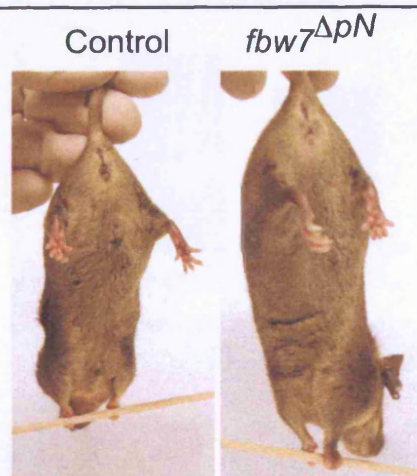
Figure 6.2 fbw7^{ΔpN} mice have a hindlimb defect. Wildtype adult animals of either 2 month of age (A) or 4 month of age (B) spread their hindlimbs when suspended by the tail whereas fbw7^{ΔpN} animals are not able to do so.
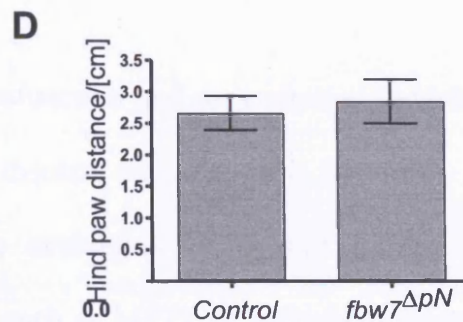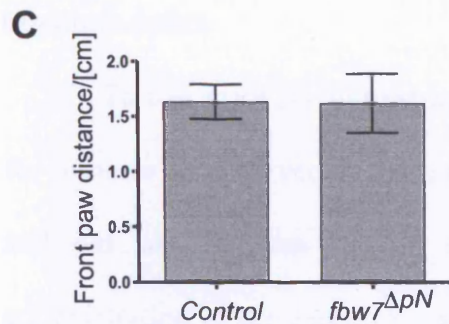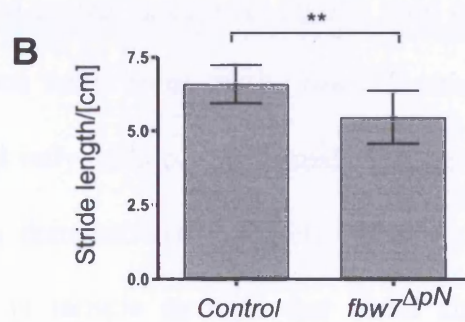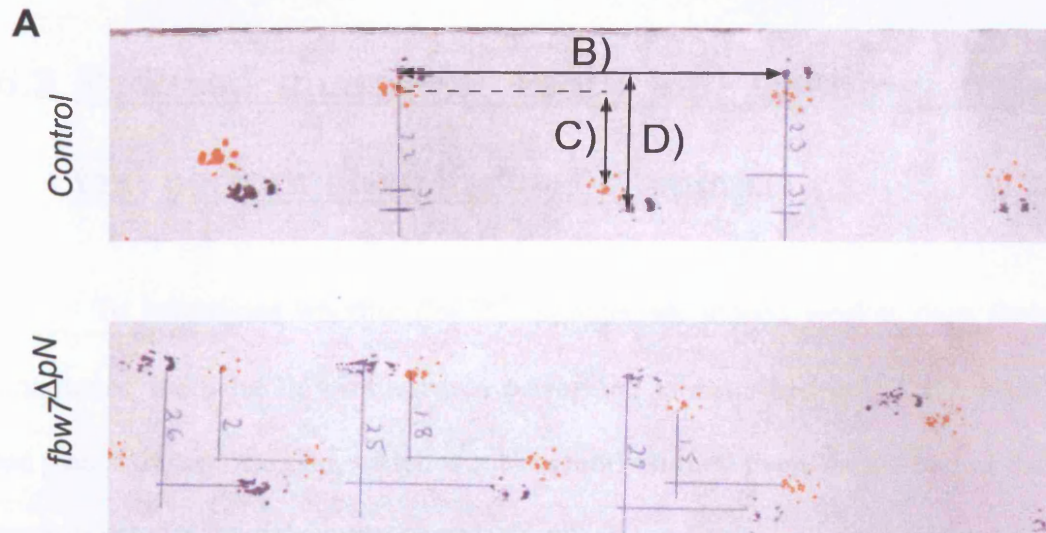
Figure 6.3 fbw7$^{\Delta pN}$ animals are mildly ataxic. Gait analysis on fbw7$^{\Delta pN}$ animals The front paws were painted in orange non-toxic ink and the back paws were painted in purple non-toxic ink. Animals were left to run towards housing at the end of the channel. A) Example of gait analysis. Distances were manually measured as indicated. B) Stride length measurement of control and fbw7$^{\Delta pN}$animals C) Front paw width and D) Hind paw width measurements. Mean +/-SD values are shown. Control: n=16, fbw7$^{\Delta pN}$:n=9.

6.3 <u>Reduced muscle strength and impaired pole test performance in *fbw7$^{\Delta pN}$* mice</u>

To investigate whether *fbw7$^{\Delta pN}$* animals are indeed weaker than their littermates, the hanging wire test was performed as described in 2.3.4.2. Mice are placed on top of a grid, which is subsequently turned over. At the end of the experiment the animals were scored "hold" if they were able to hold on or climbed on top of the turned grid 2 out of 3 times, and "fall" if they fell twice or more. As expected control mice were able to hold on or climb on top of the grid in 92% of cases while most of the *fbw7$^{\Delta pN}$* animals fell down into the nesting material and only 23% of the animals managed to hang onto the grid (Figure 6.4A). This demonstrates that Fbw7 deletion in postmitotic neurons causes a reduction in muscle strength that could also be the cause of the hindlimb defect.

To test mice for nigrostriatal dysfunction and degeneration, which can for instance be observed in Parkinson's disease, the pole test is frequently used and has been proven helpful in the evaluation of striatal lesions after administration of the neurotoxic agents such as MPTP or 6-Hydroxydopamine (K. Matsuura et al., 1997). For the pole test the mice are placed on top of a vertical, rough surfaced pole and the latency time to climb down the pole is measured as described in 2.3.4.1. Control animals traverse the pole easily and quick (4.6 seconds on average) whereas *fbw7$^{\Delta pN}$* mutant animals are slower, needing 6.6 seconds on average to climb down (Figure 6.4B). Additionally the

walking pattern of $fbw7^{\Delta pN}$ animals is different. While control animals wind their tail around the pole and walk downwards with ease, $fbw7^{\Delta pN}$ animals move down the pole in a caterpillar like fashion (see supplementary movies M3 and M4).

Taken together the results from the behavioural analysis indicate that the motor performance of $fbw7^{\Delta pN}$ mice is impaired and that $fbw7^{\Delta pN}$ animals display a phenotype, the hindlimb defect, which is similar to a mouse model for HD (L. Mangiarini et al., 1996). Interestingly the hindlimb defect was also observed in mice where another protein degradation pathway, autophagy, is impaired (M. Komatsu et al., 2006). No cellular defects, apart from a smaller brain and the hindlimb defect, could be observed in the HD model whilst mice knockout for the autophagy-involved protein ATG7 under the Nestin-cre promoter displayed an atrophic cerebral cortex and loss of Purkinje cells (M. Komatsu et al., 2006). Based on these observations and because I had already observed a reduction in Purkinje cells in $fbw7^{\Delta Cb}$ animals, I wanted to investigate whether there are similar abnormalities in the brains of $fbw7^{\Delta pN}$ animals and they were analysed by immunohistochemical stainings as described below.
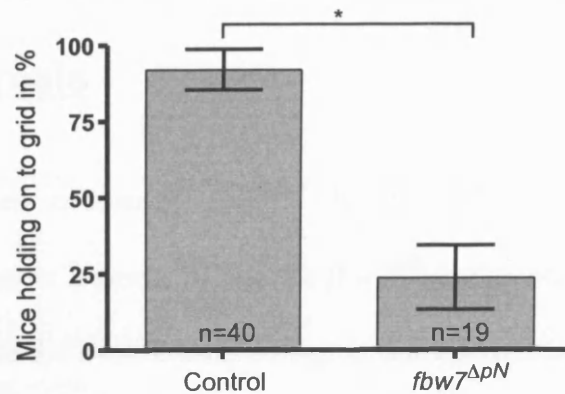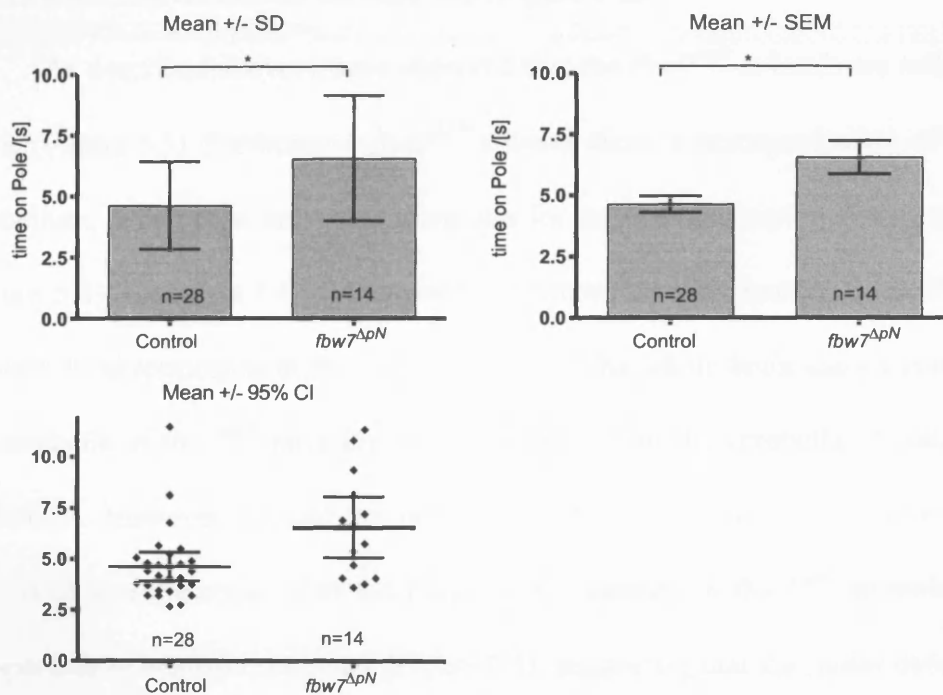
Fig 6.4 Impaired hanging wire and pole test perfomance in fbw7$^{\Delta pN}$ animals. A) Hanging wire test performed on 2-3 month old animals. Animals were placed on a grid, the grid was moved up and down to promote the animal to grip and turned over for 30 seconds. The time mice were able to hold on, climb on top of the lid, or fall off was measured. The experiment was repeated 3 times and the outcome quantified as Hold if the animal held on for at least 2 times, and fall if it fell of the grid 2 or more times. p=0.0286 Mean +/- SD B) A pole test was performed on 1-3 month old animals. Animals were placed on a vertical pole and the time to transverse the pole downwards was measured for 3 consecutive runs. The slowest value, falls and stops were excluded form the measurements. two tailed t-test, p=0.0117. To illustrate the variance of the data a graph with the original datapoints and the 95% CI were includedFor the impaired walking patters see supplementary movies M3 and M4.

6.4 No gross abnormalities of the brain in fbw7$^{\Delta PN}$ animals

When comparing fbw7$^{\Delta PN}$ brains with wt counterparts it became apparent that at 3 weeks of age the fbw7$^{\Delta PN}$ brains are slightly smaller than wt brains while the overall morphology is not altered. In the adult animal on the other hand there are no major size differences between the brains and again no gross morphological defects are observed (Figure 6.5A).

As described above, I have observed that the fbw7$^{\Delta PN}$ animals are mildly ataxic (Figure 6.3). Furthermore fbw7$^{\Delta Cb}$ animals show a misorganisation of the cerebellum, which is an important integrator for motor coordination in the brain (Figure 5.1) Therefore I first examined the cerebellar morphology in fbw7$^{\Delta PN}$ animals. In agreement with the size difference of the whole brain shown above, the cerebella of fbw7$^{\Delta PN}$ mice are slightly smaller than the cerebella of control littermates. However, I could not observe any foliation defects or positioning defects of granule cells. Also the Purkinje cell density in fbw7$^{\Delta PN}$ animals is comparable to control littermates (Figure 6.5), suggesting that the motor defects of the fbw7$^{\Delta PN}$ mice do not originate in the cerebellum.

Analysis of the fbw7$^{\Delta PN}$ brains by in situ hybridisation demonstrated a strong reduction of the fbw7 signal in the cortex and dentate gyrus (Figure 3.9). To investigate whether there are any abnormalities in neuronal morphology in these or other brain regions, fbw7$^{\Delta PN}$ brains sections were stained with a NeuN antibody to visualise neuronal nuclei. Sagittal sections of seven month-old

214

control and *fbw7^{4pN}* mutant animals were then compared. Whilst the hypothalamus, pons and dentage gyrus of *fbw7^{4pN}* animals appear normal in NeuN stained sections and no major morphological differences could be found, the cellularity of the cerebral cortex appears slightly reduced in *fbw7^{4pN}* animals (Figure 6.6). To investigate whether there are indeed alterations in the cortical cellularity in *fbw7^{4pN}* animals, coronal NeuN stained sections were further analysed.
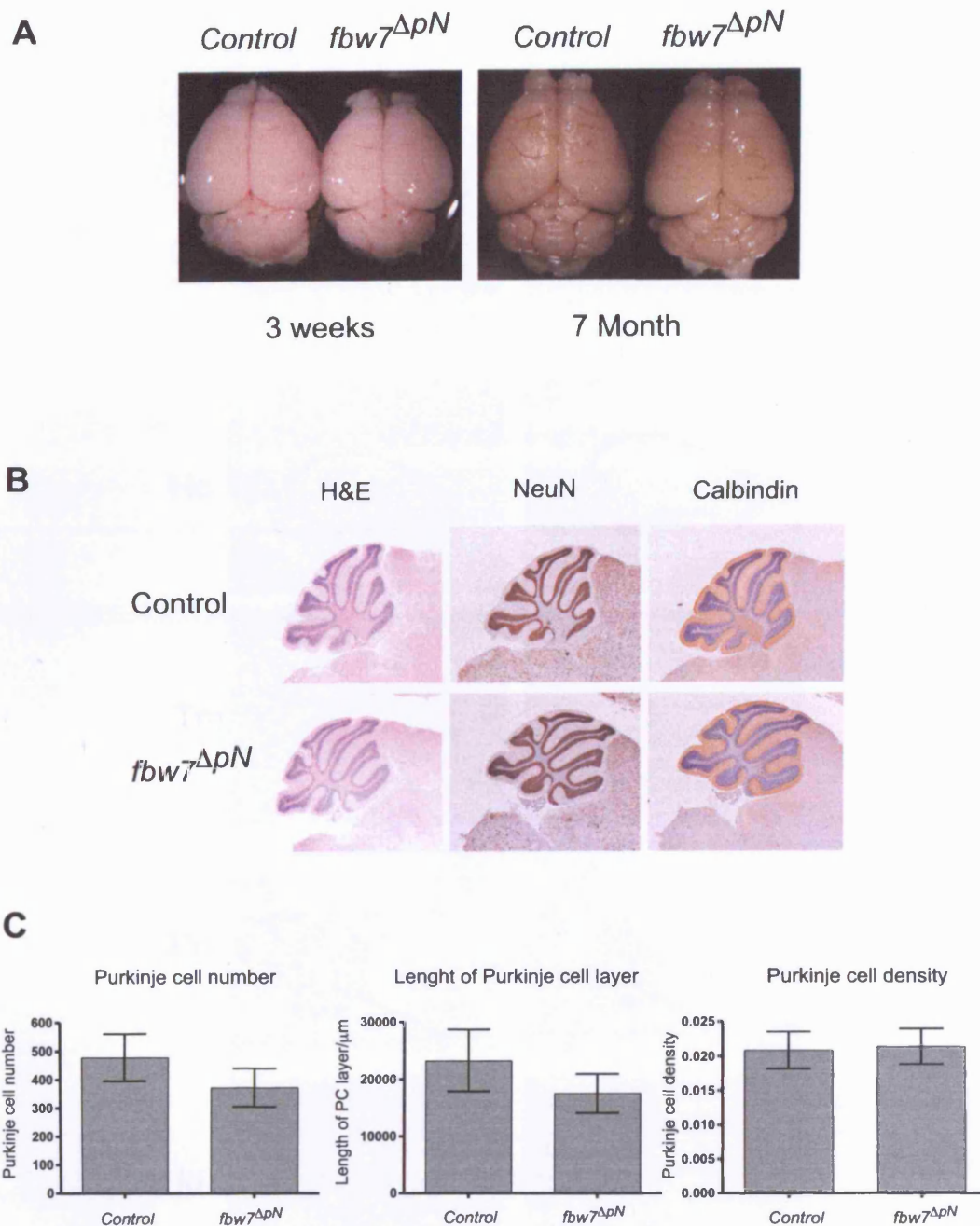
Figure 6.5 No gross morphological changes and no loss of Purkinje cells in fbw7$^{\Delta pN}$ mouse brains A) Brains of 3 week old animals and 7 month old fbw7$^{\Delta pN}$ animals do not display differences compared with wt brains apart from a reduced size. B) H&E, NeuN and Calbindin stained sections of sagittal cut cerebella of a control and fbw7$^{\Delta pN}$ animal. No foliation defects or granule cells defects are present. C) Purkinje cell parameters were determined as previously described in two to six month old fbw7$^{\Delta pN}$ animals and littermate controls. A) The number of Purkinje cells is reduced in fbw7$^{\Delta pN}$ animals but so is the Purkinje cell layer lenght (B) in in fbw7$^{\Delta pN}$ animals. The density obtained from the ration between Purkinje cell number and Purkinje cell layer lenght is not altered. Mean +/-SD shown, Control: n=4, fbw7$^{\Delta pN}$: n=3
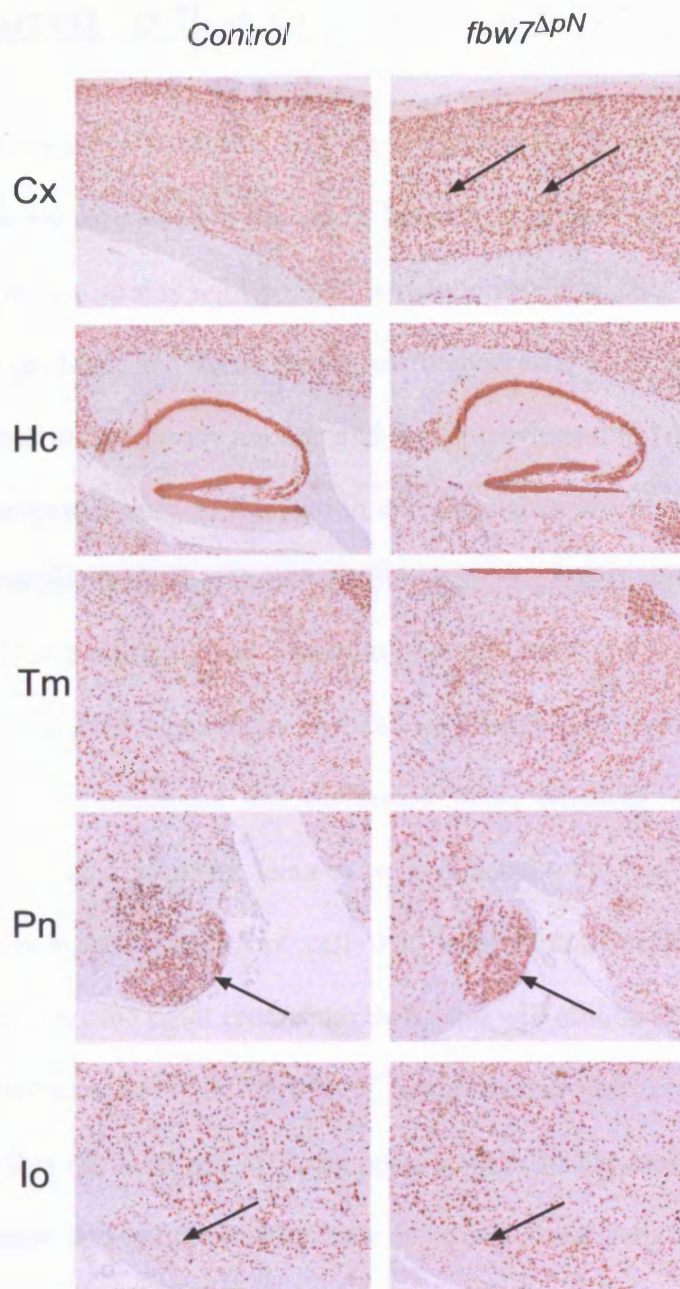
Figure 6.6 Reduced cortical cellularity in *fbw7*$^{\Delta pN}$ animals but normal pons, hippocampus and brain stem. Sagittal sections of control and *fbw7*$^{\Delta pN}$ 7 month old animals were stained with NeuN. A) The cellularity of the cortical layer is reduced (arrow) The hippocampus (Hc) and dentage gyrus are formed normal as is the thalamus (Tm). The pons (Pn) and inferior olive (Io) are normal in *fbw7*$^{\Delta pN}$ animals and no gross morphological defect can be observed.

6.5 Reduced cortical cellularity in *fbw7^{ΔpN}* animals

NeuN stainings in coronal sections confirmed that the cortical cellularity in *fbw7^{ΔpN}* brains is reduced in the the cerbral cortex (Figure 6.7). Interestingly a variety of mouse strains with cortical lamination defects also display motor-coordination problem and some strains are named after their walking pattern phenotype such as *staggerer*, *lurcher* and *reeler* (reviewed in (A. Gupta et al., 2002)). An impaired cortical lamination and cellularity are often the result of defects in neuronal migration during development, especially during the period of E11 to E17 when the cortical layers are formed (see also 1.4.1). Therefore I wanted to investigate whether the reduced cellularity is a consequence of an impaired neuronal migration and performed BrdU labelling experiments of neurons. Time mated pregnant females were injected with BrdU at E14.5 and pups were taken at E17.5. Any cell that incorporated BrdU and became postmitotic at this time point retains the BrdU and will still be BrdU positive at E17.5. Sagittal sections of E17.5 *fbw7^{ΔpN}* embryos that had received BrdU at E14.5 show that the numbers of BrdU positive cells in the intermediate zone, ventricular zone and subventricular zone is strongly reduced. In addition the BrdU labelling of the ganglionic eminence is much weaker in *fbw7^{ΔpN}* animals than in the control (Figure 6.8). This suggests that the *fbw7^{ΔpN}* animals indeed display migration defects. Whilst the reduction in BrdU positive migrating cells can explain the reduced cellularity of the cerebral cortex in *fbw7^{ΔpN}* animals, a further detailed analysis of neuronal subpopulations and migration patterns is

required to fully elucidate the role of Fbw7 in the development of the strong

behavioural phenotype and cortical migration (see also discussion).
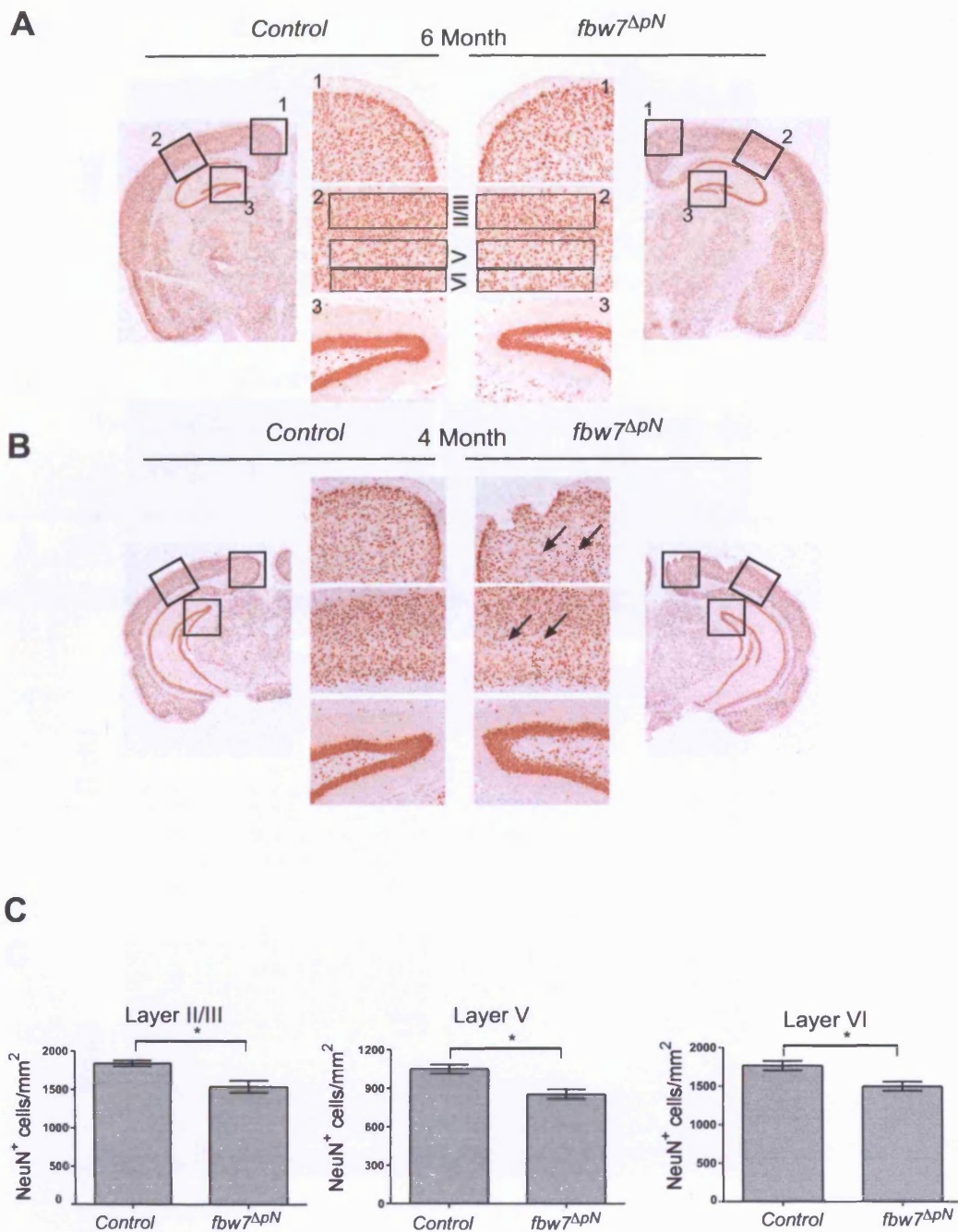
Figure 6.7 Reduced cortical cellularity in *fbw7^ΔpN^* animals
A) Coronal sections of 6 month old control and *fbw7^ΔpN^*animal. The cortical cellularity is reduced particularly in the lower part of the molecular layer which is likely to be layer V. B) Coronal more caudal section of 4 month old control and *fbw7^ΔpN^* animals. Again the cellularity is reduced and appears not to be progressive as the loss has a similar extend as in 6 month old animals. C) NeuN positive cells in coronal cortical sections of the indicated area 2 in A were counted as described in Methods. The cell density per mm² was calculated control: n=3, mutant n=3 LayerII/III: p= 0.0271, Layer V: p=0.0197, Layer VI: p=0.0357,Mean +/- SEM shown
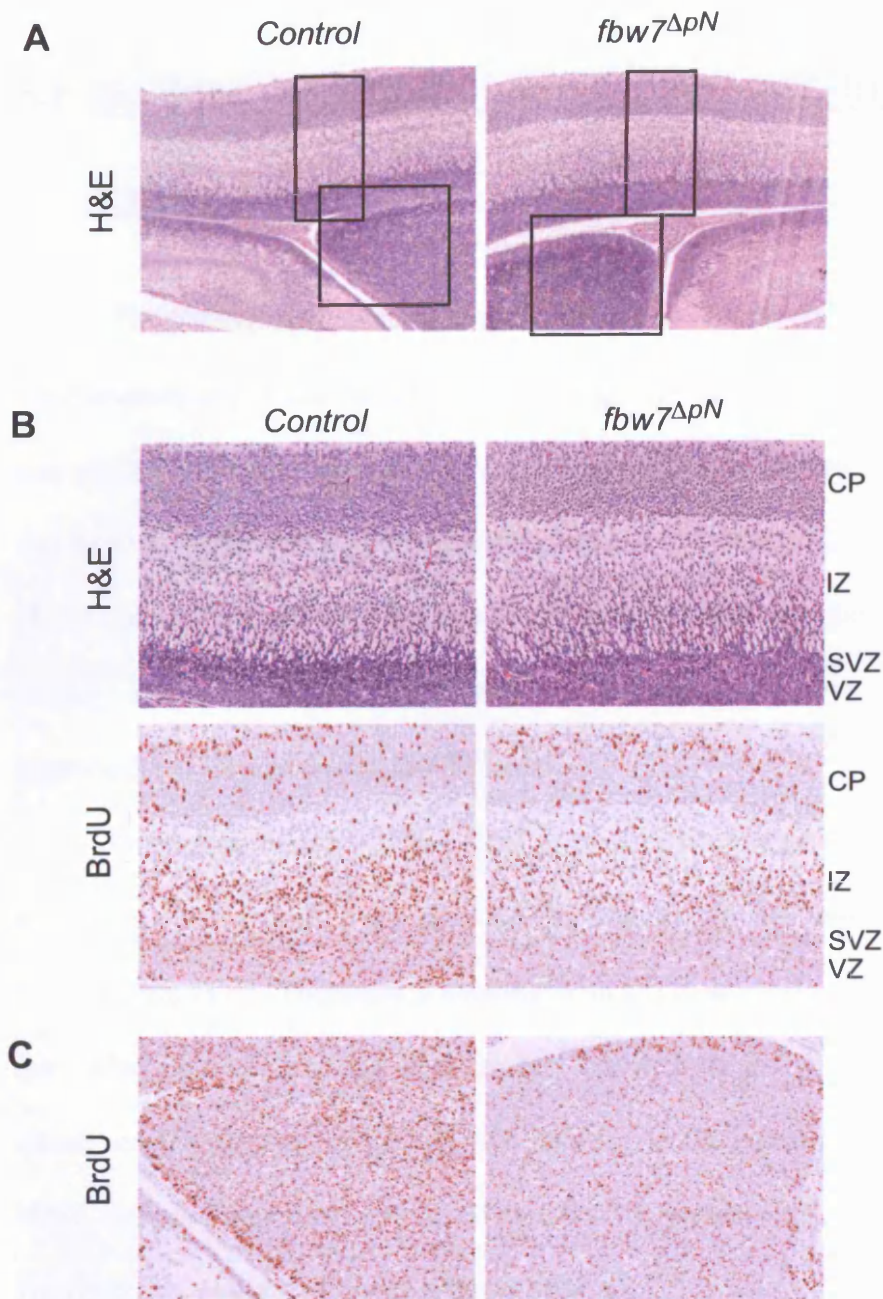
Figure 6.8 Reduced number of BrdU positive cells in the *fbw7$^{\Delta pN}$* cortex at E17. A time mated pregnant female was BrdU injected at E14.5. Sagittal sections of E17.5 embryos were taken and stained for BrdU A) H&E of the cerebral cortex and ganglionic eminence in a E17.5 control and *fbw7$^{\Delta pN}$* animal. Indicated areas are shown in B. B) H&E and BrdU stained sections from the cortex and the ganglionic eminence. The number of BrdU positive cells in the ventricular zone (VZ) subventricular zone (SVZ) as well as in the intermediate zone(IZ) and the ganglionic eminence (C) is strongly reduced while the number of BrdU positive cells in the cortical plate is similar.

6.6 <u>No loss of dopaminergic neurons in $fbw7^{\Delta pN}$</u>

<u>animals</u>

The behavioural phenotyping carried out in $fbw7^{\Delta pN}$ mice indicated that these animals might have a defect in their nigrostriatal pathway. In humans the loss of dopaminergic neurons in the substantia nigra, which is part of the nigrostriatal pathway, is the cause for Parkinson's disease (PD). Given that Fbw7 can interact with Parkin (see chapter 1.3.4) and that the $fbw7^{\Delta pN}$ mice display a tremor, it was imperative to investigate whether dopaminergic neurons die or degenerate in $fbw7^{\Delta pN}$ mice.

Dopamine belongs to the class of catecholaminergic neurotransmitters and it is synthesised from tyrosine by means of the enzyme Tyrosine Hydroxylase (TH). Therefore a staining with a TH antibody can give insights into whether dopaminergic neurons are affected in the $fbw7^{\Delta pN}$ animals. I quantified the number of TH positive neurons in the substantia nigra and the VTA, regions that show a reduced number of dopaminergic neurons in PD. However, in neither of these areas a loss of TH positive neurons could be observed (Figures 6.9 and 6.10), indicating that the motor defects do not originate from loss of dopaminergic neurons. Neurons from the VTA and the substantia nigra project into the striatum in which the TH stain is present as a diffuse stain due to its axonal localisation (Figure 6.10 left panel). Although I did not quantify the staining intensities, there is no indication that there are major alterations in striatal TH expression or in the number of TH positive

neurons in the locus coeruleus (Figure 6.10B right panel). Finally, a further step in investigating whether the Fbw7 knockout in postmitotic neurons has any effect on the nigrostriatal pathway was to analyse the GAD-67 immunoreactivity in the striatum as degeneration of GABA-ergic neurons in this brain region occurs in HD (see chapter 1.4.4). The quantification of GAD-67 levels in the striatum of $fbw7^{\Delta pN}$ animals shows, that the levels of GAD-67 immunoreactivity in the striatum of $fbw7^{\Delta pN}$ animals is comparable to that of controls (Figure 6.11) and no differences in striatal structure could be observed.

In parallel to the above analysis, I set up breedings with a mouse line in which the Cre-recombinase expression is driven by the rat tyrosine hydroxylase promoter, leading to the selective deletion of a floxed gene in catecholaminergic neurons (D. M. Gelman et al., 2003). The hypothesis was that, if the observed phenotype in $fbw7^{\Delta pN}$ animals was caused by defects in catecholaminergic neurons, the behavioural defects of $fbw7^{\Delta pN}$ animals should be reproduced in these $fbw7^{f/f},Th\text{-}cre^{+}$ ($fbw7^{\Delta CN}$) animals. However, $fbw7^{\Delta CN}$ animals appear normal and do not display any of the behavioural defects such as hindlimb clasping or a tremor that were observed in the $fbw7^{\Delta pN}$ animals (data not shown). Thus, taken together with the unaltered numbers of dopaminergic neurons in the VTA and substantia nigra of $fbw7^{\Delta pN}$ animals, I conclude that the phenotype in $fbw7^{\Delta pN}$ animals is not caused by a loss of dopaminergic neurons in the nigrostriatal system. It remains to be established where the observed defect in $fbw7^{\Delta pN}$ animals originates. (see also discussion).
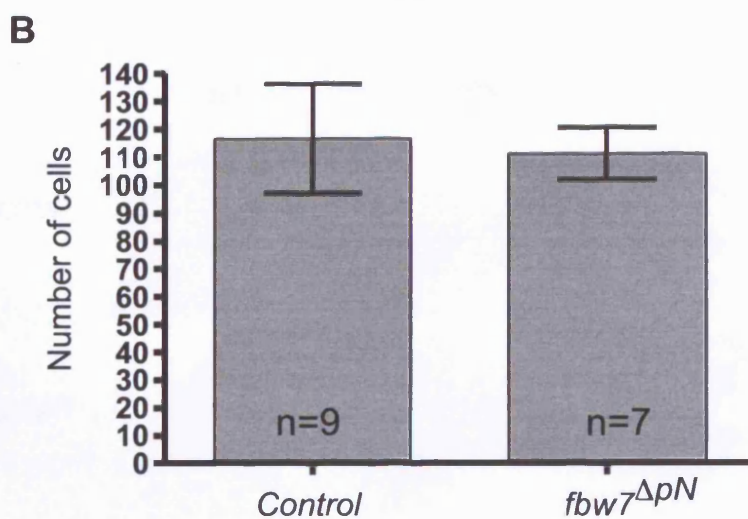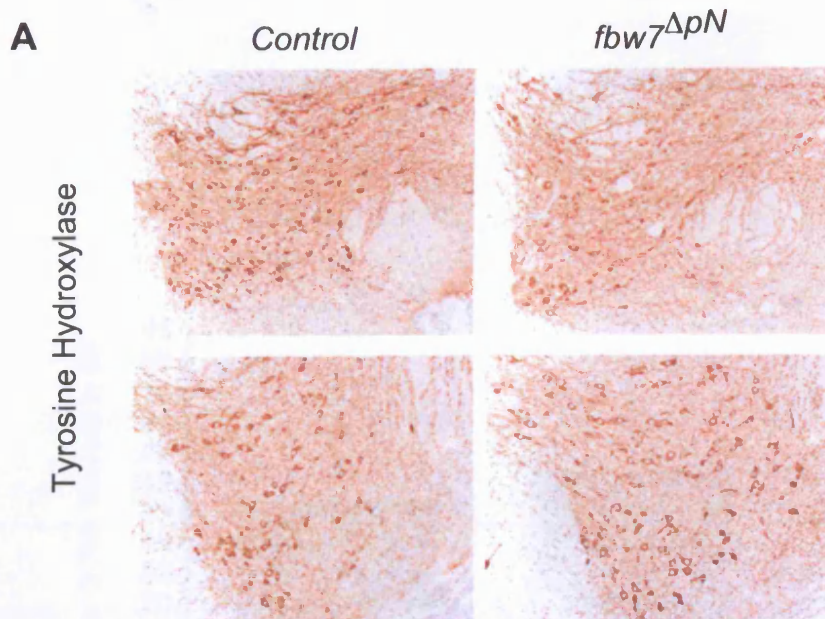
Figure 6.9 No loss of dopaminergic neurons in the VTA in *fbw7*$^{\Delta pN}$ animals. A) Example of 2 sections per genotype that were chosen for quantification of Tyrosine Hydroxylase positve neurons in the Ventral tegmetal area. B) Quantification of Tyrosine hydroxylase positive neurons in control and *fbw7*$^{\Delta pN}$ animals. TH positive neurons in the VTA in both hemishperes were quantified and the obtained cell number averaged per animal. Data are shown as Mean+/- SD of indicated animals. No significant difference could be detected.
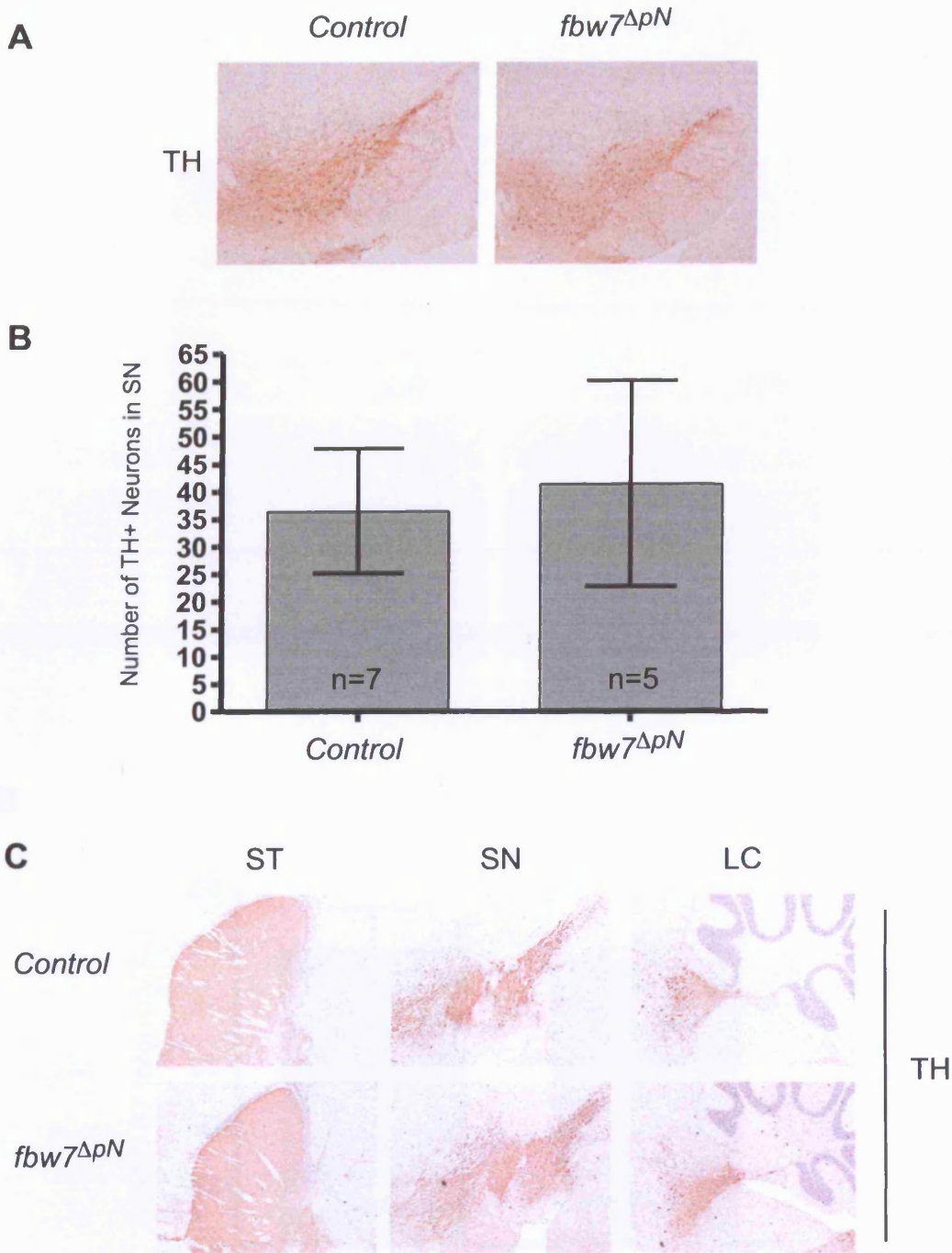
Figure 6.10 No loss of dopaminergic neurons in the Substantia Nigra. A) Coronal section of 1 month old control and $fbw7^{\Delta pN}$ animals stained with Tyrosine Hydroxylase (TH) antibody. The arrangement of TH positive neurons is comparable and no difference could be detected when the number of TH positive neurons was quantified in B) Mean +/- SD are shown. C) Sagittal sections of control and $fbw7^{\Delta pN}$ animal stained stained against TH. Additionally to the Substantia nigra (SN, middle panel) also the Striatum (St, left panel) and the Locus Coeruleus (LC, right panel) are immunoreactive for Tyrosine Hydroxylase. No apparent difference could be found in the Striatum and Locus Coeruleus.

A
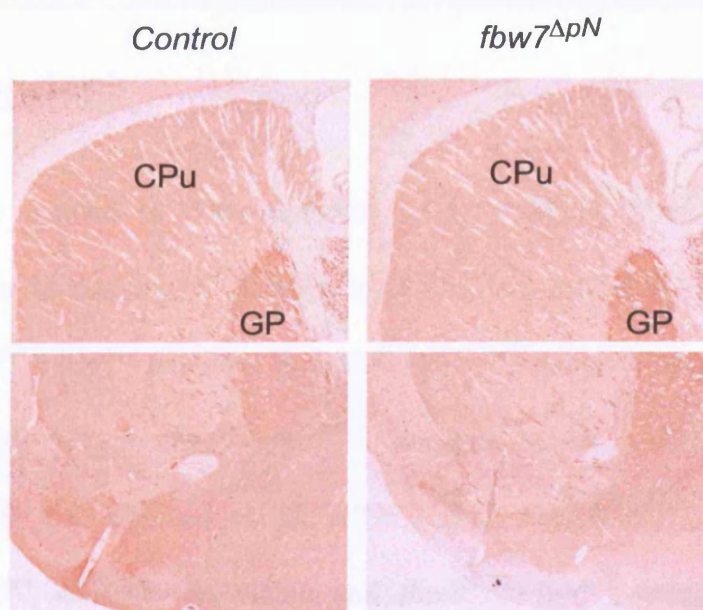
Control $fbw7^{\Delta pN}$

B
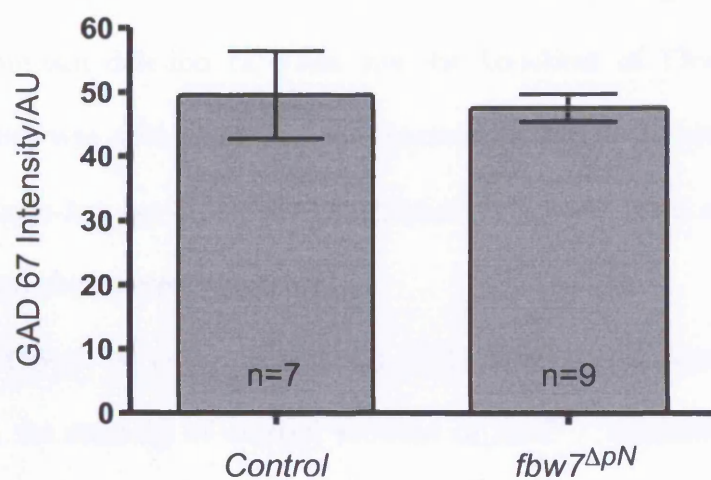
Figure 6.11 No alterations in GAD-67 levels in the striatum of $fbw7^{\Delta pN}$ mice A) Sagittal sections from control and $fbw7^{\Delta pN}$ animals were stained with a GAD-67 antibody. CPu: Caudate Putamen GP:Globus Pallidus No gross morphological differences or loss of striatal innervation can be observed B) GAD67 Intensities in the striatum were quantified as arbitrary units and no difference could be detected. Mean +/-SD values are shown

6.7 The phenotype of *fbw7*$^{\Delta PN}$ animals is not c-Jun dependent

I also wanted to determine the c-Jun dependency of the *fbw7*$^{\Delta PN}$ phenotype. To do this *fbw7*$^{\Delta PN}$ animals were firstly crossed with *cjun*$^{f/f}$ mice to obtain *fbw7*$^{\Delta PN}$:*c-jun*$^{\Delta PN}$ animals. In parallel *fbw7*$^{\Delta PN}$ animals were bred with *jun*^{AA} mice to obtain *fbw7*$^{\Delta PN}$:*jun*$^{AA/AA}$ animals where c-Jun cannot be phosphorylated (A. Behrens et al., 1999). Both the *fbw7*$^{\Delta PN}$:*c-jun*$^{\Delta PN}$ and *fbw7*$^{\Delta PN}$:*jun*$^{AA/AA}$ animals are viable and *fbw7*$^{\Delta PN}$:*c-jun*$^{\Delta PN}$ animals are also smaller that their wt littermates. A size comparison for *fbw7*$^{\Delta PN}$:*jun*$^{AA/AA}$ was not possible as the *jun*^{AA} animals are larger and heavier than wt mice and subsequently the *fbw7*$^{\Delta PN}$:*jun*$^{AA/AA}$ mice were heavier and larger as well. Neither the concomitant deletion of c-Jun, nor the knockout of Fbw7 in the *jun*^{AA} background, was able to rescue the observed hindlimb defect. This suggests that neither c-Jun nor c-Jun phosphorylation is not the main mediator for the behavioural phenotype (Figure 6.12).

Although no c-Jun dependency of the behavioural phenotype could be observed, the staining of coronal sections of *fbw7*$^{\Delta PN}$ animals with the c-Jun (H79) antibody showed an increase of c-Jun in the dentate gyrus, a brain region where Fbw7 is efficiently deleted (Figure 6.13). Since c-Jun and particularly phospho-c-Jun have been connected to the induction of neuronal apoptosis, a TUNEL labelling was performed. In line with the observation that in NeuN stained sections the Dentate gyrus appears normal, no aberrant apoptosis or loss

of cells could be observed in the Dentate gyrus or any other part of $fbw7^{\Delta pN}$

brains (Figure 6.13C and data not shown). Thus elevated c-Jun levels alone are

not sufficient to cause neuronal apoptosis. Phospho-c-Jun levels, however,

remain to be determined by immunohistocheminal stainings using phospho-

specific antibodies.
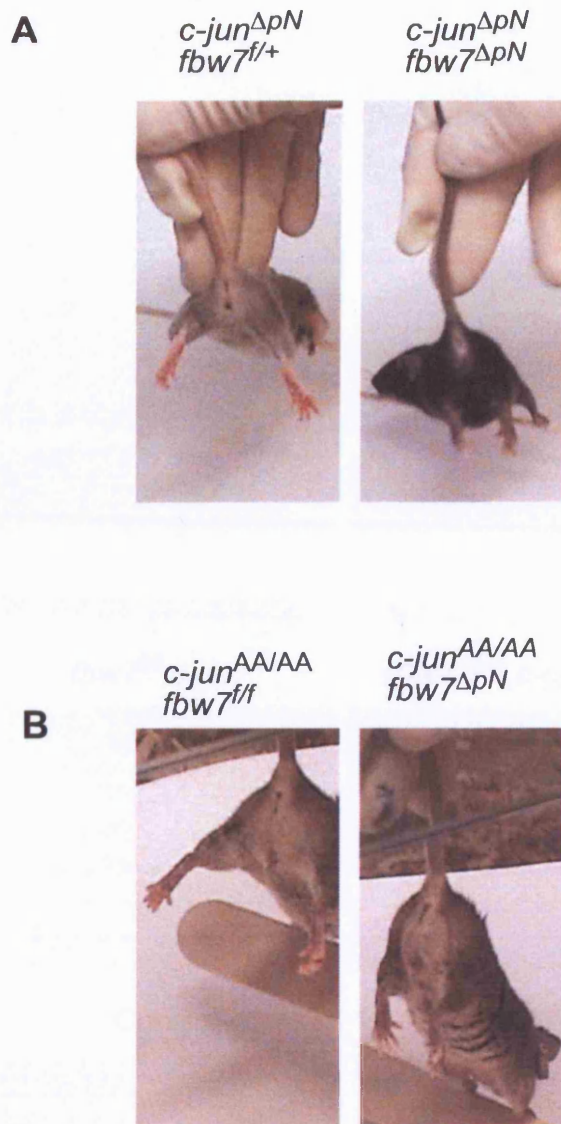
Figure6.12 The hindlimb defect is not c-Jun dependent
A) *c-jun^{ΔpN}* animals do not display a hindlimb defect whilst concomitant deletion of Fbw7 and c-Jun in *fbw7^{ΔpN}:c-jun^{ΔpN}* animals does not rescue the phenotype. B) Deletion of Fbw7 in the *jun^{AA}* background also results in a hindlimb defect, demonstrating that c-Jun is not the main mediator of this phenotypic aspect
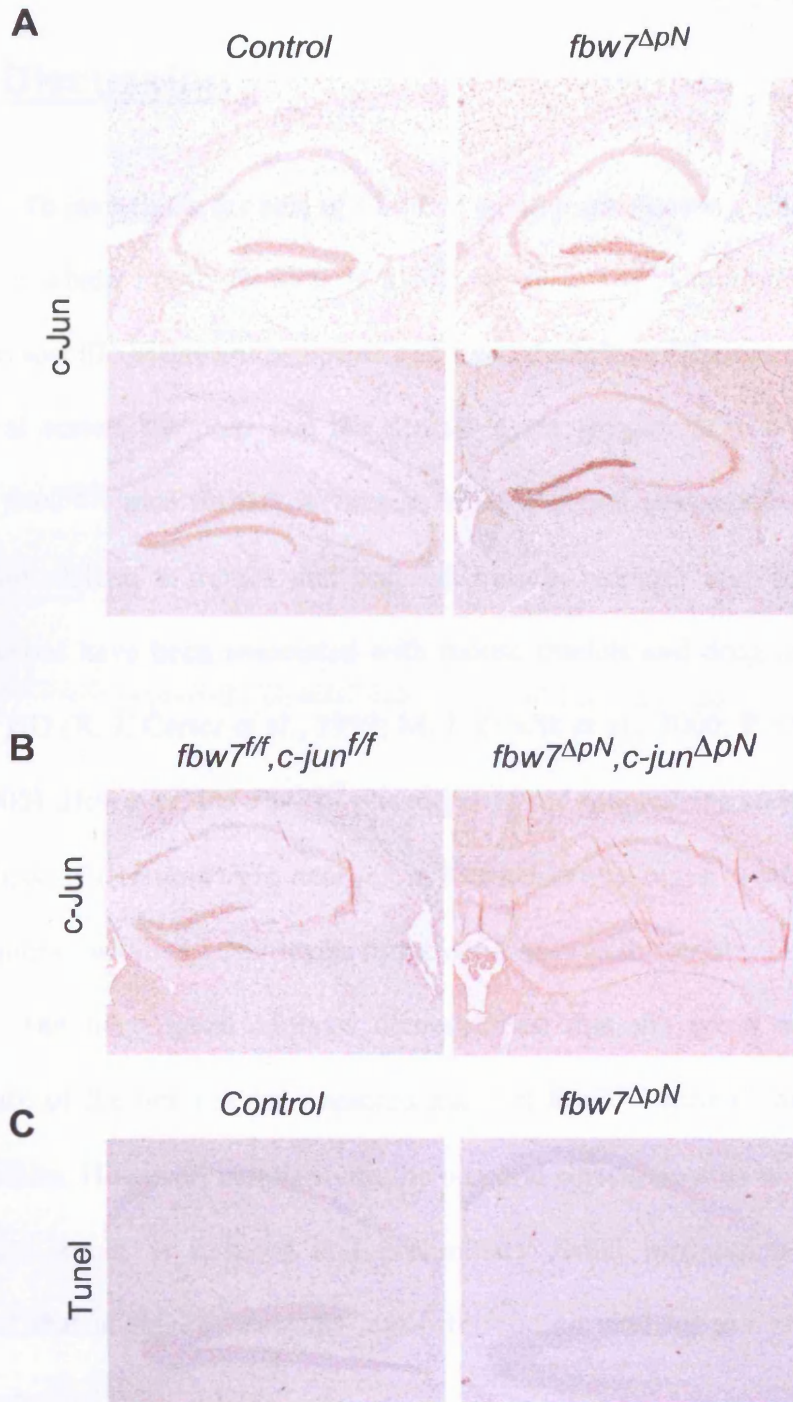
Figure 6.13 Elevated c-jun levels but no apoptosis in the dentate gyrus of *fbw7*$^{\Delta pN}$ animals All sections were stained with a c-Jun H79 antibody. A) Control and *fbw7*$^{\Delta pN}$ saggital sections of 1 month (top) and 5 month old (bottom) animals.In *fbw7*$^{\Delta pN}$ animals c-Jun levels are elevated in the dentate gyrus. B) The c-Jun stain in the dentate gyrus disappears upon concomitant deletion of Fbw7 and c-Jun, demonstrating that the staining is specific. C) No apoptosis in *fbw7*$^{\Delta pN}$ animals. Neither the Hippocampus nor the dentate gyrus display TUNEL positive cells.

6.8 <u>Discussion</u>

To investigate the role of Fbw7 in postmitotic neurons, I have generated mice in which Fbw7 deletion is mediated by a Cre recombinase under the neuron specific SynapsinI promoter and I could confirm efficient deletion in the cerebral cortex, the pons and the dentate gyrus (Figure 3.9). I observed that these $fbw7^{\Delta pN}$ mice display a variety of behavioural abnormalities such as a hindlimb defect, a tremor and reduced muscle strength and some of those phenotypes have been associated with mouse models and drug models for for PD or HD (R. J. Carter et al., 1999; M. J. Zuscik et al., 2000; P. O. Fernagut et al., 2005). However, the $fbw7^{\Delta pN}$ phenotype is not progressive and is not caused by a loss of dopaminergic neurons in the substantia nigra, ventral tegmental area, alterations in GAD67 levels or the cellularity in the striatum.

The histological analysis demonstrated that the gross morphological structure of the brain is not impaired and that $fbw7^{\Delta pN}$ animals have a normal cerebellum. However, cellularity in the cerebral cortex, an area with high Fbw7 message levels, is reduced and preliminary BrdU birthdating experiments suggest that in $fbw7^{\Delta pN}$ animals less proliferating neurons are present at E17 after labelling them at E14.

6.8.1 <u>The reduced cortical cellularity could cause the phenotype</u>

The histological analysis of the $fbw7^{\Delta pN}$ animals demonstrated a reduced cellularity in the adult cortex throughout the cortical layers (Figures 6.6 and

6.7). During development the cortical layering is established in an inside out pattern by radial migrating neurons between E14 and E18 and migration defects at this stage lead to an altered cortical lamination (see also Fig. 1.7). Preliminary results from the BrdU birthdating of neurons at E14 demonstrated that the overall number of BrdU labelled cells, particularly in the intermediate and ventricular zone but also in the ganglionic eminence, is reduced at E17 (Figure 6.8). This could indicate that at the time of the BrdU injection fewer cells were in S phase and incorporated the BrdU in $fbw7^{\Delta pN}$.

If the switch from symmetric cell division, which generates more precursors, to asymmetric division occurred prematurely, or cells are not able to differentiate properly, this could also lead to a depletion of $BrdU^+$ cells at E17. The loss of cells due to premature differentiating divisions was for instance observed in the cerebellar Notch1 knockout mice. There premature differentiating neurons die and this ultimately leads to a smaller cerebellum due to the lack of progenitor cells (S. Lutolf et al., 2002) (see also chapter 5.7.3).

It is also possible that the cells that were labelled at E14, die during the three-day period before the brains were extracted. Based on the data obtained from the $fbw7^{\Delta N}$ neurospheres where differentiation defects were observed, one can envisage that also in $fbw7^{\Delta pN}$ brains the Fbw7 deletion interferes with the final differentiation. Therefore further BrdU labelling experiments over different times will be essential to identify the reason for the reduced cell number in the cerebral cortex. If cells were able to undergo the initial asymmetric division, one would expect a comparable BrdU labelling after a short time such as for instance 3hours. However, one would then expect the inappropriate expression of neuronal markers as cells migrate to their final

position in the cortex, which should be accompanied by an increase in apoptosis. A subsequent loss of cells and fewer BrdU positive cells in the cerebral cortex at E17 would be the final outcome. The above-described experiments are planned and setup, however I could not perform them yet due to the lack of females that could be used for time matings. Once these experiments are set up, one could aim to identify whether a specific subclass of neurons is affected by Fbw7 deletion. The neurons in layer V of the cortex are mainly pyramidal projection neurons that reach distant targets outside the cerebral cortex (Z. Molnar and A. F. Cheung, 2006). Among them are also corticospinal neurons. As the name suggests, they project towards the spinal cord and if these neurons were affected in $fbw7^{\Delta pN}$ animals, this could also explain the behavioural phenotype. A number of genes that can be used as a marker for layer V neurons have been identified and are summarised in a recent review by Molyneaux (B. J. Molyneaux et al., 2007). Among them are also markers whose expression changes during development such as Ctip2 and therefore they could also be employed to characterise the cortical migration during development. Furthermore Chan et al have demonstrated that Emx1 is a marker for pyramidal neurons in the adult cortex, which are projection neurons that connect the cortex with other brain regions (C. H. Chan et al., 2001). The use of such markers could help to identify whether only a subtype of neuron, eg. neurons that use a certain neurotransmitter, or target a specific area, are particularly sensitive to the loss of Fbw7. The analysis of corticalspinal neurons together with the analysis of the spinal cord itself would be crucial in elucidating the origin of the behavioural phenotype in $fbw7^{\Delta pN}$ animals.

Finally, similar to the $fbw7^{\Delta Cb}$ and $fbw7^{\Delta N}$ animals, it is also possible that different substrates mediate the phenotype. Notch1 for instance is expressed in cortical neurons and is involved in the regulation of neurite outgrowth (O. Berezovska et al., 1999; L. Redmond et al., 2000). It would therefore be one possible target of Fbw7 in the cortex. Additionally there is emerging evidence that cell cycle regulators, including Cyclin E, are important in the nervous system and that a cell cycle re-entry in postmitotic neurons does mediate neuronal apoptosis (E. B. Becker and A. Bonni, 2004, 2005), (A. Lukaszewicz et al., 2005). It is therefore mandatory to investigate the different Fbw7 substrates in parallel with BrdU labelling experiments and apoptosis assays. Immunohistochemistry, western blotting and also FACS sorting of neuronal subpopulation (S. Sergent-Tanguy et al., 2003) could be employed to characterise the fate and differentiation of neurons in $fbw7^{\Delta pN}$ animals.

6.8.2 Other possible reasons for the observed phenotype

6.8.2.1 Hypothesis I: Defects in axonal and/or dendritic development in $fbw7^{\Delta pN}$ neurons

E3 ligases have also been implicated in the regulation of neuronal differentiation, which includes extension of the growth cone and dendritogenesis. It has been demonstrated that in culture retinal xenopus neurons the ubiquitin-conjugate concentration increases dramatically if a growth cone encounters the guidance molecule netrin and that blocking the proteasome blocks the netrin dependent turning of the growth cone (D. S. Campbell and C. E. Holt, 2001). Additionally the ubiquitin proteasome system

has been implicated in the establishment of neuronal polarity. It has for instance been shown that the proteasoma turnover of Akt in dendrites is essential for the establishment of dendrites and axons (D. Yan et al., 2006). Suppression of the proteasome in hippocampal cultures led to the symmetric distribution of Akt and resulted in the formation of multiple axons. Furthermore proteasomes can be sequestered to dendritic spines in an activity dependent manner, suggesting that they are involved in the activity dependent remodelling of the synapse (B. Bingol and E. M. Schuman, 2006) and an initial study that supports this model based on findings with the Fbw7 homologue in *c.elegans*, Sel-10, is described below.

6.8.2.2 Hypothesis 2: the motor defects are caused by deficits in synapse elimination or synaptic transmission

The *c.elegans* homologue of Fbw7, Sel-10, has recently been implicated in the elimination of synapses (M. Ding et al., 2007; D. M. Miller, 2007). Ding et al. observed that an SCF complex containing Sel-10 is active at a primary neuromuscular synapse and that the complex is inhibited in its function by the inhibitory protein Syg-1. Syg-1 binding to Skr-1, the *c.elegans* homologue to Skp-1 and thereby blocks the ubiquitination and degradation of synaptic proteins at the primary synaptic site Interestingly, this interactions stimulates the ubiquitination of proteins and subsequent elimination of secondary synapses by a yet to be identified mechanism (M. Ding et al., 2007). Furthermore Ding et al. show that artificial elevation of SCF activity causes the elimination of primary and secondary synapses. Also in mammals neuron-muscular synapses are eliminated during development (reviewed in (H. Colman

and J. W. Lichtman, 1993)). If one extrapolates the finding by Ding et al. to the mouse this would predict that deletion of Fbw7 and subsequent impairment of the SCF^{Fbw7} complex should result in an impaired synapses elimination and subsequently alter the transmission from the nerve to the muscle, which is interesting with regards to the impaired motor function of the $fbw7^{\Delta pN}$ animals. To investigate this, an analysis of the spinal cord and neuromuscular junctions in $fbw7^{\Delta pN}$ animals should be performed. One could for instance repeat the *in situ* hybridisation to determine the expression levels of Fbw7 in the neuromuscular junction (NMJ), and analyse the NMJ in $fbw7^{\Delta pN}$ animals. Established markers for the NMJ that could be used for such an analysis are antibodies against the acetylcholine-receptor and labelled bungarotoxin (reviewed in (J. Lu and J. W. Lichtman, 2007)). Studies in *Drosophila* have further implicated E3-ligase is the development of the neuromuscular junction. There the disruption of the locus of the RING-E3 ligase highwire results in defects at the neuromuscular junctions (C. Wu et al., 2005). If the observed motor defects in $fbw7^{\Delta pN}$ animals are caused by defects in the spinal cord, an area where Synapsin-cre mediated deletion takes place, but the TH-cre recombinase is not active.

It has also been demonstrated that in addition to acute lesions, changes in neurotransmitter levels can cause an impaired pole test performance and this could also be the reason for the altered behaviour in $fbw7^{\Delta pN}$ animals. The $DAT^{-/-}$ mice, where the dopamine transporter (DAT) is deleted, are also impaired in their pole test performance (P. O. Fernagut et al., 2003). These mice display persistent elevated extracellular dopamine levels due to the lack of

DAT, which is normally responsible for the re-uptake of dopamine as part of an auto-regulatory loop. To test whether deletion of Fbw7 impairs the synapse elimination in the brain one could stain or western blot with presynaptic (synaptophysin) or postsynaptic markers (eg. PSD-95) or synaptic vesicle proteins in a complementary approach with the use of electron microscopy to analyse the synapses at a high resolution level. The levels of neurotransmitters in the brain can be investigated by HPLC on dissected brain regions. This method has been used in the Parkin knockout mice, where altered neurotransmitter levels without a concurrent loss of dopaminergic neurons was observed (see chapter 1.4.4). A similar bioanalytical approach in $fbw7^{\Delta PN}$ animals could clarify whether the loss of Fbw7 causes alterations in neurotransmitter levels in the brain. Since the resulting changes in synaptic transmission would be permanent, this could also explain why there is no progression in the phenotype. If neurotransmitter levels were altered to a different degree in $fbw7^{\Delta PN}$ animals and $fbw7^{\Delta cN}$ animals, this could explain the phenotypic differences between those two mouse lines.

6.8.3 The observed phenotype is not c-Jun dependent

To establish whether the observed behavioural and histological phenotype is c-Jun dependent, crosses with either $c\text{-}jun^{\,f/f}$ or jun^{AA} mice were set up. By using the hindlimb defect as a first indicator of the $fbw7^{\Delta PN}$ phenotype, I established that the hindlimb defect is not rescued in the $fbw7^{\Delta PN}:c\text{-}jun^{\Delta PN}$ or the $fbw7^{\Delta PN}:jun^{AA/AA}$ mice, indicating that this part of the phenotype is not c-Jun dependent (Figure 6.12). Furthermore I observed that the elevated c-Jun levels in the dentate gyrus were not sufficient to cause

apoptosis. Interestingly, this is similar to the effect observed in *c-jun* transgenic Purkinje cells where high c-Jun levels alone also did not cause apoptosis (see chapter 5). However, if neurons in the dentate gyrus of *fbw7^{ΔpN}* animals were more sensitive to stress, as are c-Jun transgenic Purkinje cells, one would predict that administration of the excitotoxic agent kainate should aggravate the seizures compared to wt animals as the excitotoxicity of kainate is mediated via the JNK signalling pathway (see also chapter 1.1.1 and references therein).

The hippocampus is implicated in learning and memory formation and it will be interesting to see how *fbw7^{ΔpN}* animals perform in behavioural tests for learning and memory formation and whether elevated c-Jun levels play a role in these processes. To further investigate the effect of Fbw7 in the hippocampus I set up crosses where Fbw7 is deleted using CamK2-cre transgenic mice (*fbw7^{ΔHc}*) (L. Minichiello et al., 1999). Preliminary data suggest that *fbw7^{ΔHc}* mice do not display a hindlimb defect or tremor such as the *fbw7^{ΔpN}* animals (data not shown), which further supports the notion that the hippocampal alterations in *fbw7^{ΔpN}* animals are not responsible for the observed behavioural phenotype. However, a detailed behavioural analysis of the *fbw7^{ΔHc}* animals has yet to be performed. One would predict that like in *fbw7^{ΔpN}* animals, c-Jun levels in the dentate gyrus should be elevated. Although ablation of c-Jun in the nervous system (*c-jun^{ΔN}*) was shown not to alter the performance in the Morris water maze test (G. Raivich et al., 2004), the presence of elevated c-Jun levels in either the *fbw7^{ΔpN}* (Figure 6.13) or *fbw7^{ΔHc}* mice, will allow to test whether the presence of c-Jun alone modulates the hippocampal function and to what extent it is involved in learning and memory formation.

7 CONCLUDING REMARKS AND OUTLOOK

The aim of this thesis was to test the hypothesis that the E3-ligase Fbw7 is a key regulator of phospho-c-Jun levels in the nervous system. For this reason I generated various brain specific conditional knockout lines for Fbw7 (summarised in Table 7.1). Based on the finding that Fbw7 is mutated in cancers and that it has many substrates, an important role of Fbw7 in the organism was predicted and confirmed in early publications demonstrating that the lethal effect of a germline knockout of Fbw7 are caused by elevated Notch and cyclin E levels during vascular development (M. T. Tetzlaff et al., 2004; R. Tsunematsu et al., 2004). By means of the combinatorial use of different conditional Fbw7 knockout lines I could demonstrate that Fbw7 is important during brain development and that a nervous system specific deletion in the neural lineage also causes lethality whilst the regional or temporal restricted Fbw7 deletion in the brain does not impair viability. I obtained data that suggest that in addition to c-Jun Fbw7 has other substrates in the brain as some of the observed phenotypes are not c-Jun dependent.

7.1 Fbw7 deletion causes distinct phenotypes in different mouse lines

Using the Nestin-cre line I investigated the role of Fbw7 during early neuronal development and observed that deletion in the neural lineage results in a reduced cellularity and perinatal lethality (chapter 4). However, compared to the severe defects of the germline knockout animals, which display an

impairment of the neural tube closure, the gross brain morphology was preserved in $fbw7^{\Delta N}$ animals. This demonstrates that apart from being essential during neurulation, Fbw7 continues to play an important role in the brain after E10.5. Interestingly Nestin-cre mediated Fbw7 deletion in neurons and glia is lethal whilst deletion in exclusively postmitotic neurons by the Synapsin-driven Cre-recombinase does not. The initial studies on these mouse lines demonstated that the expression pattern of these different promoter elements is almost complementary. Whilst it was shown in Nestin-GFP mice that Nestin-promoter driven expression is high in the ventricular zone, no synapsin-cre mediated deletion can be detected within this brain region in lacZ:Synapsin-cre reporter mice (J. L. Mignone et al., 2004) (Y. Zhu et al., 2001). A loss of cells during the initial differentiation could explain why the cellularity is more strongly reduced in the $fbw7^{\Delta N}$ cortex than in the $fbw7^{\Delta pN}$ cortex, where deletion takes place after this lineage decision has been initiated and where a major population of the brain cells, namely glia, are not affected. Experiments performed by Jörg Hoeck showed that $fbw7^{\Delta N}$ neurospheres display differentiation defects (J. Hoeck personal communication). Taken together with the reduced cellularity in $fbw7^{\Delta N}$ animals it is possible that Fbw7 is involved in the regulation of progenitor- differentiation during brain development. The fact that the $fbw7^{\Delta pN}$ mice display also a reduced cellularity suggests however, that Fbw7 is also involved in additional later occurring processes. These possibilities are discussed below.

7.2 Fbw7 in the cortex

Fbw7 is highly expressed in the cerebral cortex as shown by in situ hybridisation on E18 $fbw7^{\Delta N}$ and adult $fbw7^{\Delta pN}$ animals. I observed that Fbw7 deletion in the cortex causes a reduced cortical cellularity in two different mouse lines ($fbw7^{\Delta pN}$ and $fbw7^{\Delta N}$). Defects in cortical development can occur at different stages in development, early during the initial asymmetric division, during cell migration and when cells finish migration and assume their cortical position in the respective cortical layers. Although the gross structure of the cortical layering appears preserved in $fbw7^{\Delta pN}$ animals, the cellularity is reduced (Fig 6.7). This suggests that cells die during migration or early development. It will be interesting to analyse whether as part of the reduced cellularity certain neuronal subpopulations are more affected by the Fbw7 deletion than others. To do this, established markers that label distinct neuronal subpopulations such as for instance Ctip for layer V, which also contains corticospinal neurons, will be employed (B. J. Molyneaux et al., 2007).

To monitor the migration and differentiation of neurons in $fbw7^{\Delta Cb}$ or $fbw7^{\Delta pN}$ animals a GFP-Fbw7 reporter line where GFP expression is induced by Cre-recombinase mediated deletion could be used. However, I would anticipate a lower number of GFP positive cells in the $fbw7^{\Delta pN}$ cortex due to cell death as a result of Fbw7 deletion. Although TUNEL assays were not performed on the mouse lines described here, it is feasible to hypothesise that the analysis of earlier developmental stages in the $fbw7^{\Delta Cb}$ animals and a closer monitoring of migrating neurons in $fbw7^{\Delta pN}$ animals will show an increase in neuronal apoptosis that precedes the loss of cells.

7.3 **Fbw7 in the cerebellum**

Deletion of Fbw7 in the cerebellar vermis, $fbw7^{\Delta Cb}$, caused a reduction in vermis size, a reduced Purkinje cell density and an additional fissure. In contrast mice harbouring the Fbw7 deletion in postmitotic neurons did not show any cerebellar phenotype. At a first glance this indicates that the observed cerebellar defect is due to deletion in progenitor cells as postmitotic cells appear unaffected. However, there exists some ambiguity regarding Synapsin-cre mediated deletion in the cerebellum. The initial characterisation of the Synapsin-cre transgenic line showed that Cre expression in the cerebellum is only detectable in some Purkinje cells and not the granule cell layer (Y. Zhu et al., 2001). Thus the absence of a cerebellar phenotype could be explained by the absence of cre-mediated recombination. Nonetheless, the in situ hybridisation in the cerebellum of $fbw7^{\Delta pN}$ mice showed some reduction of signal with the generic and the exon 5 specific probe and furthermore the deletion PCR for Fbw7 displayed efficient deletion in the cerebellum (Figure 3.10 and data not shown). Another study has also observed an efficient cerebellar deletion of their protein of interest using the synapsin-cre mouse line to knockout the β3-subunit of the γ-aminobutyric acid type A receptor (C. Ferguson et al., 2007). Thus based on the *in situ* hybridisation data, the deletion PCR and the report by Ferguson et al. one can speculate that deletion of Fbw7 in cerebellar progenitors that will form the cerebellar vermis has a more dramatic effect on the overall cerebellar structure than deletion in postmitotic cerebellar neurons. Purkinje cells become postmitotic between E11 and E13 and Synapsin-cre mediated deletion can be detected from E12.5 onwards as

observed in some Purkinje cells by Zhu et al. in the initial characterisation of the synapsin-cre mouse line (J. Altman and S. A. Bayer, 1978; Y. Zhu et al., 2001). Therefore if Purkinje cells expressed Fbw7 and the observed cerebellar knockout phenotype were Purkinje cell autonomous, the $fbw7^{\Delta pN}$ cerebella should display the same morphological defects in arborisation as $fbw7^{\Delta Cb}$ Purkinje cells. Based on the performed quantification and macroscopic analysis, this is not the case. This argues in favour of hypothesis-1 that was proposed in chapter 5.7 and suggests that the observed Purkinje cell defect is due to defects in granule cells, which provide essential afferent input to Purkinje cells (chapter 5.7). Since there is a loss of signal in the granule cell layer in $fbw7^{\Delta pN}$ animals without any cerebellar foliation defects when the deletion occurs at the postmitotic stage, this furthermore suggests, that Fbw7 deletion in granule cell precursors is responsible for the observed foliation defects in $fbw7^{\Delta Cb}$ animals (see also Chapter 5.7.4). However, the analysis of synapsin-cre reporter mice by analogous β-galactosidase staining as performed for the Engrailed-2 cre line (see appendix) could help to clarify this issue and asses the onset and the extent of deletion in the cerebellum of $fbw7^{\Delta pN}$ mice.

Additionally, the previously mentioned cross of different knockout animals with mice where Cre-expression also induces the expression of a GFP reporter could provide a tool to investigate the fate of Fbw7 deleted cells in the cerebellum as well. Based on the data that deletion of Fbw7 leads to a reduced cellularity and a smaller cerebellum, I would anticipate that the number of GFP positive granule cells is strongly reduced in $fbw7^{\Delta Cb}$ granule cells whilst in the $fbw7^{\Delta pN}$ GFP-positive granule cells would be present. The analysis of the

Purkinje cell maturation and synapse formation in cerebellar slices of $fbw7^{\Delta Cb}$-GFP reporter mice could also give insights into how Fbw7 influences the differentiation and arborisation of Purkinje cells. Whilst I could demonstrate that in the $fbw7^{\Delta Cb}$ the loss of Purkinje cells is phospho-c-Jun dependent, an analogous analysis of $fbw7^{\Delta pN}$ mice has still to be carried out. Although the behavioural phenotype was not rescued in $fbw7^{\Delta pN}$:c-$jun^{\Delta pN}$ animals, this does not exclude a rescue of the cortical phenotype as the phenotype of conditional Fbw7 knockout animals is composed of c-Jun dependent and independent components. If the cortical cellularity were rescued in $fbw7^{\Delta Cb}$:c-$jun^{\Delta Cb}$ animals, one could conclude that the behavioural phenotype is not caused by loss of these neurons. If it were not rescued, this could indicate, that the phenotype is caused by the cortical defects and that other substrates are responsible for the observed phenotype.

7.4 Fbw7 and neuronal connectivity

Deletion of Fbw7 in the cerebellum impaired the arborisation in Purkinje cells. Analysis of the parallel and climbing fibres indicated that the number of Vglut1 and Vglut2 positive synapses is reduced, although this has still to be quantified. Furthermore, given the behavioural phenotype of the $fbw7^{\Delta pN}$ animals together with the lack of loss of dopaminergic neurons, it is possible that the loss of Fbw7 in postmitotic neurons impairs the synaptic transmission. Interestingly, preliminary data from electron microscopy experiments demonstrate a pre- and post synaptic as well as cytoplasmic localisation of Fbw7 in wt brains (Gennadij Raivich, personal communication).

Furthermore, a number of reports have demonstrated various roles for E3 ligases in the regulation of synapse formation, transmission and signalling. In *Drosophila*, the disruption of the locus of the RING-E3-ligase highwire results in defects at the neuromuscular junctions (C. Wu et al., 2005). Presynaptic proteins that are components of synaptic vesicles such as syntaxin and synaptophysin are targeted for degradation by the E3 ligases Siah1 and Siah2 (T. C. Wheeler et al., 2002) and it has been shown that the post-synaptic-density protein PSD-95 is ubiquitinated by Mdm2 and thereby efficiently removed after synapse activation (M. Colledge et al., 2003). As, the above studies show that E3 ligases fulfil diverse regulatory roles at the synapse; Fbw7 might also participate in such processes. It remains to be established, to what extent a putative synaptic function would relate to already known Fbw7 substrates such as c-Jun, c-Myc, N-myc or cyclin E. So far I could demonstrate that Fbw7 mediated c-Jun regulation is important for the arborisation of Purkinje cells by a mechanism which remains to be fully elucidated. Many of the known Fbw7 substrates are normally localised to the nucleus, however, it cannot be excluded that Fbw7 shuttles to the nucleus upon a still unknown stimulus, and thus exerts its E3 ligase function in a signal dependent manner.

Further investigation into the identified Fbw7 substrates and also possible upstream regulators is therefore mandatory for understanding the role of Fbw7 in the nervous system. One could for instance screen for Fbw7 interacting proteins with a yeast-two- hybrid system using a brain library, or by using GST-pulldowns or Tap-tagging. These experiments could potentially identify novel substrates and upstream regulators of Fbw7 itself. In parallel a bioinformatics approach could be employed to identify putative neuronal or

even synaptic substrates by applying criteria that appear to be common in many

Fbw7 substrates such as the phospho-degron, interaction with GSK-3 and Pin1,

or ERK.

In summary this thesis clearly demonstrates that Fbw7 has an important,

non-redundant function in the nervous system. The observation that the deletion

of Fbw7 in postmitotic neurons causes a hindlimb defect and tremor similar to

other neurodegenerative pathologies indicates that Fbw7 could also play a role

in diseases of the nervous system. While some of the phenotypes were c-Jun

dependent, others were not, indicating that on a molecular level Fbw7 is an

important regulator of the function of potentially many substrates.

Finally, but importantly the generation of $fbw7^{f/f}$ mice provides a

valuable tool to extend the characterisation of Fbw7 functions to other parts of

the organisms in addition to the brain by crossing theses $fbw7^{f/f}$ animals to other

tissue specific Cre expression lines.

Table 7.1 Summary of generated mouse lines

8 REFERENCES

Abraham WC, Mason SE, Demmer J, Williams JM, Richardson CL, Tate WP, Lawlor PA, Dragunow M (1993) Correlations between immediate early gene induction and the persistence of long-term potentiation. Neuroscience 56:717-727.

Altman J (1972a) Postnatal development of the cerebellar cortex in the rat. I. The external germinal layer and the transitional molecular layer. The Journal of comparative neurology 145:353-397.

Altman J (1972b) Postnatal development of the cerebellar cortex in the rat. 3. Maturation of the components of the granular layer. The Journal of comparative neurology 145:465-513.

Altman J (1972c) Postnatal development of the cerebellar cortex in the rat. II. Phases in the maturation of Purkinje cells and of the molecular layer. The Journal of comparative neurology 145:399-463.

Altman J, Anderson WJ (1972) Experimental reorganization of the cerebellar cortex. I. Morphological effects of elimination of all microneurons with prolonged x-irradiation started at birth. The Journal of comparative neurology 146:355-406.

Altman J, Winfree AT (1977) Postnatal development of the cerebellar cortex in the rat. V. Spatial organization of purkinje cell perikarya. The Journal of comparative neurology 171:1-16.

Altman J, Bayer SA (1978) Prenatal development of the cerebellar system in the rat. I. Cytogenesis and histogenesis of the deep nuclei and the cortex of the cerebellum. The Journal of comparative neurology 179:23-48.

Ardley HC, Scott GB, Rose SA, Tan NG, Robinson PA (2004) UCH-L1 aggresome formation in response to proteasome impairment indicates a role in inclusion formation in Parkinson's disease. J Neurochem 90:379-391.

Baptista CA, Hatten ME, Blazeski R, Mason CA (1994) Cell-cell interactions influence survival and differentiation of purified Purkinje cells in vitro. Neuron 12:243-260.

Barnes WM (1994) PCR amplification of up to 35-kb DNA with high fidelity and high yield from lambda bacteriophage templates. Proc Natl Acad Sci U S A 91:2216-2220.

Becker EB, Bonni A (2004) Cell cycle regulation of neuronal apoptosis in development and disease. Prog Neurobiol 72:1-25.

Becker EB, Bonni A (2005) Beyond proliferation--cell cycle control of neuronal survival and differentiation in the developing mammalian brain. Seminars in cell & developmental biology 16:439-448.

Behrens A, Sibilia M, Wagner EF (1999) Amino-terminal phosphorylation of c-Jun regulates stress-induced apoptosis and cellular proliferation. Nat Genet 21:326-329.

Ben-Arie N, Bellen HJ, Armstrong DL, McCall AE, Gordadze PR, Guo Q, Matzuk MM, Zoghbi HY (1997) Math1 is essential for genesis of cerebellar granule neurons. Nature 390:169-172.

Bengoechea-Alonso MT, Ericsson J (2007) SREBP in signal transduction: cholesterol metabolism and beyond. Curr Opin Cell Biol 19:215-222.

Berezovska O, McLean P, Knowles R, Frosh M, Lu FM, Lux SE, Hyman BT (1999) Notch1 inhibits neurite outgrowth in postmitotic primary neurons. Neuroscience 93:433-439.

Besirli CG, Wagner EF, Johnson EM, Jr. (2005) The limited role of NH2-terminal c-Jun phosphorylation in neuronal apoptosis: identification of the nuclear pore complex as a potential target of the JNK pathway. The Journal of cell biology 170:401-411.

Bianchi E, Denti S, Catena R, Rossetti G, Polo S, Gasparian S, Putignano S, Rogge L, Pardi R (2003) Characterization of human constitutive photomorphogenesis protein 1, a RING finger ubiquitin ligase that interacts with Jun transcription factors and modulates their transcriptional activity. J Biol Chem 278:19682-19690.

Bingol B, Schuman EM (2006) Activity-dependent dynamics and sequestration of proteasomes in dendritic spines. Nature 441:1144-1148.

Bogoyevitch MA, Kobe B (2006) Uses for JNK: the many and varied substrates of the c-Jun N-terminal kinases. Microbiol Mol Biol Rev 70:1061-1095.

Brecht S, Kirchhof R, Chromik A, Willesen M, Nicolaus T, Raivich G, Wessig J, Waetzig V, Goetz M, Claussen M, Pearse D, Kuan CY, Vaudano E, Behrens A, Wagner E, Flavell RA, Davis RJ, Herdegen T (2005) Specific pathophysiological functions of JNK isoforms in the brain. Eur J Neurosci 21:363-377.

Bredel M, Bredel C, Juric D, Harsh GR, Vogel H, Recht LD, Sikic BI (2005) Functional network analysis reveals extended gliomagenesis pathway maps and three novel MYC-interacting genes in human gliomas. Cancer Res 65:8679-8689.

Campbell DS, Holt CE (2001) Chemotropic responses of retinal growth cones mediated by rapid local protein synthesis and degradation. Neuron 32:1013-1026.

Cang Y, Zhang J, Nicholas SA, Bastien J, Li B, Zhou P, Goff SP (2006) Deletion of DDB1 in mouse brain and lens leads to p53-dependent elimination of proliferating cells. Cell 127:929-940.

Carter RJ, Lione LA, Humby T, Mangiarini L, Mahal A, Bates GP, Dunnett SB, Morton AJ (1999) Characterization of progressive motor deficits in mice transgenic for the human Huntington's disease mutation. J Neurosci 19:3248-3257.

Carulli D, Buffo A, Botta C, Altruda F, Strata P (2002) Regenerative and survival capabilities of Purkinje cells overexpressing c-Jun. Eur J Neurosci 16:105-118.

Chae T, Kwon YT, Bronson R, Dikkes P, Li E, Tsai LH (1997) Mice lacking p35, a neuronal specific activator of Cdk5, display cortical lamination defects, seizures, and adult lethality. Neuron 18:29-42.

Chan CH, Godinho LN, Thomaidou D, Tan SS, Gulisano M, Parnavelas JG (2001) Emx1 is a marker for pyramidal neurons of the cerebral cortex. Cereb Cortex 11:1191-1198.

Cheng S, Fockler C, Barnes WM, Higuchi R (1994) Effective amplification of long targets from cloned inserts and human genomic DNA. Proc Natl Acad Sci U S A 91:5695-5699.

Chow CW, Rincon M, Cavanagh J, Dickens M, Davis RJ (1997) Nuclear accumulation of NFAT4 opposed by the JNK signal transduction pathway. Science 278:1638-1641.

Chow LM, Tian Y, Weber T, Corbett M, Zuo J, Baker SJ (2006) Inducible Cre recombinase activity in mouse cerebellar granule cell precursors and inner ear hair cells. Dev Dyn 235:2991-2998.

Chung KK, Zhang Y, Lim KL, Tanaka Y, Huang H, Gao J, Ross CA, Dawson VL, Dawson TM (2001) Parkin ubiquitinates the alpha-synuclein-interacting protein, synphilin-1: implications for Lewy-body formation in Parkinson disease. Nature medicine 7:1144-1150.

Colledge M, Snyder EM, Crozier RA, Soderling JA, Jin Y, Langeberg LK, Lu H, Bear MF, Scott JD (2003) Ubiquitination regulates PSD-95 degradation and AMPA receptor surface expression. Neuron 40:595-607.

Colman H, Lichtman JW (1993) Interactions between nerve and muscle: synapse elimination at the developing neuromuscular junction. Developmental biology 156:1-10.

Copp AJ, Greene ND, Murdoch JN (2003) The genetic basis of mammalian neurulation. Nat Rev Genet 4:784-793.

Corrales JD, Blaess S, Mahoney EM, Joyner AL (2006) The level of sonic hedgehog signaling regulates the complexity of cerebellar foliation. Development 133:1811-1821.

Cowan KJ, Storey KB (2003) Mitogen-activated protein kinases: new signaling pathways functioning in cellular responses to environmental stress. The Journal of experimental biology 206:1107-1115.

Cragg SJ (2006) Meaningful silences: how dopamine listens to the ACh pause. Trends in neurosciences 29:125-131.

D'Arcangelo G, Miao GG, Chen SC, Soares HD, Morgan JI, Curran T (1995) A protein related to extracellular matrix proteins deleted in the mouse mutant reeler. Nature 374:719-723.

D'Mello SR, Galli C, Ciotti T, Calissano P (1993) Induction of apoptosis in cerebellar granule neurons by low potassium: inhibition of death by insulin-like growth factor I and cAMP. Proc Natl Acad Sci U S A 90:10989-10993.

Dauer W, Przedborski S (2003) Parkinson's disease: mechanisms and models. Neuron 39:889-909.

Davis RJ (2000) Signal transduction by the JNK group of MAP kinases. Cell 103:239-252.

Derijard B, Hibi M, Wu IH, Barrett T, Su B, Deng T, Karin M, Davis RJ (1994) JNK1: a protein kinase stimulated by UV light and Ha-Ras that binds and phosphorylates the c-Jun activation domain. Cell 76:1025-1037.

Di Marcotullio L, Ferretti E, Greco A, De Smaele E, Po A, Sico MA, Alimandi M, Giannini G, Maroder M, Screpanti I, Gulino A (2006) Numb is a suppressor of Hedgehog signalling and targets Gli1 for Itch-dependent ubiquitination. Nat Cell Biol 8:1415-1423.

Ding M, Chao D, Wang G, Shen K (2007) Spatial regulation of an E3 ubiquitin ligase directs selective synapse elimination. Science 317:947-951.

Dong C, Yang DD, Wysk M, Whitmarsh AJ, Davis RJ, Flavell RA (1998) Defective T cell differentiation in the absence of Jnk1. Science 282:2092-2095.

Dumesnil-Bousez N, Sotelo C (1992) Early development of the Lurcher cerebellum: Purkinje cell alterations and impairment of synaptogenesis. Journal of neurocytology 21:506-529.

Ekholm-Reed S, Spruck CH, Sangfelt O, van Drogen F, Mueller-Holzner E, Widschwendter M, Zetterberg A, Reed SI (2004) Mutation of hCDC4 leads to cell cycle deregulation of cyclin E in cancer. Cancer Res 64:795-800.

Estus S, Zaks WJ, Freeman RS, Gruda M, Bravo R, Johnson EM, Jr. (1994) Altered gene expression in neurons during programmed cell death: identification of c-jun as necessary for neuronal apoptosis. The Journal of cell biology 127:1717-1727.

Fang D, Kerppola TK (2004) Ubiquitin-mediated fluorescence complementation reveals that Jun ubiquitinated by Itch/AIP4 is localized to lysosomes. Proc Natl Acad Sci U S A 101:14782-14787.

Fang S, Jensen JP, Ludwig RL, Vousden KH, Weissman AM (2000) Mdm2 is a RING finger-dependent ubiquitin protein ligase for itself and p53. J Biol Chem 275:8945-8951.

Feng L, Allen NS, Simo S, Cooper JA (2007) Cullin 5 regulates Dab1 protein levels and neuron positioning during cortical development. Genes Dev 21:2717-2730.

Ferguson C, Hardy SL, Werner DF, Hileman SM, Delorey TM, Homanics GE (2007) New insight into the role of the beta3 subunit of the GABAA-R in development, behavior, body weight regulation, and anesthesia revealed by conditional gene knockout. BMC Neurosci 8:85.

Ferkany JW, Coyle JT (1983) Kainic acid selectively stimulates the release of endogenous excitatory acidic amino acids. J Pharmacol Exp Ther 225:399-406.

Fernagut PO, Ghorayeb I, Diguet E, Tison F (2005) In vivo models of multiple system atrophy. Mov Disord 20 Suppl 12:S57-63.

Fernagut PO, Chalon S, Diguet E, Guilloteau D, Tison F, Jaber M (2003) Motor behaviour deficits and their histopathological and functional correlates in the nigrostriatal system of dopamine transporter knockout mice. Neuroscience 116:1123-1130.

Flechsig E, Hegyi I, Leimeroth R, Zuniga A, Rossi D, Cozzio A, Schwarz P, Rulicke T, Gotz J, Aguzzi A, Weissmann C (2003) Expression of truncated PrP targeted to Purkinje cells of PrP knockout mice causes Purkinje cell death and ataxia. Embo J 22:3095-3101.

Fleming SM, Fernagut PO, Chesselet MF (2005) Genetic mouse models of parkinsonism: strengths and limitations. NeuroRx 2:495-503.

Fremeau RT, Jr., Kam K, Qureshi T, Johnson J, Copenhagen DR, Storm-Mathisen J, Chaudhry FA, Nicoll RA, Edwards RH (2004) Vesicular glutamate transporters 1 and 2 target to functionally distinct synaptic release sites. Science 304:1815-1819.

Fremeau RT, Jr., Troyer MD, Pahner I, Nygaard GO, Tran CH, Reimer RJ, Bellocchio EE, Fortin D, Storm-Mathisen J, Edwards RH (2001) The expression of vesicular glutamate transporters defines two classes of excitatory synapse. Neuron 31:247-260.

Frey B, Suppmann, B. (1995) Demonstration of the Expand PCR System's Greater Fidelity and Higher Yields with a lacI-based PCR fidelity assay. Biochemica.

Friocourt G, Kappeler C, Saillour Y, Fauchereau F, Rodriguez MS, Bahi N, Vinet MC, Chafey P, Poirier K, Taya S, Wood SA, Dargemont C, Francis F, Chelly J (2005) Doublecortin interacts with the ubiquitin protease DFFRX, which associates with microtubules in neuronal processes. Molecular and cellular neurosciences 28:153-164.

Gallagher E, Gao M, Liu YC, Karin M (2006) Activation of the E3 ubiquitin ligase Itch through a phosphorylation-induced conformational change. Proc Natl Acad Sci U S A 103:1717-1722.

Gao M, Labuda T, Xia Y, Gallagher E, Fang D, Liu YC, Karin M (2004) Jun turnover is controlled through JNK-dependent phosphorylation of the E3 ligase Itch. Science 306:271-275.

Garcia M, Charvin D, Caboche J (2004) Expanded huntingtin activates the c-Jun terminal kinase/c-Jun pathway prior to aggregate formation in striatal neurons in culture. Neuroscience 127:859-870.

Gaveriaux-Ruff C, Kieffer BL (2007) Conditional gene targeting in the mouse nervous system: Insights into brain function and diseases. Pharmacology & therapeutics 113:619-634.

Ge W, Martinowich K, Wu X, He F, Miyamoto A, Fan G, Weinmaster G, Sun YE (2002) Notch signaling promotes astrogliogenesis via direct CSL-mediated glial gene activation. Journal of neuroscience research 69:848-860.

Gelman DM, Noain D, Avale ME, Otero V, Low MJ, Rubinstein M (2003) Transgenic mice engineered to target Cre/loxP-mediated DNA recombination into catecholaminergic neurons. Genesis 36:196-202.

Giardina SF, Cheung NS, Reid MT, Beart PM (1998) Kainate-induced apoptosis in cultured murine cerebellar granule cells elevates expression of the cell cycle gene cyclin D1. J Neurochem 71:1325-1328.

Gillardon F, Baurle J, Grusser-Cornehls U, Zimmermann M (1995) DNA fragmentation and activation of c-Jun in the cerebellum of mutant mice (weaver, Purkinje cell degeneration). Neuroreport 6:1766-1768.

Gilmore EC, Ohshima T, Goffinet AM, Kulkarni AB, Herrup K (1998) Cyclin-dependent kinase 5-deficient mice demonstrate novel developmental arrest in cerebral cortex. J Neurosci 18:6370-6377.

Goldberg MS, Fleming SM, Palacino JJ, Cepeda C, Lam HA, Bhatnagar A, Meloni EG, Wu N, Ackerson LC, Klapstein GJ, Gajendiran M, Roth BL, Chesselet MF, Maidment NT, Levine MS, Shen J (2003) Parkin-deficient mice exhibit nigrostriatal deficits but not loss of dopaminergic neurons. J Biol Chem 278:43628-43635.

Goldowitz D, Hamre K (1998) The cells and molecules that make a cerebellum. Trends in neurosciences 21:375-382.

Grant P, Pant HC (2000) Neurofilament protein synthesis and phosphorylation. Journal of neurocytology 29:843-872.

Graus-Porta D, Blaess S, Senften M, Littlewood-Evans A, Damsky C, Huang Z, Orban P, Klein R, Schittny JC, Muller U (2001) Beta1-class integrins regulate the development of laminae and folia in the cerebral and cerebellar cortex. Neuron 31:367-379.

Gu Z, Inomata K, Ishizawa K, Horii A (2007) The FBXW7 beta-form is suppressed in human glioma cells. Biochem Biophys Res Commun 354:992-998.

Guillemot F, Joyner AL (1993) Dynamic expression of the murine Achaete-Scute homologue Mash-1 in the developing nervous system. Mech Dev 42:171-185.

Gupta A, Tsai LH, Wynshaw-Boris A (2002) Life is a journey: a genetic look at neocortical development. Nat Rev Genet 3:342-355.

Gupta S, Barrett T, Whitmarsh AJ, Cavanagh J, Sluss HK, Derijard B, Davis RJ (1996) Selective interaction of JNK protein kinase isoforms with transcription factors. Embo J 15:2760-2770.

Gusella JF, MacDonald ME (2000) Molecular genetics: unmasking polyglutamine triggers in neurodegenerative disease. Nat Rev Neurosci 1:109-115.

Hagedorn M, Delugin M, Abraldes I, Allain N, Belaud-Rotureau MA, Turmo M, Prigent C, Loiseau H, Bikfalvi A, Javerzat S (2007) FBXW7/hCDC4 controls glioma cell proliferation in vitro and is a prognostic marker for survival in glioblastoma patients. Cell division 2:9.

Haglund K, Sigismund S, Polo S, Szymkiewicz I, Di Fiore PP, Dikic I (2003) Multiple monoubiquitination of RTKs is sufficient for their endocytosis and degradation. Nat Cell Biol 5:461-466.

Ham J, Babij C, Whitfield J, Pfarr CM, Lallemand D, Yaniv M, Rubin LL (1995) A c-Jun dominant negative mutant protects sympathetic neurons against programmed cell death. Neuron 14:927-939.

Hao B, Oehlmann S, Sowa ME, Harper JW, Pavletich NP (2007) Structure of a Fbw7-Skp1-cyclin E complex: multisite-phosphorylated substrate recognition by SCF ubiquitin ligases. Mol Cell 26:131-143.

Hatten ME, Heintz N (1995) Mechanisms of neural patterning and specification in the developing cerebellum. Annual review of neuroscience 18:385-408.

Hatten ME, Alder J, Zimmerman K, Heintz N (1997) Genes involved in cerebellar cell specification and differentiation. Current opinion in neurobiology 7:40-47.

Hatton BA, Knoepfler PS, Kenney AM, Rowitch DH, de Alboran IM, Olson JM, Eisenman RN (2006) N-myc Is an Essential Downstream Effector of Shh Signaling during both Normal and Neoplastic Cerebellar Growth. Cancer Res 66:8655-8661.

Hentze MW, Kulozik AE (1999) A perfect message: RNA surveillance and nonsense-mediated decay. Cell 96:307-310.

Herdegen T, Skene P, Bahr M (1997) The c-Jun transcription factor--bipotential mediator of neuronal death, survival and regeneration. Trends in neurosciences 20:227-231.

Herdegen T, Kovary K, Buhl A, Bravo R, Zimmermann M, Gass P (1995) Basal expression of the inducible transcription factors c-Jun, JunB, JunD, c-Fos, FosB, and Krox-24 in the adult rat brain. The Journal of comparative neurology 354:39-56.

Herdegen T, Claret FX, Kallunki T, Martin-Villalba A, Winter C, Hunter T, Karin M (1998) Lasting N-terminal phosphorylation of c-Jun and activation of c-Jun N-terminal kinases after neuronal injury. J Neurosci 18:5124-5135.

Herrero MT, Levy R, Ruberg M, Luquin MR, Villares J, Guillen J, Faucheux B, Javoy-Agid F, Guridi J, Agid Y, Obeso JA, Hirsch EC (1996) Consequence of nigrostriatal denervation and L-dopa therapy on the expression of glutamic acid decarboxylase messenger RNA in the pallidum. Neurology 47:219-224.

Herrup K, Mullen RJ (1979) Staggerer chimeras: intrinsic nature of Purkinje cell defects and implications for normal cerebellar development. Brain research 178:443-457.

Hoesche C, Sauerwald A, Veh RW, Krippl B, Kilimann MW (1993) The 5'-flanking region of the rat synapsin I gene directs neuron-specific and

developmentally regulated reporter gene expression in transgenic mice. J Biol Chem 268:26494-26502.

Huard JM, Forster CC, Carter ML, Sicinski P, Ross ME (1999) Cerebellar histogenesis is disturbed in mice lacking cyclin D2. Development 126:1927-1935.

Hubbard EJ, Wu G, Kitajewski J, Greenwald I (1997) sel-10, a negative regulator of lin-12 activity in Caenorhabditis elegans, encodes a member of the CDC4 family of proteins. Genes Dev 11:3182-3193.

Hunot S, Vila M, Teismann P, Davis RJ, Hirsch EC, Przedborski S, Rakic P, Flavell RA (2004) JNK-mediated induction of cyclooxygenase 2 is required for neurodegeneration in a mouse model of Parkinson's disease. Proc Natl Acad Sci U S A 101:665-670.

Huot P, Parent A (2007) Dopaminergic neurons intrinsic to the striatum. J Neurochem 101:1441-1447.

Imai Y, Soda M, Inoue H, Hattori N, Mizuno Y, Takahashi R (2001) An unfolded putative transmembrane polypeptide, which can lead to endoplasmic reticulum stress, is a substrate of Parkin. Cell 105:891-902.

Isaksson A, Musti AM, Bohmann D (1996) Ubiquitin in signal transduction and cell transformation. Biochim Biophys Acta 1288:F21-29.

Itier JM et al. (2003) Parkin gene inactivation alters behaviour and dopamine neurotransmission in the mouse. Human molecular genetics 12:2277-2291.

Jackson PK, Eldridge AG (2002) The SCF ubiquitin ligase: an extended look. Mol Cell 9:923-925.

Jandke A (2003) Characterisation of FBW7 domains. In: Mammalian Genetics Lab, p 65. Senftenberg, Germany: University of Applied Sciences Senftenberg.

Jiang YH, Armstrong D, Albrecht U, Atkins CM, Noebels JL, Eichele G, Sweatt JD, Beaudet AL (1998) Mutation of the Angelman ubiquitin ligase in mice causes increased cytoplasmic p53 and deficits of contextual learning and long-term potentiation. Neuron 21:799-811.

Jin J, Cardozo T, Lovering RC, Elledge SJ, Pagano M, Harper JW (2004) Systematic analysis and nomenclature of mammalian F-box proteins. Genes Dev 18:2573-2580.

Joazeiro CA, Wing SS, Huang H, Leverson JD, Hunter T, Liu YC (1999) The tyrosine kinase negative regulator c-Cbl as a RING-type, E2-dependent ubiquitin-protein ligase. Science 286:309-312.

Julien JP, Mushynski WE (1982) Multiple phosphorylation sites in mammalian neurofilament polypeptides. J Biol Chem 257:10467-10470.

Kamura T, Koepp DM, Conrad MN, Skowyra D, Moreland RJ, Iliopoulos O, Lane WS, Kaelin WG, Jr., Elledge SJ, Conaway RC, Harper JW, Conaway JW (1999) Rbx1, a component of the VHL tumor suppressor complex and SCF ubiquitin ligase. Science 284:657-661.

Kapfhammer JP (2004) Cellular and molecular control of dendritic growth and development of cerebellar Purkinje cells. Prog Histochem Cytochem 39:131-182.

Karsan A (2005) The role of notch in modeling and maintaining the vasculature. Canadian journal of physiology and pharmacology 83:14-23.

Kenney AM, Cole MD, Rowitch DH (2003) Nmyc upregulation by sonic hedgehog signaling promotes proliferation in developing cerebellar granule neuron precursors. Development 130:15-28.

Kerjan G, Gleeson JG (2007) A missed exit: Reelin sets in motion Dab1 polyubiquitination to put the break on neuronal migration. Genes Dev 21:2850-2854.

Kim SY, Herbst A, Tworkowski KA, Salghetti SE, Tansey WP (2003) Skp2 regulates Myc protein stability and activity. Mol Cell 11:1177-1188.

Kimura T, Gotoh M, Nakamura Y, Arakawa H (2003) hCDC4b, a regulator of cyclin E, as a direct transcriptional target of p53. Cancer Sci 94:431-436.

Kishino T, Lalande M, Wagstaff J (1997) UBE3A/E6-AP mutations cause Angelman syndrome. Nat Genet 15:70-73.

Kitagawa M, Hatakeyama S, Shirane M, Matsumoto M, Ishida N, Hattori K, Nakamichi I, Kikuchi A, Nakayama K (1999) An F-box protein, FWD1, mediates ubiquitin-dependent proteolysis of beta-catenin. Embo J 18:2401-2410.

Knoepfler PS, Cheng PF, Eisenman RN (2002) N-myc is essential during neurogenesis for the rapid expansion of progenitor cell populations and the inhibition of neuronal differentiation. Genes Dev 16:2699-2712.

Koch HB, Zhang R, Verdoodt B, Bailey A, Zhang CD, Yates JR, 3rd, Menssen A, Hermeking H (2007) Large-scale identification of c-MYC-associated proteins using a combined TAP/MudPIT approach. Cell Cycle 6:205-217.

Komatsu M, Waguri S, Chiba T, Murata S, Iwata J, Tanida I, Ueno T, Koike M, Uchiyama Y, Kominami E, Tanaka K (2006) Loss of autophagy in

the central nervous system causes neurodegeneration in mice. Nature 441:880-884.

Kuan CY, Yang DD, Samanta Roy DR, Davis RJ, Rakic P, Flavell RA (1999) The Jnk1 and Jnk2 protein kinases are required for regional specific apoptosis during early brain development. Neuron 22:667-676.

Kumar S, Kao WH, Howley PM (1997) Physical interaction between specific E2 and Hect E3 enzymes determines functional cooperativity. J Biol Chem 272:13548-13554.

Lai EC (2002) Protein degradation: four E3s for the notch pathway. Curr Biol 12:R74-78.

Laine J, Axelrad H (1994) The candelabrum cell: a new interneuron in the cerebellar cortex. The Journal of comparative neurology 339:159-173.

Lallemand Y, Luria V, Haffner-Krausz R, Lonai P (1998) Maternally expressed PGK-Cre transgene as a tool for early and uniform activation of the Cre site-specific recombinase. Transgenic Res 7:105-112.

Lambert de Rouvroit C, Goffinet AM (2001) Neuronal migration. Mech Dev 105:47-56.

Landis SC, Mullen RJ (1978) The development and degeneration of Purkinje cells in pcd mutant mice. The Journal of comparative neurology 177:125-143.

Leah JD, Herdegen T, Bravo R (1991) Selective expression of Jun proteins following axotomy and axonal transport block in peripheral nerves in the rat: evidence for a role in the regeneration process. Brain research 566:198-207.

Leclerc N, Gravel C, Plioplys A, Hawkes R (1985) Basket cell development in the normal and hypothyroid rat cerebellar cortex studied with a monoclonal anti-neurofilament antibody. Can J Biochem Cell Biol 63:564-576.

Lee JK, Hwang WS, Lee YD, Han PL (1999) Dynamic expression of SEK1 suggests multiple roles of the gene during embryogenesis and in adult brain of mice. Brain Res Mol Brain Res 66:133-140.

Lerma J (2003) Roles and rules of kainate receptors in synaptic transmission. Nat Rev Neurosci 4:481-495.

Lewis PM, Gritli-Linde A, Smeyne R, Kottmann A, McMahon AP (2004) Sonic hedgehog signaling is required for expansion of granule neuron precursors and patterning of the mouse cerebellum. Developmental biology 270:393-410.

Lewis TS, Shapiro PS, Ahn NG (1998) Signal transduction through MAP kinase cascades. Advances in cancer research 74:49-139.

Li J, Pauley AM, Myers RL, Shuang R, Brashler JR, Yan R, Buhl AE, Ruble C, Gurney ME (2002) SEL-10 interacts with presenilin 1, facilitates its ubiquitination, and alters A-beta peptide production. J Neurochem 82:1540-1548.

Li W, Tu D, Brunger AT, Ye Y (2007) A ubiquitin ligase transfers preformed polyubiquitin chains from a conjugating enzyme to a substrate. Nature 446:333-337.

Louvi A, Artavanis-Tsakonas S (2006) Notch signalling in vertebrate neural development. Nat Rev Neurosci 7:93-102.

Lu J, Lichtman JW (2007) Imaging the neuromuscular junction over the past centuries ? Sheng Li Xue Bao 59:683-696.

Lukaszewicz A, Savatier P, Cortay V, Giroud P, Huissoud C, Berland M, Kennedy H, Dehay C (2005) G1 phase regulation, area-specific cell cycle control, and cytoarchitectonics in the primate cortex. Neuron 47:353-364.

Luscher B (2001) Function and regulation of the transcription factors of the Myc/Max/Mad network. Gene 277:1-14.

Lutolf S, Radtke F, Aguet M, Suter U, Taylor V (2002) Notch1 is required for neuronal and glial differentiation in the cerebellum. Development 129:373-385.

Maat-Schieman ML, Dorsman JC, Smoor MA, Siesling S, Van Duinen SG, Verschuuren JJ, den Dunnen JT, Van Ommen GJ, Roos RA (1999) Distribution of inclusions in neuronal nuclei and dystrophic neurites in Huntington disease brain. Journal of neuropathology and experimental neurology 58:129-137.

Mangiarini L, Sathasivam K, Seller M, Cozens B, Harper A, Hetherington C, Lawton M, Trottier Y, Lehrach H, Davies SW, Bates GP (1996) Exon 1 of the HD gene with an expanded CAG repeat is sufficient to cause a progressive neurological phenotype in transgenic mice. Cell 87:493-506.

Mao JH, Perez-Losada J, Wu D, Delrosario R, Tsunematsu R, Nakayama KI, Brown K, Bryson S, Balmain A (2004) Fbxw7/Cdc4 is a p53-dependent, haploinsufficient tumour suppressor gene. Nature 432:775-779.

Marin O, Rubenstein JL (2001) A long, remarkable journey: tangential migration in the telencephalon. Nat Rev Neurosci 2:780-790.

Marin O, Rubenstein JL (2003) Cell migration in the forebrain. Annual review of neuroscience 26:441-483.

Marino S, Hoogervoorst D, Brandner S, Berns A (2003) Rb and p107 are required for normal cerebellar development and granule cell survival but not for Purkinje cell persistence. Development 130:3359-3368.

Marino S, Krimpenfort P, Leung C, van der Korput HA, Trapman J, Camenisch I, Berns A, Brandner S (2002) PTEN is essential for cell migration but not for fate determination and tumourigenesis in the cerebellum. Development 129:3513-3522.

Maruyama S, Hatakeyama S, Nakayama K, Ishida N, Kawakami K (2001) Characterization of a mouse gene (Fbxw6) that encodes a homologue of Caenorhabditis elegans SEL-10. Genomics 78:214-222.

Marzban H, Hawkes R (2007) Fibroblast growth factor promotes the development of deep cerebellar nuclear neurons in dissociated mouse cerebellar cultures. Brain research 1141:25-36.

Mata IF, Lockhart PJ, Farrer MJ (2004) Parkin genetics: one model for Parkinson's disease. Human molecular genetics 13 Spec No 1:R127-133.

Mathis L, Bonnerot C, Puelles L, Nicolas JF (1997) Retrospective clonal analysis of the cerebellum using genetic laacZ/lacZ mouse mosaics. Development 124:4089-4104.

Matsushime H, Quelle DE, Shurtleff SA, Shibuya M, Sherr CJ, Kato JY (1994) D-type cyclin-dependent kinase activity in mammalian cells. Mol Cell Biol 14:2066-2076.

Matsuura K, Kabuto H, Makino H, Ogawa N (1997) Pole test is a useful method for evaluating the mouse movement disorder caused by striatal dopamine depletion. Journal of neuroscience methods 73:45-48.

Matus AI, Ng M, Jones DH (1979) Immunohistochemical localization of neurofilament antigen in rat cerebellum. Journal of neurocytology 8:513-525.

McEvoy JD, Kossatz U, Malek N, Singer JD (2007) Constitutive turnover of cyclin E by Cul3 maintains quiescence. Mol Cell Biol 27:3651-3666.

Miale IL, Sidman RL (1961) An autoradiographic analysis of histogenesis in the mouse cerebellum. Exp Neurol 4:277-296.

Migheli A, Piva R, Wei J, Attanasio A, Casolino S, Hodes ME, Dlouhy SR, Bayer SA, Ghetti B (1997) Diverse cell death pathways result from a single missense mutation in weaver mouse. The American journal of pathology 151:1629-1638.

Mignone JL, Kukekov V, Chiang AS, Steindler D, Enikolopov G (2004) Neural stem and progenitor cells in nestin-GFP transgenic mice. The Journal of comparative neurology 469:311-324.

Miller DM (2007) Neuroscience. Synapses here and not everywhere. Science 317:907-908.

Minella AC, Welcker M, Clurman BE (2005) Ras activity regulates cyclin E degradation by the Fbw7 pathway. Proc Natl Acad Sci U S A 102:9649-9654.

Minichiello L, Korte M, Wolfer D, Kuhn R, Unsicker K, Cestari V, Rossi-Arnaud C, Lipp HP, Bonhoeffer T, Klein R (1999) Essential role for TrkB receptors in hippocampus-mediated learning. Neuron 24:401-414.

Miura E, Fukaya M, Sato T, Sugihara K, Asano M, Yoshioka K, Watanabe M (2006) Expression and distribution of JNK/SAPK-associated scaffold protein JSAP1 in developing and adult mouse brain. J Neurochem 97:1431-1446.

Miura M, Hatakeyama S, Hattori K, Nakayama K (1999) Structure and expression of the gene encoding mouse F-box protein, Fwd2. Genomics 62:50-58.

Molnar Z, Cheung AF (2006) Towards the classification of subpopulations of layer V pyramidal projection neurons. Neuroscience research 55:105-115.

Molyneaux BJ, Arlotta P, Menezes JR, Macklis JD (2007) Neuronal subtype specification in the cerebral cortex. Nat Rev Neurosci 8:427-437.

Moroy T, Geisen C (2004) Cyclin E. Int J Biochem Cell Biol 36:1424-1439.

Mugnaini E, Floris A (1994) The unipolar brush cell: a neglected neuron of the mammalian cerebellar cortex. The Journal of comparative neurology 339:174-180.

Mukhopadhyay D, Riezman H (2007) Proteasome-independent functions of ubiquitin in endocytosis and signaling. Science 315:201-205.

Muller U (1999) Ten years of gene targeting: targeted mouse mutants, from vector design to phenotype analysis. Mech Dev 82:3-21.

Muratani M, Tansey WP (2003) How the ubiquitin-proteasome system controls transcription. Nat Rev Mol Cell Biol 4:192-201.

Musti AM, Treier M, Bohmann D (1997) Reduced ubiquitin-dependent degradation of c-Jun after phosphorylation by MAP kinases. Science 275:400-402.

Musti AM, Treier M, Peverali FA, Bohmann D (1996) Differential regulation of c-Jun and JunD by ubiquitin-dependent protein degradation. Biological chemistry 377:619-624.

Nateri AS, Riera-Sans L, Da Costa C, Behrens A (2004) The ubiquitin ligase SCFFbw7 antagonizes apoptotic JNK signaling. Science 303:1374-1378.

Nishina H, Vaz C, Billia P, Nghiem M, Sasaki T, De la Pompa JL, Furlonger K, Paige C, Hui C, Fischer KD, Kishimoto H, Iwatsubo T, Katada T, Woodgett JR, Penninger JM (1999) Defective liver formation and liver cell apoptosis in mice lacking the stress signaling kinase SEK1/MKK4. Development 126:505-516.

Noguchi K, Kitanaka C, Yamana H, Kokubu A, Mochizuki T, Kuchino Y (1999) Regulation of c-Myc through phosphorylation at Ser-62 and Ser-71 by c-Jun N-terminal kinase. J Biol Chem 274:32580-32587.

Oberdick J, Smeyne RJ, Mann JR, Zackson S, Morgan JI (1990) A promoter that drives transgene expression in cerebellar Purkinje and retinal bipolar neurons. Science 248:223-226.

Oberg C, Li J, Pauley A, Wolf E, Gurney M, Lendahl U (2001) The Notch intracellular domain is ubiquitinated and negatively regulated by the mammalian Sel-10 homolog. J Biol Chem 276:35847-35853.

Oliver TG, Grasfeder LL, Carroll AL, Kaiser C, Gillingham CL, Lin SM, Wickramasinghe R, Scott MP, Wechsler-Reya RJ (2003) Transcriptional profiling of the Sonic hedgehog response: a critical role for N-myc in proliferation of neuronal precursors. Proc Natl Acad Sci U S A 100:7331-7336.

Patrick GN, Zhou P, Kwon YT, Howley PM, Tsai LH (1998) p35, the neuronal-specific activator of cyclin-dependent kinase 5 (Cdk5) is degraded by the ubiquitin-proteasome pathway. J Biol Chem 273:24057-24064.

Paysan J, Conroy WG, Coggan JS, Berg DK (2000) The neurofilament infrastructure of a developing presynaptic calyx. The Journal of comparative neurology 425:284-294.

Pearson AG, Byrne UT, MacGibbon GA, Faull RL, Dragunow M (2006) Activated c-Jun is present in neurofibrillary tangles in Alzheimer's disease brains. Neuroscience letters 398:246-250.

Pellet JB, Haefliger JA, Staple JK, Widmann C, Welker E, Hirling H, Bonny C, Nicod P, Catsicas S, Waeber G, Riederer BM (2000) Spatial, temporal and subcellular localization of islet-brain 1 (IB1), a homologue of JIP-1, in mouse brain. Eur J Neurosci 12:621-632.

Perez FA, Palmiter RD (2005) Parkin-deficient mice are not a robust model of parkinsonism. Proc Natl Acad Sci U S A 102:2174-2179.

Perez-Losada J, Mao JH, Balmain A (2005) Control of genomic instability and epithelial tumor development by the p53-Fbxw7/Cdc4 pathway. Cancer Res 65:6488-6492.

Petzold A (2005) Neurofilament phosphoforms: surrogate markers for axonal injury, degeneration and loss. J Neurol Sci 233:183-198.

Pickart CM (2001) Mechanisms underlying ubiquitination. Annu Rev Biochem 70:503-533.

Pickart CM, Eddins MJ (2004) Ubiquitin: structures, functions, mechanisms. Biochim Biophys Acta 1695:55-72.

Pierce ET (1975) Histogenesis of the deep cerebellar nuclei in the mouse: an autoradiographic study. Brain research 95:503-518.

Polleux F, Dehay C, Kennedy H (1998) Neurogenesis and commitment of corticospinal neurons in reeler. J Neurosci 18:9910-9923.

Polymeropoulos MH, Lavedan C, Leroy E, Ide SE, Dehejia A, Dutra A, Pike B, Root H, Rubenstein J, Boyer R, Stenroos ES, Chandrasekharappa S, Athanassiadou A, Papapetropoulos T, Johnson WG, Lazzarini AM, Duvoisin RC, Di Iorio G, Golbe LI, Nussbaum RL (1997) Mutation in the alpha-synuclein gene identified in families with Parkinson's disease. Science 276:2045-2047.

Popov N, Wanzel M, Madiredjo M, Zhang D, Beijersbergen R, Bernards R, Moll R, Elledge SJ, Eilers M (2007) The ubiquitin-specific protease USP28 is required for MYC stability. Nat Cell Biol 9:765-774.

Qiu L, Joazeiro C, Fang N, Wang HY, Elly C, Altman Y, Fang D, Hunter T, Liu YC (2000) Recognition and ubiquitination of Notch by Itch, a hect-type E3 ubiquitin ligase. J Biol Chem 275:35734-35737.

Raivich G, Bohatschek M, Da Costa C, Iwata O, Galiano M, Hristova M, Nateri AS, Makwana M, Riera-Sans L, Wolfer DP, Lipp HP, Aguzzi A, Wagner EF, Behrens A (2004) The AP-1 transcription factor c-Jun is required for efficient axonal regeneration. Neuron 43:57-67.

Redmond L, Oh SR, Hicks C, Weinmaster G, Ghosh A (2000) Nuclear Notch1 signaling and the regulation of dendritic development. Nature neuroscience 3:30-40.

Ridet JL, Malhotra SK, Privat A, Gage FH (1997) Reactive astrocytes: cellular and molecular cues to biological function. Trends in neurosciences 20:570-577.

Riederer BM, Porchet R, Marugg RA (1996) Differential expression and modification of neurofilament triplet proteins during cat cerebellar development. The Journal of comparative neurology 364:704-717.

Rottmann S, Luscher B (2006) The Mad side of the Max network: antagonizing the function of Myc and more. Current topics in microbiology and immunology 302:63-122.

Sabapathy K, Jochum W, Hochedlinger K, Chang L, Karin M, Wagner EF (1999) Defective neural tube morphogenesis and altered apoptosis in the absence of both JNK1 and JNK2. Mech Dev 89:115-124.

Sanyal S, Sandstrom DJ, Hoeffer CA, Ramaswami M (2002) AP-1 functions upstream of CREB to control synaptic plasticity in Drosophila. Nature 416:870-874.

Savinainen A, Garcia EP, Dorow D, Marshall J, Liu YF (2001) Kainate receptor activation induces mixed lineage kinase-mediated cellular signaling cascades via post-synaptic density protein 95. J Biol Chem 276:11382-11386.

Savio MG, Rotondo G, Maglie S, Rossetti G, Bender JR, Pardi R (2007) COP1D, an alternatively spliced constitutive photomorphogenic-1 (COP1) product, stabilizes UV stress-induced c-Jun through inhibition of full-length COP1. Oncogene.

Sears R, Nuckolls F, Haura E, Taya Y, Tamai K, Nevins JR (2000) Multiple Ras-dependent phosphorylation pathways regulate Myc protein stability. Genes Dev 14:2501-2514.

Sergent-Tanguy S, Chagneau C, Neveu I, Naveilhan P (2003) Fluorescent activated cell sorting (FACS): a rapid and reliable method to estimate the number of neurons in a mixed population. Journal of neuroscience methods 129:73-79.

Shaulian E, Karin M (2002) AP-1 as a regulator of cell life and death. Nat Cell Biol 4:E131-136.

Shen J, Kelleher RJ, 3rd (2007) The presenilin hypothesis of Alzheimer's disease: evidence for a loss-of-function pathogenic mechanism. Proc Natl Acad Sci U S A 104:403-409.

Shklyaev SS, Namba H, Sautin Y, Mitsutake N, Nagayama Y, Ishikawa N, Ito K, Zeki K, Yamashita S (2001) Involvement of wild-type p53 in radiation-induced c-Jun N-terminal kinase activation in human thyroid cells. Anticancer Res 21:2569-2575.

Sidman RL, Lane PW, Dickie MM (1962) Staggerer, a new mutation in the mouse affecting the cerebellum. Science 137:610-612.

Sillitoe RV, Joyner AL (2007) Morphology, molecular codes, and circuitry produce the three-dimensional complexity of the cerebellum. Annual review of cell and developmental biology 23:549-577.

Singer JD, Gurian-West M, Clurman B, Roberts JM (1999) Cullin-3 targets cyclin E for ubiquitination and controls S phase in mammalian cells. Genes Dev 13:2375-2387.

Smidt MP, Burbach JP (2007) How to make a mesodiencephalic dopaminergic neuron. Nat Rev Neurosci 8:21-32.

Spillantini MG, Schmidt ML, Lee VM, Trojanowski JQ, Jakes R, Goedert M (1997) Alpha-synuclein in Lewy bodies. Nature 388:839-840.

Spruck CH, Strohmaier H, Sangfelt O, Muller HM, Hubalek M, Muller-Holzner E, Marth C, Widschwendter M, Reed SI (2002) hCDC4 gene mutations in endometrial cancer. Cancer Res 62:4535-4539.

Staropoli JF, McDermott C, Martinat C, Schulman B, Demireva E, Abeliovich A (2003) Parkin is a component of an SCF-like ubiquitin ligase complex and protects postmitotic neurons from kainate excitotoxicity. Neuron 37:735-749.

Stegmeier F, Rape M, Draviam VM, Nalepa G, Sowa ME, Ang XL, McDonald ER, 3rd, Li MZ, Hannon GJ, Sorger PK, Kirschner MW, Harper JW, Elledge SJ (2007) Anaphase initiation is regulated by antagonistic ubiquitination and deubiquitination activities. Nature 446:876-881.

Sternberger LA, Sternberger NH (1983) Monoclonal antibodies distinguish phosphorylated and nonphosphorylated forms of neurofilaments in situ. Proc Natl Acad Sci U S A 80:6126-6130.

Strohmaier H, Spruck CH, Kaiser P, Won KA, Sangfelt O, Reed SI (2001) Human F-box protein hCdc4 targets cyclin E for proteolysis and is mutated in a breast cancer cell line. Nature 413:316-322.

Sudarov A, Joyner AL (2007) Cerebellum morphogenesis: the foliation pattern is orchestrated by multi-cellular anchoring centers. Neural Develop 2:26.

Sundqvist A, Bengoechea-Alonso MT, Ye X, Lukiyanchuk V, Jin J, Harper JW, Ericsson J (2005) Control of lipid metabolism by phosphorylation-dependent degradation of the SREBP family of transcription factors by SCF(Fbw7). Cell Metab 1:379-391.

Takahashi K, Akiyama H, Shimazaki K, Uchida C, Akiyama-Okunuki H, Tomita M, Fukumoto M, Uchida T (2007) Ablation of a peptidyl prolyl isomerase Pin1 from p53-null mice accelerated thymic hyperplasia by increasing the level of the intracellular form of Notch1. Oncogene 26:3835-3845.

Tetzlaff MT, Yu W, Li M, Zhang P, Finegold M, Mahon K, Harper JW, Schwartz RJ, Elledge SJ (2004) Defective cardiovascular development and elevated cyclin E and Notch proteins in mice lacking the Fbw7 F-box protein. Proc Natl Acad Sci U S A 101:3338-3345.

Thakur A, Wang X, Siedlak SL, Perry G, Smith MA, Zhu X (2007) c-Jun phosphorylation in Alzheimer disease. Journal of neuroscience research 85:1668-1673.

Tournier C, Dong C, Turner TK, Jones SN, Flavell RA, Davis RJ (2001) MKK7 is an essential component of the JNK signal transduction pathway activated by proinflammatory cytokines. Genes Dev 15:1419-1426.

Treier M, Staszewski LM, Bohmann D (1994) Ubiquitin-dependent c-Jun degradation in vivo is mediated by the delta domain. Cell 78:787-798.

Tronche F, Kellendonk C, Kretz O, Gass P, Anlag K, Orban PC, Bock R, Klein R, Schutz G (1999) Disruption of the glucocorticoid receptor gene in the nervous system results in reduced anxiety. Nat Genet 23:99-103.

Tsujita M, Mori H, Watanabe M, Suzuki M, Miyazaki J, Mishina M (1999) Cerebellar granule cell-specific and inducible expression of Cre recombinase in the mouse. J Neurosci 19:10318-10323.

Tsunematsu R, Nishiyama M, Kotoshiba S, Saiga T, Kamura T, Nakayama KI (2006) Fbxw8 is essential for Cul1-Cul7 complex formation and for placental development. Mol Cell Biol 26:6157-6169.

Tsunematsu R, Nakayama K, Oike Y, Nishiyama M, Ishida N, Hatakeyama S, Bessho Y, Kageyama R, Suda T, Nakayama KI (2004) Mouse Fbw7/Sel-10/Cdc4 is required for notch degradation during vascular development. J Biol Chem 279:9417-9423.

Uyttendaele H, Ho J, Rossant J, Kitajewski J (2001) Vascular patterning defects associated with expression of activated Notch4 in embryonic endothelium. Proc Natl Acad Sci U S A 98:5643-5648.

van Drogen F, Sangfelt O, Malyukova A, Matskova L, Yeh E, Means AR, Reed SI (2006) Ubiquitylation of cyclin E requires the sequential function of SCF complexes containing distinct hCdc4 isoforms. Mol Cell 23:37-48.

Vitadello M, Denis-Donini S (1990) Expression of neurofilament proteins in granule cells of the cerebellum. Brain research 509:47-54.

Von Coelln R, Thomas B, Savitt JM, Lim KL, Sasaki M, Hess EJ, Dawson VL, Dawson TM (2004) Loss of locus coeruleus neurons and reduced startle in parkin null mice. Proc Natl Acad Sci U S A 101:10744-10749.

von der Lehr N, Johansson S, Larsson LG (2003a) Implication of the ubiquitin/proteasome system in Myc-regulated transcription. Cell Cycle 2:403-407.

von der Lehr N, Johansson S, Wu S, Bahram F, Castell A, Cetinkaya C, Hydbring P, Weidung I, Nakayama K, Nakayama KI, Soderberg O, Kerppola TK, Larsson LG (2003b) The F-box protein Skp2 participates in c-Myc proteosomal degradation and acts as a cofactor for c-Myc-regulated transcription. Mol Cell 11:1189-1200.

Wallace VA (1999) Purkinje-cell-derived Sonic hedgehog regulates granule neuron precursor cell proliferation in the developing mouse cerebellum. Curr Biol 9:445-448.

Wang X, Taplick J, Geva N, Oren M (2004) Inhibition of p53 degradation by Mdm2 acetylation. FEBS Lett 561:195-201.

Watson A, Eilers A, Lallemand D, Kyriakis J, Rubin LL, Ham J (1998) Phosphorylation of c-Jun is necessary for apoptosis induced by survival signal withdrawal in cerebellar granule neurons. J Neurosci 18:751-762.

Wei W, Jin J, Schlisio S, Harper JW, Kaelin WG, Jr. (2005) The v-Jun point mutation allows c-Jun to escape GSK3-dependent recognition and destruction by the Fbw7 ubiquitin ligase. Cancer cell 8:25-33.

Welcker M, Clurman BE (2007) Fbw7/hCDC4 dimerization regulates its substrate interactions. Cell division 2:7.

Welcker M, Orian A, Grim JE, Eisenman RN, Clurman BE (2004a) A nucleolar isoform of the Fbw7 ubiquitin ligase regulates c-Myc and cell size. Curr Biol 14:1852-1857.

Welcker M, Orian A, Jin J, Grim JE, Harper JW, Eisenman RN, Clurman BE (2004b) The Fbw7 tumor suppressor regulates glycogen synthase kinase 3 phosphorylation-dependent c-Myc protein degradation. Proc Natl Acad Sci U S A 101:9085-9090.

Welcker M, Singer J, Loeb KR, Grim J, Bloecher A, Gurien-West M, Clurman BE, Roberts JM (2003) Multisite phosphorylation by Cdk2 and GSK3 controls cyclin E degradation. Mol Cell 12:381-392.

Wertz IE, O'Rourke KM, Zhang Z, Dornan D, Arnott D, Deshaies RJ, Dixit VM (2004) Human De-etiolated-1 regulates c-Jun by assembling a CUL4A ubiquitin ligase. Science 303:1371-1374.

Wheeler TC, Chin LS, Li Y, Roudabush FL, Li L (2002) Regulation of synaptophysin degradation by mammalian homologues of seven in absentia. J Biol Chem 277:10273-10282.

Willesen MG, Gammeltoft S, Vaudano E (2002) Activation of the c-Jun N terminal kinase pathway in an animal model of Parkinson's disease. Ann N Y Acad Sci 973:237-240.

Wilson SW, Rubenstein JL (2000) Induction and dorsoventral patterning of the telencephalon. Neuron 28:641-651.

Winston JT, Koepp DM, Zhu C, Elledge SJ, Harper JW (1999) A family of mammalian F-box proteins. Curr Biol 9:1180-1182.

Wisden W, Seeburg PH (1993) A complex mosaic of high-affinity kainate receptors in rat brain. J Neurosci 13:3582-3598.

Woelk T, Sigismund S, Penengo L, Polo S (2007) The ubiquitination code: a signalling problem. Cell division 2:11.

Wu C, Wairkar YP, Collins CA, DiAntonio A (2005) Highwire function at the Drosophila neuromuscular junction: spatial, structural, and temporal requirements. J Neurosci 25:9557-9566.

Wu G, Hubbard EJ, Kitajewski JK, Greenwald I (1998) Evidence for functional and physical association between Caenorhabditis elegans SEL-10, a Cdc4p-related protein, and SEL-12 presenilin. Proc Natl Acad Sci U S A 95:15787-15791.

Wulf GM, Ryo A, Wulf GG, Lee SW, Niu T, Petkova V, Lu KP (2001) Pin1 is overexpressed in breast cancer and cooperates with Ras signaling in increasing the transcriptional activity of c-Jun towards cyclin D1. Embo J 20:3459-3472.

Yada M, Hatakeyama S, Kamura T, Nishiyama M, Tsunematsu R, Imaki H, Ishida N, Okumura F, Nakayama K, Nakayama KI (2004) Phosphorylation-dependent degradation of c-Myc is mediated by the F-box protein Fbw7. Embo J 23:2116-2125.

Yan D, Guo L, Wang Y (2006) Requirement of dendritic Akt degradation by the ubiquitin-proteasome system for neuronal polarity. The Journal of cell biology 174:415-424.

Yang D, Tournier C, Wysk M, Lu HT, Xu J, Davis RJ, Flavell RA (1997) Targeted disruption of the MKK4 gene causes embryonic death,

inhibition of c-Jun NH2-terminal kinase activation, and defects in AP-1 transcriptional activity. Proc Natl Acad Sci U S A 94:3004-3009.

Yang DD, Kuan CY, Whitmarsh AJ, Rincon M, Zheng TS, Davis RJ, Rakic P, Flavell RA (1997) Absence of excitotoxicity-induced apoptosis in the hippocampus of mice lacking the Jnk3 gene. Nature 389:865-870.

Yang DD CD, Whitmarsh AJ, Barrett T, Davis RJ, Rincón M, Flavell RA. (1998) Differentiation of CD4+ T cells to Th1 cells requires MAP kinase JNK2. Immunity 9:575-585.

Yeh ES, Lew BO, Means AR (2006) The loss of PIN1 deregulates cyclin E and sensitizes mouse embryo fibroblasts to genomic instability. J Biol Chem 281:241-251.

Yoshida H, Hastie CJ, McLauchlan H, Cohen P, Goedert M (2004) Phosphorylation of microtubule-associated protein tau by isoforms of c-Jun N-terminal kinase (JNK). J Neurochem 90:352-358.

Zagrebelsky M, Buffo A, Skerra A, Schwab ME, Strata P, Rossi F (1998) Retrograde regulation of growth-associated gene expression in adult rat Purkinje cells by myelin-associated neurite growth inhibitory proteins. J Neurosci 18:7912-7929.

Zeiss CJ (2005) Neuroanatomical phenotyping in the mouse: the dopaminergic system. Veterinary pathology 42:753-773.

Zhang W, Koepp DM (2006) Fbw7 isoform interaction contributes to cyclin E proteolysis. Mol Cancer Res 4:935-943.

Zhu Y, Romero MI, Ghosh P, Ye Z, Charnay P, Rushing EJ, Marth JD, Parada LF (2001) Ablation of NF1 function in neurons induces abnormal development of cerebral cortex and reactive gliosis in the brain. Genes Dev 15:859-876.

Zinyk DL, Mercer EH, Harris E, Anderson DJ, Joyner AL (1998) Fate mapping of the mouse midbrain-hindbrain constriction using a site-specific recombination system. Curr Biol 8:665-668.
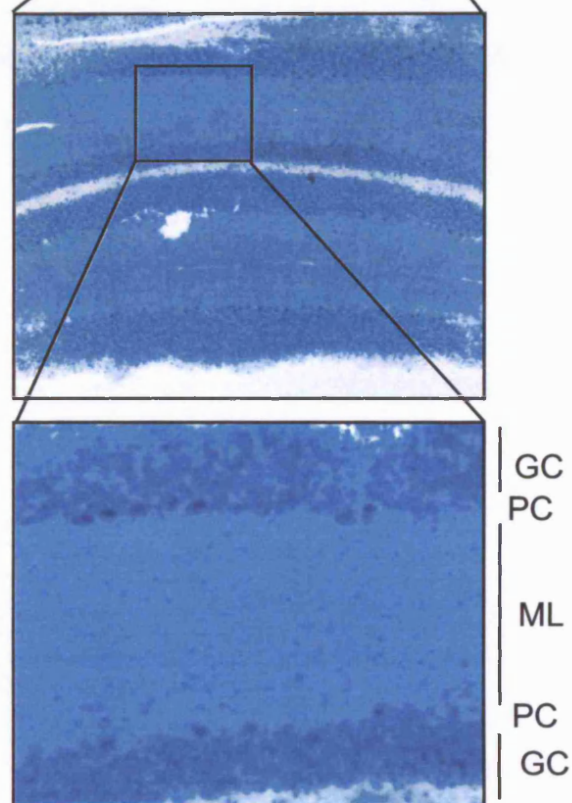
Zuscik MJ, Sands S, Ross SA, Waugh DJ, Gaivin RJ, Morilak D, Perez DM (2000) Overexpression of the alpha1B-adrenergic receptor causes apoptotic neurodegeneration: multiple system atrophy. Nature medicine 6:1388-1394.

Appendix : Engrailed2-mediated deletion in the cerebellar vermis

A

B

GC
PC

ML

PC

GC
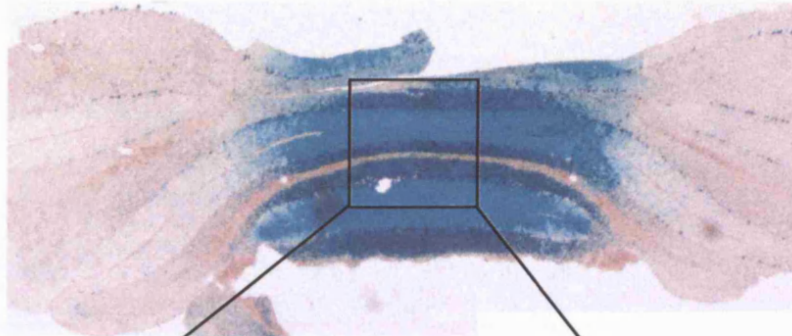
Appendix 1: Deletion under the Engrailed promoter is limited to the cerebellar vermis. A coronal cryosection obtained from a *En2cre:pten$^{flox/+}$:p53$^{flox/+}$:ROSA26lacZ$^{flox/+}$* mouse was stained for β-galactosidase to visualise areas affected by Engrailed-2 mediated deletion. A) Deletion is restricted to the cerebellar vermis and affects the cells in the vermis as demonstrated in high magnification in B: granule cells (GC), Purkinje cells (PC) and Molecular layer (ML)